LASER-INDUCED BREAKDOWN SPECTROSCOPY OF ACTINIDES – RAPID ISOTOPIC AND ELEMENTAL ANALYSIS FOR NUCLEAR FORENSICS

A thesis submitted to The University of Manchester for the degree of

Doctor of Philosophy

in the Faculty of Science and Engineering

2020

Gregory Hull

School of Engineering

Department of Chemical Engineering and Analytical Science

Table of Contents

List of Figures

List of Tables

List of Abbreviations

CF-LIBS	Calibration-Free LIBS
CRM	Certified Reference Material
DAQ	Data Acquisition card
DP-LIBS	Double-Pulsed LIBS
ECDL	External Cavity Diode Laser
F^2-LAMIS	Femtosecond Filament-LAMIS
FPs	Fission Products
FTIR	Fourier Transform Infrared spectroscopy
FWHM	Full Width at Half Maximum (of spectral line)
GC-MS	Gas Chromatography-Mass Spectrometry
GS	Gas Chromatography
HFS	Hyperfine Splitting
HRGS	High-Resolution Gamma-ray Spectroscopy
IAEA	International Atomic Energy Agency
ICP-MS	Inductively Coupled Plasma-Mass Spectrometry
IDMS	Isotope Dilution Mass Spectrometry
IR	Infrared
IS	Isotope Shift
ITU	Institute for Transuranic Elements at Karlsruhe, Germany
ITWG	Nuclear Forensics International Technical Working Group
LAMIS	Laser Ablation Molecular Isotopic Spectroscopy
LANL	Los Alamos National Laboratory, New Mexico, USE
LAS	Laser Absorption Spectroscopy
LA-TDLAS	Laser Ablation-Tuneable Diode Laser Absorption Spectroscopy
LIBS	Laser-Induced Breakdown Spectroscopy
LIF	Laser-Induced Fluorescence
LoD	Limit of Detection
LoQ	Limit of Quantification
LPP	Laser Produced Plasma or Laser ablation Produced Plasma
LSD	Laser Supported Detonation
LTE	Local Thermal Equilibrium
MDA	Multivariate Data Analysis
MoX	Mixed Oxide (nuclear fuels)
MS	Mass Spectrometry
Nd:YAG	Neodymium-doped yttrium-aluminium garnet (laser)
n_e	electron number density (usually in cm-3)
NF	Nuclear Forensics
PCA	Principal Component Analysis
PFC	Plasma Facing Component
PLS	Partial Least Squares
RMSECV	Root Mean Square Error of Cross-Validation
SEM	Scanning Electron Microscopy
SIMS	Secondary Ionisation Mass Spectrometry
SNM	Special Nuclear Material - Pu, 233U and U enriched in 235U
SP-LIBS	Single-Pulsed LIBS

t_d	Time delay (between laser ablation pulse and start of recording window)
TDLAS	Tuneable-Diode Laser Absorption Spectroscopy
TEM	Transmission Electron Microscopy
t_{gate} or t_g	Time gate (length of time for light acquisition)
TIMS	Thermal Ionisation Mass Spectrometry
UV	Ultraviolet
UV/Vis	Ultraviolet-Visible spectroscopy
XRF	X-Ray Fluorescence

Abstract

The laser-induced breakdown spectroscopy (LIBS) technique permits rapid elemental analysis of a material regardless of its nature, physical state or environment. The ability to perform immediate analysis from a stand-off distance offers significant advantages for applications which require the analysis of hazardous materials contained within controlled or inaccessible environments. This capability is particularly attractive to applications in the nuclear industry and in nuclear forensics. One potential hindrance to the technique with regard to adoption in the nuclear industry is the difficulty with isotopic analysis, owing to the narrow separation of isotopic emission lines. As a means to add isotopic capability to an already powerful analysis method, this project explored hyphenation of LIBS with tuneable diode laser absorption spectroscopy (TDLAS) to simultaneously interrogate a sample for elemental and isotopic characterisation.

Experiments were carried out using the LIBS technique with multivariate data analysis tools to analyse trace concentrations of rare earth elements dissolved in quenched salt samples. To aid the modelling, specific spectral regions, centred on known emission lines, were pre-selected. Next, a more complex system of uranium oxide samples with more than twenty trace elements was analysed with a similar methodology. The results demonstrated that the analysis was more accurate with a simple matrix, as the high density of uranium emission lines created a high background in the uranium oxide samples.

Apparatus for laser ablation-tuneable diode laser absorption spectroscopy (LA-TDLAS) was constructed, including building of an external cavity diode laser to reduce the laser linewidth for isotope-selective absorption spectroscopy. A proof of concept study was undertaken to analyse lithium isotopics around the lithium D lines at 670.78 nm. Double-pulsed laser ablation was found to reduce the absorption linewidth. For uranium isotopic experiments, the challenging isotopic ratio (0.7% ^{235}U : 99.3% ^{238}U) necessitated modification to the LA-TDLAS setup to include a balanced detection method to reduce the noise caused by shot-to-shot variations in the plasma. Using this method, both uranium isotopes were observed in the spectra, and an isotope ratio prediction could be performed. Simultaneous recording of absorption and emission spectra enabled the plasma electron density and temperature to be calculated for both lithium and uranium experiments.

Declaration

No portion of the work referred to in this thesis has been submitted in support of an application for another degree or qualification of this or any other university of other institute of learning.

Copyright Statement

Acknowledgements

First and foremost I would like to thank my team of supervisors for their continued patience and guidance through a busy four and a bit years. Dr Eddie McNaghten from the Atomic Weapons Establishment has been a consistently rigorous editor and a great technical advisor with his years of experience in the fields of laser-based spectroscopy and nuclear materials. Prof Philip Martin struck the perfect balance between a hands-off supervisor who let me take my research wherever I wanted it to go, and always being available for guidance when I hit dead ends. His knowledge of plasma science and atomic spectroscopy was incredibly valuable. Dr Clint Sharrad (when located) was supportive of all the radioactive chemistry work I planned and carried out and was helpful with the nuclear-focussed areas of my research. I am deeply indebted to them all.

After now nine years living and studying in the city of Manchester, I am very proud to call myself an honorary Mancunian. The other students and Postdocs I have known in the Martin group have been constant companions in the laboratory or the wider world (read: pub). I would like to thank in particular Dr James Thomson, Dr Paul Coffey, Dr Ali Arafeh, Dr Zac Zhang, Kiran Haroon and Dr Shaojun Xu for their help with everything from risk assessments and paperwork to computer coding, modelling, laser-systems and electronics. Members of the Sharrad research group were kind enough to teach me how to work in a radiochemical laboratory and include me in their experiments. In particular, I am very grateful to Dr Hugues Lambert and Dr Tim Kerry for inviting our group to join their research into pyroprocessing and introducing me to the interesting field of molten salt systems.

I am also grateful for the uranium samples provided by Dr Matt Higginson from AWE, and from Dr Nicholas Stevens at the University of Manchester. Additionally, the project benefitted from technical advice on constructing my external cavity diode laser from Prof Andrew Murray.

I would like to thank the Atomic Weapons Establishment and the Engineering and Physical Sciences Research Council who funded my project through the Materials for Demanding Environments Centre for Doctoral Training. I have benefitted from being part of a cohort of fantastic humans and scientists who are friends for life.

Finally, without the love and support of my brilliant family I would not be so fortunate to have had the opportunities or the education I have had in my life up to now. My Mum, Dad and sister are constant sources of motivation and inspiration to me, and I could not have completed my PhD without them. My girlfriend Kristina (who has become my office companion during the last six months of lockdown) has been an omnipresent source of hilarious conversation and emotional support. I thank her for all the meals she has prepared for me during my studies, despite earning several times my PhD salary.

Chapter 1 – General Introduction

1.1 The need for rapid in situ characterisation of nuclear materials

The analysis and characterisation of nuclear or radiological materials present complex and interesting scientific challenges. Hazards to the public and staff conducting the measurements are some of the most obvious sources of concern. In addition to this, measurement of certain materials can lead to equipment contamination and require its disposal. In the UK, legacy waste management throws up innumerable problems involving archaic contaminated environments. Famous industrial examples include Hot Cells at Sellafield which have been closed for decades, but contain unknown nuclear and radiological materials - holding unknown risks for cleaning and decommissioning. Detection, characterisation and monitoring of nuclear materials and environments are all vital for the safe management of activities across the nuclear fuel cycle.

Detection of illicit nuclear material at ports and border crossings also requires dedicated infrastructure to guard against nuclear proliferation and terrorism. Nuclear weapons are incredibly difficult to manufacture, store, maintain, transport and conceal. However, radiological dispersal devices – so called 'Dirty Bombs' – could conceivably be much easier for terrorist organisations or rouge states to acquire and deploy. Estimates about the lethality of radiological dispersion devices are difficult to predict, and depend on many factors such as local weather, height of release, dispersion effectiveness and the radiological substance used. Nonetheless, the psychological damage to the public would be immeasurable. Therefore, the prevention of such an attack has long been a priority for governments around the world.

All freight and passengers crossing controlled international borders are subject to scrutiny: it is common for shipping containers, lorry cargo, car boots and passengers' pockets to be emptied and inspected by customs officials. Also now commonplace are on-line scanners which detect concealed contraband or hidden items on a vehicle or person passing through them – a familiar example would be x-ray machines and metal detectors at airport security. In preparation for the London 2012 Olympic and Paralympic Games, the UK Government installed gamma-ray detectors at ferry crossings and the Channel Tunnel to detect nuclear and radiological material hidden inside vehicles ("Project Cyclamen"). These large devices

not only serve as detectors, but can also mark an obvious deterrent to anyone wishing to bring such material into the country.

An interesting juxtaposition is presented. If such detectors signal that a vehicle contains nuclear or radiological materials which might well be incredibly hazardous to anyone in their vicinity, how should customs officials or border Police proceed? The actual risk posed by suspect materials is unknown until detailed chemical characterisation or other identification can take place. The process of 1) categorising a suspect nuclear material 2) precisely identifying it using its most important signatures 3) tracing its movements 4) discerning its intended use and 5) ultimately attributing blame for its unlawful possession is termed Nuclear Forensics (NF).

Ideally, in the above scenario, border agents would have an analytical test which could identify the material quickly, safely, accurately and remotely. This could inform their next moves, such as: immediate seizure and isolation of the material and its courier; further, more detailed, analysis (i.e. in a laboratory); or confirmation that the carriage is legitimate due to a justifiable reasoning for the material's possession. Such an 'ideal' test is difficult to imagine, let alone design. However, the ability to quickly, accurately, remotely and non-destructively characterise the elemental constituents of a sample could be realised using laser-based spectroscopy.

The main research effort of this PhD project has been to investigate the potential of Laser-Induced Breakdown Spectroscopy (LIBS) for incorporation into the nuclear industry. LIBS is an emerging elemental analysis technique which has the ability to mitigate some of the hazards involved in nuclear and radiological sampling. Additionally, LIBS shows the potential to equal or better results obtained using established techniques in terms of accuracy, elemental coverage and particularly speed.

1.2 Laser spectroscopy for nuclear environments

Laser spectroscopy enables characterisation of material without requiring physical contact, as lasers require only non-attenuated line of sight to interact with matter. Therefore, it is possible for a machine and its operator to avoid exposure to dangerous nuclear and radiological materials they are examining. As mentioned above, the Hot Cells at Sellafield

are a good example of an environment with hazardous materials where operators cannot safely enter. Inspection of the cell contents through leaded-glass windows using laser spectroscopy can enable some characterisation to take place without opening the cell.

Sampling from a contaminated site and transporting hazardous samples for analysis costs thousands of pounds – particularly when potential nuclear or radiological material may be present. The time and cost saved by measuring at the point of interest is immeasurable compared to the need for sample collection, transit, preparation, analysis, storage and eventual disposal.

The speed at which laser-measurements can be acquired eclipses most other spectroscopic techniques, such as Mass Spectroscopy (MS) or X-Ray Fluorescence (XRF). Rapid sampling opens the door to in-line measurements – particularly useful for characterisation of conveyor-type transportation as seen during uranium mining and deconstruction of decommissioned nuclear sites. In-line monitoring of elemental concentrations within operating nuclear reactor systems could also be accomplished using laser-spectroscopy.

For many reasons, non-destructive analysis is preferable to its counterpart. Most laser techniques leave the sample in place and intact. This can enable changes over time to be reliably measured in an undisturbed environment. In the nuclear industry, for example, monitoring the leakage rate of steel storage drums could be completed in situ, therefore avoiding disturbing the vessel and causing further contamination.

The inherent safety, increased speed and reduced cost of laser-based analytical techniques could make them suitable for adoption across the nuclear industry. However, there is currently a reliance on proven elemental analysis techniques such as mass spectroscopy. It could be argued that the standards of reliability and robustness required for deployment in such a safety-rigorous industry are higher than have yet been proven by laser-based spectroscopy techniques. The safety record of the nuclear industry in the UK is very good, and the risk in adopting modifications which could fail is dangerous to overlook, both in terms of economic and reputation damage. However, conversely, it is difficult to justify the slow acceptance of novel technology to increase the speed of analysis, reduce cost and improve some safety aspects. Only through practical demonstrations in controlled settings

followed by phased implementation can new analysis techniques be accepted and utilised to their fullest.

1.3 Research themes

LIBS has yet to be widely employed in the nuclear industry. Briefly, the technique involves using a pulsed laser to create a plasma from a small volume of sample material. The emissions from this plasma are recorded and analysed to reveal the elemental constitution of the sample. LIBS requires no physical access to a sample, no high-vacuum and no sample preparation, and yet demonstrates rapid measurement speed, high sample throughput and simultaneous multi-elemental capability. Off-the-shelf LIBS products are available, from large, powerful, table-top sized apparatus down to handheld, battery-operated devices with various degrees of analytical precision and cost.

The research presented in this thesis covers four main projects of work, all of which incorporate LIBS. The overall aim has been to create an analytical method which could confirm a material's major and trace elemental composition and provide isotopic information in a single test. This could be used by border security to immediately identify suspect Special Nuclear Material (SNM), inform which safety procedures should be implemented and indicate next steps to carry out.

In order to meet this challenge, isotopic speciation has obviously been of great importance. Isotopic analysis with LIBS is considerably more difficult than elemental analysis due to the narrow separation of isotopic emission lines. For example, between ^{235}U and ^{238}U the largest splitting is 25 pm. In order to resolve such close emission lines, a high resolution spectrometer would be needed, or the analysis time would have to be increased. This increases the cost, size, power requirements and complexity of a machine, and therefore limits the opportunity for field deployment.

In this work, in order to increase isotopic analysis capability, LIBS has been used in a hyphenated system with Laser Ablation Tuneable Diode Laser Absorption Spectroscopy (LA-TDLAS). A tuneable diode laser was used to measure the absorption of the laser produced plasma. By controlling the wavelength of the diode laser to match either the ^{235}U or ^{238}U electronic transition, it is possible to measure the absorption of each isotope individually

and calculate the isotopic ratio. Forming this combined LIBS and LA-TDLAS system allows complementary results to be obtained: LIBS offers elemental analysis of both major constituents and trace impurities, whilst LA-TDLAS provides precise isotopic abundances of ^{235}U:^{238}U. The benefits of laser-based spectroscopy are maintained using the two laser techniques.

1.4 Thesis outline

Chapter 2 is an introduction to the thesis. The history of nuclear forensics is discussed. The role of spectroscopy and different elemental analysis techniques used in nuclear forensics is overviewed. LIBS is introduced with a fundamental overview of the laser ablation process and a discussion of the various impacting factors. The history of LIBS is reviewed from a technological viewpoint, concluding with recent developments and modifications which enhance the technique. Throughout, there is a deliberate focus on the literature concerning U samples and other nuclear-themed topics. A particular emphasis is placed on using LIBS for isotopic analysis, and the most recent solutions are referenced.

Chapter 3 describes experiments using LIBS with two multivariate data analysis techniques to calculate concentrations of rare earth elements dissolved in alkali metal chloride salt. This work package was undertaken to investigate the possibility of using LIBS for in situ measurements of molten salt solutions within nuclear reactors or pyrochemical reprocessing facilities.

Chapter 4 reports a series of experiments using LIBS with partial least squares regression to analyse trace element impurities within uranium-containing samples. The work is framed as a feasibility study for using LIBS in nuclear forensics investigations. More than twenty elements at known trace concentrations were analysed simultaneously by selecting known emission lines corresponding to each element.

Chapter 5 is a proof of concept study for the combined LIBS and LA-TDLAS setup. Lithium was used as a surrogate for uranium because the 15 pm separation of Li D lines at 670 nm, coupled with the isotopic split of around 15 pm for ^{6}Li and ^{7}Li at this wavelength, creates a similar absorption profile. Temporal differences between absorption and emission are discussed. Physical parameters such as plasma temperature and number density are

calculated for both single-pulsed and double-pulsed (DP-) LIBS. To my knowledge, this is the first work detailing the differences in absorption spectra acquired using multiple laser pulses for ablation.

Chapter 6 is a feasibility study of using the LA-TDLAS technique analysing uranium isotopics. The plasma electron density and temperature were calculated using a similar procedure to the lithium experiments. The effect of pulse energy on the absorption spectrum was also investigated. The limits of detection of the LA-TDLAS technique are calculated. Some sources of error and the overall suitability of the technique for applications in the nuclear industry are discussed.

Chapter 7 is a summary of all experimental results and conclusions. Future work for continuing and advancing this research is suggested.

Chapter 2 – Literature Review

2.1 Nuclear Forensics

Nuclear Forensics (NF) is the process of categorisation, characterisation, identification and attribution of suspect nuclear material [1]. A sample is firstly categorised into a subset of materials such as 'special nuclear material' (Pu, ^{235}U, ^{233}U), other nuclear material (Am, Np, natural U, LEU, Th etc.) or radioactive sources for medical or industrial applications (certain isotopes of Sr, Cs, Co, Ir, I etc.). This indicates how first responders should proceed in terms of sample handling, what level of personal protective equipment is required, what next steps to take and how best to treat the suspect. Characterisation involves more detailed analysis of the sample to ascertain key signatures. This includes material characteristics such as: dimensions and physical form; major, minor and trace elemental constituents; key isotopic compositions (e.g. ^{233}U:^{235}U:^{238}U and ^{239}Pu:^{240}Pu); and other chemical or molecular information. Identification requires involvement from scientists to compare signatures found in the sample to those of known stockpiles around the globe. This can be accomplished with input from industry experts, national registers and nuclear materials or international databases (such as the IAEA Incident Tracking Database (ITDB) [2]). Finally, suspect nuclear material must be attributed to a specific source so security failures can be identified and subsequent action taken. The point at which the material left regulatory control is usually identified.

Historically, categorisation, characterisation, identification and attribution procedures have evolved as the fields of nuclear weapons and atomic energy progressed. The first example of NF date to the beginning of the Cold War, when American reconnaissance planes detected radioactive particles (captured in the air-filters of a weather reconnaissance plane) over the USSR [3]. Nuclear scientists were able to estimate specific features of the nuclear device used to create them and, with subsequent flights, worked out the location of the detonation [4,5]. This test – designated "Joe 1" by the American Government – marked the start of the USA-USSR nuclear arms race.

The end of the Cold War and thawing of the USA-Russian relationship alleviated the potential for direct nuclear conflict between world powers. However, the nuclear legacy left behind by the Cold War continues to impact NF strongly. The lifting of the Iron Curtain as the USSR collapsed created a power-vacuum in post-Soviet Eastern Europe and led to large

amounts of nuclear material being more vulnerable. Around the same time, several high-profile seizures of nuclear material in Europe (see ref. [6] Table 1 and ref. [7] Figure 21) highlighted the need for the field to advance from post-explosion analysis to play more of a role in sample-identification and attribution [8]. As of 31st December 2019 the IAEA ITDB showed 3686 confirmed incidents of possession of nuclear or radiological material since 1993 [2]. Figure 2.1 shows a chart of the number of those incidents proven to be related to trafficking or malicious use. These results include twelve cases of high enriched uranium, two of plutonium and five plutonium-beryllium neutron sources [2].

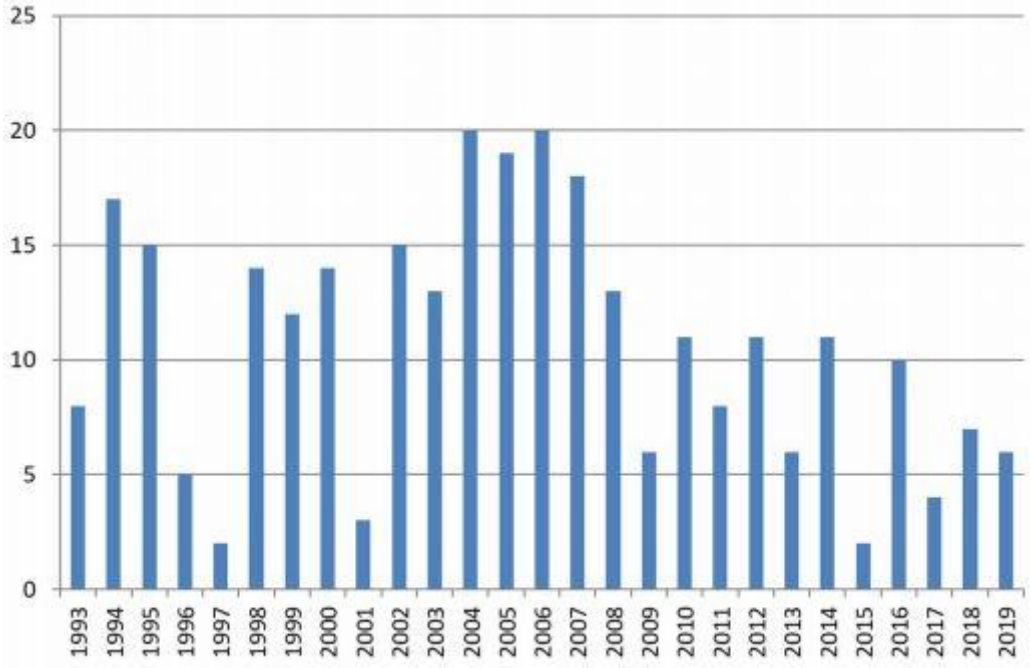

Figure 2.1. Incidents reported to the ITDB related to trafficking or malicious use of nuclear or radiological material from 1993-2019 (taken from the ITDB [2])

In the present day, many countries possess some degree of NF capability. In order to help member states implement best practices, the International Atomic Energy Agency (IAEA) began producing a 'Nuclear Security Series' in 2006 [9,10]. Specific NF advice has continued to be updated (e.g. ref. [11]) with contribution from the Nuclear Forensics International Technical Working Group (ITWG) – a working group of NF experts from around the globe affiliated with the IAEA and various law enforcement agencies [8].

As well as national capabilities such as border detection, crime scene management, sample collection, storage and handling and dedicated radiochemical analytical laboratories, the

wider field of nuclear security involves vigilance on a global scale to ensure compliance with international nuclear arms control treaties. For example, enforcing the Comprehensive Nuclear Test Ban Treaty (CTBT) [12] necessitates techniques such as forensic seismology, hydroacoustics and infrasound which enable identification of the location of a nuclear blast anywhere in the world using a global network of detectors. The Treaty on the Non-Proliferation of Nuclear Weapons (NPT) [13] came into effect in 1970 and continues to lead the fight against the spread of nuclear weapons by facilitating inspection and monitoring of nuclear stockpiles by the IAEA. In 2015 the UK Government published a national report [14] into their efforts around nuclear security and non-proliferation in line with NPT guidelines.

Nuclear terrorism is seen as a real threat to the public [15]. Well-funded and well-organised terrorist groups (such as the Islamic State group until their collapse) were seen to be the most likely source of such an attack [16]. Rouge States such as North Korea and Iran are considered dangerous not only because of their nuclear capabilities, but also the revenue they could procure by selling material to terrorist groups. Although the chances of a nuclear explosion being caused by non-state actors is remote [17,18], an attack using a Radiological Dispersion Device (RDD) (or so called “dirty bomb”) is much more attainable [19]. Yet more simplistic would be a terrorist attack on a nuclear facility – a power plant, research reactor or even a hospital – to cause mass terror [15]. After the Paris terror attacks in November 2015, investigators found videotape recordings of a Belgian nuclear official inside the home of one of the attackers [20] – proving that an act of nuclear terrorism had at least been considered.

In terms of NF research, Europe and the USA appear to be the two main drivers. In Europe, the Institute for Transuranium Elements (ITU) in Karlsruhe, Germany has been at the forefront of research and investigations since the 1990s. It’s fair to say that ITU helped write the book on NF. Klaus Mayer has been a staff member at ITU since 1996 and also chair of the ITWG since 2004 [21]. In the USA, Los Alamos National Lab (LANL) has been critical to the advancement of research into NF. Lawrence Livermore National Lab (LLNL) and Oak Ridge National Lab (ORNL) have also played their parts. The vast network of nuclear-research across America means lots of papers have been published by lots of groups across the country. However, most literature on NF have at least one or two authors from one of

these national laboratories. The US Department of Energy seems to play a key role in funding this research, along with the Department of Defence.

2.2 Spectroscopic Techniques used in NF

NF is an iterative process which requires input from border security, law enforcement, intelligence agencies and scientists. The characterisation and identification stages of NF depend principally on spectroscopic signatures which are used to compare a material with known possible identities. Numerous spectroscopic techniques can and indeed have been applied to NF as reviewed by Mayer et al [22] in 2005. Another thorough review on the analytical approaches used in NF was put forward by Stanley et al in 2013 [23]**.** Interpretation of results depends on the expert knowledge of investigators in the fields of radiochemistry, nuclear physics, reactor physics, materials science and the nuclear fuel cycle [22].

Depending on the signatures collected, the person in possession of said material may be any combination of: 1) in need of medical assistance, 2) a danger to all people in the vicinity, or 3) apparently intent on causing harm to others. Investigators and border security personnel must take every precaution to prevent themselves and other members of the public from being exposed to such material. To perform preliminary analysis whilst remaining a safe distance from suspect materials, stand-off techniques can be employed. Stand-off analysis usually takes place by collecting electromagnetic radiation emitted, reflected or scattered from a sample. Such techniques are non-destructive, which is beneficial as forensic evidence remains undamaged. Additionally, analysing a sample *in situ* eliminates the need for timely and costly sample containment, transport, preparation and eventual storage or disposal.

An important consideration of each technique is the time it takes for the analysis to reveal an answer. Some techniques can give information about a sample *in situ* within seconds. Detailed analysis could require samples to be transported to radiochemical analytical laboratories for Scanning Electron Microscopy (SEM) followed by destructive assay and Mass Spectrometry (MS). Such a sampling and analysis procedure could take weeks. The time taken to obtain an accurate result should be used to inform decision making in NF investigations, as noted by the IAEA in their Nuclear Security Series [11]. Table 2.1 gives an example from the 2015 Implementing Guide ‘Nuclear Forensics in Support of Investigations’

[11] of spectroscopic and spectrometric analytical procedures and their suggested timescales.

Table 2.1. Laboratory Methods and Techniques with typical timescales for completion of analyses. Taken from IAEA Nuclear Security Series [11] (see Scientific Glossary for acronym list)

Technique/method	Conducted within		
	24 hours	1 week	2 months
Radiological	Dose rate (α, β, γ, n) Surface contamination Radiography		
Physical characterization	Visual inspection Photography Weight determination Dimensional determination Optical microscopy Density	Microstructure, morphology and other physical characteristics SEM X ray diffraction	Nanostructure, morphology and other physical characteristics TEM
Isotopic analysis	HRGRS	TIMS ICP-MS	SIMS Radioactive counting techniques
Radiochronometry	HRGRS (for Pu)	TIMS ICP-MS	HRGRS (for U) Alpha spectrometry
Elemental/chemical composition	X ray fluorescence	ICP-MS Chemical assay FTIR spectrometry SEM/X ray spectrometry IDMS	GC–MS
Traditional forensic science disciplines	Collection of evidence associated with traditional forensic disciplines		Analysis and interpretation of evidence associated with traditional forensic disciplines

Many of the important techniques for isotopic and elemental characterisation revolve around MS. Indeed, ICP-MS was referred to as one of the 'superstar' techniques in analytical

atomic spectroscopy by Winefordner et al [24] in 2004. The analytical figures of merit (i.e. Limit of Detection (LoD), linear dynamic range, precision [RSD] etc.) achievable by MS outweigh those of many other atomic spectrographic techniques, and as such it has been used in numerous NF investigations. The work by Mayer, Varga and Wallenius [6,22,25–30] (amongst other authors) at ITU centres around TIMS and SIMS. In one example from Mayer's 2011 paper [30], the group analysed nuclear materials used in WWII by Werner Heisenberg's laboratory on the German atomic weapons program. Using the ratio of ^{234}U to ^{230}Th, they were able to 'age' two samples to 1940 and 1943 – matching historical records and therefore confirming their authenticity.

However, MS necessitates large experimental apparatus to create a high vacuum and contain the quadrupole magnets and ion counting channels. Additionally, the repetition rate for MS measurements is poor for most configurations as the vacuum must be re-established after each sample introduction. Finally, a key disadvantage for MS-based techniques is the impossibility of stand-off measurements.

Gamma ray Spectroscopy (GS) has been used in the 'categorisation' [31] and 'characterisation' [32,33] stages of NF. As categorisation requires more simplistic sample information, such as major element compositions, it can be accomplished in minutes using GS and High Resolution GS (HRGS). In contrast, detailed characterisation such as sample isotopics or parent:daughter nuclide ratios may require hours or days of counting and require a laboratory-based liquid nitrogen cooled high-purity germanium (HPGe) detector. Specific computer codes can be used to automatically interrogate HRGS spectra to reveal key elemental and isotopic ratios [22]. However, these codes fail with specific isotopes whose photon-energies are narrowly separated (e.g. ^{242}Pu) [22,34]. The ability to analyse a sample material whilst it remains sealed inside a container is a key benefit of HRGS; a feat possible because of the penetrating power of gamma ray photons. GS is therefore naturally stand-off, however samples must be placed in close proximity to detectors and at specific configurations for HRGS. The ITWG Guideline on HRGS published in 2013 by Zsingrai et al [34] states a minimum sample size of 0.5 g of nuclear material is usually required for HRGS analysis of isotopic composition. In contrast, MS techniques can require µg masses for accurate measurements. The speed and stand-off nature of GS has enabled on-line

detectors to be deployed at strategic sites around the UK, for example the Cyclamen Program at the Channel Tunnel and various ferry ports [35].

2.3 Laser-Induced Breakdown Spectroscopy

Laser-Induced Breakdown Spectroscopy (LIBS) offers the ability to elementally characterise a sample within seconds, independent of its size, physical state, and without sample preparation [36]. These attributes would be an obvious advantage in a NF application. However, LIBS has not been deployed in a NF investigation – possibly because the number of NF investigations has reduced in recent years as the LIBS technique has become more accepted. Numerous papers have demonstrated elemental 'fingerprinting' of different samples [37]. Such approaches could be easily applied to nuclear material to probe, for example, parent:daughter nuclide ratios, trace impurities to reveal a processing route, or contaminants remaining in a material throughout the nuclear fuel cycle. This section touches on the historical development of LIBS before describing the fundamentals of the laser-sample-plasma interaction and plasma lifecycle. Some of the opportunities and challenges are then discussed along with recent applications. A deliberate focus is placed on involvement of nuclear materials and nuclear environments.

2.3.1 Research and development history

LIBS has been an active area of research since the invention of the pulsed laser and first observations of Laser ablation-Produced Plasma (LPP) in the 1960s [38]. Initially termed 'laser ablation optical emission spectroscopy' or 'laser-induced plasma spectroscopy', research into applications for LIBS has been linked to the nuclear industry through its history. The 'LIBS' name was first coined in 1981 in two papers by Tom Loree and Leon Radziemski [39,40] while working at LANL. Significant contributors to the technique's early development are Radziemski and David Cremers (also from LANL) [41,42], who have co-authored over 20 publications since 1982.

Since the invention of the Q-switched laser in the 1990s, LIBS apparatus has become more available. The technology is now well matured and the number of research papers (Figure 2.2) and industrial applications continues to climb. Possibly the most well-known field-deployed setting is the ChemCam instrument on the Mars curiosity rover [43]. In this

system, a laser analyses rock types up to 7 m away to discern elemental compositions of minerals directly on the Martian surface.

Significant LIBS-breakthroughs were achieved in the UK in the 1990s and early 2000s, specifically centred around Swansea University. Collaborations between the group of Helmut Telle with Nuclear Electric plc and Sellafield Ltd led to several research papers involving underwater [44] and fibre-coupled [45,46] LIBS in response to problems in the nuclear industry with in situ monitoring of fuel rods. The group also spearheaded the first attempts to utilise chemometric methods with LIBS for various applications [47,48].

Interest in LIBS has spurred the creation of several international conferences. The 11th International Conference on LIBS will be held in Kyoto, Japan in September 2020 – now a virtual event due to the Coronavirus pandemic. Regional symposia are also running. The 10th Euro-Mediterranean Symposium on LIBS was held in Brno in the Czech Republic in September 2019, while Asian (ASLIBS) and Latin American (LAMLIBS) conferences held their third and inaugural events in 2019, respectively. Reading the members of the organising panels of these events reveals the great and the good of LIBS research groups.

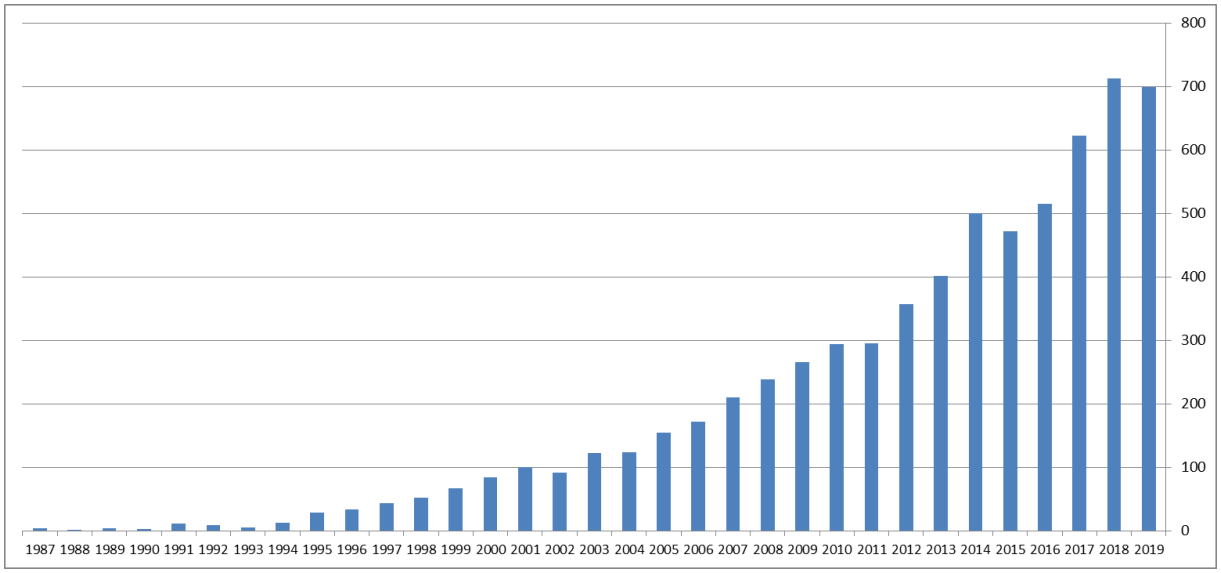

Figure 2.2. Number of papers with topic "Laser-Induced Breakdown Spectroscopy" on Web of Science per year from 1987 to 2019

2.3.2 Fundamentals of the LIBS process

A pulsed laser is focussed onto the surface of a sample, creating a power density at the point of focus which usually surpasses 10^{10} W cm^{-2}. The energy superheats nano- to micrograms of material and forces it to be rapidly ejected from the surface as a LPP. Continuum emissions caused by bremsstrahlung effects are emitted from the hot expanding plasma for the first few µs. As the plasma expands and cools further over 10's of µs, the excited atomic and ionic species relax by emitting radiation. This light is dependent on the upper and lower energy states of the emitter, so characteristic wavelengths of light are emitted from each species present within the plasma. Plasma emissions are collected – usually via fibre optic cable – and analysed using a spectrograph. By comparing the emission line wavelengths and intensities to reference databases (e.g. NIST atomic spectra database [49]), it is possible to identify any elements present over a certain concentration within the sample material. To reject the bremsstrahlung radiation and record the useful atomic and ionic emissions, a time delay is used before the light-collection window. The plasma finally fully relaxes to form a neutral gas which cools and dissipates into the local atmosphere [50]. A graphic of the LIBS process timing sequence is shown below in Figure 2.3.

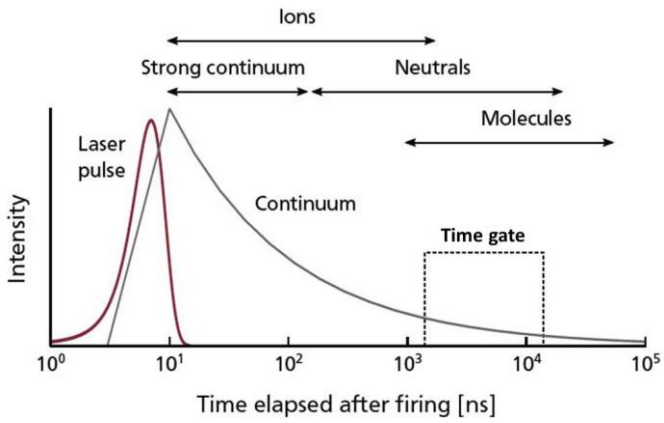

Figure 2.3. Plasma evolution with time, showing laser pulse (red) and emission intensity (black). Estimated emitting species are shown above graph. Taken from [51]

The emissions from the plasma change throughout its lifecycle. The time delay (t_d) between laser-pulse and light-collection and the duration of collection time (time gate (t_{gate})) must be controlled to record only as much of the useful information as possible and limit the bremsstrahlung background. By controlling the t_d and t_{gate}, the emissions of a particular

species can be maximised compared to the measurement background or to other emission lines. Ions appear in the plasma before atoms, therefore ionic emission lines are observed before atomic lines. For some compounds, molecular emission lines can also be seen at greater delay times. A simplified example of the changing emission spectra is shown in Figure 2.4 for three increasing delay times.

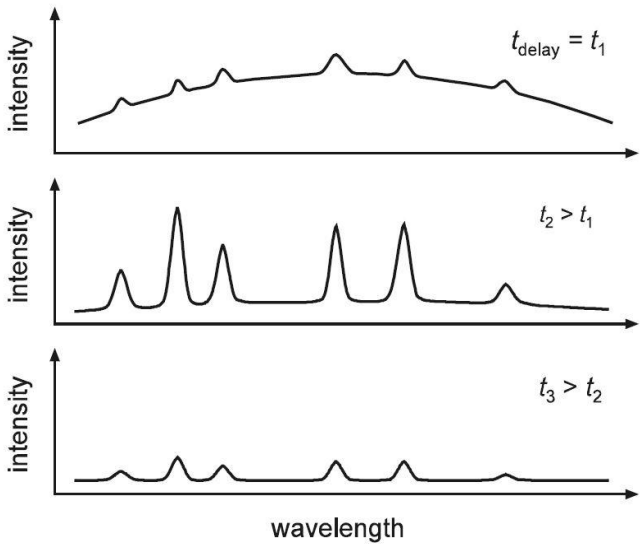

Figure 2.4. Illustration of LIBS emission spectra at increasing time delays. Taken from [50]

At any given point in the LPP lifecycle, the electron and gas temperatures and electron number density (n_e) can be estimated by studying the emission lines. This requires knowledge of the species present in the sample and an assumption of ideal plasma conditions: optically thin and homogenous plasma under Local Thermal Equilibrium (LTE). Unfortunately, these conditions are unlikely in a non-stationary, inhomogeneous non-thermal plasma [52]. Most temperature estimations therefore use a very narrow t_{gate} to analyse a quasi-stationary plasma. Temperature estimations can be carried out with assumptions of certain experimental parameters (e.g. $n_e = 10^{16}$ cm^{-3}) using the Saha-Eggert relation and Boltzmann/Maxwell distributions.

Typical instrumentation for LIBS apparatus consists simply of a pulsed laser (normally <10 ns shot duration), focussing and light collection optics, an optical fibre and a spectrograph, plus a computer for synchronisation of laser trigger and spectrometer readings and data visualisation. Innumerable hardware setups have been employed – some of which will be described in the following sections. A basic setup is shown in Figure 2.5.

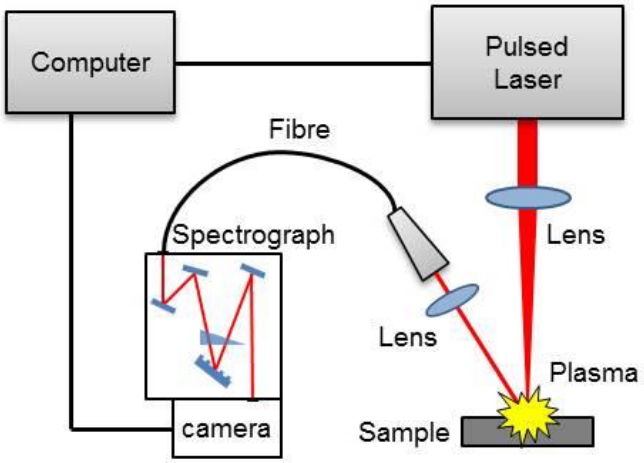

Figure 2.5. Schematic of LIBS experimental apparatus

One key aspect which makes LIBS so desirable is the facility for stand-off and remote analysis. 'Conventional stand-off' LIBS and 'remote' LIBS are distinguished by Li et al [53] as follows. Stand-off uses optics with long focal lengths to target laser pulses onto and receive emitted radiation from a distant target. In contrast, remote setups use fibre optic cables to transport the laser light and the emissions from hardware to sample. Both designs allow expensive laser and spectroscopic equipment to be distant from the sample environment, which is beneficial in many applications but none more so than in the nuclear industry.

2.3.3 Matrix Effects

The interaction of laser, sample, plasma and gas is complex; it depends on many factors and directly influences many more. For a start, the energy transmitted to the sample depends on the wavelength, pulse energy and pulse duration of the laser shot. Experimental parameters such as spot size (which can be varied by changing the sample height relative to the focal length of the optics), ambient pressure and sheath gas also have an effect. Concerning the sample material itself, density, surface finish and absorbance/transmittance at the laser-wavelength all help determine the penetration depth and interaction volume. Variables such as these combine to influence the ablation event and lead to changes in: volume of ablated material; speed and size of the shockwave and plasma plume; sample damage caused by crater formation, melting and re-deposition; and ultimately the intensity of emission lines on a spectrum. The final point here is of paramount importance from a

spectroscopic point of view. The impact of sample matrix and surface finish on the spectroscopic results are termed matrix effects.

The formation of an ablation crater after each laser shot can be used to perform depth-profiling of a material. Subsequent pulses in the same location ablate from the bottom of the crater and so vaporise material from the bulk rather than the surface. The additional depth is not strictly linear with number of shots, as the bottom of a narrow crater is naturally a different ablation-surface, so a different volume of material is removed. Additionally, some of the ablated material has been shown to re-settle inside the crater after ablation [54,55], which complicates the elemental analysis. Nonetheless, good results showing elemental layering have been demonstrated. Margetic et al [56] detected multiple layers of Cu-Ag on a Si wafer by ablating 15-30 nm of material per pulse with a fs laser. Papazoglou et al [57] also analysed thin films of multi-layer semiconductor materials, with excellent visualisation of the crater formation using in-situ interferometry. Glaus and Hahn [58] analysed high temperature alloys covered in stainless steel foil as well as corroded roman rings with a fibre-coupled ns laser.

2.3.4 Laser-Induced Shockwave and Hydrodynamics

An interesting by-product of laser ablation is the formation of a shockwave which expands from the point of plasma creation. The shockwave consists of a spherical high-pressure front of sheath-gas, within which lies a low-pressure region. Fascinating images of the shockwave expansion have been produced using shadowgraphy methods by Harilal et al [59], Harilal et al [60] and Lahaye et al [61] from Pacific Northwest National Laboratory. The Harilal group also used optical time-of-flight to study the expansion plumes, persistence and hydrodynamics of uranium LPP under different gas pressures [62]. The Miyabe group used Shadowgraphy and laser-induced fluorescence to study the population of atomic and ionic species in gadolinium LPP [63]. They showed that the gas pressure and gas atomic weight influence the laser-induced shockwave size, the temporal expansion and the population of atomic and ionic species.

The mathematics behind shockwave speed and radius were recently reviewed by Campanella et al [64]. The authors note that at pulse energies above 8×10^8 W cm^{-2} (commonly achieved by LIBS) the shock wave has the energy to ionize surrounding gas in so

called ‘laser-supported detonation’. This allows a plasma of sheath gas ions to absorb energy directly from the laser (as the gas is no longer transparent) and can result is a preliminary plasma-front which expands with the shockwave. Interestingly, investigations by Cristoforetti et al [65], Ma et al [66] and Harilal et al [67] have revealed mixing between sheath gas and plasma only occurs if the pulse energy is high enough to create this primary plasma front by laser-supported detonation. At lower pulse energies, results suggest the plasma contains significantly less contribution from the gas due to the ‘barrier shockwave’ which pushes the gas away. Harilal et al [68] have shown the interactions differ substantially when using ns, fs or filamentation-LIBS (discussed below).

2.4 Adaptations to the basic LIBS methodology

2.4.1 Double-Pulsed LIBS

Firing the pulsed laser twice in rapid succession has the effect of reheating the LPP. The adaptation is called Double-Pulsed LIBS (DP-LIBS), and has been shown to increase the analytical figures of merit substantially when compared to Single-Pulsed-LIBS (SP-LIBS) [69]. Multiple pulsing is often quite straightforward to accomplish using a Q-switched Pockels cell laser. The cell simply opens and shuts twice with the correctly timed electrical triggers to allow two distinct regions of laser emission from the same flashlamp pulse. The two pulses used in DP-LIBS can be dissimilar in terms of pulse energy, pulse duration, pulse orientation (i.e. coaxial or orthogonal to one another), laser wavelength and laser focal point. Different combinations of these parameters have been reported in literature (e.g. see ref. [70] Table 1 for 30 references on different configurations of DP-LIBS), and some of the most common are shown in the schematics in Figure 2.6.

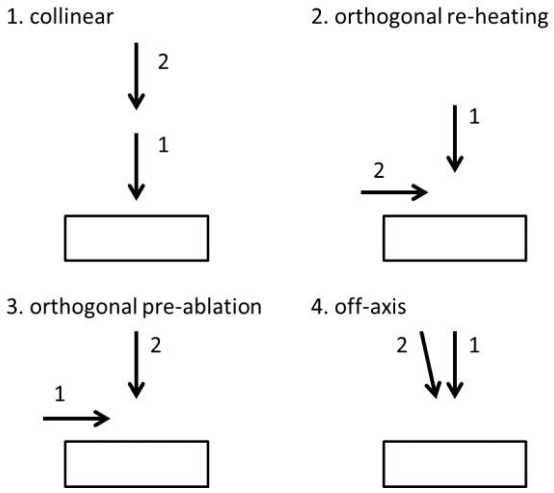

Figure 2.6. Schematics of different configurations for DP-LIBS. Arrows depict direction of laser ablation pulses and numbers 1 and 2 distinguish their temporal order

Experimental an theoretical comparisons were performed by De Giacomo et al [71] with different metal alloy samples. Their measurements of plume expansion indicated that the DP-LPP moved 5 times faster than SP-LPP as it was able to expand into the rarefied region behind the shockwave caused by the first pulse. They also discussed various theories into why the signal of DP-LIBS is enhanced, including increased ablation-efficiency, higher gas temperatures and greater DP-LPP lifetime. Corsi et al [72] produced interesting results in 2004 by using Shadowgraphy to capture images the expanding shockwaves caused by SP- and DP-LIBS. This technique was first used to record LPP in the Soviet Union in 1968 by Basov et al [73]. Overlapping long and short laser pulses was demonstrated by Cui et al [74]. One 60 μs pulse was fired first, and at the maximum intensity of the plasma formed by that pulse, a second shorter pulse was fired. The results showed greater signal intensity by a factor of 5-7 compared to SP-LIBS. In 2019 an interesting paper by Hai et al [75] demonstrated two pulses which were spatially different, with annular and circular laser pulses interacting with the same sample surface. Firing the circular laser 12 μs before the annular laser gave the best signal enhancement of around 4 compared to synchronised firing pulses. LoD was also increased by around a factor of 3. A comparative study of SP- and DP-LIBS analysing uranium emissions from a glass sample matrix was carried out by Skrodzki et al [76]. Their near coaxial arrangement with two dissimilar laser wavelengths and pulse energies led to increased emission intensities and SBR compared to a single pulse, and no increase in sample damage. Coaxial DP-LIBS was applied to the study of Plasma Facing

Components (PFCs) at low pressures in a Tokamak reactor by Hai et al [77]. They found that the emission lines of molybdenum were enhanced by 6.5 times compared to SP-LBIS when an ideal delay time of 1.5 µs was used. Fantoni et al [78] also investigated PFCs with coaxial DP-LIBS. They detected hydrogen isotopes present in samples designed to simulate the tungsten diverter found in a Tokamak reactor design. The ability to measure elemental changes of PFCs *in situ* in a fusion core (during downtime) is highly advantageous, and the hardware could conceivably be quite straightforward.

Orthogonal orientation of the two laser pulses has been shown to increase spectral quality compared to a co-axial arrangement [79–81]. Chinni et al [80] showed an enhancement factor of between 6 and 65 for orthogonal DP-LIBS compared to only 1 to 22 for coaxial DP-LIBS (both compared to SP-LIBS) for uranium emission lines. Interestingly, the best results were obtained using vastly different delay times of 1 µs for coaxial DP-LIBS and 15 to 25 µs for orthogonal DP-LIBS, which suggests very different ablation dynamics. Lindner et al [79] showed how the presence of particles in the gas above a sample has a significant impact on the laser-sample interaction and by result on the analytical signals. They used a pre-pulse shockwave to rarefy the local atmosphere above the sample and remove these particles (present from previous ablation shots) to demonstrate the impact they can have. Klus et al [81] used an orthogonal re-heating pulse to enhance the emission signals. They were able to combine XRF and multivariate analysis tools to spatially map uranium ores in a sandstone sample. Wang et al [82] investigated the possible improvements of orthogonal DP-LIBS with both an orthogonal pre-pulse and re-heating pulse. They found that using a re-heating orthogonal pulse rather than a pre-pulse gave significantly more reliable emission line intensities, with average RSD of 1.69% for the re-heating pulse and 5.83% for the pre-ablation. They concluded that the influence of particles and un-atomised material in the plasma hindered the repeatability so the re-heating pulse was able to atomise or ionise these particles. Lu et al [83] used a fs laser pulse followed by an orthogonal ns re-heating pulse to analyse silicon. Their results show dramatic improvements in Si emission line intensities of up to 360 times compared to a single fs pulse and improvements to Signal to Noise Ratio (SNR) also. Their use of a dual fs-ns system allowed excellent spatial resolution (<2 µm) without compromising on spectral quality. Hai et al [84] applied the orthogonal DP-LIBS technique to simultaneously clean a mirror surface from within a Tokamak reactor and

analyse the ablated metals. They were able to clearly identify the boundary between the deposition later and the silicon beneath in an on-line analysis.

2.4.2 Underwater LIBS

It is important to note that a powerful pulsed laser has the capability to form a LPP at any solid surface as well as within or immediately above a liquid or gas, and so LIBS can be used to analyse any sample material. However, sampling of liquid samples can prove difficult because of lower LPP temperature, emission intensity and shorter lifetime [85] plus macroscopic events such as bubble formation and splashing [86,87]. Applied Photonics ltd (based in Skipton, UK) developed a novel gas flow device for underwater analysis of solid samples in the late 2000s [88]. This adaptation creates a pseudo-atmospheric LIBS measurement by bubbling N_2 gas across the solid surface at the point of laser focus. An alternative to gas flow in underwater LIBS is double pulsing the fibre-coupled laser. The first laser pulse creates a cavitation-bubble into which the LPP produced by the second pulse can expand [89,90].

Underwater LIBS was used to study simulated debris within the Fukushima Daiichi nuclear power plant's flooded pressure vessel by Saeki et al [91]. Spectra were compared from underwater SP-LIBS, the aforementioned gas flow technique (with various gases) and DP-LIBS. The best results were recorded using a N_2 gas flow similar to the Applied Photonics instrument mentioned previously. Their setup suggests such a fibre-coupled probe would be suitable for analysis of the metals within the reactor core and would be able to survive the high radiation field. Sakka et al [92] showed that, for single pulses of the same pulse energy, longer pulses (up to 150 ns) increased the intensity of Cu(I) lines compared to shorter pulses. They suggest that the elongated laser pulse may heat the periphery of the expanding plume and eliminate the temperature gradient which causes self-absorption in the shorter pulse ablations – giving the spectral results of narrower and sharper peaks. Underwater LIBS has been used to great effect for cultural heritage applications, for example analysing solid samples of archaeological interest on shipwrecks [93]. The Laserna group from the university of Malaga are the most active in submarine LIBS, with numerous papers over many years [88,94–96].

2.4.3 Femtosecond Lasers

Femtosecond (fs) lasers have recently been used for LIBS ('fs-LIBS') and have shown improved analytical figures of merit and reduced sample damage (i.e. crater formation, melting) [97,98]. The ablation process differs from the traditional ns-LIBS in several ways. Firstly, the laser pulse is so short lived that by the time the plasma begins to form the radiation has ceased. This means the plasma is free to expand from the surface without further energy transfer, resulting in cooler plasma and less ionisation [99] compared to ns ablation [100]. The immediate presence of cooler plasma means there is less Bremsstrahlung emission so the continuum background is significantly weaker in fs-LIBS, which can improve the quality of spectra [99]. Moreover, the pulse energy needed to create a LPP with a fs laser is significantly lower than for ns-LPP [101]. Additionally, the heat affected zone is smaller in fs-LIBS, and gives rise to less sample melting and associated damage. Although Harilal et al [68] showed fs-LIBS gives a deeper crater than similar ns-LIBS, they note the sample damage is worse in ns-LIBS because of ring structures around the crater caused by re-solidification of ablated material. The emissive state from a fs-LPP is naturally much shorter than a ns-LPP [102] because the plasma is cooler so dissipates its energy more quickly. Oba et al [103] increased the emission period from a fs-LPP by using an orthogonal re-heating ns laser pulse. This technique permitted the advantages of improved spatial resolution and less sample damage given by fs-LIBS whilst intensifying emissions by a factor of 25 (compared to sp-fs-LIBS).

The use of fs lasers with LIBS has also given rise to filamentation-LIBS, which has the capability to create plasmas over a km away [104]. Filamentation beams can be caused by high power (TW) ultrashort laser pulses (>100 fs) by inducing a change in the refractive index of air to focus the laser beam. The focussing effects are balanced by diffusion caused by LPP – leading to a dynamic equilibrium and thus self-guided laser filaments. A filamentation beam over a km long was observed by Rodriguez in 2004 [105], and put to effect for a surface analysis by Durand et al in 2013 [106]. In 2009 Judge et al [107] compared results of fs-LIBS and filamentation-LIBS for the remote analysis of carbon and clay mixtures. They found that filamentation-ablation caused more stable plasma and gave better SNR, which allowed more accurate discrimination between clay and graphite

samples. Ghebregziabher et al [108] examined the effect of propagating filament beam distance on signal intensity using a copper sample. They used the Cu I atomic emission and acoustic measurements to determine that the ablated mass and signal intensity was maximised nearer the end of the filament's possible path. Hou et al [109] studied the expansion of the plasma plume created by filamentation-LIBS to understand how the expansion differed when using a filament of weakly-ionised air (created by the ablation laser) as oppose to a focussed laser. Their results revealed the expansion differs substantially, with two plasma 'zones' created: one more usual LPP zone closer to the sample surface and a second which expands back towards the laser along the filament. They note that analysing the different zones with spatially and temporally resolved-spectroscopy could increase the intensity of different emissive species and aid quantification. The promising new research theme of filamentation-LIBS could increase the stand-off capability of traditional LIBS and open up new applications [110–113], including isotopic LIBS which is discussed in the following sections.

2.4.4 Chemometric Techniques

One of the benefits of LIBS is the ability to measure multiple emission lines from multiple species simultaneously. However, increasing the number of elements in the sample increases the complexity of the spectrum and necessitates the use of specialist Multivariate Analysis (MVA) tools to decrypt useful information. A well reported problem with nuclear LIBS analysis is the complex spectra of high-Z elements such as actinides and lanthanides. This is due to the high number of energy levels – and therefore electronic transitions – in such systems [26,114,115]. For example, Chinni et al [80] reference 5000 uranium lines in a hollow cathode lamp (HCL) discharge between 384.8 and 908.4 nm and state that more than 92,000 lines of U(I) have been reported. Numerous chemometric and MVA techniques have been applied to LBIS, as shown by Table 2.2 (taken from Galbács 2015 review [116]).

Table 2.2. List of chemometric methods used in recent LIBS literature – taken from [116]

Table 2 A list of chemometric methods used in recent LIBS literature for qualitative discrimination (classification) and for quantitative analysis (calibration)

Methods used for qualitative discrimination	Methods used for quantitative analysis
Principle component analysis (PCA)	Partial least squares (PLS-1, PLS-2)
Partial least squares (PLS)	Nonlinearized dominant-factor-based partial least squares (NDFPLS)
Discriminant analysis (DA)	Multi-linear regression (MLR)
Classification tree (CT)	Principal component regression (PCR)
Linear correlation (LC)	Generalized linear correlation (GLCM)
Rank correlation (RC)	Least-absolute-shrinkage-and-selection-operator (LASSO)
Overlapping integrals (OI)	Sparse multivariate regression with covariance estimation (MRCE)
Support vector machines (SVM)	Artifical neural networks (ANN)
Soft independent modeling of class analogy (SIMCA)	Wavelet transform hybride model (WTM)
Independent component analysis (ICA)	Polinomial multivariate inverse regression (PMIR)
Artifical neural networks (ANN)	Multi-spectral line calibration (MSLC)
Hierarchical cluster analysis (HCA)	Random forest regression (RFR)
k-nearest neighbors (KNN)	Discarding and kriging
Receiver operating characteristics (ROC)	–
Random forest (RF)	–

Partial Least Squares (PLS) is a MVA technique commonly applied to LIBS spectral to improve the quality of results [117–120]. PLS can be used to select only intense peaks or well resolved peaks to use for regression plots [121]. For example, Castro *et al* [122] compared various normalisation strategies used in combination with PLS to select the best peaks for univariate and multivariate analysis for numerous elements in 80 different metal alloys. The Phongikaroon group have published papers using PLS models to quantify uranium [123] and lanthanide elements [124]. Martin et al [125] and Weisberg et al [126] have also used PLS to quantify rare earth element concentrations; Martin et al from solid pellets and Weisberg et al in a molten salt sample.

Additionally, PLS has helped increase the certainty of conclusions draw from LIBS analysis by allowing more information to be extracted from lower resolution spectra. Doucet et al [127] used PLS to create concentration models of uranium and hydrogen isotopes with lower-end spectroscopic equipment as may be used in field-deployed apparatus. Similarly, in a computer simulated study of uranium isotopics, Chan et al [120] found that using PLS enabled accurate isotopic estimations of uranium samples without requiring the peaks to be completely resolved. They also showed that using multiple emission lines improved their results by up to nine times compared to univariate analysis.

Another useful chemometric technique is Principal Component Analysis (PCA), which allows classification of large datasets by reducing the dimensionality [128,129]. This enables unknown samples to be more easily grouped towards known materials or concentrations, and appears well suited to the 'categorisation' stage of NF rather than the 'characterisation'. Yang et al [130] showed how PCA could be applied to LIBS spectra to help resolve two overlapping fingerprints at a crime scene. PCA was used to confirm the peak selection methodology, and the results showed spectra obtained from regions of the two fingerprints were divided into separate clusters. Sarkar et al [131] validated different LIBS normalisation and pre-treatment procedures by examining the groupings offered by PCA of the resulting spectra. De Lucia et al [132] and Gottfried et al [133] demonstrated that DP-LIBS combined with PCA was capable of discriminating different types of explosives, biological species and organic material (diesel) at stand-off distances. Klus et al [81] showed that resolution-related issued caused by the high density of uranium emission lines could be overcome by analysing a region of apparent baseline (which contained numerous undetectable uranium peaks) instead of identifying individual peaks. PCA was used to indicate which regions of the spectrum correlated with uranium concentration and indicated that the 'apparent baseline' could be used rather than a uranium peak.

The research effort into data analytics and artificial intelligence is constantly gathering pace. It seems inevitable that techniques such as PCA will become more common not only in spectroscopy but in many walks of life as global computer power continues to grow into and beyond the digital age. Other novel methods such as artificial neural networks have been applied to LIBS for online monitoring of metal casting [134] and have in fact already been proposed for nuclear forensics by Bhatt et al [135]. The interesting field of chemometrics will undoubtedly continue to grow and develop [119].

2.4.5 Calibration-Free LIBS (CF-LIBS)

A method to overcome the issue of matrix effects named Calibration Free-LIBS (CF-LIBS) was proposed by Ciucci et al [136] in 1999. The method involves attributing every peak in a spectrum to an emissive species (element or ion) including the sample matrix. Then, after a calculation of plasma temperature using Boltzmann plots, the concentration of each species can be estimated using known parameters of wavelength and intensity (taken from NIST

database). Several assumptions are made throughout the procedure, such as LTE conditions, stoichiometric ablation and optically thin and homogenous plasma [116]. Additionally, arguably the most important assumption is that *every* peak is successfully identified and fitted which is difficult to achieve in practice. However, CF-LIBS has become a popular method for quantifiable chemical characterisation of unknown samples due to its standardless approach. Indeed, Hahn and Omenetto state in their LIBS review in 2012 that the accuracy of the CF-LIBS approach tends to justify itself and prove that worries about LTE and optically thin and homogenous plasma are overstated [137]. A detailed list of applications of CF-LIBS can be found in a recent review by Tognoni et al [138] from the same group which invented the technique in 1999. An improvement on the quantitative ability of CF-LIBS was proposed by Cavalcanti et al [139] in 2013. One-point calibration-LIBS (OPC-LIBS) uses a single matrix-matched sample of known composition to aid with the calculations of plasma temperature, electron number density, stoichiometry etc. and was shown by the authors to aid concentration predictions of minor and major constituent elements. This method was employed by Senesi et al [140] to analyse metallic element composition of meteorites, with improvements over traditional CF-LIBS. In 2014, Aragón and Aguilera [141,142] pioneered a method using curves of growth and multiple emission lines from each element to improve plasma temperature estimations by reducing the impact of self-absorption [119].

2.5 Isotopic LIBS

Hopefully the sections above have given the reader an understanding of the complex processes involved in the LIBS technique and how they can be controlled and manipulated to suit different environments. The number of applications of LIBS increased from the 1990's because of the relatively simple apparatus and the advantages of no sample preparation, rapid analysis time, multi-element capabilities and quantitative results. The numerous applications used in the references thus far give a taste of how the technique has matured and widened its appeal into numerous fields. However, there remains technological hurdles which LIBS has great difficulty overcoming. One such issue particularly prevalent in the nuclear industry is the difficulty of isotopic calculations with LIBS.

In its most basic form, the problem is the very narrow separation of isotopic emission lines. This causes complications in spectral analysis and deconvolution and renders quantitative measurements often impossible without all but the most powerful spectrometers. Even using such ideal equipment, spectral line broadening caused by Stark and Doppler effects can increase the FWHM of emission peaks and make them unresolvable. Altering the measurement environment – for example by using reduced gas pressure or a different gas such as N_2 or Ar – can soften some broadening effects [143]. However, this increases the physical footprint of the instrumentation and lengthens the measurement time – eliminating some of the key advantages which make LIBS so appealing. Isotope ratios can be determined from partially overlapped spectral lines. However, precision and sensitivity of the determination improve with increasing ratio of peak separation to peak width [144,145].

The difference between emission lines of two isotopes – the isotopic shift (IS) – is caused by a combination of two effects: the mass effect and the field (or volume) effect [146–148]. The mass effect applies to lighter elements such as H or Li, whereas the field effect relates to heavy elements like the actinides. Elements in the centre of the periodic table offer very small IS (smaller than Doppler or Stark widths) and require high resolution Doppler-free spectroscopy techniques at reduced gas pressures to resolve, as demonstrated by Obrebski et al [149].

This section will review the literature on technical adaptations, inclusion of additional spectroscopy in hyphenated approaches and other enhancements which have sought to enable isotopic LIBS. An up to date review of spectroscopic approaches applied to the issue of isotopic LIBS is included in section VI. of ref. [148]. Other reviews and detailed discussions are given Hahn and Omenetto 2012 [137]; Russo et al 2013 [150]; Harmon et al 2013 [151]; and Wu et al 2020 [85]. For reference, Table 2.3 gives some commonly investigated atomic transitions and the associated ISs.

Table 2.3. Commonly investigated transition lines and their isotopic shifts

Species	Isotopes	Wavelength (nm)	Isotope Shift (pm)
H I	^{1}H / ^{2}D	656.279	176
Li I	^{6}Li / ^{7}Li	670.776	16
U II	^{235}U / ^{238}U	424.437	25
U I	^{235}U / ^{238}U	682.691	18
Pu I	^{239}Pu / ^{240}Pu	594.522	13

2.5.1 Reduced Pressure Isotopics

The different emission properties of uranium isotopes have been observed and studied since the very genesis of the atomic age at Oak Ridge National Laboratory in the 1940s [152]. Burkhart et al [152] observed more than 900 uranium emission lines with separation between isotopes with arc discharge plasmas. The first uses of LIBS for isotope ratio measurements occurred several decades later, and were performed in low pressure atmosphere to limit spectral line broadening so as to enable isotopic lines to be more easily resolved. Pietsch et al [153] used an air pressure of 2.67 Pa to analyse the U II 424.467 nm emission line in 1998. They reported a relative precision of 5% was obtained on the isotopic ratio calculation, although they admit this would be reduced at lower enrichment than the 3.5% ^{235}U sample they used. In the same year, Niki et al [154] analysed molecular emission lines of boron monoxide at 400 Pa (more information on the analysis of molecular emission lines is given in the following section). In 2002, Smith et al [155] examined plutonium isotopics in a helium atmosphere at 13 kPa using the Pu I line at 594.522 nm. By using a higher pressure than previous work by Pietsch et al [153], the plutonium plasma lasted for a significantly longer time after ablation. The LPP cooled more slowly at this higher pressure, which enabled emission to be recorded for a longer time under a reduced Doppler broadening regime, allowing an IS of 12.5 pm between ^{239}Pu and ^{240}Pu to be resolved. Mercadier et al [156] resolved hydrogen and deuterium emission lines under reduced argon

pressure in 2010. Their study on the segregation of species within the LPP (due to different expansion velocities of heavy and light elements) in PFCs revealed the ablation depth was dependent on the gas pressure above the sample. They attribute this to the plasma shielding effect (where the expanding LPP absorbs laser energy rather than the sample), as at higher pressures the plasma remained for a longer time and also had a greater density. In 2006, D'Ulivo et al [157] also recorded isotopic emission lines from hydrogen and deuterium gas at reduced pressures of around 7 kPa. Their setup produced an RSD better than 2.5% for 15 samples of different isotopic gas mixes, although they note that their system is limited to molar fractions of between 0.5 and 1 hydrogen:deuterium.

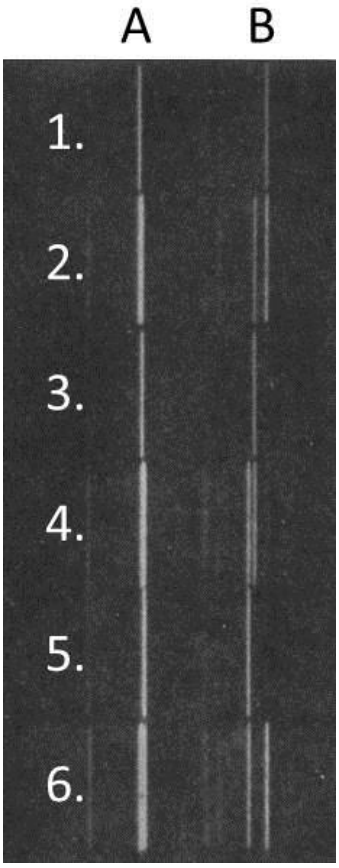

Figure 2.7. Uranium emission lines from an arc discharge plasma, recorded in 1949 at Oak Ridge National Laboratory. Samples 1 through 6 are combinations of uranium isotopes as follows: 1. U^{238}; 2. U^{238} and U^{235}; 3. U^{235}; 4. U^{235} and U^{233}; 5. U^{233}; 6. U^{238} and U^{233}. Lines under A are the 424.167 nm emission with no isotope shift. Lines under B are the 424.437 nm emission, with a clear separation between lines in mixtures 2, 4 and 6. Taken from [152]

2.5.2 Atmospheric Pressure Isotopics

In their 2011 paper on isotopic LIBS with a specific focus on NF, Doucet et al [127] argued that LIBS could be used for rapid isotopic analysis under atmospheric pressure conditions. They used a PLS1 algorithm to deconvoluted unresolved uranium and hydrogen emission lines at atmospheric pressure. Their models have an accuracy between 6% and 8% RSD for uranium enrichment from natural abundance (0.7%) to 3% ^{235}U. They state that this level of accuracy is acceptable for a handheld instrument or for an alert notification (i.e. as a categorisation rather than characterisation). The model accuracies improved significantly with higher enrichment of uranium: 20% and 93% ^{235}U giving relative accuracies of 3% and 0.1%, respectively. However, aside from their spectrometer and hardware apparatus which were quite usual for LIBS, their spectra and were recorded under idealised experimental conditions. For example the uranium samples were of high chemical purity and the samples themselves were created on ceramic disks at well controlled concentrations – allowing 300 identical repeat measurements per sample. *In situ* on a NF investigation, this methodology would be unattainable. Hundreds of identical shots might prove impossible because of small sample sizes, and the chemical purity of a sample could vary significantly. Nonetheless, their results are impressive and highlight how chemometrics can be used to aid LIBS analysis and the field of NF.

Chan et al [144] also used chemometrics to create concentration-predictive models for uranium isotopics. They demonstrated improved results (i.e. lower RSD) when a spectrometer with greater resolving power was used. However, the increased spectral resolution created the additional complication of detecting hyperfine splitting (HFS) of some uranium lines (e.g. the most intense emission they recorded at 682.691 nm) which required additional investigations and adjustments to their model. Despite this, their models taking into account of HFS and other fitting parameters accurately predicted the isotopic ratios of known samples. They also created models to predict the total uranium concentrations, with the best LoD score of 500 ppm. Choi et al [146] discussed the effect of spectrometer resolving power and line selection concerning the isotopic analysis of uranium. Using two narrowly separated lines from a mercury lamp as a surrogate for uranium isotope emissions, they were able to accurately deconvolve emissions with line widths significantly greater

than the line separation. They also showed that despite complex spectra and low concentrations of uranium, high resolution spectrometers and spectral deconvolution can reveal LoD values as small as 3 ppm with optimised parameters such as time delay and gate width. However, without practical LIBS apparatus or data their results remain theoretical.

Cremers et al [114] compared the isotopic speciation possible with two spectrometers with different resolving powers. Their apparatus consisted of a hand-held LIBS probe with backpack-sized batteries, electronics and spectrometers to demonstrate a fully man-portable system. With their highest resolution spectrometer they were able to observe isotope shifts in uranium, hydrogen and lithium for samples with high and low isotopic ratios, although they state that uranium enrichments on the order of 4-5% remain challenging. Burger et al [158] analysed deuterated water with SP- and DP-LIBS. By studying the Balmer series, they found a shorter inter-pulse delay time of just 50 ns improved the persistence and linewidth of emission lines compared to a longer inter-pulse delay DP-LIBS and also compared to SP-LIBS. In 2016, the same research group based under Igor Jovanovic in Pennsylvania revealed a simple hybrid interferometric/dispersive spectroscopic device capable of resolving the 25 pm uranium IS at 424.44 nm [159]. Morgan et al [159] used a Fabry-Perot etalon coupled with a Czerzy-Turner spectrometer to give a resolution of 6 pm around the 424 nm region. Using this relatively simple setup, they were able to clearly identify two separate uranium emissions and their respective isotopically-shifted partners. Effenberger and Scott [160] possibly led the way with this hyphenated Fabry-Perot/Czerny-Turner setup with their work analysing the mercury doublet at 313.2 nm (separated by 29 pm) in 2011.

2.5.3 Laser Ablation Molecular Isotopic Spectrometry (LAMIS)

A promising avenue of ongoing research involves analysing molecular emission lines rather than elemental lines in the LIBS spectrum. Molecular species are formed either through direct vaporisation from the sample surface, or from plasma-assisted chemical reactions between ablation plume and the surrounding atmosphere. The key difference between atomic and molecular emissions is that molecular emissions from diatomics are significantly more sensitive to the mass of either partner. For example, the largest IS of an atomic boron line is 0.002 nm, whereas for boron monoxide the greatest IS is more than two orders of

magnitude larger at 0.73 nm [154,161]. The increased IS is due mainly to differences in rotational and vibrational states between isotopes [161]. The first experimental evidence of isotopic evaluation from molecular emission lines was shown by Niki et al [154] in 1998, using boron monoxide. However, the term 'Laser Ablation Molecular Isotopic Spectrometry' (LAMIS) was proposed by Russo et al in 2011 [161] in the first of a series of papers by the same group of authors based in the USA [101,162–164]. Table 2.4 lists elements which have been studied using LAMIS and the associated references. Molecular emissions appear later in the LPP lifecycle than ionic and atomic lines, and are characteristically weaker than atomic emissions [101] due to the lower number density of emitting species. However, through control of spectral integration time, the SNR for molecular lines can usually be made comparable to atomic emissions. An additional complication is the presence of various rotational and vibrational bands within each molecular emission spectrum, causing a repeating Lorentzian peak. These emissions can obscure overlapping isotopics and must be accounted for – usually with modelling and spectral fitting as presented in the review by Bol'shakov et al [101] with various elements. Ran et al [165] used a complex model with corrections for self-absorption and band-interference to reconstruct AlO spectra with good results.

Table 2.4. Literature published on the use of LAMIS (Laser Ablation Molecular Isotopic Spectrometry) and the elements used in the study

Element	Reference
hydrogen	[164,166]
boron	[101,131,161,162,164,167]
carbon	[101,164,168–170]
nitrogen	[164]
oxygen	[101,164]
aluminium	[165,171]
chlorine	[164]
calcium	[101]
strontium	[101,163]
zirconium	[101,172,173]
uranium	[171,174–176]

An interesting adaptation to LAMIS to increase the spectral intensity was proposed by Zhu et al in 2019 [177]. They used Laser-Induced Fluorescence (LIF) to increase the concentration of molecules in the upper energy state and therefore increase the emission intensity from molecular species. Although laser ablation-LIF (LA-LIF) is not novel (e.g. ref. [178]), this was the first demonstrated use of LIF for analysis of molecular species within a LPP for the purpose of isotopic quantification. The group examined BO and CN emissions with different boron and carbon isotopes, and found that the use of LIF increased the emission intensity by up to 34 times compared to usual LAMIS. Additionally, the use of LIF reduced the effect of complex rotational-vibrational bands which tend to confuse LAMIS measurements.

Adapting LAMIS to enable remote measurements could be instrumental to the ambition for isotopic and elemental characterisation from distance. To that end, femtosecond lasers and the associated phenomenon of 'filamentation' discussed in the previous sections was applied to LAMIS in 2015 by Hou et al [172]. The group measured zirconium isotopes at distances of up to 7.8 m using a setup of Femtosecond Filament-LAMIS (F^2-LAMIS). They found that the emission intensity of the ZrO lines around 482.73 nm was comparable to that of atomic zirconium at 482.80 nm, which is in contrast to many other studies where the molecular emission intensity is far smaller [101]. Ratios of four zirconium isotopes were accurately identified at various propagation distances using the single ZrO molecular emission and without calibration standards, demonstrating how remote isotopic analysis could be achieved. Hartig et al [175,179] used F^2-LAMIS to analyse uranium oxides. They discerned that atomic, ionic and molecular uranium emissions are maximised at different distances of filament propagation, concluding that these differences are caused by differences in plasma temperature and pressure.

2.5.4 Hyphenation with other spectroscopic techniques

A final way in which the isotopic capability of LIBS has been improved is through inclusion of additional spectroscopic techniques. By hyphenating LIBS with other laser-based analyses, the resolution needed for isotopic emissions lines can be provided by the laser source rather than through spectroscopic enhancements. Complementary information can be ascertained using hyphenation, with LIBS providing elemental characterisation and an additional

technique providing isotopic quantification. Hyphenated techniques also maintain the advantages of LIBS over traditional MS (standoff capability, short analysis time, no sample preparation etc.), making the resulting combination highly attractive. Two of the most promising hyphenated approaches are Laser Absorption Spectroscopy (LAS) and the aforementioned LIF.

The key requirement for isotopics is that the hyphenated laser source has a narrow enough linewidth to enable selective interrogation of each isotope in turn. For this purpose, semiconductor diode lasers are the obvious choice for spectroscopy due to their tunability, high spectral radiance, small size, low power demand, high stability and low cost [180]. Although initially confined to the IR region, the spectral coverage of diode lasers has been increasing ever since their commercial introduction in the 1980's because of advances in semiconductor technology [181]. Wavelengths of as low as 375 nm are commercially available from numerous manufacturers and suppliers. Several review articles about the use of diode lasers in spectroscopic and industrial applications have been published [180–184]. Other review articles focus on the field of Tuneable Diode Laser Absorption Spectroscopy (TDLAS) specifically [185–188].

The Niemax group, based in Germany, published a series of papers on uranium isotopics using LA-LIF in 1999 [178] and LA-TDLAS in 2001 and 2002 [189,190]. The LoD achieved using time integrated measurement of isotopic fluorescence in 1999 [178] was 6 mg g^{-1} (of the minor ^{235}U isotope). They reported better precision using time integrated measurements (holding the diode laser wavelength stationary on each transition in sequence) rather than rapidly ramping the laser diode wavelength across both isotopic transitions in a single ablation event, due to the transient nature of the LPP. They reached a similar conclusion with their next paper [189], this time using LA-TDLAS with a single laser diode. Although the LoD was improved to 100 µg g^{-1}, ramping the wavelength to provide an isotopic ratio in a single ablation again proved difficult. Additionally, the absorbance of each isotope was optimised at different spatial and temporal points in the LPP. The major isotope (^{238}U) was best measured at a greater distance from the sample surface where the number density of absorbing species was lower. In contrast, the ^{235}U isotope signal was optimised at a smaller distance and earlier in the LPP lifecycle. A trade-off between these two positions was reached, however the absorption measurement for the ^{238}U isotope had to be made

with the wavelength shifted 7.5 pm from peak centre as the LPP was optically thick at the centre wavelength of the transition. These effects limited the RSD of the isotopic prediction to 4.1%. In the final paper in 2002 [190], a second laser diode was incorporated to simultaneously measure both isotopic transitions. Although the region of plasma under analysis was slightly different (as the beams were crossed at an angle of 4°), the results of LoD (50 μg g^{-1}) and RSD (1.1%) were significantly better as shot-to-shot variations in plasma size and temperature were automatically accounted for by measuring both isotopes simultaneously.

Niemax's previous work on isotopics had used low pressure graphite furnaces and either Doppler-limited or Doppler-free spectroscopy [147,191]. However, these three papers on LIF and TDLAS around the turn of the century showed how isotopics could be analysed using laser-ablation as sources for atomisation rather than graphite furnaces, which opened up new possibilities for rapid *in situ* analysis. Having said that, these studies by Niemax and simultaneous work by Winefordner based at the University of Florida (King et al with rubidium isotopes [192] and Smith et al with lithium isotopes [193]) all relied on reduced pressures and inert atmospheres, neither of which are perfectly suitable for field-deployment.

More recently, Taylor and Phillips [194,195] and others [196] have used differential LAS to show the feasibility of uranium isotopics in a LPP at atmospheric pressure. This method of balanced detection used two laser beams analysing precisely the same plasma to remove noise caused by background effects. Two orthogonally polarised beams were spatially overlapped using polarising beamsplitters. In this way, the two beams were combined before intersection with the plasma then separated after absorption – allowing removal of the shot to shot variations common in LPP. Taylor and Phillips [194] showed that such a technique could be used for isotopic analysis in low concentration samples by measuring an absorbance spectrum of a weak U I line (861 nm) and reporting a linewidth of 5.51 pm.

Phillips et al [145] published another hyphenated technique using LIBS-LIF in 'two-dimensional fluorescence spectroscopy' (2D-FS). This method involves simultaneous LIBS and LIF recording (at different time domains) using a standard resolution spectrometer with resolving power of around 40,000. By moving from aluminium electronic transitions in their

first paper [197] to uranium isotopic transitions in their second [145], the separation between peaks was reduced from 2.75 nm to 4.6 pm. Nonetheless, 2D-FS was able to differentiate the two isotopic peaks at atmospheric pressure using fs-LA. A LoD of 240 ppm for the ^{235}U isotope was also achieved (this improved to 120 ppm at reduced pressure). The same paper [145] discusses LAS experiments using a similar experimental setup. Their results showed dramatically increased broadening as the gas pressure was increased to 700 Torr which could make isotopic analysis impossible with absorption. Despite an improved LoD for LAS compared to LIF at reduced pressures, the authors seem satisfied that 2D-FS would be better suited to stand-off analysis of nuclear material in the future as the capacity for analysis at atmospheric pressure is desirable.

2.5.5 Recent Developments

An unavoidable problem with LA-LIF and LA-TDLAS is that as the resolution of the measurement is increased by refining the linewidth of the laser, the tuning range of the measurement is reduced. That is to say, increasing the resolution negatively effects the spectral coverage, and so less transitions can be analysed simultaneously. Indeed, in practically all of the literature around LA-LIF and LA- TDLAS only a single transition (or group of isotopic transitions) was probed in each experiment. One of the benefits of LIBS is the ability to record multiple wavelengths across the whole emission spectrum simultaneously, allowing multiple species to be identified and measured. To date, the only hyphenated technique which promises to enable a wider spectral bandwidth with high spectral resolution is dual-comb spectroscopy. This method relies on pulsed femtosecond lasers with slightly mismatched pulse trains. Stepping the wavelength of each pulse effectively enables very rapid wavelength ramping, and offsetting the pulse trains means the ‘gaps’ between wavelength ‘teeth’ of each comb can be better covered to increase the resolution. The technique was well reviewed by Coddington et al [198] in 2016, and was applied to laser ablation plasmas by Bergevin et al [199] in 2018 to investigate potassium and rubidium line hyperfine structures. The absorption peaks of the two elements were separated by around 15 nm, and yet could be analysed with 1 pm resolution by the dual frequency combs. In 2019, Shang et al [200] used dual frequency comb measurements to track the evolution of ionic and elemental species within an iron plasma. They were able to calculate number

densities and excitation temperatures at multiple delay times, and proposed that the accuracy of such calculations would be improved with inclusion of more transitions from different species which is possible with dual-comb spectroscopy.

A slightly different approach was taken by Merten and Johnson [201], who used a 'pseudocontinuum' laser to record the absorption of multiple isotopic transitions simultaneously. They stretched the bandwidth of a laser using an optical parametric oscillator to create a probe beam which was wider than the absorption feature, but narrow enough to be analysed with a standard Echelle spectrometer. They analysed three absorption peaks (separated by just 30 pm) in the lithium spectrum with a single laser ablation shot, which dramatically reduced the noise compared to stepping the probe wavelength and using multiple shots.

2.6 Conclusions and direction of future research and developments

LIBS offers a set of advantages which are unachievable using other elemental analysis techniques. The combination of immediate, in situ, multi-element characterisation of a material, down to trace levels of contamination, is favourable for many applications. The proven capability for stand-off or remote measurements opens more doors for analysis of hazardous materials and environments. Quantification of each constituent can be achieved with matrix-matched calibration samples. Without such samples, calibration-free approaches can still offer semi-quantitative information. High throughput settings and in-line deployments have been successful in a number of settings. The hardware required for LIBS is rugged and relatively inexpensive, and a balance can be achieved between the required capabilities and level of investment owing to the growing number of providers. Vehicle-portable, man-portable (i.e. backpack sized) and handheld instruments have all been developed and commercialised. Minor changes in the operation of LIBS equipment, such as incorporating multiple laser pulses (DP-LIBS) or using different sheath gases and pressures, have been shown to increase the analytical figures of merit without fundamentally increasing the complexity of the measurement.

The benefits of LIBS are numerous, but the poorer precision of the technique (compared to TIMS for example) should not be overlooked. No analytical technique is perfect, and there is no 'one size fits all' elemental analysis. Rather, it is the specific application and setting which

dictates the choice of method. For analysis of nuclear environments, LIBS offers improved safety, analysis speed and in situ analysis which is preferable to the established process of sample collection, transport, analysis, storage and disposal. Other benefits include the inherent stand-off capability of laser based analytical methods which could permit investigation of very hazardous environments from a safe distance, and the lack of impact from isobaric elements which present a problem for MS. For nuclear forensics, the LIBS method does not aim to compare with the precision attainable with TIMS. The benefits of LIBS lie with the: immediate in situ measurement and short analysis time; semi-quantitative and multi-elemental results; non-destructive sampling; possibility for stand-off data acquisition; and rugged, man-portable apparatus.

Chemometric methods have been applied to LIBS and several different approaches have been shown to improve the limit of detection, reduce the uncertainties and enable less user-involvement. All of these attributes are attractive to the end user. For nuclear forensics in particular, the breadth of knowledge required for an investigator to make key decisions is huge considering the number of different processes, techniques and materials used in the nuclear industry all over the world. Were LIBS to be more widely applied across the nuclear industry, it would be prevalent to construct a data library to compile spectra of known samples and information on specific spectroscopic signatures. This could be used in conjunction with principal component analysis or artificial neural networks to rapidly compare seized material with known stockpiles. Almost every country appears (at least ostensibly) positive towards prevention of nuclear proliferation, so such an international database should be a popular idea, and could even stimulate better nuclear safeguarding practices and collaboration.

The key problem which has persisted throughout the history of LIBS and, I would argue, has inhibited its adoption across the nuclear industry is the difficulty associated with isotopic speciation. Narrowly separated isotopic emission lines have consistently proved impossible to resolve when recorded from a LPP. Resolution of isotopic peaks is complicated by spectral line broadening (Stark and Doppler effects). Increasing the resolution of most emission-based methods could be achieved by recording over a longer time period and using a spectrometer with narrower slits. However, these solutions are impossible with LIBS because of the short-lived and transient nature of the LPP. Additionally, shot-to-shot

variations in the ablation process immediately introduce noise and uncertainty which renders isotopic characterisation impossible.

Numerous methods have been advocated to enhance the isotopic capability of LIBS. Initially, many of these were performed under reduced pressure to lessen spectral line broadening effects. However, the requirement for vacuum chambers and different sheath gases increases the complexity of the apparatus and the physical footprint of a device, which reduces the portability and ruggedness which are some of the key benefits of LIBS. Most recently, the introduction of LAMIS to characterise molecular rather than atomic emission lines has shown promise, and has been applied to numerous molecular species. Hyphenation of the laser ablation process with a second laser-based analytical technique could maintain many of the advantages of LIBS and additionally facilitate isotopic characterisation. The application of methods such as LA-LIF and LA-TDLAS to isotopic analysis was pioneered by the Niemax group in Germany twenty years ago. The improvement and evolution of these methods continues to this day with the work of Phillips and Harilal (among others) with two-dimensional fluorescence spectroscopy and differential laser absorption spectroscopy.

Technological progress with femtosecond laser ablation has seen the number of papers on fs-LIBS growing in recent years. It seems likely that as the cost of femtosecond lasers continues to fall, the number of applications and breadth of research will continue to grow, as it did for nanosecond laser ablation after the commercialisation of the Q-switched laser.

2.7 References

[1] V. Fedchenko, The Role of Nuclear Forensics in Nuclear Security, Strateg. Anal. 38 (2014) 230–247. doi:10.1080/09700161.2014.884442.

[2] IAEA, IAEA Incident and Trafficking Database (ITDB): 2020 Fact Sheet, Vienna, Austria, 2020. http://www-ns.iaea.org/downloads/security/itdb-fact-sheet.pdf.

[3] J.T. Richelson, Spying on the Bomb, First, Norton, New York, 2007.

[4] C.A. Ziegler, D. Jacobson, Spying Without Spies, First, Praeger, Westport, CT, 1995.

[5] A. Glaser, T. Bielefeld, Nuclear Forensics: Capabilities, Limits, and the “CSI Effect,” in: Sci.

Glob. Secur. Conf., Cambridge, MA, 2008: pp. 56–57. http://www.princeton.edu/~aglaser/talk2008_forensics.pdf.

[6] T. Fanghänel, K. Mayer, Z. Varga, M. Wallenius, 20 Years of Nuclear Forensics at ITU: between R&D and Case Work, in: Int. Conf. Adv. Nucl. Forensics - IAEA CN-218, 2014: p. IAEA-CN-218-44. https://conferences.iaea.org/event/16/sessions/564/#20140707.

[7] IAEA, Combating illicit trafficking in nuclear and other radioactive material, Vienna, Austria, 2007. https://www.iaea.org/publications/7806/combating-illicit-trafficking-in-nuclear-and-other-radioactive-material.

[8] S. Niemeyer, L. Koch, The Historical Evolution of Nuclear Forensics: A Technical Viewpoint, in: Int. Conf. Adv. Nucl. Forensics - IAEA CN-218, International Atomic Energy Agency, Vienna, Austria, 2014: p. IAEA-CN-218-117. http://www-pub.iaea.org/MTCD/Publications/PDF/SupplementaryMaterials/P1706/Plenary_Session_1A.pdf.

[9] IAEA, IAEA Nuclear Security Series, IAEA Nucl. Secur. Ser. (n.d.). http://www-ns.iaea.org/security/nuclear_security_series.asp?s=5&l=35 (accessed July 1, 2016).

[10] IAEA, Nuclear Forensics Support, International Atomic Energy Agency, Vienna, Austria, 2006. http://www-pub.iaea.org/MTCD/publications/PDF/Pub1241_web.pdf.

[11] IAEA, Nuclear Forensics in Support of Investigations, Vienna, Austria, 2015. http://www-pub.iaea.org/books/IAEABooks/10797/Nuclear-Forensics-in-Support-of-Investigations.

[12] United Nations, Comprehensive Nuclear-Test-Ban Treaty (CTBT), (n.d.). https://www.un.org/disarmament/wmd/nuclear/ctbt/ (accessed February 18, 2020).

[13] United Nations, Treaty on the Non-Proliferation of Nuclear Weapons (NPT), (n.d.). https://www.un.org/disarmament/wmd/nuclear/npt/ (accessed February 18, 2020).

[14] United Kingdom Government, National report on the implementation of actions 5, 20, and 21 of the action plan of the 2010 Review Conference of the Parties to the Treaty on the Non-Proliferation of Nuclear Weapons, New York, 2015. https://undocs.org/NPT/CONF.2015/29.

[15] R.S. Litwak, Recalibrating deterrence to prevent nuclear terrorism, Wash. Q. 40 (2017) 55–70. doi:10.1080/0163660X.2017.1302739.

[16] J. Herbach, Yearbook of International Humanitarian Law Volume 17, 2014, First, T.M.C. Asser

Press, 2014. doi:10.1007/978-94-6265-091-6.

[17] N. Salik, Nuclear Terrorism: Assessing the Danger, Strateg. Anal. 38 (2014) 173–184. doi:10.1080/09700161.2014.884437.

[18] L. Weiss, On fear and nuclear terrorism, Bull. At. Sci. 71 (2015) 75–87. doi:10.1177/0096340215571909.

[19] I.D. Hutcheon, P.M. Grant, K.J. Moody, Handbook of Nuclear Chemistry. Chapter 62 - Nuclear Forensic Materials and Methods, 2nd Editio, Springer, Boston, Ma, 2011. doi:10.1007/978-1-4419-0720-2.

[20] M. Schreuer, A.J. Rubin, Video Found in Belgium of Nuclear Official May Point to Bigger Plot, New York Times. (2016) 4. https://www.nytimes.com/2016/02/19/world/europe/belgium-nuclear-official-video-paris-attacks.html.

[21] IAEA, Advances in Nuclear Forensics: Countering the Evolving Threat of Nuclear and Other Radioactive Material out of Regulatory Control, in: IAEA Proc. Ser., Vienna, Austria, 2014: p. 149. http://www-pub.iaea.org/books/IAEABooks/10881/Advances-in-Nuclear-Forensics-Countering-the-Evolving-Threat-of-Nuclear-and-Other-Radioac.

[22] K. Mayer, M. Wallenius, I. Ray, Nuclear forensics - a methodology providing clues on the origin of illicitly trafficked nuclear materials, Analyst. 130 (2005) 433–441. doi:10.1039/b412922a.

[23] F.E. Stanley, A.M. Stalcup, H.B. Spitz, A brief introduction to analytical methods in nuclear forensics, J. Radioanal. Nucl. Chem. 295 (2013) 1385–1393. doi:10.1007/s10967-012-1927-3.

[24] J.D. Winefordner, I.B. Gornushkin, T. Correll, E. Gibb, B.W. Smith, N. Omenetto, Comparing several atomic spectrometric methods to the super stars: special emphasis on laser induced breakdown spectrometry, LIBS, a future super star, J. Anal. At. Spectrom. 19 (2004) 1061–1083. doi:10.1039/b400355c.

[25] Z. Varga, M. Wallenius, K. Mayer, Age determination of uranium samples by inductively coupled plasma mass spectrometry using direct measurement and spectral deconvolution, J. Anal. At. Spectrom. 25 (2010) 1958–1962. doi:10.1039/c0ja00048e.

[26] Z. Varga, R. Katona, Z. Stefánka, M. Wallenius, K. Mayer, A. Nicholl, Determination of rare-earth elements in uranium-bearing materials by inductively coupled plasma mass spectrometry, Talanta. 80 (2010) 1744–1749. doi:10.1016/j.talanta.2009.10.018.

[27] M. Srncik, K. Mayer, E. Hrnecek, M. Wallenius, Z. Varga, P. Steier, G. Wallner, Investigation of the 236U/238U isotope abundance ratio in uranium ores and yellow cake samples, Radiochim. Acta. 99 (2011) 335–339. doi:10.1524/ract.2011.1840.

[28] M. Wallenius, A. Morgenstern, A. Nicholl, R. Fiedler, C. Apostolidis, K. Mayer, Age Determination of Highly Enriched Uranium, in: Symp. Int. Safeguards - Verif. Nucl. Mater. Secur. - IAEA-SM-376, International Atomic Energy Agency, Vienna, Austria, 2001: p. 76. http://www-pub.iaea.org/MTCD/publications/PDF/ss-2001/PDF files/Session 5/Paper 5-07.pdf.

[29] M. Wallenius, K. Mayer, Age determination of plutonium material in nuclear forensics by thermal ionisation mass spectrometry, Fresenius. J. Anal. Chem. 366 (2000) 234–238. doi:10.1007/s002160050046.

[30] K. Mayer, M. Wallenius, K. Lützenkirchen, J. Galy, Z. Varga, N. Erdmann, R. Buda, J. V Kratz, N. Trautmann, K. Fifield, Nuclear forensics: A methodology applicable to nuclear security and to non-proliferation, J. Phys. Conf. Ser. 312 (2011). doi:10.1088/1742-6596/312/6/062003.

[31] E. Keegan, M.J. Kristo, M. Colella, M. Robel, R. Williams, R. Lindvall, G. Eppich, S. Roberts, L. Borg, A. Gaffney, J. Plaue, H. Wong, J. Davis, E. Loi, M. Reinhard, I. Hutcheon, Nuclear forensic analysis of an unknown uranium ore concentrate sample seized in a criminal investigation in Australia, Forensic Sci. Int. 240 (2014) 111–121. doi:10.1016/j.forsciint.2014.04.004.

[32] S.E. Shaban, N.M. Ibrahiem, S.A. El-Mongy, E.E. Elshereafy, Validation of scanning electron microscope (SEM), energy dispersive X-ray (EDX) and gamma spectrometry to verify source nuclear material for safeguards purposes, J. Radioanal. Nucl. Chem. 296 (2013) 1219–1224. doi:10.1007/s10967-012-2374-x.

[33] R.P. Keegan, R.J. Gehrke, A method to determine the time since last purification of weapons grade plutonium, Appl. Radiat. Isot. 59 (2003) 137–143. doi:10.1016/S0969-8043(03)00149-0.

[34] J. Zsigrai, C. Larsson, S.P. Holloway, M. Wallenius, N. Cong Tam, J. Safar, Nuclear Forensics ITWG Guideline on High-Resolution Gamma Spectroscopy, 2013.

[35] Home Office, Supplementary memorandum from UK Border Agency, Home Office, London, 2009. https://publications.parliament.uk/pa/cm200809/cmselect/cmpubacc/336/9030910.htm#:~:text=Programme Cyclamen is a joint,UK from a terrorist attack.

[36] S. Musazzi, U. Perini, Laser-Induced Breakdown Spectroscopy Theory and Applications, Springer, 2014. doi:10.1007/978-3-642-45085-3.

[37] R.S. Harmon, R.R. Hark, C.S. Throckmorton, E.C. Rankey, M.A. Wise, A.M. Somers, L.M. Collins, Geochemical Fingerprinting by Handheld Laser-Induced Breakdown Spectroscopy, Geostand. Geoanalytical Res. 41 (2017) 563–584. doi:10.1111/ggr.12175.

[38] L.J. Radziemski, D.A. Cremers, A brief history of laser-induced breakdown spectroscopy: From the concept of atoms to LIBS 2012, Spectrochim. Acta - Part B At. Spectrosc. 87 (2013) 3–10. doi:10.1016/j.sab.2013.05.013.

[39] L.J. Radziemski, T.R. Loree, Laser-induced breakdown spectroscopy: Time-resolved spectrochemical applications, Plasma Chem. Plasma Process. 1 (1981) 281–293. doi:10.1007/BF00568836.

[40] T.R. Loree, L.J. Radziemski, Laser-Induced Breakdown Spectroscopy: Time-Integrated Applications, Plasma Chem. Plasma Process. 1 (1981) 271–279. https://link.springer.com/article/10.1007/BF00568835.

[41] D.A. Cremers, L.J. Radziemski, T.R. Loree, Spectrochemical Analysis of Liquids Using the Laser Spark., Appl. Spectrosc. 38 (1984) 721–729. doi:10.1366/0003702844555034.

[42] L.J. Radziemski, D.A. Cremers, Laser-induced plasmas and applications, M. Dekker, 1989. https://inis.iaea.org/search/search.aspx?orig_q=RN:21084624 (accessed March 5, 2020).

[43] R.C. Wiens, S. Maurice, B. Barraclough, M. Saccoccio, W.C. Barkley, J.F. Bell, S. Bender, J. Bernardin, D. Blaney, J. Blank, M. Bouye, N. Bridges, N. Bultman, P. CaIs, R.C. Clanton, B. Clark, S. Clegg, A. Cousin, D.A. Cremers, A. Cros, L. Deflores, D. Delapp, R. Dingler, C. D'Uston, M. Darby Dyar, T. Elliott, D. Enemark, C. Fabre, M. Flores, O. Forni, O. Gasnault, T. Hale, C. Hays, K. Herkenhoff, E. Kan, L. Kirkland, D. Kouach, D. Landis, Y. Langevin, N. Lanza, F. Larocca, J. Lasue, J. Latino, D. Limonadi, C. Lindensmith, C. Little, N. Mangold, G. Manhes, P. Mauchien, C.P. McKay, E. Miller, J. Mooney, R. V Morris, L. Morrison, T. Nelson, H. Newsom, A. Ollila, M. Ott, L. Pares, R. Perez, F. Poitrasson, C. Provost, J.W. Reiter, T. Roberts, F. Romero, V. Sautter, S. Salazar, J.J. Simmonds, R. Stiglich, S. Storms, N. Striebig, J.J. Thocaven, T. Trujillo, M. Ulibarri, D. Vaniman, N. Warner, R. Waterbury, R. Whitaker, J. Witt, B. Wong-Swanson, The ChemCam instrument suite on the Mars Science Laboratory (MSL) rover: Body unit and combined system tests, Space Sci. Rev. 170 (2012) 167–227. doi:10.1007/s11214-012-9902-4.

[44] D.C.S. Beddows, O. Samek, M. Liška, H.H. Telle, Single-pulse laser-induced breakdown

spectroscopy of samples submerged in water using a single-fibre light delivery system, Spectrochim. Acta - Part B At. Spectrosc. 57 (2002) 1461–1471. doi:10.1016/S0584-8547(02)00083-6.

[45] C.M. Davies, H.H. Telle, D.J. Montgomery, R.E. Corbett, Quantitative analysis using remote laser-induced breakdown spectroscopy (LIBS), Spectrochim. Acta Part B At. Spectrosc. 50 (1995) 1059–1075. doi:10.1016/0584-8547(95)01314-5.

[46] A.I. Whitehouse, J. Young, I.M. Botheroyd, S. Lawson, C.P. Evans, J. Wright, Remote material analysis of nuclear power station steam generator tubes by laser-induced breakdown spectroscopy, Spectrochim. Acta - Part B At. Spectrosc. 56 (2001) 821–830. doi:10.1016/S0584-8547(01)00232-4.

[47] O. Samek, H.H. Telle, D.C.S. Beddows, Laser-induced breakdown spectroscopy: A tool for real-time, in vitro and in vivo identification of carious teeth, BMC Oral Health. 1 (2001) 1–9. doi:10.1186/1472-6831-1-1.

[48] O. Samek, V. Krzyzanek, D.C.S. Beddows, H.H. Telle, J. Kaiser, M. Liska, Material identification using laser spectroscopy and pattern recognition algorithms, Lect. Notes Comput. Sci. (Including Subser. Lect. Notes Artif. Intell. Lect. Notes Bioinformatics). 2124 (2001) 443–450. doi:10.1007/3-540-44692-3_54.

[49] A. Kramida, Y. Ralchenko, J. Reader, The NIST ASD Team (2018), NIST Atomic Spectra Database, NIST At. Spectra Database (Ver. 5.6.1). [Online] (2019) http://physics.nist.gov/asd. doi:10.18434/T4W30F.

[50] R. Noll, Laser-Induced Breakdown Spectroscopy, First Edit, Springer, 2012. doi:10.1007/978-3-642-20668-9.

[51] I.R.R. Roman, Semi-Automatic Elemental Identification and Quantification by Laser–Induced Breakdown Spectroscopy, Centro de Investigaciones en Optica A.C., 2017. https://cio.repositorioinstitucional.mx/jspui/bitstream/1002/213/1/17159.pdf.

[52] G. Cristoforetti, A. De Giacomo, M. Dell'Aglio, S. Legnaioli, E. Tognoni, V. Palleschi, N. Omenetto, Local Thermodynamic Equilibrium in Laser-Induced Breakdown Spectroscopy: Beyond the McWhirter criterion, Spectrochim. Acta - Part B At. Spectrosc. 65 (2010) 86–95. doi:10.1016/j.sab.2009.11.005.

[53] W. Li, X. Li, X. Li, Z. Hao, Y. Lu, X. Zeng, A review of remote laser-induced breakdown

spectroscopy, Appl. Spectrosc. Rev. (2018) 1–25. doi:10.1080/05704928.2018.1472102.

[54] N. Farid, S.S. Harilal, H. Ding, A. Hassanein, Emission features and expansion dynamics of nanosecond laser ablation plumes at different ambient pressures, J. Appl. Phys. 115 (2014). doi:10.1063/1.4862167.

[55] X. Wang, V. Motto-Ros, G. Panczer, D. De Ligny, J. Yu, J.M. Benoit, J.L. Dussossoy, S. Peuget, Mapping of rare earth elements in nuclear waste glass-ceramic using micro laser-induced breakdown spectroscopy, Spectrochim. Acta - Part B At. Spectrosc. 87 (2013) 139–146. doi:10.1016/j.sab.2013.05.022.

[56] V. Margetic, M.A. Bolshov, A. Stockhaus, K. Niemax, R. Hergenroder, Depth profiling of multi-layer samples using femtosecond laser ablation, J. Anal. At. Spectrom. 16 (2001) 616–621. doi:10.1039/b100016k.

[57] D.G. Papazoglou, V. Papadakis, D. Anglos, In situ interferometric depth and topography monitoring in LIBS elemental profiling of multi-layer structures, J. Anal. At. Spectrom. 19 (2004) 483–488. doi:10.1039/b315657r.

[58] R. Glaus, D.W. Hahn, Fiber-coupled laser-induced breakdown and Raman spectroscopy for flexible sample characterization with depth profiling capabilities, Spectrochim. Acta - Part B At. Spectrosc. 100 (2014) 116–122. doi:10.1016/j.sab.2014.06.026.

[59] S.S. Harilal, G. V. Miloshevsky, P.K. Diwakar, N.L. Lahaye, A. Hassanein, Experimental and computational study of complex shockwave dynamics in laser ablation plumes in argon atmosphere, Phys. Plasmas. 19 (2012). doi:10.1063/1.4745867.

[60] S.S. Harilal, P.J. Skrodzki, A. Miloshevsky, B.E. Brumfield, M.C. Phillips, G. Miloshevsky, On- and off-axis spectral emission features from laser-produced gas breakdown plasmas, Phys. Plasmas. 24 (2017). doi:10.1063/1.4985678.

[61] N.L. Lahaye, S.S. Harilal, P.K. Diwakar, A. Hassanein, Characterization of laser ablation sample introduction plasma plumes in fs-LA-ICP-MS, J. Anal. At. Spectrom. 29 (2014) 2267–2274. doi:10.1039/c4ja00200h.

[62] S.S. Harilal, P.K. Diwakar, N.L. Lahaye, M.C. Phillips, Spatio-temporal evolution of uranium emission in laser-produced plasmas, Spectrochim. Acta - Part B At. Spectrosc. 111 (2015) 1–7. doi:10.1016/j.sab.2015.06.003.

[63] M. Miyabe, M. Oba, H. Iimura, K. Akaoka, K. Ali, M. Kato, I. Wakaida, Ablation plume structure

and dynamics in ambient gas observed by laser-induced fluorescence imaging spectroscopy, Spectrochim. Acta - Part B At. Spectrosc. 110 (2015) 101–117. doi:10.1016/j.sab.2015.06.004.

[64] B. Campanella, S. Legnaioli, S. Pagnotta, F. Poggialini, V. Palleschi, Shock waves in laser-induced plasmas, Atoms. 7 (2019) 1–14. doi:10.3390/ATOMS7020057.

[65] G. Cristoforetti, G. Lorenzetti, S. Legnaioli, V. Palleschi, Investigation on the role of air in the dynamical evolution and thermodynamic state of a laser-induced aluminium plasma by spatial- and time-resolved spectroscopy, Spectrochim. Acta - Part B At. Spectrosc. 65 (2010) 787–796. doi:10.1016/j.sab.2010.07.002.

[66] Q.L. Ma, V. Motto-Ros, W.Q. Lei, M. Boueri, X.S. Bai, L.J. Zheng, H.P. Zeng, J. Yu, Temporal and spatial dynamics of laser-induced aluminum plasma in argon background at atmospheric pressure: Interplay with the ambient gas, Spectrochim. Acta - Part B At. Spectrosc. 65 (2010) 896–907. doi:10.1016/j.sab.2010.08.005.

[67] S.S. Harilal, B.E. Brumfield, B.D. Cannon, M.C. Phillips, Shock Wave Mediated Plume Chemistry for Molecular Formation in Laser Ablation Plasmas, Anal. Chem. 88 (2016) 2296–2302. doi:10.1021/acs.analchem.5b04136.

[68] S.S. Harilal, J. Yeak, B.E. Brumfield, J.D. Suter, M.C. Phillips, Dynamics of molecular emission features from nanosecond, femtosecond laser and filament ablation plasmas, J. Anal. At. Spectrom. 31 (2016) 1192–1197. doi:10.1039/c6ja00036c.

[69] V.I. Babushok, F.C. DeLucia, J.L. Gottfried, C.A. Munson, A.W. Miziolek, Double pulse laser ablation and plasma: Laser induced breakdown spectroscopy signal enhancement, Spectrochim. Acta - Part B At. Spectrosc. 61 (2006) 999–1014. doi:10.1016/j.sab.2006.09.003.

[70] Y. Li, D. Tian, Y. Ding, G. Yang, K. Liu, C. Wang, X. Han, A review of laser-induced breakdown spectroscopy signal enhancement, Appl. Spectrosc. Rev. 53 (2018) 1–35. doi:10.1080/05704928.2017.1352509.

[71] A. De Giacomo, M. Dell'Aglio, D. Bruno, R. Gaudiuso, O. De Pascale, Experimental and theoretical comparison of single-pulse and double-pulse laser induced breakdown spectroscopy on metallic samples, Spectrochim. Acta - Part B At. Spectrosc. 63 (2008) 805–816. doi:10.1016/j.sab.2008.05.002.

[72] M. Corsi, G. Cristoforetti, M. Giuffrida, M. Hidalgo, S. Legnaioli, V. Palleschi, A. Salvetti, E. Tognoni, C. Vallebona, Three-dimensional analysis of laser induced plasmas in single and

double pulse configuration, Spectrochim. Acta - Part B At. Spectrosc. 59 (2004) 723–735. doi:10.1016/j.sab.2004.02.001.

[73] N. Basov, V. Gribkov, O. Krokhin, G. Sklizkov, High Temperature Effects on Intense Laser Emission Focused on a Solid Target, Sov. J. Exp. Theor. Phys. 27 (1968) 575. http://jetp.ac.ru/cgi-bin/dn/e_027_04_0575.pdf.

[74] M. Cui, Y. Deguchi, Z. Wang, Y. Fujita, R. Liu, F.J. Shiou, S. Zhao, Enhancement and stabilization of plasma using collinear long-short double-pulse laser-induced breakdown spectroscopy, Spectrochim. Acta - Part B At. Spectrosc. 142 (2018) 14–22. doi:10.1016/j.sab.2018.02.002.

[75] R. Hai, L. Sun, D. Wu, Z. He, H. Sattar, J. Liu, W. Tong, C. Li, C. Feng, H. Ding, Enhanced laser-induced breakdown spectroscopy using the combination of circular and annular laser pulses, J. Anal. At. Spectrom. 34 (2019) 1982–1987. doi:10.1039/c9ja00230h.

[76] P.J. Skrodzki, J.R. Becker, P.K. Diwakar, S.S. Harilal, A. Hassanein, A Comparative Study of Single-pulse and Double-pulse Laser-Induced Breakdown Spectroscopy with Uranium-containing Samples, Appl. Spectrosc. 70 (2016) 467–473. doi:10.1177/0003702815626670.

[77] R. Hai, P. Liu, D. Wu, H. Ding, J. Wu, G.N. Luo, Collinear double-pulse laser-induced breakdown spectroscopy as an in-situ diagnostic tool for wall composition in fusion devices, Fusion Eng. Des. 89 (2014) 2435–2439. doi:10.1016/j.fusengdes.2014.04.065.

[78] R. Fantoni, S. Almaviva, L. Caneve, F. Colao, G. Maddaluno, P. Gasior, M. Kubkowska, Hydrogen isotope detection in metal matrix using double-pulse laser-induced breakdown-spectroscopy, Spectrochim. Acta - Part B At. Spectrosc. 129 (2017) 8–13. doi:10.1016/j.sab.2016.12.008.

[79] H. Lindner, K.H. Loper, D.W. Hahn, K. Niemax, The influence of laser-particle interaction in laser induced breakdown spectroscopy and laser ablation inductively coupled plasma spectrometry, Spectrochim. Acta - Part B At. Spectrosc. 66 (2011) 179–185. doi:10.1016/j.sab.2011.01.002.

[80] R.C. Chinni, D.A. Cremers, L.J. Radziemski, M. Bostian, C. Navarro-Northrup, Detection of uranium using laser-induced breakdown spectroscopy, Appl. Spectrosc. 63 (2009) 1238–1250. http://www.osapublishing.org/abstract.cfm?uri=as-63-11-1238.

[81] J. Klus, P. Mikysek, D. Prochazka, P. Pořízka, P. Prochazková, J. Novotný, T. Trojek, K. Novotný,

M. Slobodník, J. Kaiser, Multivariate approach to the chemical mapping of uranium in sandstone-hosted uranium ores analyzed using double pulse Laser-Induced Breakdown Spectroscopy, Spectrochim. Acta - Part B At. Spectrosc. 123 (2016) 143–149. doi:10.1016/j.sab.2016.08.014.

[82] Q. Wang, J.-G. Wang, Y. Liang, X. Chen, B. Wu, Z. Ni, F. Dong, Investigation on emission spectra of reheating and pre-ablation dual-pulse laser-induced breakdown spectroscopy, 2011 Int. Conf. Opt. Instruments Technol. Optoelectron. Meas. Technol. Syst. 8201 (2011) 82012I. doi:10.1117/12.907258.

[83] Y. Lu, V. Zorba, X. Mao, R. Zheng, R.E. Russo, UV fs-ns double-pulse laser induced breakdown spectroscopy for high spatial resolution chemical analysis, J. Anal. At. Spectrom. 28 (2013) 743–748. doi:10.1039/c3ja30315b.

[84] R. Hai, X. Wu, Y. Xin, P. Liu, D. Wu, H. Ding, Y. Zhou, L. Cai, L. Yan, Use of dual-pulse laser-induced breakdown spectroscopy for characterization of the laser cleaning of a first mirror exposed in HL-2A, J. Nucl. Mater. 447 (2014) 9–14. doi:10.1016/j.jnucmat.2013.12.019.

[85] J. Wu, Y. Qiu, X. Li, H. Yu, Z. Zhang, A. Qiu, Progress of laser-induced breakdown spectroscopy in nuclear industry applications, J. Phys. D. Appl. Phys. 53 (2020) 023001. doi:10.1088/1361-6463/ab477a.

[86] P. Fichet, D. Menut, R. Brennetot, E. Vors, A. Rivoallan, Analysis by laser-induced breakdown spectroscopy of complex solids, liquids, and powders with an echelle spectrometer, Appl. Opt. 42 (2003) 6029. doi:10.1364/AO.42.006029.

[87] P. Fichet, P. Mauchien, J.F. Wagner, C. Moulin, Quantitative elemental determination in water and oil by laser induced breakdown spectroscopy, Anal. Chim. Acta. 429 (2001) 269–278. doi:10.1016/S0003-2670(00)01277-0.

[88] S. Guirado, F.J. Fortes, V. Lazic, J.J. Laserna, Chemical analysis of archeological materials in submarine environments using laser-induced breakdown spectroscopy. On-site trials in the Mediterranean Sea, Spectrochim. Acta - Part B At. Spectrosc. 74–75 (2012) 137–143. doi:10.1016/j.sab.2012.06.032.

[89] A. De Giacomo, M. Dell'Aglio, O. De Pascale, M. Capitelli, From single pulse to double pulse ns-Laser Induced Breakdown Spectroscopy under water: Elemental analysis of aqueous solutions and submerged solid samples, Spectrochim. Acta - Part B At. Spectrosc. 62 (2007) 721–738. doi:10.1016/j.sab.2007.06.008.

[90] A. Casavola, A. De Giacomo, M. Dell'Aglio, F. Taccogna, G. Colonna, O. De Pascale, S. Longo, Experimental investigation and modelling of double pulse laser induced plasma spectroscopy under water, Spectrochim. Acta - Part B At. Spectrosc. 60 (2005) 975–985. doi:10.1016/j.sab.2005.05.034.

[91] M. Saeki, A. Iwanade, C. Ito, I. Wakaida, B. Thornton, T. Sakka, H. Ohba, Development of a fiber-coupled laser-induced breakdown spectroscopy instrument for analysis of underwater debris in a nuclear reactor core, J. Nucl. Sci. Technol. 51 (2014) 930–938. doi:10.1080/00223131.2014.917996.

[92] T. Sakka, H. Oguchi, S. Masai, K. Hirata, Y.H. Ogata, M. Saeki, H. Ohba, Use of a long-duration ns pulse for efficient emission of spectral lines from the laser ablation plume in water, Appl. Phys. Lett. 88 (2006) 1–4. doi:10.1063/1.2172235.

[93] A. Botto, B. Campanella, S. Legnaioli, M. Lezzerini, G. Lorenzetti, S. Pagnotta, F. Poggialini, V. Palleschi, Applications of laser-induced breakdown spectroscopy in cultural heritage and archaeology: A critical review, J. Anal. At. Spectrom. 34 (2019) 81–103. doi:10.1039/c8ja00319j.

[94] S. Guirado, F.J. Fortes, J.J. Laserna, Elemental analysis of materials in an underwater archeological shipwreck using a novel remote laser-induced breakdown spectroscopy system, Talanta. 137 (2015) 182–188. doi:10.1016/j.talanta.2015.01.033.

[95] M. López-Claros, F.J. Fortes, J.J. Laserna, Subsea spectral identification of shipwreck objects using laser-induced breakdown spectroscopy and linear discriminant analysis, J. Cult. Herit. 29 (2018) 75–81. doi:10.1016/j.culher.2016.12.015.

[96] F.J. Fortes, S. Guirado, A. Metzinger, J.J. Laserna, A study of underwater stand-off laser-induced breakdown spectroscopy for chemical analysis of objects in the deep ocean, J. Anal. At. Spectrom. 30 (2015) 1050–1056. doi:10.1039/c4ja00489b.

[97] E.L. Gurevich, R. Hergenröder, Femtosecond laser-induced breakdown spectroscopy: Physics, applications, and perspectives, Appl. Spectrosc. 61 (2007) 233–242. doi:10.1366/000370207782217824.

[98] T.A. Labutin, V.N. Lednev, A.A. Ilyin, A.M. Popov, Femtosecond laser-induced breakdown spectroscopy, J. Anal. At. Spectrom. 31 (2016) 90–118. doi:10.1039/c5ja00301f.

[99] L.A. Emmert, R.C. Chinni, D.A. Cremers, C.R. Jones, W. Rudolph, Comparative study of

femtosecond and nanosecond laser-induced breakdown spectroscopy of depleted uranium, Appl. Opt. 50 (2011) 313–317.

[100] J.R. Freeman, S.S. Harilal, P.K. Diwakar, B. Verhoff, A. Hassanein, Comparison of optical emission from nanosecond and femtosecond laser produced plasma in atmosphere and vacuum conditions, Spectrochim. Acta - Part B At. Spectrosc. 87 (2013) 43–50. doi:10.1016/j.sab.2013.05.011.

[101] A.A. Bol'shakov, X. Mao, J.J. Gonzlez, R.E. Russo, Laser ablation molecular isotopic spectrometry (LAMIS): current state of the art, J. Anal. At. Spectrom. 31 (2016) 119. doi:10.1039/c5ja00310e.

[102] N.L. LaHaye, M.C. Phillips, A.M. Duffin, G.C. Eiden, S.S. Harilal, The influence of ns- and fs-LA plume local conditions on the performance of a combined LIBS/LA-ICP-MS sensor, J. Anal. At. Spectrom. 31 (2016) 515–522. doi:10.1039/c5ja00317b.

[103] M. Oba, Y. Maruyama, K. Akaoka, M. Miyabe, I. Wakaida, Double-pulse LIBS of gadolinium oxide ablated by femto- and nano-second laser pulses, Appl. Phys. A Mater. Sci. Process. 101 (2010) 545–549. doi:10.1007/s00339-010-5894-7.

[104] K. Stelmaszczyk, P. Rohwetter, G. Méjean, J. Yu, E. Salmon, J. Kasparian, R. Ackermann, J.P. Wolf, L. Wöste, Long-distance remote laser-induced breakdown spectroscopy using filamentation in air, Appl. Phys. Lett. 85 (2004) 3977–3979. doi:10.1063/1.1812843.

[105] M. Rodriguez, R. Bourayou, G. Méjean, J. Kasparian, J. Yu, E. Salmon, A. Scholz, B. Stecklum, J. Eislöffel, U. Laux, A.P. Hatzes, R. Sauerbrey, L. Wöste, J.P. Wolf, Kilometer-range nonlinear propagation of femtosecond laser pulses, Phys. Rev. E - Stat. Nonlinear, Soft Matter Phys. 69 (2004) 1–7. doi:10.1103/PhysRevE.69.036607.

[106] M. Durand, A. Houard, B. Prade, A. Mysyrowicz, A. Durécu, B. Moreau, D. Fleury, O. Vasseur, H. Borchert, K. Diener, R. Schmitt, F. Théberge, M. Chateauneuf, J.-F. Daigle, J. Dubois, Kilometer range filamentation, Opt. Express. 21 (2013) 26836. doi:10.1364/oe.21.026836.

[107] E.J. Judge, G. Heck, E.B. Cerkez, R.J. Levis, Discrimination of composite graphite samples using remote filament-induced breakdown spectroscopy, Anal. Chem. 81 (2009) 2658–2663. doi:10.1021/ac802080q.

[108] I. Ghebregziabher, K.C. Hartig, I. Jovanovic, Propagation distance-resolved characteristics of filament-induced copper plasma, Opt. Express. 24 (2016) 5263. doi:10.1364/oe.24.005263.

[109] H. Hou, B. Yang, X. Mao, V. Zorba, P. Ran, R.E. Russo, Characteristics of plasma plume in ultrafast laser ablation with a weakly ionized air channel, Opt. Express. 26 (2018) 13425. doi:10.1364/oe.26.013425.

[110] N. Jhajj, E.W. Rosenthal, R. Birnbaum, J.K. Wahlstrand, H.M. Milchberg, Demonstration of long-lived high-power optical waveguides in air, Phys. Rev. X. 4 (2014) 1–8. doi:10.1103/PhysRevX.4.011027.

[111] J.K. Wahlstrand, N. Jhajj, E.W. Rosenthal, R. Birnbaum, S. Zahedpour, H.M. Milchberg, Long-lived high power optical waveguides in air, in: Opt. InfoBase Conf. Pap., 2014. doi:10.1364/hilas.2014.hth2b.4.

[112] N. Jhajj, E.W. Rosenthal, R. Birnbaum, J.K. Wahlstrand, H.M. Milchberg, Demonstration of long-lived high power optical waveguides in air, in: Conf. Lasers Electro-Optics Eur. - Tech. Dig., 2014. doi:10.1364/cleo_si.2014.sth1e.3.

[113] P. Rohwetter, K. Stelmaszczyk, L. Woste, R. Ackermann, G. Mejean, E. Salmon, J. Kasparian, J. Yu, J.P. Wolf, Filament-induced remote surface ablation for long range laser-induced breakdown spectroscopy operation, Spectrochim. Acta - Part B At. Spectrosc. 60 (2005) 1025–1033. doi:10.1016/j.sab.2005.03.017.

[114] D.A. Cremers, A. Beddingfield, R. Smithwick, R.C. Chinni, C.R. Jones, B. Beardsley, L. Karch, Monitoring Uranium, Hydrogen, and Lithium and Their Isotopes Using a Compact Laser-Induced Breakdown Spectroscopy (LIBS) Probe and High-Resolution Spectrometer, Appl. Spectrosc. 66 (2012) 250–261. doi:10.1366/11-06314.

[115] E.J. Judge, J.E. Barefield, J.M. Berg, S.M. Clegg, G.J. Havrilla, V.M. Montoya, L.A. Le, L.N. Lopez, Laser-induced breakdown spectroscopy measurements of uranium and thorium powders and uranium ore, Spectrochim. Acta - Part B At. Spectrosc. 83–84 (2013) 28–36. doi:10.1016/j.sab.2013.03.002.

[116] G. Galbács, A critical review of recent progress in analytical laser-induced breakdown spectroscopy, Anal. Bioanal. Chem. 407 (2015) 7537–7562. doi:10.1007/s00216-015-8855-3.

[117] K. Kuhn, J.A. Meima, D. Rammlmair, C. Ohlendorf, Chemical mapping of mine waste drill cores with laser-induced breakdown spectroscopy (LIBS) and energy dispersive X-ray fluorescence (EDXRF) for mineral resource exploration, J. Geochemical Explor. 161 (2016) 72–84. doi:10.1016/j.gexplo.2015.11.005.

[118] J.-I. Yun, R. Klenze, J.-I. Kim, Laser-induced breakdown spectroscopy for the on-line multielement analysis of highly radioactive glass melt simulants. Part II: Analyses of molten glass samples, Appl. Spectrosc. 56 (2002) 852–858. doi:10.1366/000370202760171518.

[119] T. Takahashi, B. Thornton, Quantitative methods for compensation of matrix effects and self-absorption in LIBS signals of solids, Spectrochim. Acta - Part B At. Spectrosc. 138 (2017) 31–42. doi:10.1016/j.sab.2017.09.010.

[120] G.C.-Y. Chan, X. Mao, I. Choi, A. Sarkar, O.P. Lam, D.K. Shuh, R.E. Russo, Multiple emission line analysis for improved isotopic determination of uranium — a computer simulation study, Spectrochim. Acta - Part B At. Spectrosc. 89 (2013) 40–49. doi:10.1016/j.sab.2013.09.001.

[121] P. Devangad, V.K. Unnikrishnan, M.M. Tamboli, K.M.M. Shameem, R. Nayak, K.S. Choudhari, C. Santhosh, Quantification of Mn in glass matrices using laser induced breakdown spectroscopy (LIBS) combined with chemometric approaches, Anal. Methods. 8 (2016) 7177–7184. doi:10.1039/c6ay01930g.

[122] J.P. Castro, E.R. Pereira-Filho, Twelve different types of data normalization for the proposition of classification, univariate and multivariate regression models for the direct analyses of alloys by laser-induced breakdown spectroscopy (LIBS), J. Anal. At. Spectrom. 31 (2016) 2005–2014. doi:10.1039/C6JA00224B.

[123] A. Williams, S. Phongikaroon, Laser-Induced Breakdown Spectroscopy (LIBS) Measurement of Uranium in Molten Salt, Appl. Spectrosc. 72 (2018) 1029–1039. doi:10.1177/0003702818760311.

[124] A. Williams, K. Bryce, S. Phongikaroon, Measurement of Cerium and Gadolinium in Solid Lithium Chloride–Potassium Chloride Salt Using Laser-Induced Breakdown Spectroscopy (LIBS), Appl. Spectrosc. 71 (2017) 2302–2312. doi:10.1177/0003702817709298.

[125] M.Z. Martin, R.C. Martin, S. Allman, D. Brice, A. Wymore, N. Andre, Quantification of rare earth elements using laser-induced breakdown spectroscopy, Spectrochim. Acta - Part B At. Spectrosc. 114 (2015) 65–73. doi:10.1016/j.sab.2015.10.005.

[126] A. Weisberg, R.E. Lakis, M.F. Simpson, L. Horowitz, J. Craparo, Measuring lanthanide concentrations in molten salt using laser-induced breakdown spectroscopy (LIBS), Appl. Spectrosc. 68 (2014) 937–48. doi:10.1366/13-07390.

[127] F.R. Doucet, G. Lithgow, R. Kosierb, P. Bouchard, M. Sabsabi, Determination of isotope ratios

using Laser-Induced Breakdown Spectroscopy in ambient air at atmospheric pressure for nuclear forensics, J. Anal. At. Spectrom. 26 (2011) 536–541. doi:10.1039/c0ja00199f.

[128] M. Robel, M.J. Kristo, Discrimination of source reactor type by multivariate statistical analysis of uranium and plutonium isotopic concentrations in unknown irradiated nuclear fuel material, J. Environ. Radioact. 99 (2008) 1789–1797. doi:10.1016/j.jenvrad.2008.07.004.

[129] D.A. Cremers, R.C. Chinni, Laser-Induced Breakdown Spectroscopy—Capabilities and Limitations, Appl. Spectrosc. Rev. 44 (2009) 457–506. doi:10.1080/05704920903058755.

[130] J.-H. Yang, S.-J. Choi, J.J. Yoh, Towards reconstruction of overlapping fingerprints using plasma spectroscopy, Spectrochim. Acta - Part B At. Spectrosc. 134 (2017) 25–32. doi:10.1016/j.sab.2017.06.001.

[131] A. Sarkar, X. Mao, R.E. Russo, Advancing the analytical capabilities of laser ablation molecular isotopic spectrometry for boron isotopic analysis, Spectrochim. Acta - Part B At. Spectrosc. 92 (2014) 42–50. doi:10.1016/j.sab.2013.12.001.

[132] F.C. De Lucia, J.L. Gottfried, C.A. Munson, A.W. Miziolek, Double pulse laser-induced breakdown spectroscopy of explosives: Initial study towards improved discrimination, Spectrochim. Acta - Part B At. Spectrosc. 62 (2007) 1399–1404. doi:10.1016/j.sab.2007.10.036.

[133] J.L. Gottfried, F.C. De Lucia, C.A. Munson, A.W. Miziolek, Double-pulse standoff laser-induced breakdown spectroscopy for versatile hazardous materials detection, Spectrochim. Acta - Part B At. Spectrosc. 62 (2007) 1405–1411. doi:10.1016/j.sab.2007.10.039.

[134] G. Lorenzetti, S. Legnaioli, E. Grifoni, S. Pagnotta, V. Palleschi, Laser-based continuous monitoring and resolution of steel grades in sequence casting machines, Spectrochim. Acta - Part B At. Spectrosc. 112 (2015) 1–5. doi:10.1016/j.sab.2015.07.006.

[135] B. Bhatt, A. Dehayem-Kamadjeu, K.H. Angeyo, Rapid nuclear forensics analysis via machine-learning-enabled laser-induced breakdown spectroscopy (LIBS), AIP Conf. Proc. 060006 (2019) 1–4. doi:10.1063/1.5110124.

[136] A. Ciucci, M. Corsi, V. Palleschi, S. Rastelli, A. Salvetti, E. Tognoni, New Procedure for Quantitative Elemental Analysis by Laser-Induced Plasma Spectroscopy, Appl. Spectrosc. 53 (1999) 960–964. doi:10.1366/0003702991947612.

[137] D.W. Hahn, N. Omenetto, Laser-induced breakdown spectroscopy (LIBS), part II: Review of

instrumental and methodological approaches to material analysis and applications to different fields, Appl. Spectrosc. 66 (2012) 347–419. doi:10.1366/11-06574.

[138] E. Tognoni, G. Cristoforetti, S. Legnaioli, V. Palleschi, Calibration-Free Laser-Induced Breakdown Spectroscopy: State of the art, Spectrochim. Acta - Part B At. Spectrosc. 65 (2010) 1–14. doi:10.1016/j.sab.2009.11.006.

[139] G.H. Cavalcanti, D. V Teixeira, S. Legnaioli, G. Lorenzetti, L. Pardini, V. Palleschi, One-point calibration for calibration-free laser-induced breakdown spectroscopy quantitative analysis, Spectrochim. Acta - Part B At. Spectrosc. 87 (2013) 51–56. doi:10.1016/j.sab.2013.05.016.

[140] G.S. Senesi, G. Tempesta, P. Manzari, G. Agrosì, An Innovative Approach to Meteorite Analysis by Laser-Induced Breakdown Spectroscopy, Geostand. Geoanalytical Res. 40 (2016) 533–541. doi:10.1111/ggr.12126.

[141] C. Aragón, J.A. Aguilera, CSigma graphs: A new approach for plasma characterization in laser-induced breakdown spectroscopy, J. Quant. Spectrosc. Radiat. Transf. 149 (2014) 90–102. doi:10.1016/j.jqsrt.2014.07.026.

[142] C. Aragón, J.A. Aguilera, Quantitative analysis by laser-induced breakdown spectroscopy based on generalized curves of growth, Spectrochim. Acta - Part B At. Spectrosc. 110 (2015) 124–133. doi:10.1016/j.sab.2015.06.010.

[143] H.R. Griem, Spectral Line Broadening by Plasmas, Academic Press, New York, 1974. https://griem.obspm.fr/index.php?page=accueil.php.

[144] G.C.-Y. Chan, I. Choi, X. Mao, V. Zorba, O.P. Lam, D.K. Shuh, R.E. Russo, Isotopic determination of uranium in soil by laser induced breakdown spectroscopy, Spectrochim. Acta - Part B At. Spectrosc. 122 (2016) 31–39. doi:10.1016/j.sab.2016.05.014.

[145] M.C. Phillips, B.E. Brumfield, N. Lahaye, S.S. Harilal, K.C. Hartig, I. Jovanovic, Two-dimensional fluorescence spectroscopy of uranium isotopes in femtosecond laser ablation plumes, Sci. Rep. 7 (2017) 1–12. doi:10.1038/s41598-017-03865-9.

[146] I. Choi, G.C.Y. Chan, X. Mao, D.L. Perry, R.E. Russo, Line selection and parameter optimization for trace analysis of uranium in glass matrices by laser-induced breakdown spectroscopy (LIBS), Appl. Spectrosc. 67 (2013) 1275–1284. doi:10.1366/13-07066.

[147] H.D. Wizemann, K. Niemax, Isotope selective element analysis by diode laser atomic absorption spectrometry, Mikrochim. Acta. 129 (1998) 209–216. doi:10.1007/bf01244743.

[148] S.S. Harilal, B.E. Brumfield, N.L. Lahaye, K.C. Hartig, M.C. Phillips, Optical spectroscopy of laser-produced plasmas for standoff isotopic analysis, Appl. Phys. Rev. 5 (2018) 1–32. doi:10.1063/1.5016053.

[149] A. Obrebski, J. Lawrenz, K. Niemax, On the potential and limitations of spectroscopic isotope ratio measurements by resonant Doppler-free two-photon laser enhanced ionization spectroscopy, Spectrochim. Acta - Part B At. Spectrosc. 45 (1990) 15–36. doi:doi:10.1016/0584-8547(90)80079-X.

[150] R.E. Russo, X. Mao, J.J. Gonzalez, V. Zorba, J. Yoo, Laser ablation in analytical chemistry, Anal. Chem. 85 (2013) 6162–77. doi:10.1021/ac4005327.

[151] R.S. Harmon, R.E. Russo, R.R. Hark, Applications of laser-induced breakdown spectroscopy for geochemical and environmental analysis: A comprehensive review, Spectrochim. Acta - Part B At. Spectrosc. 87 (2013) 11–26. doi:10.1016/j.sab.2013.05.017.

[152] L.E. Burkhart, G. Stukenbroeker, S. Adams, Isotope shifts in uranium spectra, Phys. Rev. 75 (1949) 83–85. doi:10.1103/PhysRev.75.83.

[153] W. Pietsch, A. Petit, A. Briand, Isotope ratio determination of uranium by optical emission spectroscopy on a laser-produced plasma - basic investigations and analytical results, Spectrochim. Acta - Part B At. Spectrosc. 53 (1998) 751–761. doi:10.1016/S0584-8547(97)00123-7.

[154] H. Niki, T. Yasuda, I. Kitazima, Measurement Technique of Boron Isotopic Ratio by Laser-induced Breakdown Spectroscopy, J. Nucl. Sci. Technol. 35 (1998) 34–39. doi:10.1080/18811248.1998.9733817.

[155] C.A. Smith, M.A. Martinez, D.K. Veirs, D.A. Cremers, Pu-239/Pu-240 isotope ratios determined using high resolution emission spectroscopy in a laser-induced plasma, Spectrochim. Acta - Part B At. Spectrosc. 57 (2002) 929–937. doi:10.1016/S0584-8547(02)00023-X.

[156] L. Mercadier, J. Hermann, C. Grisolia, A. Semerok, Plume segregation observed in hydrogen and deuterium containing plasmas produced by laser ablation of carbon fiber tiles from a fusion reactor, Spectrochim. Acta - Part B At. Spectrosc. 65 (2010) 715–720. doi:10.1016/j.sab.2010.04.011.

[157] A. D'Ulivo, M. Onor, E. Pitzalis, R. Spiniello, L. Lampugnani, G. Cristoforetti, S. Legnaioli, V. Palleschi, A. Salvetti, E. Tognoni, Determination of the deuterium/hydrogen ratio in gas

reaction products by laser-induced breakdown spectroscopy, Spectrochim. Acta - Part B At. Spectrosc. 61 (2006) 797–802. doi:10.1016/j.sab.2006.06.001.

[158] M. Burger, P.J. Skrodzki, L.A. Finney, J. Hermann, J. Nees, I. Jovanovic, Isotopic analysis of deuterated water via single- and double-pulse laser-induced breakdown spectroscopy, Phys. Plasmas. 25 (2018). doi:10.1063/1.5042665.

[159] P.K. Morgan, J.R. Scott, I. Jovanovic, Hybrid interferometric/dispersive atomic spectroscopy of laser-induced uranium plasma, Spectrochim. Acta - Part B At. Spectrosc. 116 (2016) 58–62. doi:10.1016/j.sab.2015.12.006.

[160] A.J. Effenberger, J.R. Scott, Practical high-resolution detection method for laser-induced breakdown spectroscopy., Appl. Opt. 51 (2012) B165-70. doi:10.1364/AO.51.00B165.

[161] R.E. Russo, A.A. Bol'shakov, X. Mao, C.P. McKay, D.L. Perry, O. Sorkhabi, Laser Ablation Molecular Isotopic Spectrometry, Spectrochim. Acta - Part B At. Spectrosc. 66 (2011) 99–104. doi:10.1016/j.sab.2011.01.007.

[162] X. Mao, A.A. Bol'shakov, D.L. Perry, O. Sorkhabi, R.E. Russo, Laser Ablation Molecular Isotopic Spectrometry: Parameter influence on boron isotope measurements, Spectrochim. Acta - Part B At. Spectrosc. 66 (2011) 604–609. doi:10.1016/j.sab.2011.06.007.

[163] X. Mao, A.A. Bol'shakov, I. Choi, C.P. McKay, D.L. Perry, O. Sorkhabi, R.E. Russo, Laser Ablation Molecular Isotopic Spectrometry: strontium and its isotopes, Spectrochim. Acta - Part B At. Spectrosc. 66 (2011) 767–775. doi:10.1016/j.sab.2011.12.002.

[164] A.A. Bol'shakov, X. Mao, D.L. Perry, R.E. Russo, Laser Ablation Molecular Isotopic Spectrometry for Rare Isotopes of the Light Elements, Spectroscopy. 29 (2014). doi:10.13140/2.1.3062.3364.

[165] P. Ran, H. Hou, S.N. Luo, Molecule formation induced by non-uniform plume-air interactions in laser induced plasma, J. Anal. At. Spectrom. 32 (2017) 2254–2262. doi:10.1039/c7ja00287d.

[166] A. Sarkar, X. Mao, G.C.Y. Chan, R.E. Russo, Laser ablation molecular isotopic spectrometry of water for 1D2/1H1 ratio analysis, Spectrochim. Acta - Part B At. Spectrosc. 88 (2013) 46–53. doi:10.1016/j.sab.2013.08.002.

[167] S. Brown, A. Ford, C.C. Akpovo, J. Martinez, L. Johnson, Matrix effects in laser ablation molecular isotopic spectrometry, Spectrochim. Acta - Part B At. Spectrosc. 101 (2014) 204–

212. doi:10.1016/j.sab.2014.09.003.

[168] M. Dong, X. Mao, J.J. Gonzalez, J. Lu, R.E. Russo, Carbon isotope separation and molecular formation in laser-induced plasmas by laser ablation molecular isotopic spectrometry, Anal. Chem. 85 (2013) 2899–2906. doi:10.1021/ac303524d.

[169] M. Dong, G.C.Y. Chan, X. Mao, J.J. Gonzalez, J. Lu, R.E. Russo, Elucidation of C2 and CN formation mechanisms in laser-induced plasmas through correlation analysis of carbon isotopic ratio, Spectrochim. Acta - Part B At. Spectrosc. 100 (2014) 62–69. doi:10.1016/j.sab.2014.08.009.

[170] A.A. Bol'shakov, X. Mao, J. Jain, D.L. McIntyre, R.E. Russo, Laser ablation molecular isotopic spectrometry of carbon isotopes, Spectrochim. Acta - Part B At. Spectrosc. 113 (2015) 106–112. doi:10.1016/j.sab.2015.08.007.

[171] H. Hou, X. Mao, V. Zorba, R.E. Russo, Laser Ablation Molecular Isotopic Spectrometry for Molecules Formation Chemistry in Femtosecond-Laser Ablated Plasmas, Anal. Chem. 89 (2017) 7750–7757. doi:10.1021/acs.analchem.7b01750.

[172] H. Hou, G.C.Y. Chan, X. Mao, R. Zheng, V. Zorba, R.E. Russo, Femtosecond filament-laser ablation molecular isotopic spectrometry, Spectrochim. Acta - Part B At. Spectrosc. 113 (2015) 113–118. doi:10.1016/j.sab.2015.09.014.

[173] H. Hou, G.C.Y. Chan, X. Mao, V. Zorba, R. Zheng, R.E. Russo, Femtosecond laser ablation molecular isotopic spectrometry for zirconium isotope analysis, Anal. Chem. 87 (2015) 4788–4796. doi:10.1021/acs.analchem.5b00056.

[174] X. Mao, G.C.-Y. Chan, I. Choi, V. Zorba, R.E. Russo, Combination of atomic lines and molecular bands for uranium optical isotopic analysis in laser induced plasma spectrometry, J. Radioanal. Nucl. Chem. 312 (2017) 121–131. doi:10.1007/s10967-017-5197-y.

[175] K.C. Hartig, I. Ghebregziabher, I. Jovanovic, Standoff Detection of Uranium and its Isotopes by Femtosecond Filament Laser Ablation Molecular Isotopic Spectrometry, Sci. Rep. 7 (2017) 1–9. doi:10.1038/srep43852.

[176] D.G. Weisz, J.C. Crowhurst, W.J. Siekhaus, T.P. Rose, B. Koroglu, H.B. Radousky, J.M. Zaug, M.R. Armstrong, B.H. Isselhardt, M.R. Savina, M. Azer, M.S. Finko, D. Curreli, Formation of 238U16O and 238U18O observed by time-resolved emission spectroscopy subsequent to laser ablation, Appl. Phys. Lett. 111 (2017). doi:10.1063/1.4991824.

[177] Z.H. Zhu, J.M. Li, Z.Q. Hao, S.S. Tang, Y. Tang, L.B. Guo, X.Y. Li, X.Y. Zeng, Y.F. Lu, Isotopic determination with molecular emission using laser-induced breakdown spectroscopy and laser-induced radical fluorescence, Opt. Express. 27 (2019) 470. doi:10.1364/oe.27.000470.

[178] B.W. Smith, A. Quentmeier, M.A. Bolshov, K. Niemax, Measurement of uranium isotope ratios in solid samples using laser ablation and diode laser-excited atomic fluorescence spectrometry, Spectrochim. Acta - Part B At. Spectrosc. 54 (1999) 943–958. doi:10.1016/S0584-8547(99)00022-1.

[179] K.C. Hartig, I. Ghebregziabher, I. Jovanovic, Remote detection of uranium by fs-filamentation laser ablation molecular isotopic spectrometry, in: 2016 Conf. Lasers Electro-Optics, CLEO 2016, OSA, 2016: pp. 1–2. doi:10.1364/cleo_si.2016.sth1h.5.

[180] K. Niemax, J. Koch, C. Schnürer-Patschan, A. Zybin, Diode laser spectrometry of environmental and industrial samples, in: Proc. SPIE 3758, Appl. Tunable Diode Other Infrared Sources Atmos. Stud. Ind. Process. Monit. II, Denver, Colorado, 1999: pp. 138–141. doi:doi:10.1117/12.366446.

[181] K. Niemax, A. Zybin, C. Schnürer-Patschan, H. Groll, Semiconductor Diode Lasers in Atomic Spectrometry, Anal. Chem. News Featur. 68 (1996) 351A-356A. doi:10.1021/ac961942i.

[182] A. Zybin, C. Schnürer-Patschan, M.A. Bolshov, K. Niemax, Elemental analysis by diode laser spectroscopy, Trends Anal. Chem. 17 (1998) 513–520. doi:10.1016/S0165-9936(98)00063-6.

[183] G. Galbács, A Review of Applications and Experimental Improvements Related to Diode Laser Atomic Spectroscopy, Appl. Spectrosc. Rev. 41 (2006) 259–303. doi:10.1080/05704920600620378.

[184] M.A. Bolshov, Y.A. Kuritsyn, Y. V Romanovskii, Tunable diode laser spectroscopy as a technique for combustion diagnostics, Spectrochim. Acta - Part B At. Spectrosc. 106 (2015) 45–66. doi:10.1016/j.sab.2015.01.010.

[185] R. Hergenröder, K. Niemax, Laser atomic absorption spectroscopy applying semiconductor diode lasers, Spectrochim. Acta - Part B At. Spectrosc. 43 (1988) 1443–1449. doi:doi.org/10.1016/0584-8547(88)80183-6.

[186] D.J. Butcher, A. Zybin, M.A. Bolshov, K. Niemax, Diode laser atomic absorption spectrometry as a detector for metal speciation, Rev. Anal. Chem. 20 (2001) 79–100. doi:10.1515/REVAC.2001.20.2.79.

[187] J. Koch, A. Zybin, K. Niemax, Narrow and broad band diode laser absorption spectrometry - Concepts, limitations and applications, Spectrochim. Acta - Part B At. Spectrosc. 57 (2002) 1547–1561. doi:10.1016/S0584-8547(02)00104-0.

[188] A. Zybin, J. Koch, H.D. Wizemann, J. Franzke, K. Niemax, Diode laser atomic absorption spectrometry, Spectrochim. Acta - Part B At. Spectrosc. 60 (2005) 1–11. doi:10.1016/j.sab.2004.10.001.

[189] A. Quentmeier, M.A. Bolshov, K. Niemax, Measurement of uranium isotope ratios in solid samples using laser ablation and diode laser-atomic absorption spectrometry, Spectrochim. Acta - Part B At. Spectrosc. 56 (2001) 45–55. doi:10.1016/S0584-8547(00)00289-5.

[190] H. Liu, A. Quentmeier, K. Niemax, Diode laser absorption measurement of uranium isotope ratios in solid samples using laser ablation, Spectrochim. Acta - Part B At. Spectrosc. 57 (2002) 1611–1623.

[191] J. Lawrenz, A. Obrebski, K. Niemax, Measurement of isotope ratios by Doppler-free laser spectroscopy applying semiconductor diode lasers and thermionic diode detection, Anal. Chem. 59 (1987) 1232–1236.

[192] L.A. King, I.B. Gornushkin, D. Pappas, B.W. Smith, J.D. Winefordner, Rubidium isotope measurements in solid samples by laser ablation-laser atomic absorption spectroscopy, Spectrochim. Acta - Part B At. Spectrosc. 54 (1999) 1771–1781. doi:10.1016/S0584-8547(99)00140-8.

[193] B.W. Smith, I.B. Gornushkin, L.A. King, J.D. Winefordner, A laser ablation–atomic fluorescence technique for isotopically selective determination of lithium in solids, Spectrochim. Acta - Part B At. Spectrosc. 53 (1998) 1131–1138. doi:10.1016/S0584-8547(98)00132-3.

[194] N.R. Taylor, M.C. Phillips, Differential laser absorption spectroscopy of uranium in an atmospheric pressure laser-induced plasma, Opt. Lett. 39 (2014) 594–597. doi:10.1364/OL.39.000594.

[195] N.R. Taylor, M.C. Phillips, Measurements of Uranium Line Widths and Pressure Broadening Coefficients in Atmospheric Pressure Laser- Induced Plasmas, CLEO 2013. paper CTu2 (2013) CTu2H.2. doi:10.1364/CLEO_SI.2013.CTu2H.2.

[196] P.J. Skrodzki, N.P. Shah, N. Taylor, K.C. Hartig, N.L. LaHaye, B.E. Brumfield, I. Jovanovic, M.C. Phillips, S.S. Harilal, Significance of ambient conditions in uranium absorption and emission

features of laser ablation plasmas, Spectrochim. Acta - Part B At. Spectrosc. 125 (2016) 112–119. doi:10.1016/j.sab.2016.09.012.

[197] S.S. Harilal, N.L. LaHaye, M.C. Phillips, Two-dimensional fluorescence spectroscopy of laser-produced plasmas, Opt. Lett. 41 (2016) 3547. doi:10.1364/OL.41.003547.

[198] I. Coddington, N. Newbury, W. Swann, Dual-comb spectroscopy, Optica. 3 (2016) 414. doi:10.1364/optica.3.000414.

[199] J. Bergevin, T.H. Wu, J. Yeak, B.E. Brumfield, S.S. Harilal, M.C. Phillips, R.J. Jones, Dual-comb spectroscopy of laser-induced plasmas, Nat. Commun. 9 (2018) 1–6. doi:10.1038/s41467-018-03703-0.

[200] Y. Zhang, C. Lecaplain, R.R.D. Weeks, J. Yeak, S.S. Harilal, M.C. Phillips, R. Jason Jones, Time-resolved dual-comb measurement of number density and temperature in a laser-induced plasma, Opt. Lett. 44 (2019) 3458. doi:10.1364/ol.44.003458.

[201] J. Merten, B. Johnson, Laser continuum source atomic absorption spectroscopy: Measuring the ground state with nanosecond resolution in laser-induced plasmas, Spectrochim. Acta - Part B At. Spectrosc. 139 (2018) 38–43. doi:10.1016/j.sab.2017.11.006.

Chapter 3 - Quantitative prediction of rare earth concentrations in salt matrices using laser-induced breakdown spectroscopy for application to molten salt reactors and pyroprocessing

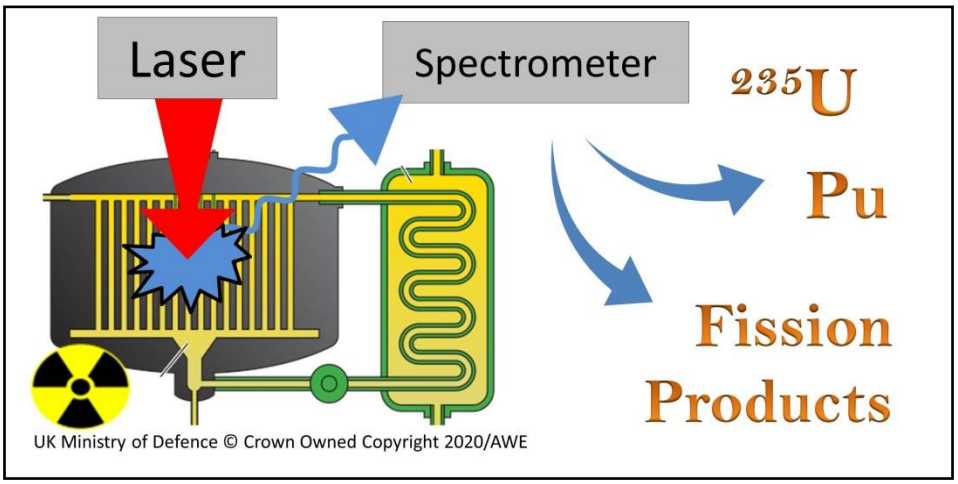

This paper has been published in *Journal of Analytical Atomic Spectroscopy*, Volume 36, Issue 1, pages 92-102, 2021.

DOI: 10.1039/D0JA00352B

Authors: Gregory Hull †[a,b], Hugues Lambert [a,c], Kiran Haroon [a], Paul Coffey [a,b], Timothy Kerry [a,d], Edward D. McNaghten [e], Clint A. Sharrad [a], Philip Martin †[a,b]

a. Department of Chemical Engineering and Analytical Science, University of Manchester, Oxford Road, Manchester, M13 9PL

b. Photon Science Institute, University of Manchester, Oxford Road, Manchester, M13 9PL

c. Lhoist Group – Business Innovation Center, rue de l'industrie 31, 1400 Nivelles, Belgium

d. Department of Materials Science and Engineering, Delft University of Technology, Mekelweg 2, CD Delft, 2628 The Netherlands

e. AWE, Aldermaston, Reading, Berkshire, RG7 4PR

† Corresponding authors

Author contribution: involved with sample preparation procedures with Hugues Lambert; performed all of the experiments with the LIBS apparatus; completed the data pre-processing steps; did the multivariate data analysis techniques together with Kiran Haroon; wrote the paper with some advice from Kiran on the methodology and data interpretation sections for the PLS analysis.

3.1 Abstract

Pyroprocessing of spent nuclear fuels is an electrochemical separation method where spent metallic fuel is dissolved in a molten salt bath to allow uranium (U) and plutonium (Pu) to be isolated from fission products (FPs) and other impurities. This allows the useful materials to be reused in mixed oxide fuel (MOx) or further refined to new reactor fuel. Monitoring the changing concentrations of U, Pu, FPs and other species inside a molten salt vessel presents a unique challenge which laser-induced breakdown spectroscopy (LIBS) may be able to overcome, due to its ability to simultaneously analyse multiple elements using a single measurement with stand-off capability *in situ*. In this study, samples of praseodymium (Pr), holmium (Ho) and erbium (Er) chloride ($LnCl_3$) in LiCl + KCl eutectic (LKE) salt were analysed with LIBS. Multiple laser pulse energies were tested to maximise the signal to background ratio, the best results were obtained at the lowest pulse energy of 85 mJ/pulse. Forward interval Partial Least Squares (iPLS) regression was used to create predicted versus measured concentration models for each element. This method achieved Root Mean Squared Error of Cross Validation (RMSECV) values of between 3.20×10^{-3} and 16.3×10^{-3} $mmol_{Ln}\ g_{LKE}^{-1}$ for single lanthanide samples and 2.84×10^{-3} and 7.62×10^{-3} $mmol_{Ln}\ g_{LKE}^{-1}$ for mixed samples of all three lanthanide elements. Limits of quantification of between 1000 and 9000 ppm suggest LIBS should be a candidate for on-line analysis of elemental concentrations during pyroprocessing.

3.2 Introduction

Reprocessing of nuclear fuels to allow multiple passes of fissile elements through a reactor, increases fuel usage and maximises the energy generated from mined uranium ores [1]. Creating a closed nuclear fuel cycle by reprocessing spent fuel to create fuel pellets of recycled uranium or Mixed Oxide (MOx) fuels improves the sustainability of uranium resources. Currently, the preferred reprocessing technique for oxide fuels is the Plutonium Uranium Reduction Extraction (PUREX) process – a liquid-liquid extraction method [2].

Pyroprocessing is a reprocessing technique that uses a molten salt bath, such as LiCl-KCl eutectic (LKE), to dissolve metallic spent nuclear fuel [3]. A key advantage for using molten salt media is its radiation stability [4] and is consequently considered to be the lead

technique for reprocessing high burn-up/fast reactor fuels where liquid-liquid extraction may not be viable. Currently, pyroprocessing methods have been developed to pilot plant scale [5,6] but have yet to be deployed at process scales. Once the spent fuel is dissolved in a molten salt bath, U is separated from Pu, other actinides and fission products (FPs) using electrochemical methods [7]. By adding extra UCl3 to the molten salt, the isotopic composition of collected U can be controlled, allowing the U to be re-cast to create new fuel rods.

Pyroprocessing was developed for use with integral fast reactors and fast neutron reactors, as these designs allow more tolerance towards impurities in the fuel [4]. Molten salt electrolysis reprocessing is able to achieve such tolerance in a single reprocessing step. This reduces the footprint of the reprocessing facility to such an extent that it can be co-located on a reactor site [8]. Additionally, the molten salts approach provides in-built safety features, such as proliferation resistance and reduced criticality risk [9].

Ideally, the concentration of the different species in a molten salt solution would be tracked as the electrochemical separation takes place during pyroprocessing. However, the use of spectroscopic methods such as fluorescence spectroscopy, absorption spectroscopy and Raman spectroscopy for this purpose have all proved difficult due to a variety of factors [10]. For example, research carried out by Schroll et al [10] using UV-vis absorption spectroscopy, showed a dependence of the molar absorptivity of lanthanides on temperature.

Laser-induced breakdown spectroscopy (LIBS) is an analytical technique which could be used to monitor pyroprocessing. In this approach, a high energy laser pulse is focused onto the sample surface to generate a luminous plasma. The plasma is formed as a result of the extreme temperature within a small volume and typically contains nano- to micrograms of the ablated material. The excited atomic and ionic species in the plasma cool and relax over a few hundred μs, emitting characteristic wavelengths of light which are collected and analysed using a spectrometer. The technique requires no sample preparation and has a fast repetition rate (typically 10 Hz), which leads to high sample throughput and enables on-line analysis. Additionally, laser-based analysis requires only line-of-sight as opposed to traditional techniques which require physical access for sample collection. The laser

radiation can be directed through access windows (such as lead-shielded glass or quartz) to the sample and the emission from the plasma can be collected using fibre optics. This enables in situ analysis of hazardous material and dangerous environments whilst shielding the instrumentation and machine-operator, and also reduces the costs associated with sample collection, transportation, storage, analysis and disposal. The possibility for stand-off and remote measurements with LIBS makes the technique very attractive for the analysis of hazardous materials and environments, for example for applications nuclear fission [11,12] and fusion [13,14]. Finally, the ability to simultaneously measure all elemental constituents using a single measurement simplifies the analysis considerably.

The capability of the LIBS technique to simultaneously record numerous emission lines from multiple elements permits the use of multivariate data analysis tools [15–17]. Elements and lines of interest can be identified using spectral databases, such as the NIST Atomic Spectra database [18]. Difficulties associated with overlapping peaks in the spectra can be overcome by using a high-resolution spectrometer. Traditionally LIBS has not been able to achieve the figures of merit associated with other techniques such as mass spectrometry, X-ray Fluorescence (XRF) and gamma spectroscopy. However, use of multivariate data analysis techniques has improved the analytical capabilities of LIBS. Moreover, the benefits of in situ, standoff, on-line, multi-elemental analysis with LIBS outweigh the higher performance of more traditional techniques in industrial applications.

LIBS has been used to analyse various types of solid [15,19–24], liquid [17,25–30] and aerosol [31,32] samples containing rare earth and actinide elements. Research on using LIBS for analysing salt matrices for pyroprocessing or molten salt reactors has been led by the Phongikaroon group [15,26,31,32] (based in Virginia, USA). They have demonstrated how multivariate analysis tools can be used to great effect with rare earth and actinide spectra. Williams et al [15] reported Root Mean Squared Error of Cross-Validation (RMSECV) values of less than 0.30 wt% for solid Ce and Gd samples in solid salt matrices using Partial Least Squares regression (PLS) models. Williams and Phongikaroon [32] also reported RMSECV values of 0.085 wt% for U in aerosolised molten salt with PLS modelling. Elsewhere in the USA, Weisberg et al [17] previously used PLS modelling to predict Eu and Pr concentrations in molten salt samples, with root mean square error of prediction (RMSEP) values of 0.13 % for both elements.

The work presented here demonstrates the use of LIBS in combination with new approaches to multivariate data analysis to predict more accurate lanthanide concentrations in quenched LKE matrices. Solid salt samples of praseodymium (Pr), holmium (Ho) and erbium (Er) in known concentrations were used to construct Principal Component Analysis (PCA) and PLS models. More detailed examinations of the effects of laser pulse energy and normalisation on the LIBS spectra are made here. Mixed lanthanide samples containing all three elements at differing concentrations were also investigated to more accurately represent a field-relevant scenario.

3.3 Experimental

3.3.1 Chemicals and Materials

To prepare the salt samples, a known molar amount of lanthanide chloride ($LnCl_3$) was mixed with LKE salt and melted at 700 °C for 18 hours in a ceramic crucible. Cylinders of each sample were created by withdrawing aliquots of the molten solution into a quartz tube using a syringe and allowing the solution to immediately quench in the tube. The mass of the removed quenched melt was measured after each withdrawal. To create additional concentrations of lanthanide, after each withdrawal, known masses of solid LKE salt were added and the mixture left to melt. Five different concentrations of Ho and four of both Pr and Er were used in this study. The concentration of each sample, measured by mass balance, is shown in Table 3.1.

Table 3.1. Lanthanide concentrations of single-lanthanide samples ($mmol_{Ln}\ g_{LKE}^{-1}$)

	Lanthanide concentration ($mmol_{Ln}\ g_{LKE}^{-1}$)				
Element	1	2	3	4	5
Pr	0.2354	0.1955	0.1405	0.0868	
Ho	0.1694	0.1233	0.0808	0.0400	0.0258
Er	0.1582	0.0764	0.0390	0.0259	

Mixed lanthanide samples were prepared by mixing known molar amounts of $PrCl_3$, $HoCl_3$, $ErCl_3$ and LKE in one crucible before melting as above. Four mixed samples were created -

the concentrations are shown in Table 3.2. The chemical homogeneity of the mixed samples was not measured, but as the samples were left in a hot crucible overnight before being withdrawn, mixing was assumed to be complete. No chemical inhomogeneities were detected during the analysis.

Table 3.2. Lanthanide concentrations of mixed-lanthanide samples ($mmol_{Ln}\ g_{LKE}^{-1}$)

	Lanthanide concentration ($mmol_{Ln}\ g_{LKE}^{-1}$)			
Element	Mix Ln1	Mix Ln2	Mix Ln3	Mix Ln4
Pr	0.4884	0.3143	0.2076	0.3134
Ho	0.1633	0.2544	0.1774	0.2096
Er	0.1789	0.0697	0.2249	0.2640

Each measurement consisted of between six and thirty repeat shots at different points on the sample surface. Recording the same number of shots on each sample was not possible because some of the samples had deteriorated as a result of exposure to moisture and no longer displayed any flat, featureless surfaces suitable for repeat analyses. LIBS data were recorded under an argon atmosphere at ambient temperature and atmospheric pressure. The samples were placed in an air-tight sample cell for analysis in order to reduce exposure to moisture and to minimise operator-exposure to the ablation products. This cell consisted of a stainless steel spherical square (Scanwell/Kimball Physics, internal diameter 3.6 in, six conflat attachments with annealed copper gaskets) with 2 mm thick quartz windows to allow radiation from the Nd:YAG laser to access the sample, and for emitted light to pass through. To fill the sample cell, the lid was loosely rested on the surface of the cell and argon gas flushed through using a Swagelok adaptor for 30 seconds, after which the lid was securely attached and the input vent sealed.

The samples were kept in position during ablation using adhesive pads. As the samples were cylindrical, the stage was positioned before each measurement to ensure that the laser radiation was focused onto the top of the tube. This maintained the highest possible pulse energy at the sample surface, and ensured the samples were at the same height with

respect to the laser focal point. A photograph of the sample cell with samples in place, along with a schematic, is presented in Figure 3.1.

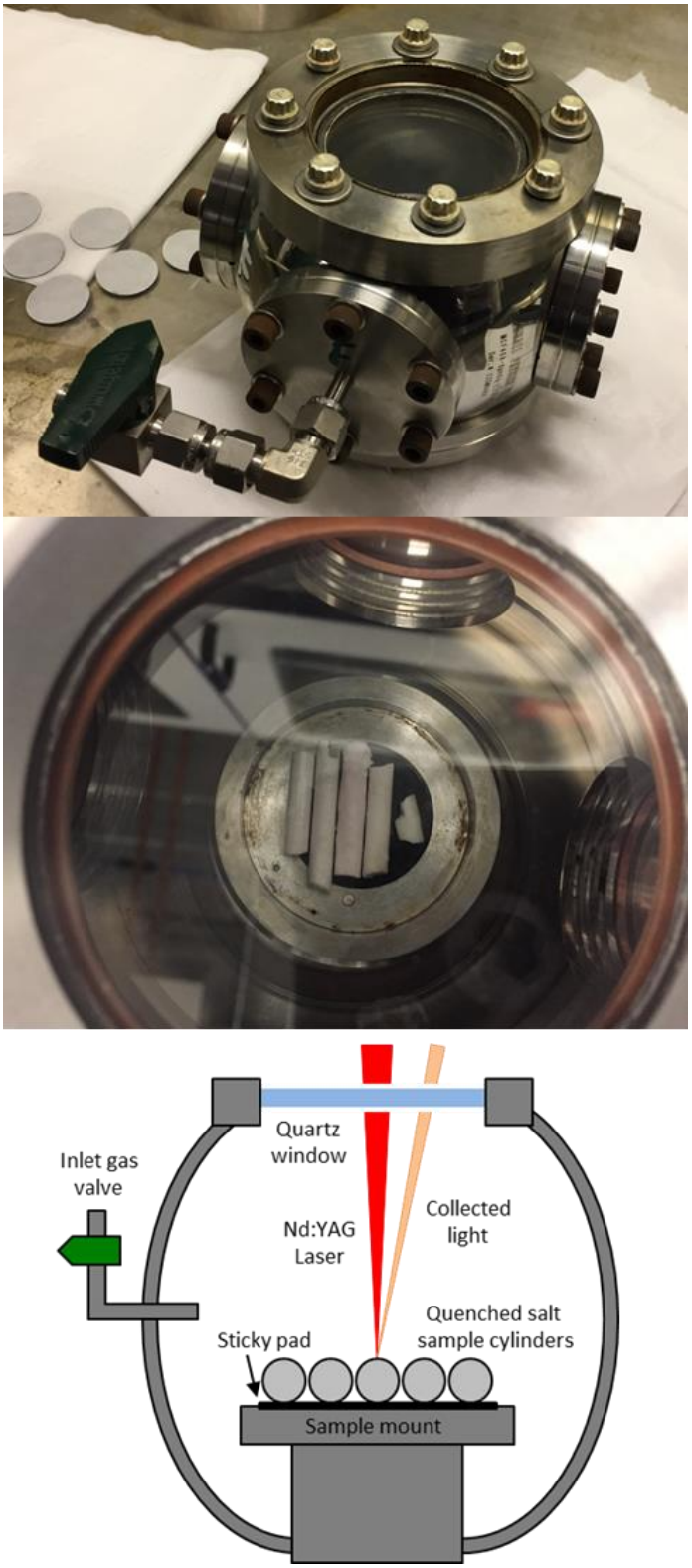

Figure 3.1. Air tight sample cell (top) with cylindrical samples inserted (middle), and schematic of samples during measurement (bottom)

3.3.2 Instrumentation

The experimental setup consisted of a Nd:YAG laser (Innolas Spitlight 600) operating at its fundamental wavelength (1064 nm) with a pulse duration of 7 ns and a repetition rate of 10 Hz, and an Echelle spectrometer (LTB Aryelle Butterfly) with ICCD camera (Andor iStar series). A labelled photograph and schematic of the system are shown in Figure 3.2. The beam delivery periscope system, sample chamber, sample cell and LIBS module were manufactured by Applied Photonics Ltd. Sophi software by LTB was used to control the laser, spectrometer and camera during analysis. The camera settings used were as follows: MCP gain, 150; gate delay, 1500 ns; gate width, 100 µs.

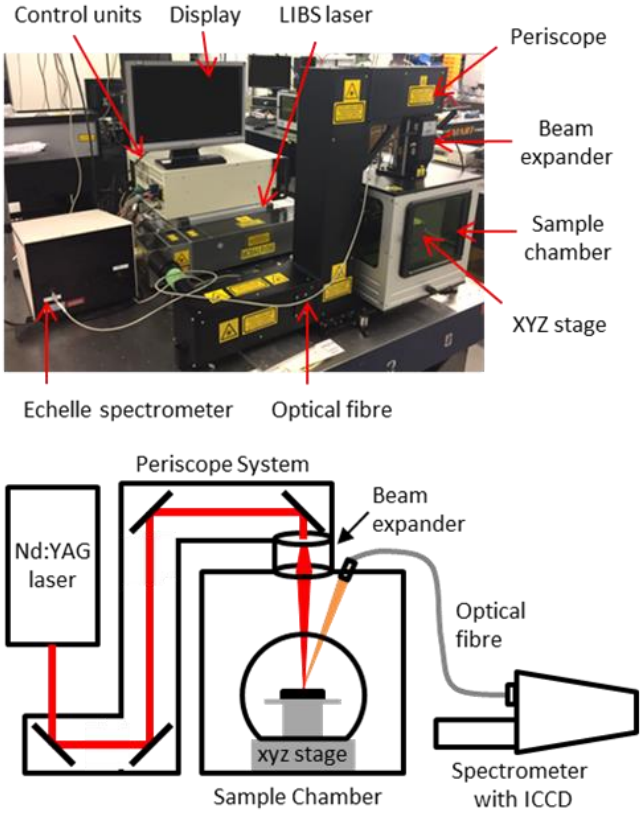

Figure 3.2.Photograph and schematic of LIBS experimental setup

The pulse energy of the laser could be varied between 85 mJ/pulse to 220 mJ/pulse (as measured with a Gentec-eo UNO laser power meter), which gave a power-density of 2.46 × 10^{10} W cm^{-2} to 6.40 × 10^{10} W cm^{-2} at the sample-surface (using spot size of 0.25 mm which was measured from post-ablated samples). To control the pulse energy, the voltage supplied to the flashlamp was modulated between 540 and 620 V (minimum and maximum

settings respectively). There was no observed change in laser pulse diameter or energy distribution at different flashlamp settings. In order to understand how the laser pulse energy affected the light emission, each single-element sample was initially tested at five different pulse energies: 85, 119, 153, 186 and 220 mJ/pulse.

3.3.3 Data pre-processing and multivariate analysis

After each measurement, the recorded spectrum was exported into csv format using a Python macro and normalised with respect to a matrix peak (Li I at 497.170 nm) with a bespoke LabView (National Instruments) Virtual Instrument (VI). This Li signal was chosen as it displayed a single peak (unlike most other Li emissions which exhibited self-absorption or self-reversal) and was in the same area of the spectrum as the majority of the lanthanide emission lines. For normalisation, a fit of two Lorentzian peaks was performed – the Li I line at 497.170 and two overlapping lanthanide lines (Pr I and Er I) at 497.600 nm (shown in Figure 3.3) – and the whole spectrum divided by the maximum intensity of the Li I fit. A similar methodology and choice of normalisation peak was reported by Williams et al [15].

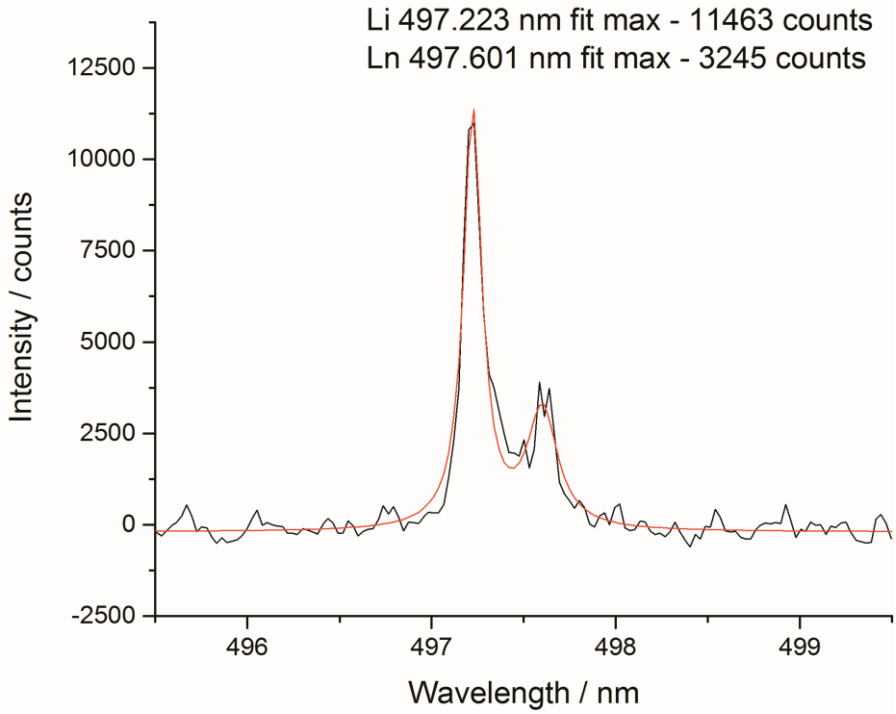

Figure 3.3. Lorentzian fit of normalisation peak (Li I 497.170 nm) and lanthanide element peak

To demonstrate the need for normalisation, charts of intensity at various emission peaks (for Er at 85 mJ/pulse) are shown below in Figure 3.4. The upper chart shows the absolute intensity as recorded by the spectrometer, whereas the lower shows the intensity normalised against the Li line at 497.170 nm. Normalising the data leads to an observable increase in emission intensity with increasing concentration, in contrast to the absolute data which shows discrepancies away from this trend. The positive correlation of the normalised signal intensity to concentration resulted in improved modelling results.

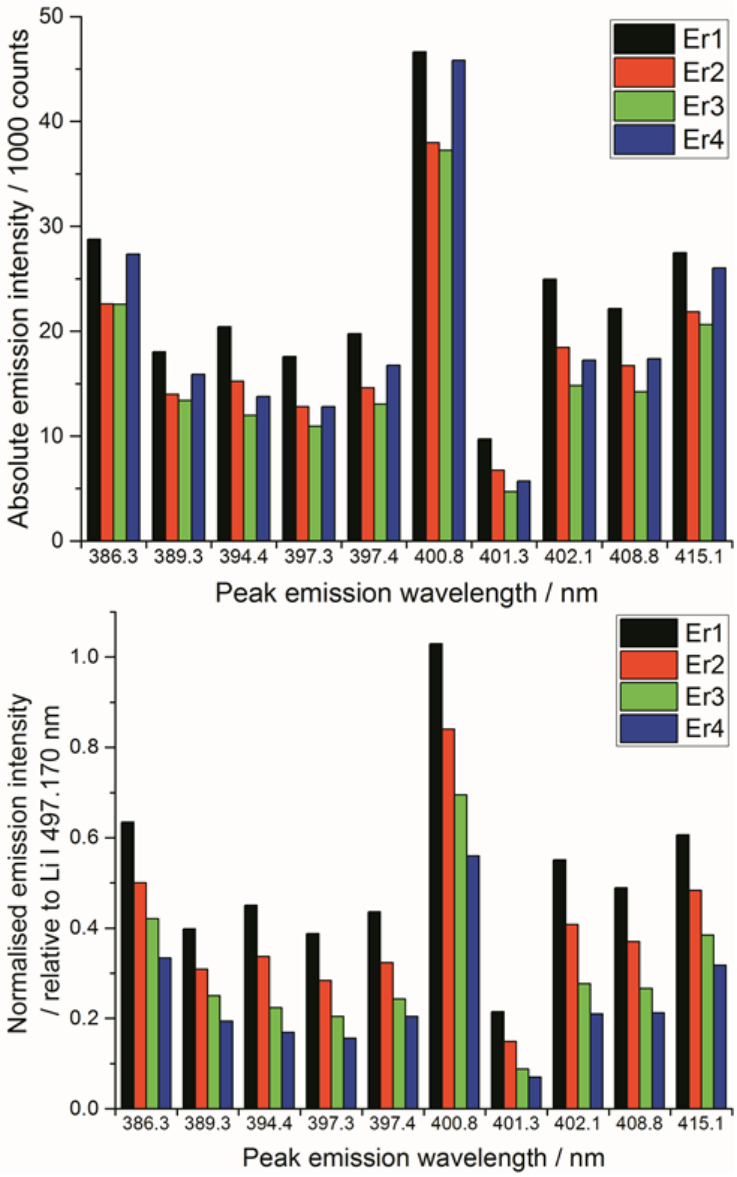

Figure 3.4. Comparison of Er emission line peak intensities with absolute intensity (above) and relative intensity (below) for four samples of erbium (Er1 = 0.158, Er2 = 0.076, Er3 = 0.039, Er 4 = 0.026 $mmol_{Er}\ g_{LKE}^{-1}$)

The Echelle spectrometer design generates an artificial intensity bias for wavelengths that fall in the centre of its pixel grid, meaning that across each order of the spectrometer there is an intensity maximum at the centre of that wavelength range. This artificially inflates the number of counts at certain periodic positions in each spectrum which increased the error of concentration models. This effect was particularly noticeable in the blank sample analyses. Since the Echelle orders are fixed at certain wavelength and pixel positions, a simple third-order fit of each order could be easily applied to all of the spectra in a dataset. To maintain the information contained in the spectral peaks whilst removing the artificial bias for the pixels at the centre of the camera grid, the fitted curve ignored vales above 1.5 times the mean for each region. One Echelle order of a blank sample is shown in Figure 3.5, along with the third order fit and resulting corrected spectrum. All repeated measurements on the same sample were then averaged together.

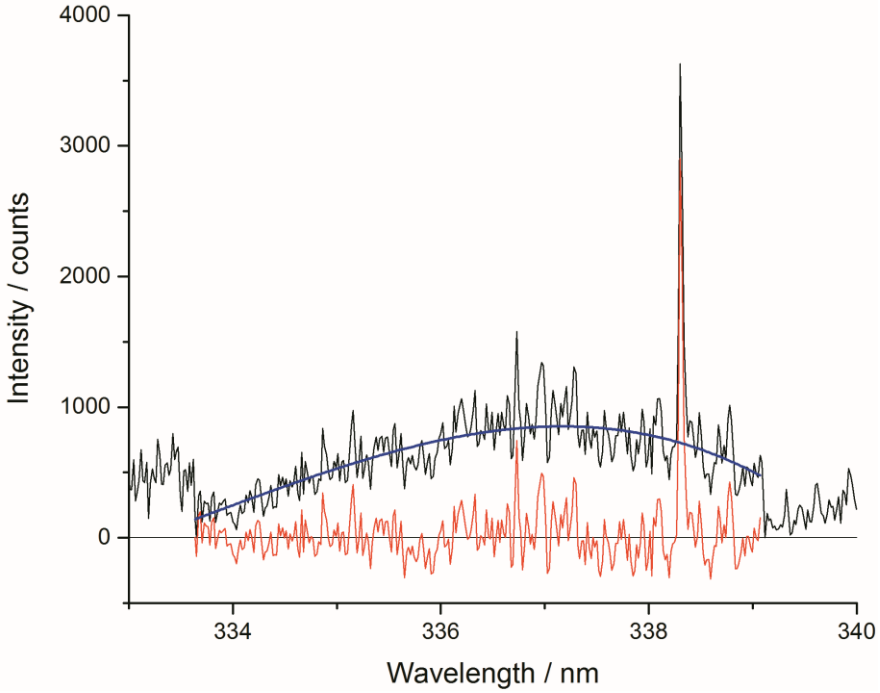

Figure 3.5. Example of Echelle order intensity bias between 332.8 and 339.2 nm (black - pre-treated spectrum; blue - third order fit; red - resulting treated spectrum)

Applying a Savitzky-Golay filter to each spectrum was tested both before and after normalisation with various combinations of side points and polynomial orders. However, the signal quality was not noticeably improved, and the processing time for normalisation

was increased from 0.1 second per spectrum to around 10 seconds per spectrum with the filter. The spectra were therefore analysed without any smoothing.

Using forward interval PLS (iPLS) (PLS Toolbox [Matlab]), predicted versus measured concentration models were plotted (using 'leave-one-out' cross-validation) for each set of single lanthanide samples and for each of the three elements present in the mixed samples. An interval of 15 data points proved adequate to create accurate models for all of the analyses bar one (mixed lanthanide samples, Pr model), where the window was reduced to 5 points to improve the quality of the results.

3.4 Results and discussion

Preliminary experiments varying the laser pulse energy were carried out to identify the settings which maximised the signal to background ratio. After the best pulse energy and sampling techniques had been determined, further experiments were undertaken to analyse the full set of both single and mixed lanthanide samples for PLS concentration modelling.

Figure 3.6 shows an example spectral region of 385 to 391 nm and the high density of emission lines present. For the preliminary (laser pulse energy) experiments, the peak intensity data (from known emission lines) was used to ascertain the signal to background ratio, whereas for the concentration modelling experiments the whole spectrum was used for iPLS.

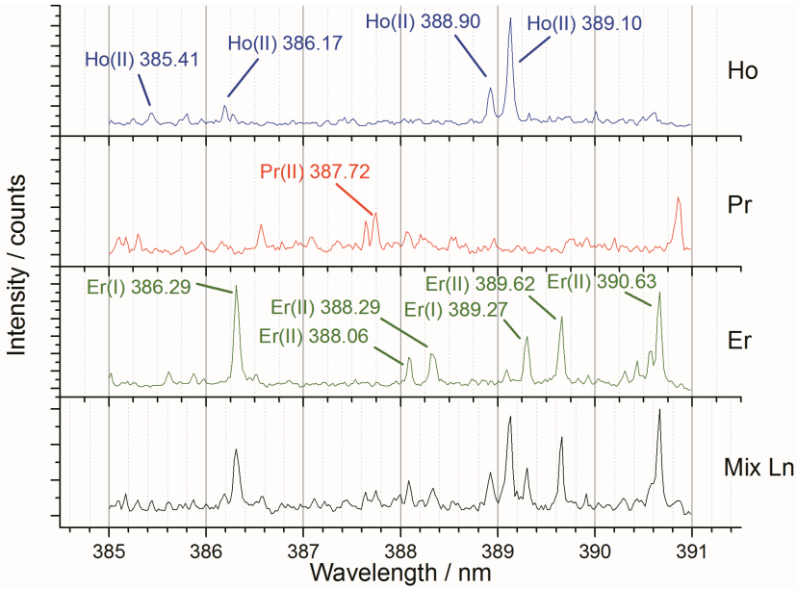

Figure 3.6. Annotated averaged LIBS spectra showing single lanthanide samples and a mixed lanthanide sample for the 385 to 391 nm window (recorded at 85 mJ/pulse)

3.4.1 Laser pulse energy

The quality of LIBS spectra can be adversely affected by line broadening mechanisms which occur in the plasma, i.e. Doppler broadening and Stark broadening. Additionally, in this experiment, signal intensities changed markedly from shot-to-shot on the same spot of sample for both Li and lanthanide emission lines. We believe this may be because a relatively large amount of material was ablated by each laser shot, particularly at higher pulse energies, due to the relatively low density of the samples. Ablating greater amounts of sample from one spot lowered the height of the local sample surface and moved it out from the focal point of the laser radiation, thereby resulting in less material being ablated and thus reducing the emission intensity [15,32]. Visual inspection of the samples indicated the ablation-craters were significantly larger for the higher pulse energies. Additionally, some of the ablation products were deposited on the sample chamber window, which reduced the power density at the sample surface [32,33]. This effect was significantly worse at higher pulse energies, due to the increased amount of material ablated. The sample chamber window was cleaned after every experiment (i.e. every new sample or new pulse energy) to ensure the consistency of the analyses.

The normalised spectral results, presented in Figure 3.7, were obtained by using the ratio of lanthanide peak intensity to Li emission, and show a negative correlation between pulse energy and intensity, as indicated by the Pr1 emission. This is unexpected, as one would assume an equal ratio of Li and lanthanide are ablated with each shot on the same sample, independent of the total amount of material. It is possible that the Li peak chosen for normalisation was slightly affected by self-absorption, whereas the very intense 610 and 671 nm Li emissions showed obvious self-reversal, the 497.170 nm line did not appear to be affected. The changing pulse energy did not appear to have any effect on the RSD of the lanthanide emission intensity after normalisation against the lithium peak.

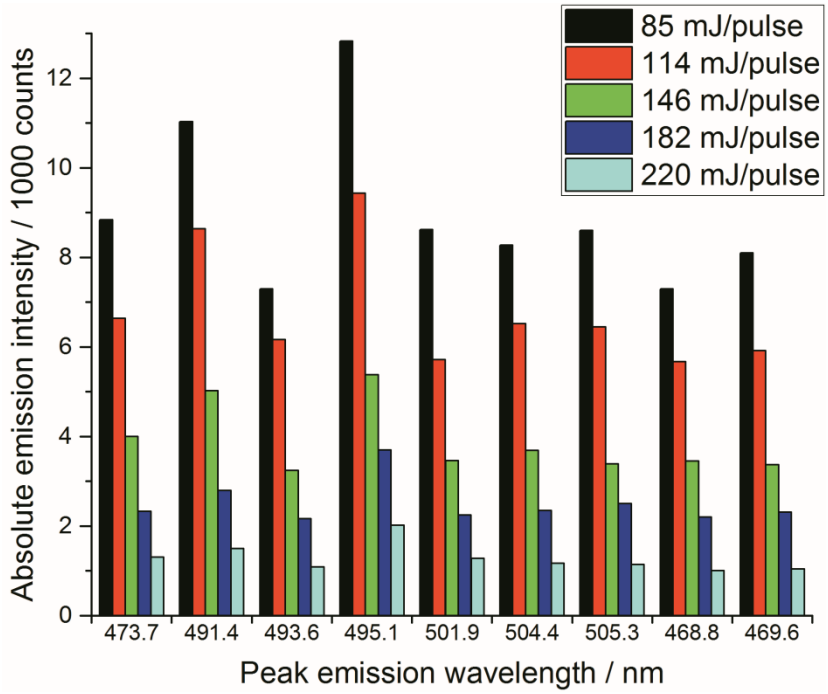

Figure 3.7. Comparison of selected Pr emission line intensities at various pulse energies (average of 30 shots at each pulse energy)

Principal Component Analysis (PCA) was used to further investigate the effect of pulse energy on the lanthanide emission spectra. The lanthanide emission peak-intensities were extracted from the averaged data for each single lanthanide sample at several pulse energies and used to construct PCA models. A full list of the emission peaks used is provided in Table 3.3. Figure 3.8 shows highest concentration samples for Ho, Pr and Er measured at variable pulse energies (from 85 mJ/pulse up to 220 mJ/pulse). Each group of elements appears as an independent cluster. Additionally, the model is completely explained by three

components (t[1] = 49%, t[2] = 40%, t[3] = 10 %). For each of the three elements, the samples with the greatest separation were measured at the lowest pulse energy. Indeed, for each set of measurements there is a linear distribution emanating from the centre of the plot, with distance from the centre increasing with decreasing pulse energy.

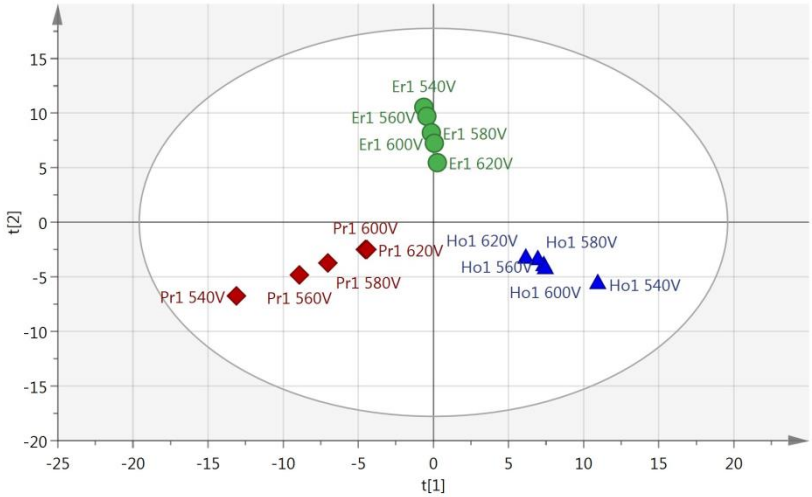

Figure 3.8. Score scatter plot of PCA using highest-concentration single lanthanide samples at various pulse energies (540V = 85 mJ/pulse; 560V = 119 mJ/pulse; 580V = 153 mJ/pulse; 600V = 186 mJ/pulse; 620V = 220 mJ/pulse). Ho – blue ▲, Pr – Red ♦, Er – green ● (x axis component 1 = 49% explained, y axis component 2 = 40% explained)

As a result of the lowest pulse energy giving the greatest separation of samples, an additional PCA was carried out using only the lowest pulse energy measurements for each of the single lanthanide samples. The scores plot of this PCA is shown in Figure 3.9. As with Figure 3.8, there is a clear separation of sample groups into three independent clusters. Within each of these clusters, the highest concentration samples are further from the origin than the lower concentrations. Additionally, the three principal components completely explain the 3 groups of data (R2X cumulative = 99.2%). The near-linear spread of samples according to their concentration in this plot shows that multivariate analysis could be used to predict the concentration of lanthanide elements in a sample.

Table 3.3. Lanthanide emission lines used for PCA

Species	λ / nm	Species	λ / nm	Species	λ / nm
Pr(II)	381.602	Ho(II)	339.898	Er(II)	290.447
Pr(II)	387.718	Ho(II)	342.163	Er(II)	291.036
Pr(II)	396.481	Ho(II)	342.534	Er(II)	296.452
Pr(II)	399.479	Ho(II)	342.813	Er(II)	323.058
Pr(II)	400.869	Ho(II)	345.314	Er(II)	326.478
Pr(II)	405.488	Ho(II)	345.600	Er(II)	331.242
Pr(II)	405.654	Ho(II)	347.426	Er(II)	334.604
Pr(II)	406.281	Ho(II)	348.484	Er(I)	336.408
Pr(II)	410.072	Ho(II)	349.476	Er(II)	336.802
Pr(II)	411.846	Ho(I)	366.229	Er(II)	337.271
Pr(II)	414.122	Ho(I)	366.797	Er(II)	338.508
Pr(II)	414.311	Ho(I)	373.140	Er(II)	339.200
Pr(II)	416.416	Ho(II)	374.817	Er(II)	347.171
Pr(II)	417.939	Ho(II)	379.675	Er(II)	349.910
Pr(II)	418.948	Ho(II)	381.073	Er(I)	355.802
Pr(II)	420.672	Ho(II)	385.407	Er(II)	355.990
Pr(II)	422.293	Ho(II)	386.168	Er(II)	359.983
Pr(II)	422.535	Ho(II)	388.896	Er(II)	360.490
Pr(II)	430.576	Ho(II)	389.102	Er(II)	361.656
Pr(II)	436.833	Ho(II)	395.573	Er(II)	369.265
Pr(II)	440.882	Ho(II)	395.968	Er(I)	381.033
Pr(II)	442.925	Ho(I)	404.081	Er(II)	383.048
Pr(II)	444.983	Ho(II)	404.544	Er(I)	386.285
Pr(II)	446.866	Ho(I)	405.393	Er(II)	388.061
Pr(II)	449.646	Ho(I)	410.384	Er(II)	388.289
Pr(I)	468.780	Ho(I)	410.862	Er(I)	389.268
Pr(I)	469.577	Ho(I)	412.020	Er(II)	389.623
Pr(II)	473.669	Ho(I)	412.565	Er(II)	390.631
Pr(I)	490.699	Ho(I)	412.716	Er(II)	393.863
Pr(I)	491.402	Ho(I)	413.622	Er(I)	394.442
Pr(I)	492.460	Ho(I)	416.303	Er(I)	397.304
Pr(I)	493.600	Ho(I)	417.323	Er(I)	397.358
Pr(I)	494.030	Ho(I)	419.435	Er(I)	400.796
Pr(I)	495.137	Ho(I)	422.704	Er(I)	401.258
Pr(I)	501.859	Ho(I)	425.443	Er(I)	402.051
Pr(I)	501.976	Ho(I)	426.405	Er(I)	408.763
Pr(I)	502.696	Ho(I)	435.073	Er(I)	415.111
Pr(I)	504.383	Ho(I)	493.901		
Pr(I)	504.552	Ho(I)	598.290		
Pr(I)	505.340				
Pr(I)	508.712				
Pr(I)	513.344				
Pr(II)	525.973				

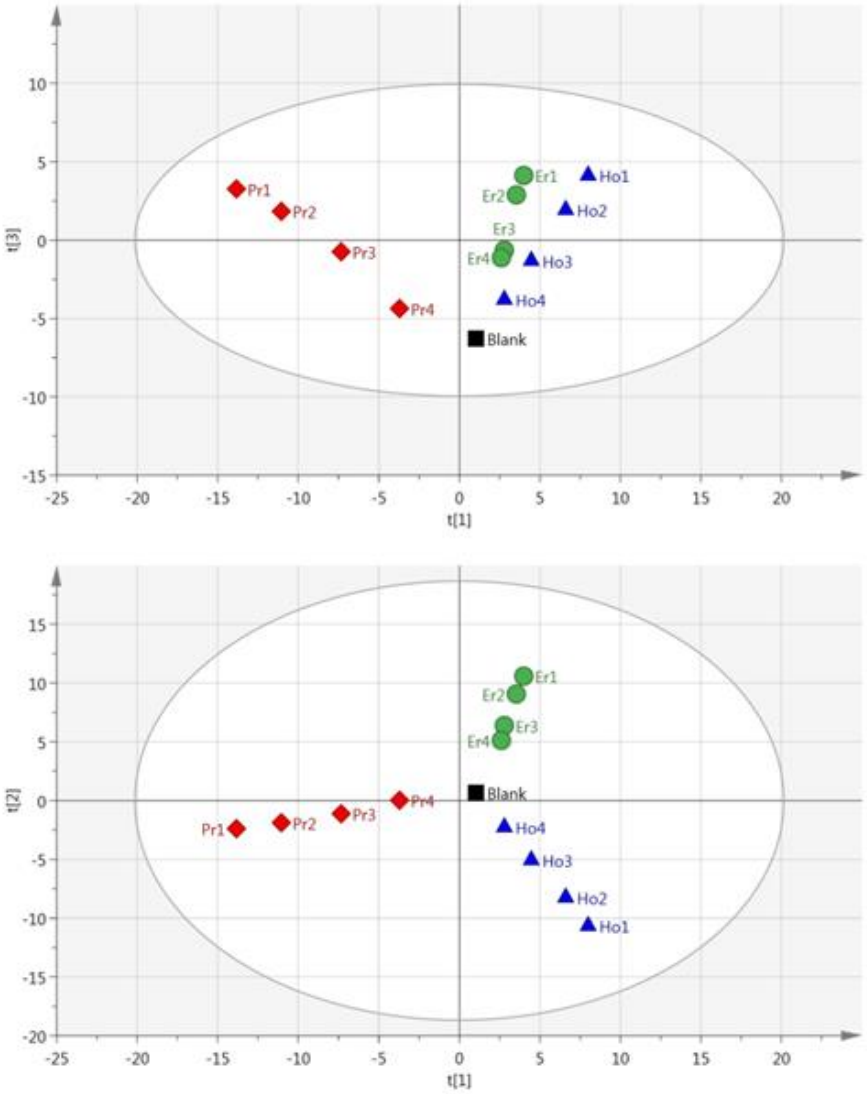

Figure 3.9. Score scatter plots using PCA analysis of peak intensity data for single lanthanide samples (pulse energy = 85 mJ/pulse). Upper figure: component 2 against component 1; lower figure: component 3 against component 1. Ho – blue ▲, Pr – Red ♦, Er – green ● (component 1 = 47% explained, component 2 = 41% explained, component 3 = 12% explained)

It was concluded that the lowest pulse energy gave the greatest normalised peak intensities and also the best separation of results in PCA modelling, whilst simultaneously damaging the sample less than higher pulse energies. On this basis the next set of experiments were conducted at the lowest possible pulse energy of 85 mJ/pulse. Additionally, only a single laser shot was used at each position to allow a repeatable sample surface for each

measurement. Although this limited the number of measurements which could be obtained from each sample, it was deemed to be the best way of ensuring consistency.

3.4.2 Concentration prediction models

Forward iPLS is a technique used for variable selection in multivariate data analysis. The dataset is first split into a number of intervals, decided by the window size, and each of these is modelled using PLS. The model which returns the lowest Root Mean Square Error (RMSE) is identified. Next, this model is used in conjunction with the model of every other interval to try and improve the RMSE. Should a set of models reduce the RMSE, then this interval is added to the variable selection. This method is repeated until the error cannot be improved by the addition of any other model, at which point the variables identified are used to model the whole dataset. Complex datasets, such as those containing multiple species, are more likely to require a small window size so peaks from different species are not included in the same interval.

Predicted versus measured concentration plots were constructed using forward iPLS with a window-size of 15 points. The plots are presented in Figure 3.10 **a** (single element samples) and **b** (mixed lanthanide samples) and the figures of merit are summarised in Table 3.4. The overall linearity of the models is promising. Using a window-size of 15 points returned excellent RMSECV results for all of the single lanthanide samples and marginally higher (poorer) results for the mixed samples (as can be expected from the increased density of emission lines). The model for Pr in the mixed samples is the obvious outlier, with a significantly worse R^2 value than the other plots. In order to improve the accuracy of this model the window size was reduced to 5 points, which increased the R^2 value to be comparable with the other mixed lanthanide samples. However, this required an increase of the processing time from 10 seconds to 5 minutes.

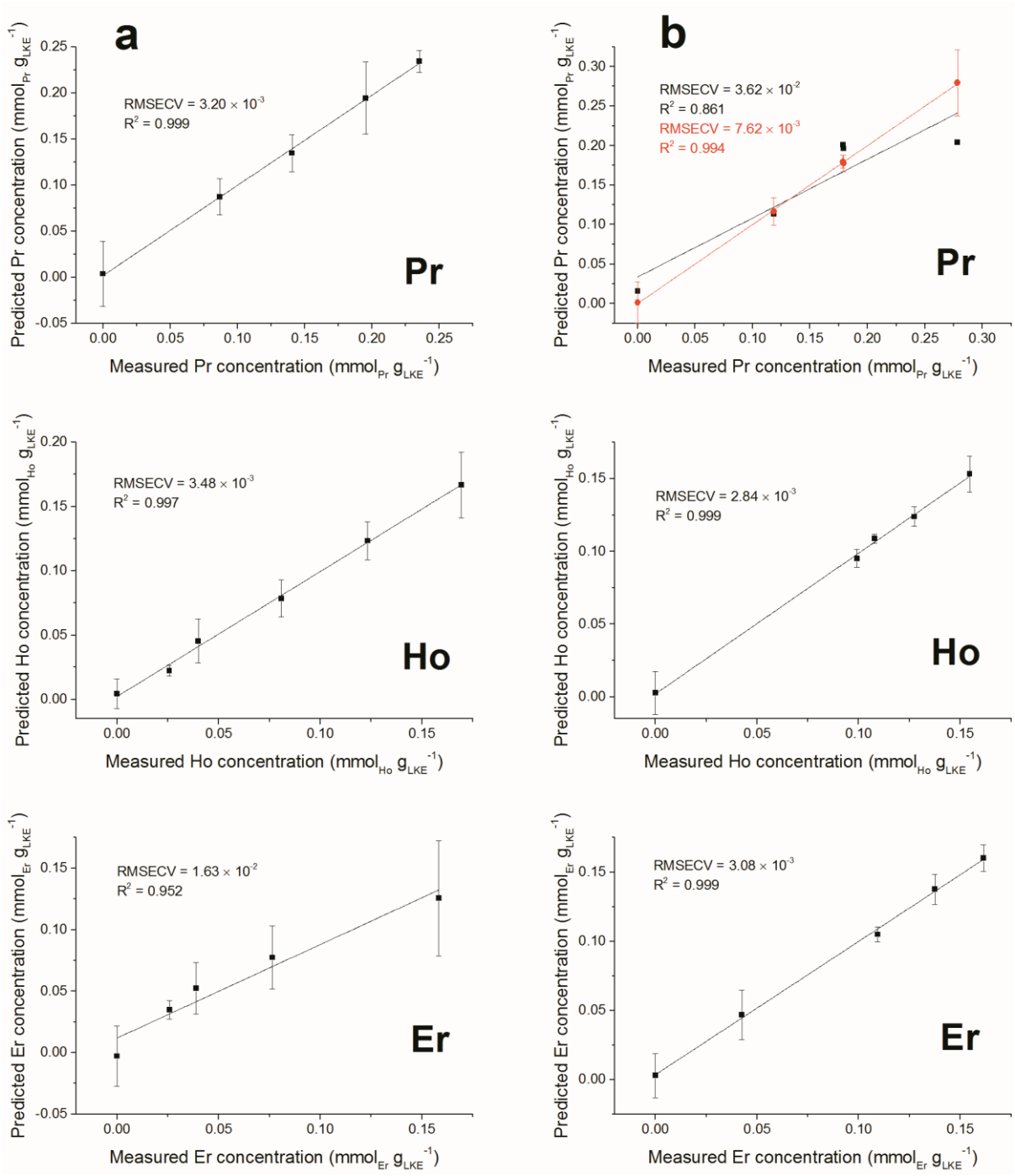

Figure 3.10. Predicted against measured concentrations for **a**) single lanthanide samples and **b**) mixed lanthanide samples (RMSECV given in units of $mmol_{Ln}\ g_{LKE}^{-1}$). Note different plots for (b) Pr: black line uses window of 15 points whereas red line uses window of 5 to increase the model accuracy

Table 3.4. iPLS modelling results for single lanthanide and mixed lanthanide samples (S: standard error of regression)

* w gives window size for Mix Pr samples

Model name	Latent variables	RMSECV ($mmol_{Ln}\ g_{LKE}^{-1}$)	R^2	S ($mmol_{Ln}\ g_{LKE}^{-1}$)	LoD ($mmol_{Ln}\ g_{LKE}^{-1}$)	LoQ ($mmol_{Ln}\ g_{LKE}^{-1}$)	LoD (ppm)	LoQ (ppm)
Pr	3	3.20×10^{-3}	0.999	0.0032	0.0097	0.0322	541	1800
Ho	5	3.48×10^{-3}	0.997	0.0037	0.0115	0.0384	644	2150
Er	3	1.63×10^{-2}	0.952	0.0121	0.0478	0.1593	2670	8900
Mix Pr (w = 15)*	4	3.62×10^{-2}	0.861	0.0354	0.1423	0.4744	7960	26500
Mix Pr (w = 5)*	4	7.62×10^{-3}	0.994	0.0018	0.0054	0.0179	300	1000
Mix Ho	3	2.84×10^{-3}	0.999	0.0025	0.0077	0.0256	429	1430
Mix Er	4	3.08×10^{-3}	0.999	0.0028	0.0088	0.0294	494	1650

Limits Of Detection (LoD) and Limits Of Quantification (LoQ) for the single and the mixed lanthanide samples, shown in Table 3.4, were calculated using Equations (1), (2) and (3), where *S* is the standard error of regression, y_i-$\hat{y}_i$ is the distance between each data point and the linear calibration line, *m* is the gradient of the linear calibration line and *df* is the degrees of freedom of the model.

$$LoD = \frac{3\,S}{m} \tag{1}$$

$$LoQ = \frac{10\,S}{m} \tag{2}$$

$$S = \sqrt{\frac{\sum(y_i - \hat{y}_i)^2}{df}} \tag{3}$$

LIBS has traditionally suffered from higher LoD than other analytical techniques (e.g. TIMS, XPS etc.) due to the complex nature of interactions between the laser radiation, sample, plasma and surrounding atmosphere. However, the LoQ values here are below the concentrations that are likely to be encountered in industrial pyroprocessing facilities of spent nuclear fuel.

The Root Mean Square Error of Cross-Validation (RMSECV) is another means to quantify the accuracy of a prediction of a PLS model. It is calculated with the average distance between values of predicted and actual lanthanide concentration using Equation (4) (*N* is the number of points used to plot each graph). RMS Error of Prediction (RMSEP) is a similar measure but uses an external prediction set for validation.

$$RMSECV = \sqrt{\frac{\sum\left(y_{predicted} - y_{actual}\right)^2}{N}} \tag{4}$$

The LoD values calculated could be more accurate if samples of much higher concentration of lanthanide were used, as these would provide a better idea on linearity. However, the experiment was designed to simulate the intended industrial application, so the very low dilution of Ln elements is justified.

Interestingly, some of the regions selected by the iPLS software did not appear to contain any lanthanide emission lines. Using the Ho models for single and mixed lanthanide samples as an example, the single-lanthanide Ho iPLS selected only two regions to construct a model: 369.12 – 369.40 nm and 451.94 – 452.29 nm. The NIST atomic spectra database [18] shows that former of these contains one Ho emission line at 369.195 nm, but the latter region does not contain any known Ho emission lines. Both intervals also are shown to contain Ar lines which may have played a role in the selection, although an Ar atmosphere was used in every measurement so should be irrelevant to the quantification process. In the case of the mixed-lanthanide Ho model, three regions were selected by the iPLS: 304.24 – 304.46 nm, 322.72 – 322.97 nm and 361.36 - 361.63 nm. The first two of these intervals do not contain any Ho emission lines according to the NIST database. The final interval does contain one Ho line at 361.331 nm (adjusting for spectrometer calibration error of up to + 40 pm) and this peak can be seen on the spectrum. It is possible that the wide Lorentzian tails of nearby peaks have overlapped into the selected regions. Also, it may be that there are unreported Ho peaks, which is not uncommon for heavy elements with complex electronic structures such as the lanthanide or actinide series.

A different way to validate the created models is to use an additional dataset as a prediction set. It is possible to use the single lanthanide samples as a prediction set for the mixed lanthanide models and vice-versa. Figure 3.11 shows the averaged Ho dataset (five samples plus blank) used as a prediction set for the mixed Ho model. Standard error of regression and R^2 values are worse than for the models created with only either single or mixed samples. However, there is still a positive correlation between the prediction and measured concentration, which is good considering there were two other elements present in the calibration set. This information can be used to demonstrate the validity of the iPLS method and, in particular, the intervals selected by the PLS Toolbox software.

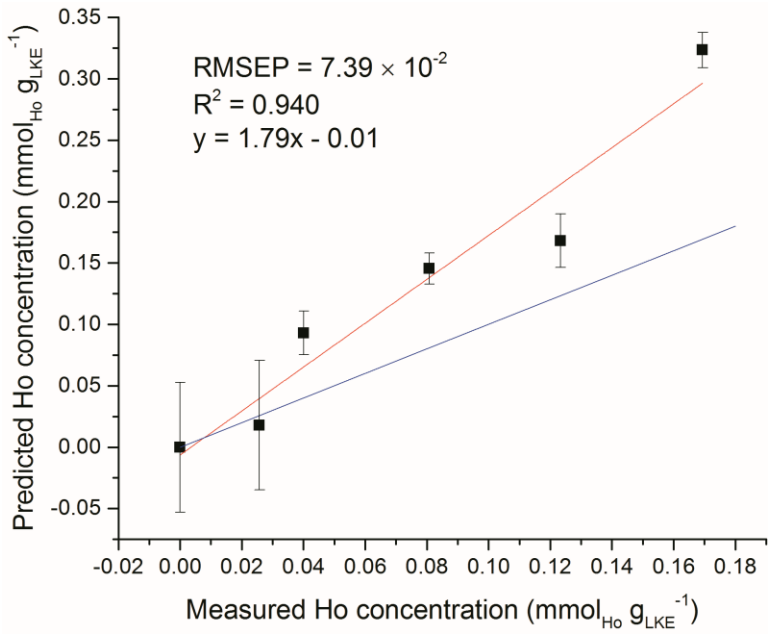

Figure 3.11. Ho single lanthanide samples as prediction set for Ho mixed lanthanide model. Red line is best fit of data points, blue line is ideal fit of y = x (RMSEP = 7.39 × 10^{-2} $mmol_{Ln}$ g_{LKE}^{-1})

Repeatability of measurements was an issue throughout the experiments. Some of the samples had clearly deteriorated in quality as a result of exposure to moisture as LKE is hygroscopic. This caused the samples to increase in diameter, resulting in an uneven sample surface. It is widely reported that LIBS analysis is particularly sensitive to sample-surface inhomogeneity [26]. The differences in sample diameter were accounted for by adjusting the height of the stage (with respect to the laser focal point) for each measurement, but it was impossible to account for the variations in surface finish between the glassy and rough salt surfaces. It is worth noting, however, that in an industrial setting the sample would be a molten salt solution. Liquid samples provide a naturally level, even and self-healing surface, so the surface finish would be less of an issue (although other handling and experimental complications are associated with liquid-samples and LIBS [17,31]). Future experiments using molten salts could be accomplished with only minor changes to the experimental setup to allow this theory to be tested.

As an example of sample inhomogeneity, an iPLS model was created using only six spectra from each Ho sample plus the blank. This analysis used the venetian blinds cross-validation method [34] with a window width of six to prevent falling into the sample replicate trap,

and the predicted versus measured Ho concentration is shown in Figure 3.12. There is a large variation in predicted concentrations for samples at the same measured concentration. There is an obvious need for brute force averaging of several repeat measurements before modelling or prediction. This is despite the spectral corrections such as normalisation and baseline-subtraction which have been detailed previously. The laser repetition rate limits the frequency of sampling in LIBS measurements. In our setup the repetition rate was 10 Hz. A similar system in an industrial setting (with more sample material) could record hundreds of repeat measurements in a matter of seconds and rapidly fulfil the need for averaging numerous spectra.

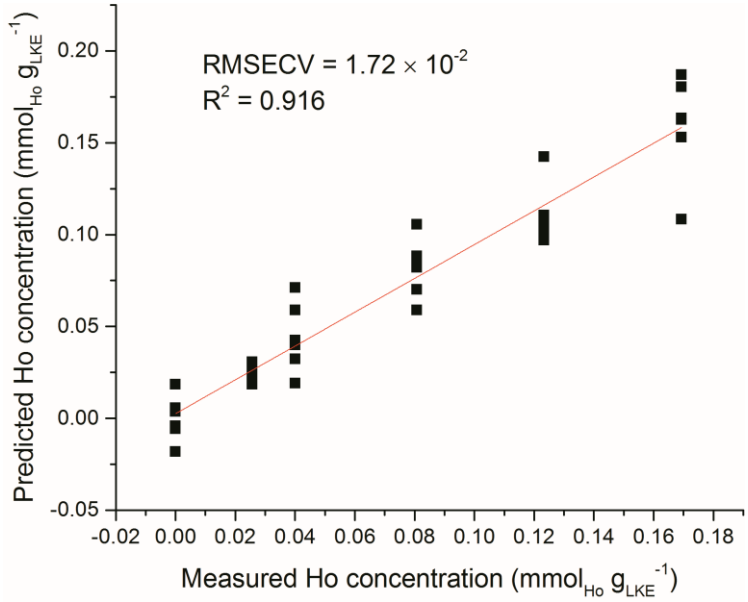

Figure 3.12. Predicted vs measured concentration of Ho samples. Model created using six individual spectra at each sample concentration rather than an average of all spectra at each sample

3.5 Conclusions

The potential for concentration-prediction using LIBS has been demonstrated for lanthanide elements. Different concentrations of Ho, Er and Pr dissolved into LKE matrices were measured within an air-tight sample cell with a quartz viewing-window. Each LIBS emission spectrum was individually normalised with respect to a Li matrix peak at 497.170 nm and the Echelle-order baseline was subtracted (using a third-order plot of each Echelle-order

wavelength range), before repeat measurements on the same sample were averaged together.

Preliminary experiments investigating the laser pulse energy showed normalised lanthanide emission signal to noise ratio was improved at lower pulse energies. This was confirmed using PCA, which gave a better separation of samples recorded at the lowest pulse energies on a scores scatter plot.

Forward iPLS regression was used to construct concentration models for single lanthanide samples and for each of the three elements within mixed lanthanide samples. Using these models, predicted versus measured concentration graphs were plotted and used to estimate RMSECV, LoD and LoQ values. A standard window size of 15 points was used for iPLS across all the samples bar one, where it was necessary to reduce the window size to increase the accuracy. Some of the windows selected for incorporation into a model were shown to not contain any reported lanthanide emission lines. However, despite this, excellent RMSECV, LoD and LoQ values were obtained for all of the samples.

The PLS results suggest that LIBS could become a useful technique for the online monitoring of molten salt during pyroprocessing – particularly if deployment to an industrial setting could be validated by analysing molten samples or different matrix-salts. Additional improvements could be found by altering the ICCD camera settings (such as gate delay time and width) or investigating double-pulsed LIBS to maximise the signal to background ratio.

Conflicts of interest

There are no conflicts to declare.

Acknowledgements

The Authors would like to thank the Atomic Weapons Establishment (AWE plc) and the EPSRC Materials for Demanding Environments Centre for Doctoral Training (M4DE CDT) for funding of the PhD research project, and AWE for the loan of the LIBS apparatus.

3.6 References

[1] T. Koyama, Y. Sakamura, M. Iizuka, T. Kato, T. Murakami, J.-P. Glatz, Development of

Pyro-processing Fuel Cycle Technology for Closing Actinide Cycle, Procedia Chem. 7 (2012) 772–778. doi:10.1016/j.proche.2012.10.117.

[2] R. Malmbeck, C. Nourry, M. Ougier, P. Souček, J.P. Glatz, T. Kato, T. Koyama, Advanced fuel cycle options, Energy Procedia. 7 (2011) 93–102. doi:10.1016/j.egypro.2011.06.013.

[3] H. Lee, G. Il Park, K.H. Kang, J.M. Hur, J.G. Kim, D.H. Ahn, Y.Z. Cho, E.H. Kim, Pyroprocessing technology development at KAERI, Nucl. Eng. Technol. 43 (2011) 317–328. doi:10.5516/NET.2011.43.4.317.

[4] IAEA, Assessment of Partitioning Processes for Transmutation of Actinides, Vienna, Austria, 2010. https://www-pub.iaea.org/MTCD/Publications/PDF/TE_1648_CD/PDF/TECDOC_1648.pdf.

[5] J.J. Laidler, J.E. Battles, W.E. Miller, J.P. Ackerman, E.L. Carls, Development of pyroprocessing technology, Prog. Nucl. Energy. 31 (1997) 131–140. doi:10.1016/0149-1970(96)00007-8.

[6] A. V. Bychkov, S.K. Vavilov, P.T. Porodnov, O. V. Skiba, G.P. Popkov, A.K. Pravdin, Pyrochemical Reprocessing of Irradiated Mixed Oxide Fuel in Molten Salts, in: H. Wendt (Ed.), Molten Salt Forum Proc. Int. Symp. Molten Salt Chem. Technol. 1998, Uetikon-Zuerich, Switzerland, 1998: pp. 525–528. https://trove.nla.gov.au/work/11482686?selectedversion=NBD10720488.

[7] Y. Sakamura, T. Murakami, K. Tada, S. Kitawaki, Electrowinning of U-Pu onto inert solid cathode in LiCl-KCl eutectic melts containing UCl3 and PuCl3, J. Nucl. Mater. 502 (2018) 270–275. doi:10.1016/j.jnucmat.2018.02.025.

[8] J. Zhang, Electrochemistry of actinides and fission products in molten salts - Data review, J. Nucl. Mater. 447 (2014) 271–284. doi:10.1016/j.jnucmat.2013.12.017.

[9] J.H. Yoo, C.S. Seo, E.H. Kim, H.S. Lee, A conceptual study of pyroprocessing for recovering actinides from spent oxide fuels, Nucl. Eng. Technol. 40 (2008) 581–592. doi:10.5516/NET.2008.40.7.581.

[10] C.A. Schroll, A.M. Lines, W.R. Heineman, S.A. Bryan, Absorption spectroscopy for the quantitative prediction of lanthanide concentrations in the 3LiCl–2CsCl eutectic at 723 K, Anal. Methods. 8 (2016) 7731–7738. doi:10.1039/C6AY01520D.

[11] A. Lang, D. Engelberg, N.T. Smith, D. Trivedi, O. Horsfall, A. Banford, P.A. Martin, P. Coffey, W.R. Bower, C. Walther, M. Weiß, H. Bosco, A. Jenkins, G.T.W. Law, Analysis of contaminated nuclear plant steel by laser-induced breakdown spectroscopy, J. Hazard. Mater. 345 (2018) 114–122. doi:10.1016/j.jhazmat.2017.10.064.

[12] J. Wu, Y. Qiu, X. Li, H. Yu, Z. Zhang, A. Qiu, Progress of laser-induced breakdown spectroscopy in nuclear industry applications, J. Phys. D. Appl. Phys. 53 (2020) 023001. doi:10.1088/1361-6463/ab477a.

[13] G. Maddaluno, S. Almaviva, L. Caneve, F. Colao, V. Lazic, L. Laguardia, P. Gasior, M. Kubkowska, Detection by LIBS of the deuterium retained in the FTU toroidal limiter, Nucl. Mater. Energy. 18 (2019) 208–211. doi:10.1016/j.nme.2018.12.029.

[14] G.S. Maurya, A. Marín-Roldán, P. Veis, A.K. Pathak, P. Sen, A review of the LIBS analysis for the plasma-facing components diagnostics, J. Nucl. Mater. 541 (2020) 152417. doi:10.1016/j.jnucmat.2020.152417.

[15] A. Williams, K. Bryce, S. Phongikaroon, Measurement of Cerium and Gadolinium in Solid Lithium Chloride–Potassium Chloride Salt Using Laser-Induced Breakdown Spectroscopy (LIBS), Appl. Spectrosc. 71 (2017) 2302–2312. doi:10.1177/0003702817709298.

[16] M.Z. Martin, R.C. Martin, S. Allman, D. Brice, A. Wymore, N. Andre, Quantification of rare earth elements using laser-induced breakdown spectroscopy, Spectrochim. Acta - Part B At. Spectrosc. 114 (2015) 65–73. doi:10.1016/j.sab.2015.10.005.

[17] A. Weisberg, R.E. Lakis, M.F. Simpson, L. Horowitz, J. Craparo, Measuring lanthanide concentrations in molten salt using laser-induced breakdown spectroscopy (LIBS), Appl. Spectrosc. 68 (2014) 937–48. doi:10.1366/13-07390.

[18] A. Kramida, Y. Ralchenko, J. Reader, The NIST ASD Team (2018), NIST Atomic Spectra Database, NIST At. Spectra Database (Ver. 5.6.1). [Online] (2019)

http://physics.nist.gov/asd. doi:10.18434/T4W30F.

[19] X. Wang, V. Motto-Ros, G. Panczer, D. De Ligny, J. Yu, J.M. Benoit, J.L. Dussossoy, S. Peuget, Mapping of rare earth elements in nuclear waste glass-ceramic using micro laser-induced breakdown spectroscopy, Spectrochim. Acta - Part B At. Spectrosc. 87 (2013) 139–146. doi:10.1016/j.sab.2013.05.022.

[20] V.K. Unnikrishnan, R. Nayak, P. Devangad, M.M. Tamboli, C. Santhosh, G.A. Kumar, D.K. Sardar, Calibration based laser-induced breakdown spectroscopy (LIBS) for quantitative analysis of doped rare earth elements in phosphors, Mater. Lett. 107 (2013) 322–324. doi:10.1016/j.matlet.2013.06.036.

[21] B.T. Manard, E.M. Wylie, S.P. Willson, Analysis of Rare Earth Elements in Uranium Using Handheld Laser-Induced Breakdown Spectroscopy (HH LIBS), Appl. Spectrosc. 72 (2018) 1653–1660. doi:10.1177/0003702818775431.

[22] P. Devangad, V.K. Unnikrishnan, R. Nayak, M.M. Tamboli, K.M. Muhammed Shameem, C. Santhosh, G.A. Kumar, D.K. Sardar, Performance evaluation of Laser Induced Breakdown Spectroscopy (LIBS) for quantitative analysis of rare earth elements in phosphate glasses, Opt. Mater. (Amst). 52 (2016) 32–37. doi:10.1016/j.optmat.2015.12.001.

[23] B. Bhatt, A. Dehayem-Kamadjeu, K.H. Angeyo, Rapid nuclear forensics analysis via machine-learning-enabled laser-induced breakdown spectroscopy (LIBS), AIP Conf. Proc. 060006 (2019) 1–4. doi:10.1063/1.5110124.

[24] P. Fichet, D. Menut, R. Brennetot, E. Vors, A. Rivoallan, Analysis by laser-induced breakdown spectroscopy of complex solids, liquids, and powders with an echelle spectrometer, Appl. Opt. 42 (2003) 6029. doi:10.1364/AO.42.006029.

[25] J.R. Wachter, D.A. Cremers, Determination of Uranium in Solution Using Laser-Induced Breakdown Spectroscopy, Appl. Spectrosc. 41 (1987) 1042–1048. doi:10.1366/0003702874447897.

[26] C. Hanson, S. Phongikaroon, J.R. Scott, Temperature effect on laser-induced breakdown spectroscopy spectra of molten and solid salts, Spectrochim. Acta - Part B

At. Spectrosc. 97 (2014) 79–85. doi:10.1016/j.sab.2014.04.012.

[27] J.-I. Yun, R. Klenze, J.-I. Kim, Laser-induced breakdown spectroscopy for the on-line multielement analysis of highly radioactive glass melt. Part I: Characterization and evaluation of the method, Appl. Spectrosc. 56 (2002) 437–448. doi:10.1366/0003702021955097.

[28] J.-I. Yun, R. Klenze, J.-I. Kim, Laser-induced breakdown spectroscopy for the on-line multielement analysis of highly radioactive glass melt simulants. Part II: Analyses of molten glass samples, Appl. Spectrosc. 56 (2002) 852–858. doi:10.1366/000370202760171518.

[29] H. Hotokezaka, S. Tanaka, A. Suzuki, S. Nagasaki, Speciation analysis on europium(III) using laser-induced breakdown spectroscopy, Radiochim. Acta. 88 (2000) 645–648. doi:10.1524/ract.2000.88.9-11.645.

[30] N.A. Smith, J.A. Savina, M.A. Williamson, Application of Laser Induced Breakdown Spectroscopy to Electrochemical Process Monitoring of Molten Chloride Salts, in: Symp. Int. Safeguards Link. Strateg. Implement. People, Vienna, Austria, 2014: pp. 1–7. https://www.semanticscholar.org/paper/Application-of-Laser-Induced-Breakdown-Spectroscopy-Smith-Savina/84faa4386f3a0991da8ec68e0ee542c6cf598269.

[31] A.N. Williams, S. Phongikaroon, Laser-Induced Breakdown Spectroscopy (LIBS) in a Novel Molten Salt Aerosol System, Appl. Spectrosc. 71 (2017) 744–749. doi:10.1177/0003702816648965.

[32] A. Williams, S. Phongikaroon, Laser-Induced Breakdown Spectroscopy (LIBS) Measurement of Uranium in Molten Salt, Appl. Spectrosc. 72 (2018) 1029–1039. doi:10.1177/0003702818760311.

[33] B. Yoo, S.H. Kim, J. Lee, Quantitative analysis of molten salt by laser-induced breakdown spectroscopy, in: Glob. Nucl. Fuel Cycle a Low-Carbon Futur., Paris, France, 2015: pp. 20–24. https://inis.iaea.org/search/search.aspx?orig_q=RN:49058543.

[34] D. Ballabio, V. Consonni, Classification tools in chemistry. Part 1: Linear models. PLS-

DA, Anal. Methods. 5 (2013) 3790–3798. doi:10.1039/c3ay40582f.

Chapter 4 - Laser-induced breakdown spectroscopy and multivariate data analysis of uranium samples with trace impurities for rapid nuclear forensics

This chapter is undergoing security clearance at the Atomic Weapons Establishment. Once this is complete, it will be submitted to *Journal of Nuclear Materials* for peer review.

Authors: Gregory Hull †[a,b], Kiran Haroon [a], Edward D. McNaghten [c], Clint A. Sharrad [a], Philip Martin †[a,b]

a. Department of Chemical Engineering and Analytical Science, University of Manchester, Oxford Road, Manchester, M13 9PL

b. Photon Science Institute, University of Manchester, Oxford Road, Manchester, M13 9PL

c. AWE, Aldermaston, Reading, Berkshire, RG7 4PR

† Corresponding Authors

Author contribution: planned and carried out all the sample preparation and LIBS experiments; completed the data pre-processing (including finding the spectral regions of interest); had help from Kiran Haroon to finish the PLS modelling work; and finally wrote the paper with some advice from Kiran about the terminology for the data analysis sections.

4.1 Abstract

Nuclear forensics is the process of determining the key signatures within a sample of nuclear material to discover its origin, destination and the legality of its possession. Laser-induced breakdown spectroscopy (LIBS) is an elemental analysis technique which could provide key benefits to the field of nuclear forensics including no sample preparation, relatively simple and portable apparatus, non-destructive analysis, and the offer of stand-off or remote measurement capabilities. In this work, uranium oxide and uranium ore concentrate samples with known trace elemental impurities were analysed using LIBS. Each elemental impurity was independently modelled with partial least squares regression (PLS) using selected spectral regions containing known emission lines for each element. The emission spectra from the two sample materials were compared and a number of differences were observed which prevented the two materials being modelled together. Modelling of the uranium oxide samples independently provided good predicted versus measured concentration graphs and root mean squared error of cross-validation (RMSECV) values between 0.8 μg g^{-1} and 94 μg g^{-1} for 23 trace elements which were not present in the blank. The uranium ore concentrate sample displayed a number of emission peaks which could be used for qualitative analysis. The results suggest that excellent limits of detection are achievable with the LIBS technique if suitable reference materials are available, and LIBS could be a useful tool to nuclear forensics investigations given its advantages over traditional techniques.

Key Words:

Nuclear forensics; LIBS; Multivariate data analysis; Partial least squares regression

4.2 Introduction

Nuclear forensics is the process of identifying a sample of nuclear or radioactive material. Typically, the stages of categorisation, characterisation, identification and attribution are performed to ascertain what the material is and where it was removed from regulatory control [1]. Traditional forensic science is utilised, along with analytical techniques which probe deeper into a material's elemental and isotopic fingerprint. Nuclear forensics is a key element of nuclear security, which also involves inspections at nuclear sites across the globe

and analysis either in situ or elsewhere after sample collection [2]. The precision and accuracy is invariably better when more sophisticated apparatus may be used at analytical laboratories rather than tests being carried out in the field. However, the costs in terms of time and money related to sample acquisition, transport, storage, analysis and eventual disposal should not be overlooked – particularly as samples of nuclear relevance are potentially hazardous.

A material can be identified by comparing characteristic 'signatures' with known stockpiles or reference materials [3,4]. Key parameters for consideration are: major and trace elemental concentrations; isotopic abundances (particularly of uranium and plutonium); oxidation state or other chemical forms; and physical properties such as dimensions or appearance [5]. Some signatures can be created by specific processing steps, while others are present in the uranium ore and remain with the sample for the majority of its lifetime. As an example, studying a uranium oxide fuel pellet could reveal where the uranium was mined, the processing steps undertaken, the time present in a reactor or time since processing took place (the sample 'age') and the design of reactor. The interpretation of analytical results leads to conclusions about a sample's history and can eventually point towards where the sample was removed from regulatory control. As such, the result of a nuclear forensics investigation can be criminal proceedings against individuals or corporations who facilitated (either knowingly or unknowingly) the release of a potentially dangerous chemical [6,7].

The analytical techniques used for nuclear forensics can be broadly separated into non-destructive and destructive analyses [8]. Generally, non-destructive analyses are less time consuming because complex sample preparation is not necessary [9]. An example is high resolution gamma-ray spectroscopy (HRGS) which can be used to identify isotopic composition of radioactive elements within around 20 minutes [10]. More precise elemental and isotopic characterisation can be interrogated from a sample with mass spectrometry techniques such as thermal ionisation mass spectrometry (TIMS) or inductively coupled plasma mass spectrometry (ICP-MS). However, such destructive analyses require sub-sampling and sample work-up before testing can begin, which increase the total analysis time [11]. More accurate HRGS necessitates longer counting times (in the order of days) and high purity germanium scintillators which require bulky cryogenic cooling. Additionally,

HRGS is best suited to powdered samples which can be evenly distributed above a counter at a calibrated distance and is less well suited to different shaped solids or non-homogenous sample materials.

Laser-induced breakdown spectroscopy (LIBS) is an analytical technique which provides rapid elemental analysis of a material irrespective of its physical state or surface finish. As a laser-based analysis, LIBS permits stand-off and remote measurements [12–16], and benefits from no sample preparation, no vacuum requirements, relatively simple and robust hardware and an ever-growing list of applications. The measurement speed is rapid enough to enable in-line analysis for waste stream management and monitoring [17,18], metal casting [19], mining [20] and other industrial processes [21,22]. Spatial mapping [23] and depth profiling [24,25] have also been demonstrated with LIBS, offering 3D information prohibited by most spectrochemical analysis.

The benefits of using LIBS in nuclear forensics are numerous. Firstly, no physical contact is required between the apparatus or the technician and the sample. Exposure to radiological hazards can therefore be minimised. Secondly, the analysis time and the repetition rate is dependent on the shot frequency of the ablation laser which is normally in the order of 10 Hz, enabling immediate categorisation of a sample material to inform next steps. Finally, emission spectroscopy can record numerous wavelengths from multiple species simultaneously. Isobaric elements, which are a problem for mass spectrometry, present no challenge in emission spectroscopy. The wide spectral coverage of most spectrometers and numerous emission lines for each element means that in practice there is never a situation where isolated emission peaks (without interference) cannot be identified. Analysing numerous emission peaks simultaneously opens the possibility of chemometrics and multivariate data analysis (MDA), which in recent years have been demonstrated to increase the accuracy of the LIBS technique [26–29]. As a result of these attributes, LIBS can accomplish elemental fingerprinting of major and trace elements safely, rapidly and with a high degree of accuracy.

LIBS has been used to study various uranium-containing samples to identify trace element impurities and limits of detection (LoDs). Fichet et al [30] identified emission lines and calculated LoDs from eighteen elements at trace concentrations in UO_2 and PuO_2 samples

using stand-off LIBS. Their setup used a laser and spectroscopic equipment in a separate room to the sample and glove box to prove the potential for shielding of the apparatus and user from restricted environments (e.g. hot cells). Chinni et al [31] demonstrated a limit of detection of 0.26% w/w of uranium in soil at a at close range, and 0.5% w/w at a stand-off distance of 30 m. Sirven et al [26] used PCA and SIMCA to discriminate between eleven uranium ore concentrate samples analysed with LIBS. Bhatt et al [28] calculated a LoD of 34 ppm of uranium oxide in cellulose, and used artificial neural networks and PCA to discriminate between samples from different regions in Kenya. Manard et al [32] used a portable handheld LIBS instrument to calculate limits of detection for three rare earth elements in uranium oxide samples. Their LoDs below 320 ppm for Eu, Nd and Yb demonstrate how handheld instrumentation can enable portability without compromising on precision.

In this feasibility study, uranium oxide and uranium ore concentrate samples with varying concentrations of elemental impurities were analysed using LIBS. The MDA technique of partial least squares regression (PLS) was used to model the trace element concentrations. The aim of the study was to identify and quantify trace elements alongside the uranium matrix material to mimic a situation which could arise in nuclear forensic applications. Our conclusions highlight both the benefits of the technique and show the main obstacles which need to be overcome for LIBS to be accepted.

4.3 Experimental

4.3.1 LIBS apparatus

A schematic of the experimental setup is shown in Figure 4.1. A 6 ns, 1064 nm pulse from a Nd:YAG laser (Spitlight 600, Innolas) was used for laser ablation, with a pulse energy of 600 mJ focussed onto the sample with a beam expander and a 10 cm lens. The stability of the pulse energy is presumed to be accurate to the manufacturer's specification with a RMS of <0.7%. Light was collected with a 10 cm lens at a nominal angle from vertical and transferred with a 2 m fibre optic cable (400 µm core) to an Echelle spectrometer (Aryelle Butterfly, Lasertechnik Berlin) with 400 mm focal length and a spectral range from 250 to 900 nm. An ICCD camera (Andor iStar series; 1024 × 1024 pixels, 13.3 × 13.3 mm^2) was used

to analyse the plasma emission with Sophi software (Lasertechnik Berlin). The spectrometer and camera had a resolving power of approximately 35000. The plasma was analysed using a time delay of 1500 ns after laser ablation and a time gate of 50 µs to allow Bremsstrahlung effects to dissipate and maximise signal to noise ratio.

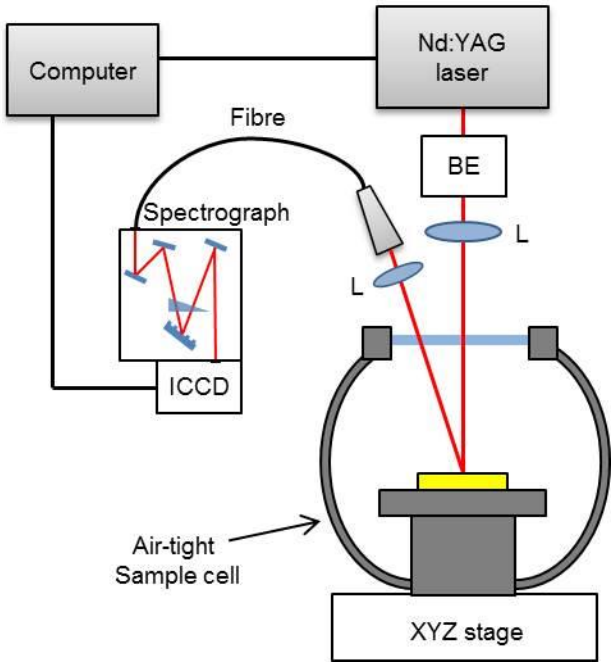

Figure 4.1. Schematic of experimental setup (BE: beam expander; L: lens; ICCD: intensified charge coupled device)

4.3.2 Sample materials

Two different uranium-containing materials were available for LIBS analysis. CRM-124 [33] is a set of seven U_3O_8 powdered solids produced in 1983 by New Brunswick Laboratories, USA. The seven samples (CRM-124-1 to CRM-124-7) contain decreasing concentrations of twenty four trace elemental impurities, as shown in Table 4.1. The final sample in the series (CRM-124-7) contained solely U_3O_8 matrix material, with only minor impurities present from the manufacturing processes. All of the CRM-124 samples were black ceramic coarse powders in physical appearance.

CUP-2 is a uranium ore concentrate (UOC) standard reference material, produced in 1986 by Blind River uranium refinery of Eldorado Resources ltd, Canada [34]. The sample was a dark orange, free running fine powder in appearance. Many of the elemental impurities in CRM-

124 were also present in CUP-2. However, the CUP-2 sample contained a significantly higher concentration of impurity elements compared to the CRM-124 samples, again shown in Table 4.1. The CUP-2 sample material contains 75.4 wt % uranium, whereas the CRM-124 sample series has around 85 wt %.

Table 4.1. Certified elemental concentrations of uranium samples used in LIBS analysis. All concentrations in μg element per g uranium

Element	**Sample Name**							
	CRM-124-1	**CRM-124-2**	**CRM-124-3**	**CRM-124-4**	**CRM-124-5**	**CRM-124-6**	**CRM-124-7**	**CUP-2**
Aluminium	205	105	55	25	15	10	5	
Beryllium	25	12.5	5	2.5	1.3	0.5	0.1	
Bismuth	50	25	10	5	2.5	1	0.2	
Boron	5.1	2.6	1.1	0.6	0.35	0.2	0.1	68
Cadmium	5.2	2.7	1.2	0.7	0.45	0.3	0.2	
Calcium	200	100	51	21	11	5.8	0.8	8221
Chromium	102	52	22	12	7	4.3	2.3	
Cobalt	25	12.5	5	2.6	1.4	0.6	0.1	
Copper	50	25	10.4	5.4	2.9	1.4	0.4	
Iron	210	110	60	30	20	15	10	4124
Lead	51	26	10.8	5.8	3.3	1.8	0.8	
Magnesium	101	51	21	11	6	3	1	3036
Manganese	51	26	11	5.7	3.2	1.7	0.7	
Molybdenum	100	50	20	10	5	2	0.1	915
Nickel	202	102	52	22	12	7	2	38
Silicon	202	102	52	22	12	7.3	2.3	2254
Silver	5	2.5	1	0.5	0.25	0.1	0.1	
Sodium	400	200	100	40	20	10	0.5	6086
Tin	51	26	10.6	5.6	3.1	1.6	0.6	
Titanium	50	25	10.3	5.3	2.8	1.3	0.3	252
Tungsten	200	100	50	20	10	5	0.1	
Vanadium	50	25	10	5	2.5	1	0.2	875
Zinc	202	102	52	22	12	6.6	1.6	
Zirconium	200	100	50	20	10	5	5	583
Arsenic								464
Phosphorus								398
Potassium								1458
Sulphur								10607

To prepare the samples for laser ablation, roughly 1 mg of material was deposited onto the centre of a 2.5 cm diameter double-sided carbon adhesive disk and spread over an area around 0.5 cm^2 using a spatula. The disk was tipped sideways and tapped to remove any excess powder. The carbon disk was secured onto a slightly larger stainless steel disk for easier handling, and sealed inside an air-tight sample cell (Scanwel ltd, Bala, UK) with an upper quartz window for laser access under air at atmospheric pressure. Judge et al [35] used a similar sample mounting procedure for their uranium LIBS experiments. The coarse ceramic grains of the CRM-124 samples were difficult to spread evenly, whereas the fine powder of the CUP-2 sample was easier to manipulate into a more homogenous surface.

Two repeat samples of each material (CRM-124-1 to -7 and CUP-2) were created, giving fourteen CRM-124 samples and two CUP-2 samples. 25 shots were recorded on each sample and averaged together. The laser shots were separated from one another by around 0.5 mm, and only recorded at points on the surface where the sample material was deposited and adhered to the sticky pad. After 25 measurements, much of the sample material had been removed from the mount by the ablation process or resulting shockwaves; however the spectra still exhibited uranium emission lines.

4.3.3 Uranium baseline correction, normalisation and averaging

LIBS measurements of uranium create inherently complex spectra due to the very high density of uranium emission lines (see [36]). The Echelle spectrometer used in our experiments also gives characteristic repetitive maxima due to the pixel order in the ICCD camera. The combined result is an apparent high noise made up of thousands of uranium emission lines. Although careful time gating can limit the effect of Bremsstrahlung emission on LIBS spectra, the uranium emission lines are impossible to remove as they appear after the same delay as the analyte emissions.

The maximum intensity of each Echelle order in a spectrum was highly dependent on the coupling of the laser with the sample material. Analysis of the un-contaminated carbon adhesive disk showed very little contribution to the baseline, whereas targeting the uranium powder gave very intense baseline regions. Therefore, the inhomogeneous distribution of sample material across the carbon disk caused varied baselines which distorted the modelling and necessitated a baseline correction pre-processing step. The baseline was

corrected using a third order plot of each Echelle-maxima spectral region. As with our previous work [29], the third order plot was formed after ignoring the 20% of points with the highest intensity within each Echelle-region. This was to preserve the information and quality of the emission peaks.

After baseline correction, each spectrum was normalised to the maximum intensity of a consistent uranium emission line. The U II emission at 367.01 nm was chosen for this purpose, as this peak was isolated and consistently high intensity in the experiments. The normalisation helped to reduce the variation between the spectra.

4.3.4 Partial least squares regression methodology

Initial modelling investigations were carried out using forward interval partial least squares regression (iPLS) (PLS Toolbox, Matlab) with leave one out cross-validation. iPLS selects a subset of adjacent wavelength scores at a time to analyse with PLS. Forward iPLS stipulates that additional intervals are added sequentially to increase the model validity until no additional benefit can be made with any interval. iPLS reduces the models' complexity and irrelevant spectral information (i.e. from other elements or the baseline). An interval region of 5 points was used after assessment of the average full width at half maximum (FWHM) of emission lines. The entire normalised spectrum was used for these analyses. However, the modelling proved unsuccessful as the intervals selected by the iPLS software did not correlate to known emission lines for particular elements. Furthermore, the software selected several duplicate regions in models for different elements, which was clearly incorrect.

To aid the modelling, rather than using the whole spectrum for iPLS and relying on the software to select intervals of interest, the spectral regions around specific LIBS emission lines were manually selected. Emission lines were selected by cross-referencing the NIST atomic spectra database [37] with the LIBS spectra of CRM-124-1 and CUP-2 samples. The criterion for selection was that the line was isolated from other analyte lines in both spectra (not necessarily isolated from the uranium emission lines). Some of the low concentration analytes were not visible above the noise at any position in the spectra. For these elements, the literature wavelength value was used. Between three and seven lines were identified for each element. For each line, a region of seven pixels centred at the literature wavelength

was selected for PLS modelling, corresponding to about 1.5 emission linewidths. It was important to include as much of the spectral peak as possible whilst minimising the impact of the background. A list of the lines selected for each element is given in Table 4.2. PLS was performed for each impurity element using the selected regions of interest.

Root mean squared error of cross-validation (RMSECV) was used to compare the accuracy of the models. RMSECV is calculated using measured versus predicted concentration plots with Equation (5), where y_i is the measured concentration and $\hat{y}_i$ is the predicted concentration.

$$\mathrm{RMSECV} = \sqrt{\frac{1}{n}\sum_{i=1}^{n}(y_i - \hat{y}_i)^2} \tag{5}$$

4.4 Results and discussion

4.4.1 Spectral observations

A blank carbon adhesive disk was analysed to identify the elements present and ascertain the influence of the sample mount on the spectra. An annotated LIBS spectrum of the blank disk is given in Figure 4.2, with some intense peaks labelled. The sodium peaks at 589.0 and 589.6 nm are problematic because they are also included in both the CRM-124 and CUP-2 samples as impurities. The presence of such intense sodium peaks in the blank measurement casts doubt over the ability of the PLS methodology to accurately predict the concentration, as discussed further in the following sections.

Initially, the CRM-124 and CUP-2 samples were modelled with PLS together (for the elements which were present in both samples). However, the addition of the CUP-2 samples significantly increased the RMSECV of the models. The samples were not matrix matched, and their different physical characteristics, surface finishes and elemental constituents meant they could not be fairly compared. In addition, the concentrations were significantly higher for elements in the CUP-2 sample compared to the CRM-124 samples, which hindered the viability of the modelling.

Table 4.2. Emission lines used for selected partial least squares regression modelling (taken from NIST atomic spectra database [37])

Element	**Wavelength / nm**						
Aluminum	308.221	309.303	344.308	396.175	783.639		
Beryllium	332.156	381.345	457.266				
Bismuth	262.791	289.798	293.830	298.903	302.464	306.772	
Boron	291.808	303.226	345.129	412.193	448.705	449.773	
Cadmium	274.854	298.062	508.582	533.748	537.813	643.847	
Calcium	445.472	585.758	643.878	646.248	649.382	714.788	
Chromium	357.869	359.349	360.533	425.435	427.480	520.844	
Cobalt	340.512	344.364	345.350	347.402	350.228	356.938	
Copper	261.837	276.637	296.116	303.610	324.754	327.396	
Iron	271.903	344.061	371.994	373.713	374.556	385.991	
Lead	280.200	283.305	357.273	363.957	368.346	405.781	470.271
Magnesium	382.932	383.162	516.739	517.292	518.394	552.785	
Manganese	257.610	259.373	279.482	403.076	403.307	403.449	
Molybdenum	313.259	317.035	379.825	386.411	390.296	550.649	
Nickel	341.457	345.847	349.296	351.505	352.454	361.939	
Silicon	252.851	504.103	505.598	566.956			
Silver	328.068	338.289	381.094	520.908	546.550	768.778	
Sodium	312.442	313.548	316.374	330.237	588.995	589.592	
Tin	270.651	283.999	286.332	300.914	303.412	317.505	
Titanium	323.452	334.941	336.121	364.268	365.350	399.864	
Tungsten	400.875	429.461	438.487	439.006	439.009	439.516	440.876
Vanadium	411.199	437.943	438.487	439.006	439.009	439.516	440.876
Zinc	255.795	328.233	330.258	334.502	491.162	636.234	
Zirconium	339.198	343.823	349.621	360.119	386.387	389.032	528.005

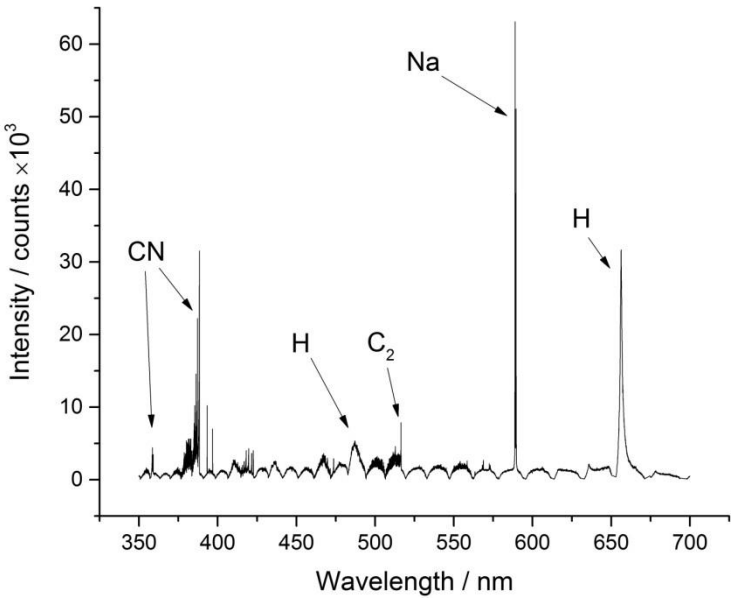

Figure 4.2. LIBS spectrum of blank carbon sticky pad

To highlight the differences between the CRM-124, CUP-2 and blank spectra, Figure 4.3 shows the nitrogen emission envelope around 820 nm as an example. The measurements were undertaken in air and there were no reported nitrogen impurities in the samples. Therefore, it is assumed that the nitrogen emissions arose from ambient N_2 gas excited by the laser ablation event. The blank and CRM-124-1 spectra show intense nitrogen peaks, whereas the CUP-2 spectrum shows very weak nitrogen emissions. The only intense peaks in the CUP-2 spectrum are sodium emissions lines which are repeated in the blank and CRM-124-1 spectra.

The hydrogen emission line at 656.28 nm (n=3 → n=2; 97492 → 82259 cm^{-1} [37]) was also quite different between the blank, CRM-124-1 and CUP-2 spectra as shown in Figure 4.4. Once again, hydrogen was not a listed impurity in the samples. Therefore, the only sources of hydrogen in the plasma were from the carbon adhesive mount or from moisture in the uranium material or the ambient gas. The documentation provided with the samples states that CUP-2 has a concentration of 2.94 wt. % moisture [34], whereas there is no description of the moisture in the CRM-124 samples [33]. The physical properties of CRM-124 suggest there should be less moisture present, as it is harder for moisture to permeate into hard ceramic granules. Figure 4.4 shows an intense hydrogen emission peak in the blank spectrum, an intermediate hydrogen peak in the CRM-124-1 spectrum and no evidence of a peak in the CUP-2 spectrum.

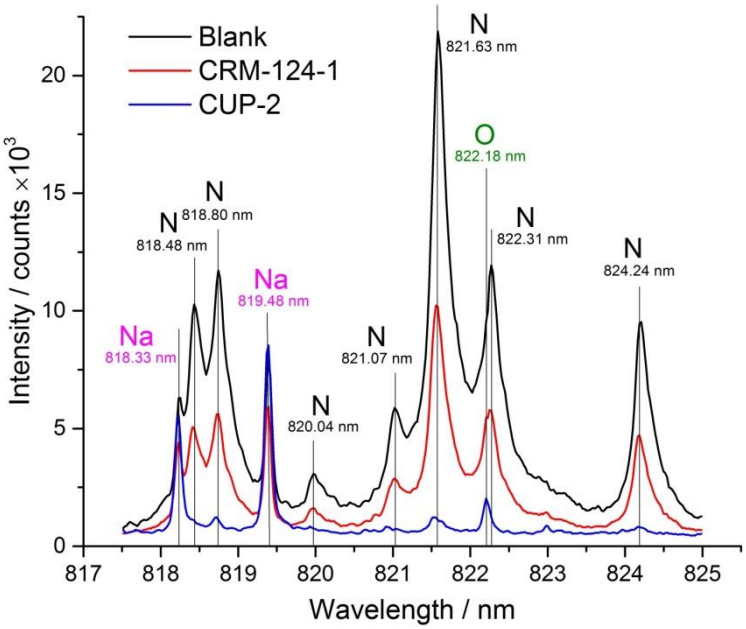

Figure 4.3. LIBS spectral region showing nitrogen, oxygen and sodium emission lines for a blank and two uranium-containing samples. Blank, black; CRM-124-1, red; CUP-2, blue (25 shots averaged)

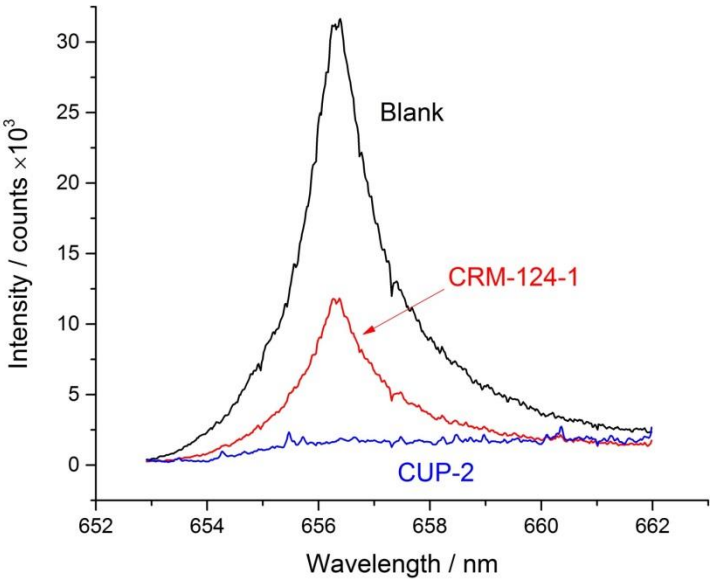

Figure 4.4. Hydrogen resonance line at 656.28 nm. Black, blank; Red, CRM-124-1; Blue, CUP-2 (25 shots averaged)

The differences in nitrogen and hydrogen emission intensities between the blank, CRM-124 and CUP-2 spectra are evidence of how the ablation process varied significantly between

the samples. LIBS measurements are traditionally strongly influenced by surface finish, as minor changes in reflectivity, texture or sample height (relative to the focal point of the ablation laser) can significantly affect the ablation process. Intense hydrogen and nitrogen peaks in the blank and CRM-124-1 spectra indicate the laser interacted less with the granular powder of the CRM-124-1 and ablated the carbon adhesive material. The lack of nitrogen and hydrogen peaks in the CUP-2 sample indicates that the laser could analyse the sample material better and resulted in reduced ablation of the carbon adhesive beneath. This fits with the physical characteristics of both samples: the CUP-2 powder was much finer and more easily manipulated into a homogenous layer, whereas the CRM-124 samples were more granular which left gaps between the grains. The result of the spectral differences was that the CUP-2 could not be used for the PLS modelling.

4.4.2 Partial least squares regression analysis

Excluding the CUP-2 samples from the PLS models gave good predicted versus measured concentration graphs for the CRM-124 sample series for most of the elements present. The results are listed in Table 4.3. The highest RMSECV value was obtained with the sodium model, which is unsurprising given the prevalence of the sodium emission peaks in the blank sample (Figure 4.2).

Examples of predicted versus measured concentration graphs for two models are shown in Figure 4.5. These models represent the lowest RMSECV of 0.84 μg g^{-1} for silver and the highest RMSECV (excluding sodium) of 81.3 μg g^{-1} for molybdenum. The outlier point marked in the molybdenum graph (panel B) shows a predicted concentration of over 400 μg g^{-1} for a measured value of 100 μg g^{-1}. Excluding this value from the RMSECV modelling improves the RMSECV from 94.3 μg g^{-1} to 27.6 μg g^{-1}. The large variation between results from identical samples is clearly a problem for the application of this technique.

Table 4.3. Trace element present in sample, measured and predicted concentration of each element in the highest concentration sample (CRM-124-1) and root mean squared error of cross-validation for each element, measured with PLS of specific spectral regions

Element	**CRM-124-1 measured concentration / μg g^{-1}**	**CRM-124-1 predicted concentration / μg g^{-1}**	**RMSECV / μg g^{-1}**	**Number of latent variables**
Aluminium	205	50	70.3	1
Beryllium	25	12	12.7	1
Bismuth	50	8	19.4	1
Boron	5.1	1	1.9	1
Cadmium	5.2	2	1.4	6
Calcium	200	118	44.3	2
Chromium	102	88	10.6	8
Cobalt	25	5	9.0	1
Copper	50	30	9.5	9
Iron	210	51	70.6	2
Lead	51	59	68.0	1
Magnesium	101	71	23.6	3
Manganese	51	25	13.0	10
Molybdenum	100	235	94.3	3
Nickel	202	39	72.4	1
Silicon	202	29	81.3	1
Silver	5	4	0.8	4
Sodium	400	65	586.0	1
Tin	51	39	10.1	6
Titanium	50	7	29.1	10
Tungsten	200	31	75.0	1
Vanadium	50	77	22.9	10
Zinc	202	72	69.4	8
Zirconium	200	30	75.8	1

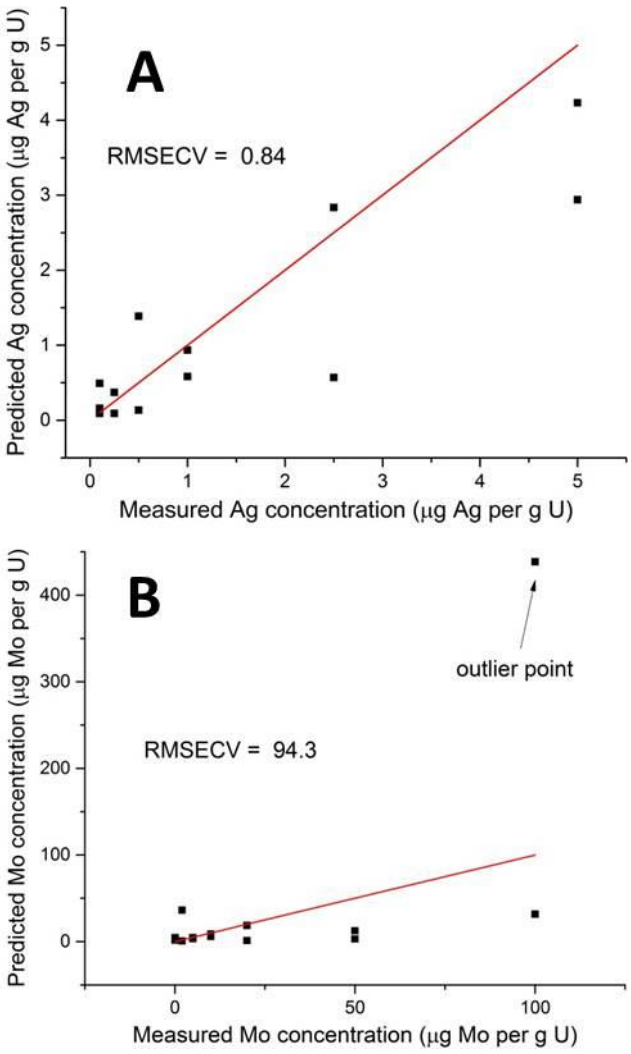

Figure 4.5. Predicted versus measured concentration graphs for A) silver and B) molybdenum, formed using PLS of selected spectral regions. Red line shows 'ideal' linear relationship between measured and predicted concentrations

(See Appendix Figure 8.3 for error bars of RMSECV)

The results in Table 4.3 show a positive correlation between element concentration and RMSECV, suggesting that the modelling was more accurate for lower concentration species. This trend is evident in Figure 4.6, which shows the RMSECV and the concentration of each element in sample CRM-124-1. However, RMSECV is a metric for the absolute error rather than the percentage error. More information can be extracted by comparing the ratio of RMSECV to sample concentration for each element, as shown in Figure 4.7. The majority of the elements are clustered between 0.1 and 0.4. The exceptions are sodium (which has been discusses previously), lead and molybdenum which have significantly higher ratio than

the other elements. Overall, the results do not seem biased towards lower concentration species.

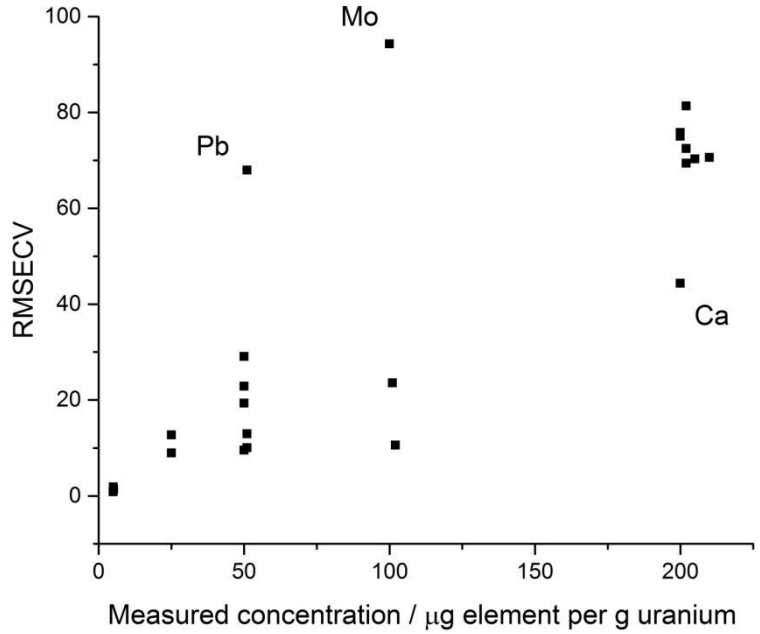

Figure 4.6. RMSECV against concentration for 23 impurity elements. Outliers Mo (molybdenum), Pb (lead) and Ca (calcium) are labelled. Data point for sodium (RMSECV = 586 μg g-1) is removed from figure for ease of reporting

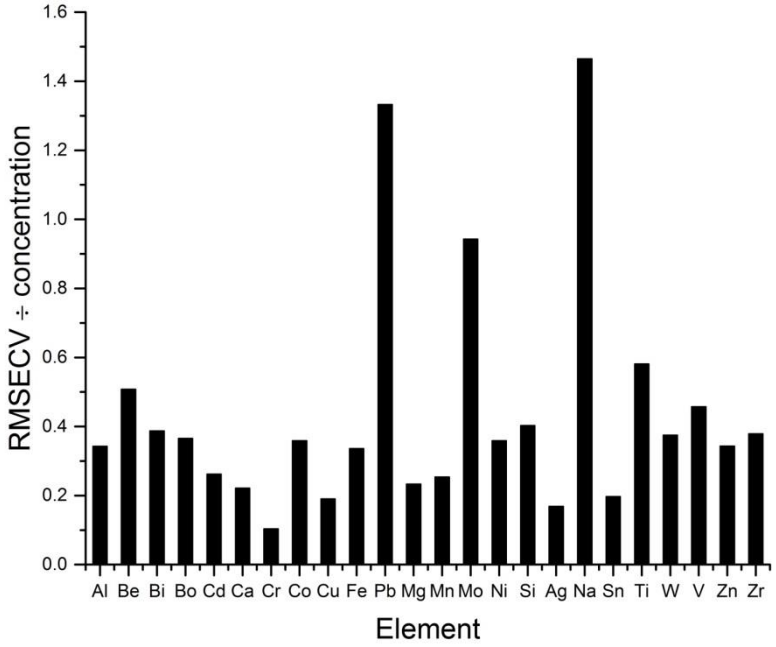

Figure 4.7. RMSECV per concentration of element in sample CRM-124-1 for each element modelled with PLS

The limit of detection (LoD) is dependent on the spectral response for the specific transitions selected for PLS analysis and as such is element-specific. Traditionally, the LIBS technique is quoted as having limits of detection down to 10 μg g^{-1} or lower [38,39]. However, this relies on numerous factors being optimised. For example, sample preparation methods and sample surface finish play an important role in the repeatability of the ablation process and so influence the standard deviation of both the noise and the analyte signal strength. Additionally, apparatus modifications such as controlling the sheath gas [40] and the pressure [41] or the use of multiple laser pulses [42,43] can be used to improve both the repeatability and the strength of analyte response. In this work, the sample preparation was kept deliberately unrefined to better simulate a field-deployed nuclear forensics investigation. However, this led to poorer repeatability and as such reduced accuracy of the modelling. It is probable that the lowest concentration elements in the samples were below the LoD. As such, the software may have been modelling the noise rather than the analyte. Analysing a greater number of replicate samples could have enabled more information to be extracted as peaks with lower intensity may have been identified above the noise.

As we have shown, the quantitative ability of LIBS is linked to using matrix-matched samples and is improved with the use of elements at higher concentrations which present a strong analyte response. In the case of nuclear materials, emission lines must be strong enough to overcome the crowded uranium spectrum. Qualitative analysis with LIBS would still be a useful addition to a nuclear forensics toolkit given the rapid measurement time and benefits of multi-element analysis, stand-off detection and portability. Numerous processes in the nuclear fuel cycle do use standardised materials. For example uranium ore concentrate is fairly ubiquitous, and uranium oxide fuel pellets are normally physically quite similar. LIBS would certainly be a useful technique for quantitative analysis in these applications where more of the sampling conditions could be controlled. The creation of a spectral library or database of LIBS measurements could enable rapid comparisons between an unknown sample and known stockpiles of nuclear materials.

4.5 Conclusions

Nuclear forensics is the process of identifying suspicious nuclear material to ascertain its characteristics and origin. Laser-induced breakdown spectroscopy (LIBS) could be a useful

tool for nuclear forensics, owing to the advantages of rapid analysis time, no sample preparation, portability and stand-off capabilities.

In this study, LIBS was used to analyse uranium oxide samples with known trace element impurities. The sample series consisted of seven uranium oxide samples with increasing levels of twenty four trace elements. A further uranium ore concentrate sample could not be included in the modelling because the samples were not matrix matched and there were significant differences between the LIBS spectra. Partial least squares regression (PLS) modelling was performed on the sample series in order to plot predicted versus measured concentration graphs and calculate the root mean squared error of cross-validation (RMSECV). Improvement to the PLS modelling was achieved by selecting specific regions of interest centred on spectral spectroscopic transitions rather than analysing the entire LIBS spectrum. This method gave RMSECV values between 0.8 $\mu g\ g^{-1}$ and 94 $\mu g\ g^{-1}$ for all but one element (sodium) which could not be modelled accurately as it appeared in the blank.

The main source of uncertainty in the modelling was from shot-to-shot variations in the laser ablation process, caused by inhomogeneity in the samples. The sample preparation was deliberately designed to simulate a field-deployed nuclear forensics investigation, so no attempt was made to control the sample surface which could have improved the repeatability and signal to noise ratio. Additionally, some elements were present at concentrations below the traditional limit of detection for the LIBS technique which casts doubt over the low RMSECV results for some elements. Future experiments could be conducted with specifically designed samples with higher concentrations of impurity elements. Furthermore, the use of rare earth elements or fission product surrogates as impurities would make the samples more applicable to the field of nuclear forensics. Additional improvements could be achieved without compromising the rapid measurement time or increasing the physical footprint of the apparatus by using double-pulsed LIBS.

Acknowledgements

The authors would like to thank AWE and EPSRC for funding the PhD project behind this work through the Materials for Demanding Environments Centre for Doctoral Training. We would also like to thank Dr Matthew Higginson from AWE for his help with sample preparation and transportation.

4.6 References

[1] IAEA, Advances in Nuclear Forensics: Countering the Evolving Threat of Nuclear and Other Radioactive Material out of Regulatory Control, in: IAEA Proc. Ser., Vienna, Austria, 2014: p. 149. http://www-pub.iaea.org/books/IAEABooks/10881/Advances-in-Nuclear-Forensics-Countering-the-Evolving-Threat-of-Nuclear-and-Other-Radioac.

[2] V. Fedchenko, The Role of Nuclear Forensics in Nuclear Security, Strateg. Anal. 38 (2014) 230–247. doi:10.1080/09700161.2014.884442.

[3] IAEA, Identification of High Confidence Nuclear Forensics Signatures, Vienna, Austria, 2017. https://www.iaea.org/publications/12231/identification-of-high-confidence-nuclear-forensics-signatures.

[4] IAEA, Development of a National Nuclear Forensics Library: A System for the Identification of Nuclear or Other Radioactive Material out of Regulatory Control, Vienna, Austria, 2018. https://www.iaea.org/publications/13438/development-of-a-national-nuclear-forensics-library-a-system-for-the-identification-of-nuclear-or-other-radioactive-material-out-of-regulatory-control.

[5] E. Keegan, M.J. Kristo, K. Toole, R. Kips, E. Young, Nuclear Forensics: Scientific Analysis Supporting Law Enforcement and Nuclear Security Investigations, Anal. Chem. 88 (2016) 1496–1505. doi:10.1021/acs.analchem.5b02915.

[6] IAEA, Planning and Organizing Nuclear Security Systems and Measures for Nuclear and Other Radioactive Material out of Regulatory Control, Vienna, Austria, 2018. doi:1.

[7] IAEA, Prevention of the inadvertent movement and illicit trafficking of radioactive materials, 2002. http://www-pub.iaea.org/MTCD/publications/PDF/te_1311_web.pdf.

[8] J.H. Rim, K.J. Kuhn, L. Tandon, N. Xu, D.R. Porterfield, C.G. Worley, M.R. Thomas, K.J. Spencer, F.E. Stanley, E.J. Lujan, K. Garduno, H.R. Trellue, Determination of origin and intended use of plutonium metal using nuclear forensic techniques, Forensic Sci. Int. 273 (2017) e1–e9. doi:10.1016/j.forsciint.2017.01.014.

[9] IAEA, Nuclear Forensics in Support of Investigations, Vienna, Austria, 2015. http://www-pub.iaea.org/books/IAEABooks/10797/Nuclear-Forensics-in-Support-of-Investigations.

[10] K. Mayer, M. Wallenius, K. Lützenkirchen, J. Galy, Z. Varga, N. Erdmann, R. Buda, J. V Kratz, N. Trautmann, K. Fifield, Nuclear forensics: A methodology applicable to nuclear security and to non-proliferation, J. Phys. Conf. Ser. 312 (2011). doi:10.1088/1742-6596/312/6/062003.

[11] IAEA, Nuclear Forensics Support, International Atomic Energy Agency, Vienna, Austria, 2006. http://www-pub.iaea.org/MTCD/publications/PDF/Pub1241_web.pdf.

[12] S.S. Harilal, B.E. Brumfield, N.L. Lahaye, K.C. Hartig, M.C. Phillips, Optical spectroscopy

of laser-produced plasmas for standoff isotopic analysis, Appl. Phys. Rev. 5 (2018) 1–32. doi:10.1063/1.5016053.

[13] S. Palanco, C. López-Moreno, J.J. Laserna, Design, construction and assessment of a field-deployable laser-induced breakdown spectrometer for remote elemental sensing, Spectrochim. Acta - Part B At. Spectrosc. 61 (2006) 88–95. doi:10.1016/j.sab.2005.12.004.

[14] C. López-Moreno, S. Palanco, J.J. Laserna, F. DeLucia, A.W. Miziolek, J. Rose, R.A. Walters, A.I. Whitehouse, Test of a stand-off laser-induced breakdown spectroscopy sensor for the detection of explosive residues on solid surfaces, J. Anal. At. Spectrom. 21 (2006) 55–60. doi:10.1039/b508055j.

[15] J.B. Sirven, B. Sallé, P. Mauchien, J.L. Lacour, S. Maurice, G. Manhès, Feasibility study of rock identification at the surface of Mars by remote laser-induced breakdown spectroscopy and three chemometric methods, J. Anal. At. Spectrom. 22 (2007) 1471–1480. doi:10.1039/b704868h.

[16] X. Wan, P. Wang, Remote quantitative analysis of minerals based on multispectral line-calibrated laser-induced breakdown spectroscopy (LIBS), Appl. Spectrosc. 68 (2014) 1132–1136. doi:10.1366/13-07203.

[17] Y. Deguchi, M. Noda, Y. Fukuda, Y. Ichinose, Y. Endo, M. Inada, Y. Abe, S. Iwasaki, Industrial applications of temperature and species concentration monitoring using laser diagnostics, Meas. Sci. Technol. 13 (2002). doi:10.1088/0957-0233/13/10/201.

[18] M.A. Gondal, T. Hussain, Determination of poisonous metals in wastewater collected from paint manufacturing plant using laser-induced breakdown spectroscopy, Talanta. 71 (2007) 73–80. doi:10.1016/j.talanta.2006.03.022.

[19] G. Lorenzetti, S. Legnaioli, E. Grifoni, S. Pagnotta, V. Palleschi, Laser-based continuous monitoring and resolution of steel grades in sequence casting machines, Spectrochim. Acta - Part B At. Spectrosc. 112 (2015) 1–5. doi:10.1016/j.sab.2015.07.006.

[20] M. Gaft, I. Sapir-Sofer, H. Modiano, R. Stana, Laser induced breakdown spectroscopy for bulk minerals online analyses, Spectrochim. Acta - Part B At. Spectrosc. 62 (2007) 1496–1503. doi:10.1016/j.sab.2007.10.041.

[21] N.A. Smith, J.A. Savina, M.A. Williamson, Application of Laser Induced Breakdown Spectroscopy to Electrochemical Process Monitoring of Molten Chloride Salts, in: Symp. Int. Safeguards Link. Strateg. Implement. People, Vienna, Austria, 2014: pp. 1–7. https://www.semanticscholar.org/paper/Application-of-Laser-Induced-Breakdown-Spectroscopy-Smith-Savina/84faa4386f3a0991da8ec68e0ee542c6cf598269.

[22] J. Wu, Y. Qiu, X. Li, H. Yu, Z. Zhang, A. Qiu, Progress of laser-induced breakdown spectroscopy in nuclear industry applications, J. Phys. D. Appl. Phys. 53 (2020) 023001. doi:10.1088/1361-6463/ab477a.

[23] M. Shattan, M. Gragston, Z. Zhang, J.D. Auxier, K.G. McIntosh, C. Parigger, Mapping of Uranium in Surrogate Nuclear Debris Using Laser-Induced Breakdown Spectroscopy (LIBS), Appl. Spectrosc. 73 (2019) 591–600. doi:10.1177/0003702819842871.

[24] V. Margetic, M.A. Bolshov, A. Stockhaus, K. Niemax, R. Hergenroder, Depth profiling of multi-layer samples using femtosecond laser ablation, J. Anal. At. Spectrom. 16 (2001) 616–621. doi:10.1039/b100016k.

[25] D.G. Papazoglou, V. Papadakis, D. Anglos, In situ interferometric depth and topography monitoring in LIBS elemental profiling of multi-layer structures, J. Anal. At. Spectrom. 19 (2004) 483–488. doi:10.1039/b315657r.

[26] J. Sirven, A. Pailloux, Y. M'Baye, N. Coulon, T. Alpettaz, S. Gossé, Towards the determination of the geographical origin of yellow cake samples by laser-induced breakdown spectroscopy and chemometrics, J. Anal. At. Spectrom. 24 (2009) 451–459. doi:10.1039/b821405k.

[27] M.Z. Martin, S. Allman, D.J. Brice, R.C. Martin, N.O. Andre, Exploring laser-induced breakdown spectroscopy for nuclear materials analysis and in-situ applications, Spectrochim. Acta - Part B At. Spectrosc. 74–75 (2012) 177–183. doi:10.1016/j.sab.2012.06.049.

[28] B. Bhatt, A. Dehayem-Kamadjeu, K.H. Angeyo, Rapid nuclear forensics analysis via machine-learning-enabled laser-induced breakdown spectroscopy (LIBS), AIP Conf. Proc. 060006 (2019) 1–4. doi:10.1063/1.5110124.

[29] G. Hull, E.D. McNaghten, C. Sharrad, P.A. Martin, Quantitative Prediction of Rare Earth Concentrations in Salt Matrices using Laser-Induced Breakdown Spectroscopy for Application to Molten Salt Reactors and Pyroprocessing, (2020).

[30] P. Fichet, P. Mauchien, C. Moulin, Determination of impurities in uranium and plutonium dioxides by laser-induced breakdown spectroscopy, Appl. Spectrosc. 53 (1999) 1111–1117. doi:10.1366/0003702991947892.

[31] R.C. Chinni, D.A. Cremers, L.J. Radziemski, M. Bostian, C. Navarro-Northrup, Detection of uranium using laser-induced breakdown spectroscopy, Appl. Spectrosc. 63 (2009) 1238–1250. http://www.osapublishing.org/abstract.cfm?uri=as-63-11-1238.

[32] B.T. Manard, E.M. Wylie, S.P. Willson, Analysis of Rare Earth Elements in Uranium Using Handheld Laser-Induced Breakdown Spectroscopy (HH LIBS), Appl. Spectrosc. 72 (2018) 1653–1660. doi:10.1177/0003702818775431.

[33] P.M. Santoliquido, Preparation and provisional certification of NBL Spectrographic Impurity Standards, CRM 123 (1-7) and 124 (1-7), Argonne, Illinois, 1983. https://inis.iaea.org/search/searchsinglerecord.aspx?recordsFor=SingleRecord&RN=15035310.

[34] G. Eppich, R. Kips, R. Lindvall, Compilation of LLNL CUP-2 Data, 2016.

[35] E.J. Judge, J.E. Barefield, J.M. Berg, S.M. Clegg, G.J. Havrilla, V.M. Montoya, L.A. Le, L.N. Lopez, Laser-induced breakdown spectroscopy measurements of uranium and thorium powders and uranium ore, Spectrochim. Acta - Part B At. Spectrosc. 83–84 (2013) 28–36. doi:10.1016/j.sab.2013.03.002.

[36] E.J. Judge, J.M. Berg, L.A. Le, L.N. Lopez, J.E. Barefield, LIBS Spectral Data for a Mixed

Actinide Fuel Pellet Containing Uranium, Plutonium, Neptunium and Americium, Los Alamos, 2012. doi:10.2172/1044103.

[37] A. Kramida, Y. Ralchenko, J. Reader, The NIST ASD Team (2018), NIST Atomic Spectra Database, NIST At. Spectra Database (Ver. 5.6.1). [Online] (2019) http://physics.nist.gov/asd. doi:10.18434/T4W30F.

[38] R. Noll, Laser-Induced Breakdown Spectroscopy, First Edit, Springer, 2012. doi:10.1007/978-3-642-20668-9.

[39] D.A. Cremers, L.J. Radziemski, Handbook of Laser-Induced Breakdown Spectroscopy, Second, Wiley, 2013. doi:10.1002/9781118567371.

[40] D. Zhang, X. Ma, S. Wang, X. Zhu, Influence of ambient gas on laser-induced breakdown spectroscopy of uranium metal, Plasma Sci. Technol. 17 (2015) 971–974. doi:10.1088/1009-0630/17/11/15.

[41] S.S. Harilal, B. O'Shay, Y. Tao, M.S. Tillack, Ambient gas effects on the dynamics of laser-produced tin plume expansion, J. Appl. Phys. 99 (2006). doi:10.1063/1.2188084.

[42] R. Ahmed, M.A. Baig, A comparative study of single and double pulse laser induced breakdown spectroscopy, J. Appl. Phys. 106 (2009). doi:10.1063/1.3190516.

[43] P.J. Skrodzki, J.R. Becker, P.K. Diwakar, S.S. Harilal, A. Hassanein, A Comparative Study of Single-pulse and Double-pulse Laser-Induced Breakdown Spectroscopy with Uranium-containing Samples, Appl. Spectrosc. 70 (2016) 467–473. doi:10.1177/0003702815626670.

Chapter 5 – Isotopic analysis and plasma diagnostics for lithium detection using combined laser ablation–tuneable diode laser absorption spectroscopy and laser-induced breakdown spectroscopy

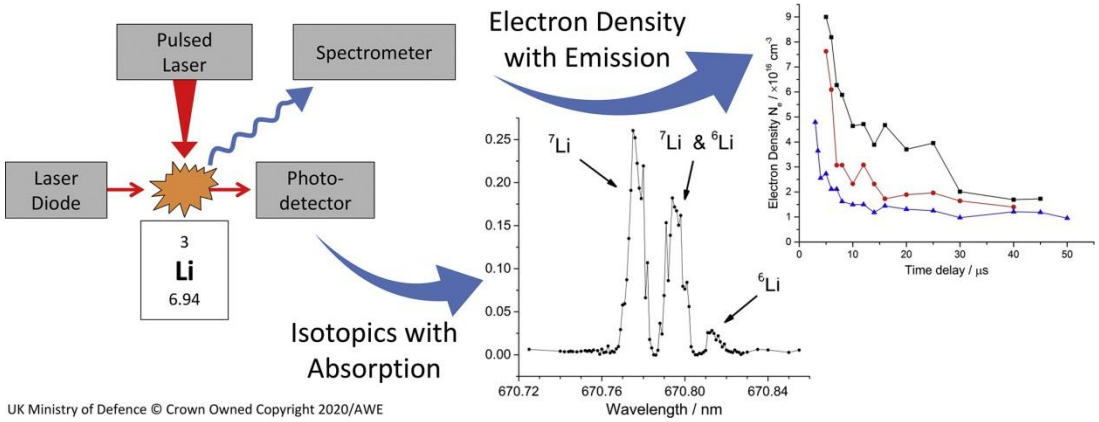

This chapter has been published in *Spectrochimica Acta Part B: Atomic Spectroscopy*, Volume 177, page 106051, March 2021.

DOI: 10.1016/j.sab.2020.106051

Authors: Gregory Hull †[a,b], Edward D. McNaghten [c], Paul Coffey [a,b], Philip Martin †[a,b]

a. Department of Chemical Engineering and Analytical Science, University of Manchester, Oxford Road, Manchester, M13 9PL

b. Photon Science Institute, University of Manchester, Oxford Road, Manchester, M13 9PL

c. AWE, Aldermaston, Reading, Berkshire, RG7 4PR

† Corresponding Authors

Author contribution: constructed the LA-TDLAS apparatus and the external cavity diode laser; fabricated the lithium samples; analysed the samples; performed the data analysis; and wrote the paper.

5.1 Abstract

Laser-Induced Breakdown Spectroscopy (LIBS) enables rapid stand-off measurements of potentially hazardous material which is particularly favourable for applications in the nuclear industry. Isotopic characterisation with LIBS remains challenging because of the narrow separation of isotopic emission lines, which demands large, high resolution spectrometers. To address this, laser ablation (LA)-Tuneable Diode Laser Absorption Spectroscopy (TDLAS) has been combined with LIBS to analyse laser-produced plasma of lithium. Isotope ratio calculations were performed by fitting multiple peaks to the Li absorption spectra, achieving a relative error of 13% at later delay times after line broadening had reduced. Double-pulsed laser ablation resulted in narrower absorption peaks but more noise in the absorption spectra. LIBS and LA-TDLAS spectra were used simultaneously to calculate plasma temperature and electron density for both single- and double-pulsed laser ablation. The Doppler broadening of absorption peaks from LA-TDLAS was used to calculate the plasma temperature after long time delays of 200 µs. The temperature followed an exponential decay which was extrapolated back to early delay times in order to predict the temperature throughout the plasma lifecycle. The electron density was calculated using the Stark broadening of emission peaks from the LIBS spectra, which were temperature-corrected by accounting for the Doppler broadening. Both single- and double-pulsed-laser ablation plasmas exhibited maximum electron densities of around 10^{16} to 10^{17} cm^{-3}, although the decay rate was reduced by around a factor of 2 using DP-laser ablation. We have shown that the combination of emission and absorption spectroscopy with LIBS and LA-TDLAS is useful for isotopic analysis and calculating laser ablation plasma properties. We have demonstrated that double pulsed laser ablation has the potential to enable more isotopic pairs to be analysed due to the narrower absorption linewidth.

Key Words:

LIBS; Tuneable diode laser absorption spectroscopy; Laser ablation; Double-pulse LIBS; Isotopic analysis

5.2 Introduction

Laser ablation (LA) -based analytical techniques offer rapid and robust atomic information, often irrespective of a samples' surface finish or physical state. LA-Inductively Coupled Plasma Mass Spectroscopy (LA-ICP-MS) and Laser-Induced Breakdown Spectroscopy (LIBS) are two examples of how commercially available pulsed lasers have rapidly advanced the field of atomic spectroscopy. Of these two techniques, LIBS is more adaptable to field-deployment and portability, as it does not require a special sample chamber or vacuum, allows standoff capabilities which can shield the user from harmful material [1–3], requires zero or minimal sample preparation, can extract multi-elemental information from any sample material and enables rapid measurements to be performed, thereby allowing in-line analysis to be achieved [4–6]. Problems associated with other elemental analysis techniques which can be used for in-line analysis, such as X-Ray Fluorescence (XRF) or Spark Discharge Optical Emission Spectroscopy (SD-OES), can be overcome by LIBS and the technique is amenable to the detection of a broader range of analytes than these methods [7].

Line broadening mechanisms, particularly Stark broadening, and bremsstrahlung background emission reduce the spectral quality of LIBS [8]. These drawbacks can be managed with control of the time delay and width of the acquisition window, but ultimately limit the potential for quantitative analytical data and isotopic information to be obtained from a measurement. Numerous attempts have been made to increase the spectral resolution and improve the detection limits which can be achieved by LIBS: these include the use of multiple laser pulses for the ablation process [9–12]; hardware additions such as spectrometer enhancements [13,14], magnetic fields [15], and electric discharges [16]; and chemometric methods [17–22]. Many chemometric techniques have become commonplace, particularly multivariate data analyses such as Partial Least Squares (PLS) and Principal Component Analysis (PCA).

Double-Pulsed-LIBS (DP-LIBS) has been shown to have an improved analytical performance over Single-Pulsed-LIBS (SP-LIBS) in terms of Limit of Detection (LoD) and shot-to-shot variation [9,23,24]. In DP-LIBS the first laser pulse ablates the sample and creates the plasma whilst the second pulse re-heats the already-vaporised analyte. Many different adaptations of DP-LIBS have been reported. A collinear design is often used, with both laser

pulses focussed from vertically above the sample surface. This has been demonstrated with multiple-pulses from the same laser [25] and with separate lasers aligned coaxially [11,26,27]. Orthogonal orientations, in which a second laser pulse interacts with the ablation plume from a position parallel to the sample surface, have also been realised [28–30]. Firing the orthogonal laser as a pre-pulse to rarefy the sheath gas also changes the dynamics of plume expansion and can improve the emission intensity (i.e. reduce bremsstrahlung effects) [28,31]. Additionally, combinations of various laser wavelengths [11], spot sizes [32], pulse energies [12] and pulse lengths [10,33] have been studied. Many of these have demonstrated significant improvements in terms of Signal to Noise Ratio (SNR) and LoDs compared to SP-LIBS.

Characteristics of LIBS such as standoff capability and immediate in situ quantification suggest the technique would be particularly suited to applications within the nuclear fuel cycle. However, a challenge limiting implementation of this approach in the nuclear industry is the inability of LIBS to offer isotopic characterisation of materials without the use of expensive, bulky, low light throughput spectrometers. Isotopic LIBS continues to be difficult to achieve because of the narrow separation of isotopic emission lines combined with line-broadening mechanisms within the laser ablation-produced plasma (LPP). For example, the largest separation of emission lines between the ^{235}U and ^{238}U isotopes is 25 pm [34], and for ^{239}Pu and ^{240}Pu just 13 pm [35]. Isotope shifts are caused by the mass shift and the volume (or 'field') shift. For elements of lower atomic mass such as H and Li, a change in mass caused by the addition of one neutron has a large effect in relative terms, whereas for the heavier elements such as U and Pu it is negligible. However, the volume shift is greater for heavier elements. As such, isotope shifts are greatest for elements at the extremities of the periodic table. The elements towards the centre of the periodic table exhibit very small isotope shifts (less than 1 pm for most elements) [36].

Tuneable semiconductor diode lasers have enhanced atomic spectroscopy because of their narrow spectral linewidth, ever increasing spectral coverage, high stability, low cost, small size and low power requirements [37–39]. Detection limits of the order of pg/g have been achieved in elemental analyses performed using Tuneable Diode Laser Absorption Spectroscopy (TDLAS) [40] under appropriate conditions. Isotope-selective measurements can be performed using TDLAS: the required high resolution provided by the narrow laser

linewidth [41]. Absorption spectroscopy is generally carried out on gas and liquid samples, as light must be detected beyond a sample and compared to a reference beam. As such, an integral part of TDLAS is atomisation of solid samples. This has been accomplished in the past using graphite furnaces [42–44], flames [45–47] and plasma [48,49] atomisers.

LA-TDLAS facilitates atomisation of solid samples with minimal sample preparation, whilst maintaining the benefits of standoff, rapid and in situ sampling associated with laser spectroscopy. Additionally, for certain elements, LA-TDLAS could determine isotopic distributions which are not easily achievable by other field-deployable techniques. As such, LA-TDLAS has been proposed as a method to analyse uranium and plutonium isotopics in the nuclear industry [48–54]. Most literature to date has focussed solely on absorption spectroscopy and not utilised the emissions from the LPP in an analytical manner (i.e. using LIBS). Additionally, there are few studies [55] conducted at atmospheric pressure due to the challenges associated with the complex LA process. Hyphenating the elemental analysis of LIBS with the isotopic analysis of LA-TDLAS would create a combined method which could find use throughout the nuclear fuel cycle. The benefits of laser-based spectroscopy of high sample throughput, minimal sample preparation, portable experimental hardware and the opportunity for stand-off analysis would be maintained with the two complimentary analyses. The combined strategy would also be appealing to the field of nuclear forensics [56,57]. The combined analysis could also use complimentary information to improve overall accuracy. For example, in most laser ablation experiments the temperature is estimated from prior knowledge of the equipment parameters and the sample material, whereas in these experiments the LA-TDLAS results were used to calculate the temperature more accurately. This led to more accurate electron density calculations as the line broadening caused by temperature (Doppler broadening) could be accounted for.

In this study, a combined LA-TDLAS with LIBS setup has been constructed and tested for analytical performance under atmospheric conditions. Lithium was chosen as a sample material because the Li isotope shift is comparable to that found in nuclear materials (^{6}Li ↔ ^{7}Li = 15 pm; ^{235}U ↔ ^{238}U = 25 pm; ^{239}Pu ↔ ^{240}Pu = 13 pm). It was important to understand the laser ablation plasma's physical conditions of temperature and electron density to improve the accuracy of the isotope predictions. As such, temporal changes of temperature and electron density were monitored by recording simultaneous absorbance (LA-TDLAS) and

emission (LIBS) measurements. Due to the aforementioned benefits of DP-LIBS on the emission spectra, combined LA-TDLAS and LIBS measurements were also performed with DP-LA. It was hoped that the longer plasma lifetime and better shot-to-shot consistency achieved with DP-LA should lead to a longer time period for LA-TDLAS measurements to take place and improve the signal to noise ratio. Increasing the plasma lifetime could enable rapid wavelength ramping across several atomic or isotopic transitions as the plasma remains in a quasi-static state for a longer duration.

5.3 Materials and methods

5.3.1 Laser ablation – tuneable diode laser absorption spectroscopy apparatus

The ablation laser was a Q-switched Nd:YAG laser (Innolas Spitlight 600) operating at the fundamental wavelength of 1064 nm with a 6 ns pulse duration and a pulse energy of 85 mJ/pulse. The sample chamber (with xyz mobile stage) and beam focussing optics were designed and manufactured by Applied Photonics ltd. (Skipton, UK).

In brief, the TDLAS setup consisted of a collimated laser diode with a wavelength centred around 671 nm (Roithner Lasertechnik QL67F6SA) with a beam diameter of 1mm, two periscopes (to control the beam height and direction), a Si photodiode (Thorlabs DET10A/M, 0.8 mm^2, 1 ns rise time) with 30 mm focussing lens and a Data Acquisition (DAQ) card (National Instruments USB-6259, 1 MHz sampling rate, 16 bit). A bespoke Virtual Instrument (VI) was developed in LabView software (version 2016, National Instruments) to synchronise the laser ablation pulse and laser-absorption measurement, utilising a TTL pulse used to trigger the Nd:YAG laser. A schematic of the hyphenated LA-TDLAS experimental system combined with LIBS is shown in Figure 5.1. In order to optimise alignment of laser diode through the LPP, a sheet of burn paper angled at 45° to both the (vertical) YAG laser and (horizontal) laser diode was used to mark the point of YAG laser focus. Then, without adjusting the paper, the laser diode was aligned to the centre of the scorch mark created on the burn paper. The height of the laser diode beam above the sample surface was precisely adjusted to 1.5 mm using the periscope system, as this height maximised the absorbance from each LPP pulse. A final lens before the collection photodiode was required to capture

the full emission of the laser diode, as the beam was slightly deflected and scattered by shockwaves (Schilleren distortions) and particles (Raleigh and Mie scattering) produced during ablation.

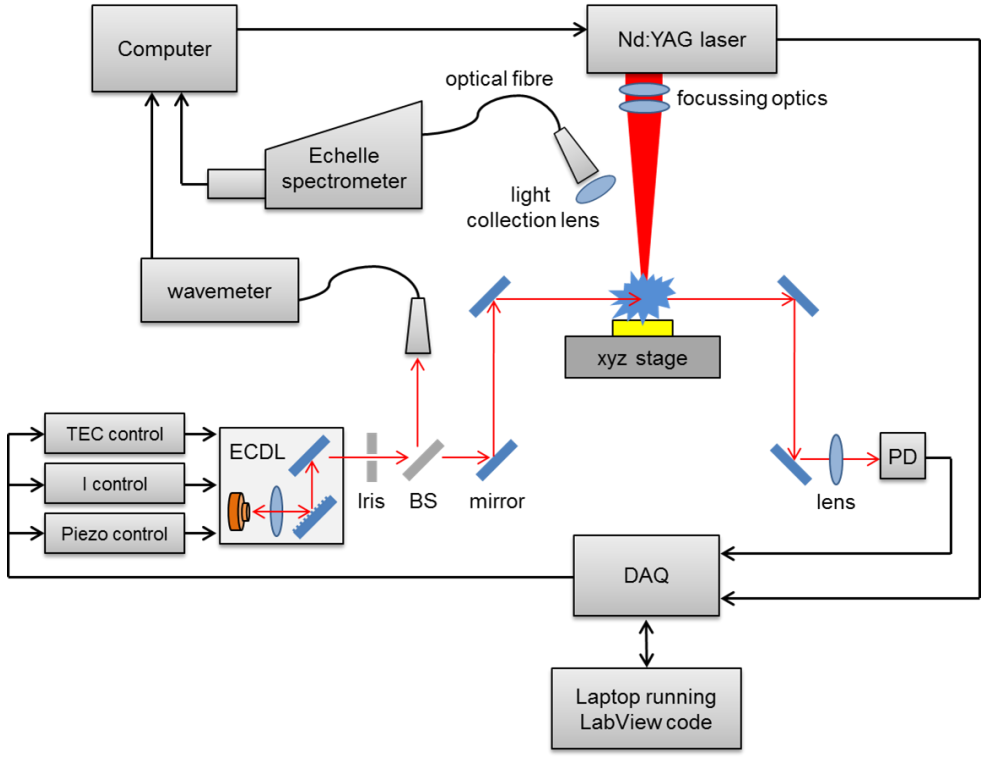

Figure 5.1. Schematic of hyphenated LIBS – LA-TDLAS setup (BS: beam splitter, PD: photodiode, DAQ: data acquisition card, TEC: thermoelectric cooler, ECDL: external cavity diode laser)

To attain the necessary spectral resolution for analysis of the Li absorption feature, the laser linewidth was reduced using a custom-built external cavity of length around 10 mm. This forced the multiple transverse-mode emission into a single-mode of around 400 kHz FWHM [58]. With temperature, current and grating-angle adjustments, the External Cavity Diode Laser (ECDL) had a mode-hop free tuning range of ±0.5 nm. The design improves upon that published by Hawthorn et al [58] in 2001. Our design uses an off-the-shelf kinematic mirror mount with piezoelectric actuators (Thorlabs KC1-PZ/M), which reduces the complexity and number of bespoke parts required (for more information see ref. [59] and Appendix Section 8.2).

5.3.2 Laser-induced breakdown spectroscopy apparatus

For the LIBS measurements, plasma emissions were collected using a lens (10 cm focal length, 12.5 mm diameter) and transferred with a 2 m fibre-optic cable to an Echelle spectrometer (Lasertechnik Berlin [LTB] Aryelle-Butterfly) with ICCD camera (Andor iStar series). All LIBS measurement variables, including time delay (t_d) between laser pulse and measurement, width of time gate (t_g) and camera-gain were controlled by Aryelle software (LTB).

For DP-LIBS experiments, a simple collinear geometry was achieved by opening the Pockels cell twice during a single flashlamp pulse. The timing of the two pulses with respect to the flashlamp was controlled to achieve two pulses of equal intensity. A photodiode inside the laser cavity measured the amplitude of the two pulses from the scattered light. The shortest inter-pulse delay at which two identical pulses could be created was 3 µs. Temporal emission and absorption measurements are reported from the time of the second laser pulse. Although different combinations of geometries and pulses with unequal intensities have had positive impacts on emission spectra in the literature, it was impossible to control the laser geometry or pulse length due to the configuration of the experimental apparatus.

5.3.3 Lithium samples

The samples used were 1.00 g lithium tetraborate pellets, approximately 20 mm diameter by 2 mm depth, produced using a hydraulic presser. Before pressing, the lithium tetraborate powder (Fisher Scientific, 98%) was dried in an oven at 150 °C for 2hrs. The samples were stored in an air-tight chamber after production to limit exposure to atmospheric moisture. The surface of each sample was smoothed and polished using grinding paper (grit = p1200, p2400 and p4000) before each set of measurements to ensure a homogenous surface was maintained. Using this method of polishing allowed repeated measurements to be performed on each pellet. To record each individual ablation pulse, the position of the sample pellet was adjusted using the xyz stage to expose a fresh surface. A total of 10 repeat measurements were taken at each laser diode wavelength, with each shot separated by 0.5 mm on the surface. A baseline (I_0) was plotted using the photodiode voltage before each ablation shot and used to calculate the absorbance with Equation (6).

$$A = -\log_{10}\frac{I}{I_0} \quad (6)$$

5.3.4 Lithium line selection and spectral line broadening

The Li I D1 and D2 transitions centred around 670.78 nm have high transition strengths and can be accessed using commercial laser diodes for absorption measurements. The two transitions of ^{7}Li ($^{2}S_{1/2} \leftarrow {}^{2}P_{1/2}$ and $^{2}S_{1/2} \leftarrow {}^{2}P_{3/2}$) shown in Table 5.1 are both red shifted by an isotope shift of 15 pm for the corresponding ^{6}Li lines. As the D1 and D2 emissions are separated by a similar wavelength, a triplet pattern is produced. The natural isotopic abundance of the two isotopes (92.5 % ^{7}Li and 7.5 % ^{6}Li) combined with the different oscillator strengths of Li D1 and D2 results in a non-symmetrical triplet.

The emission from a laser ablation plasma changes temporally as the plasma cools. Broadband emission (bremsstrahlung) is produced during the early life of the plasma, after which ionic and then neutral atomic lines are detected. After this, the plasma cools further to leave a neutral atomic vapour plume which dissipates into the sheath gas. By measuring the emission and absorption at different points throughout the plasma lifecycle, changes in plasma composition and temperature have been compared for SP- and DP-LPP.

Spectral line broadening in a LPP is mainly caused by Stark and Doppler effects. The former depends on a local electric field caused by nearby ionised nuclei and electrons and dominates earlier in the plasma lifecycle when the plasma is hotter and contains more ionised species. The Stark broadening effects rapidly diminish as the plasma undergoes recombination and relaxation to leave excited neutral atoms. Doppler broadening is caused by thermal motion of atoms and continues when the plasma has relaxed to a neutral gas. Stark broadening results in a Lorentzian lineshape, while Doppler broadening leads to a Gaussian lineshape. A Voigt profile is a convolution of these two lineshapes. The Lorentzian width and the Gaussian width can be used to infer information about the plasma composition and the plasma temperature if the broadening mechanism and the analyte species are known [61]. The values of Lorentzian and Gaussian width obtained from a Voigt fit can be directly used as an indicator of the Stark and Doppler broadening, respectively. Stark broadening is dependent on the electron density, the plasma temperature and on

Table 5.1. Spectroscopic details of the two lithium lines used for TDLAS (λ: wavelength in air, f_{ik}: oscillator strength, A_{ki}: Einstein coefficient, $E_{i,k}$: energy of lower and upper level respectively) (taken from NIST Database [58])

Transition	**λ (nm)**	**Relative Intensity**	**f_{ik}**	**A_{Ki} $\times 10^7$ (s^{-1})**	**E_i (cm^{-1})**	**E_k (cm^{-1})**	**Lower Level**			**Upper Level**		
							Config.	**Term**	**J**	**Config.**	**Term**	**J**
^{7}Li D1	670.776	1.000	0.498	3.6891	0.00	14 904.00	$1s^2 2s$	^2S	1/2	$1s^2 2p$	$^2P°$	3/2
^{6}Li D1	670.791	0.081										
^{7}Li D2	670.791	0.500	0.249	3.6890	0.00	14 903.66	$1s^2 2s$	^2S	1/2	$1s^2 2p$	$^2P°$	1/2
^{6}Li D2	670.806	0.041										

Stark broadening coefficients. Many of the coefficients for Li transitions have been reported in literature [62] and can be found in online databases [63,64]. Doppler broadening is related to the plasma temperature with Equation (7) (*k* and *c* are physical constants; *T* is the plasma temperature in Kelvin; m_A is the atomic mass of lithium, 6.941; and λ_0 is the peak centre wavelength) [61].

$$w_G = \sqrt{\frac{8kT\ ln(2)}{m_A c^2}}\lambda_0 = 7.16 \times 10^{-7}\sqrt{\frac{T}{m_A}}\lambda_0 \qquad (7)$$

Stark broadening is linear with electron density [64], so when the Stark broadening coefficients and plasma temperature are known, the electron density can be calculated from the Lorentzian width of emission peaks.

Table 5.2 lists Li transitions used for N_e calculation using Stark broadening parameters. Not all the Li transitions visible in the spectra could be used for N_e calculations as many of the emission peaks displayed self-absorption effects. Self-absorption is often seen in LPP and LIBS measurements due to the non-homogenous plasma cross-section caused by different heating and cooling rates. The plasma exterior cools faster as it is in contact with the sheath gas, creating a layer of atoms at lower energy states which absorb light emitted from the hotter plasma core [65]. Transitions to lower energy levels are particularly affected, as the cooler plasma exterior has a higher proportion of lower-energy level species. The effected emission peaks could not be accurately fitted due to self-reversal of the peak centres, and so could not be used to calculate N_e using the Stark width.

Table 5.2. Li emission lines used for electron density calculations with Stark broadening. A signal to noise ratio of 2:1 was used to judge when a line was 'visible' (td: time delay)

λ (nm)	E_i (cm^{-1})	E_k (cm^{-1})	t_d when line visible above noise (μs)	t_d when line decayed to level of noise (μs)
413.26	14904	39094	5	45
427.31	14904	38300	5	40
497.17	14904	35012	3	50

Other potential sources of line broadening were investigated but ultimately proved too minor to merit inclusion in fitting and calculations. The natural linewidth of the ^{7}Li D2 line at 670.791 nm is 0.348 pm (calculated with $1/2\pi A_{ik}$ given in Table 5.1). The effect of resonance broadening was calculated as 0.646 pm (FWHM) using Equation (8) [66] (g_i and g_k are the statistical weights of lower and upper states of resonance line; f_r is the oscillator strength; λ is the transition wavelength and λ_r is the wavelength of the resonance (perturbing) transition; and N_i is the number density of the ground state).

$$\Delta\lambda_{resonance} \approx 8.6 \times 10^{-30} \sqrt{\frac{g_i}{g_k}} \lambda^2 \lambda_r f_r N_i \qquad (8)$$

The instrument line width was calculated with an internal Hg calibration lamp to be between 10.3 and 12.4 nm for the three transitions detailed in Table 5.2. A correction was applied to the Gaussian width of the LIBS emission lines during Voigt fitting.

The effect of ion broadening on the Stark widths was not included in the N_e calculations, as the electron impact width is said to be the most dominant mechanism in the literature. Furthermore, there were no Li II (Li^+) lines visible at any part of the temporal measurements, so omitting the impact of ions on the line broadening seemed justified [65]. Assumptions must be made about the line broadening mechanisms in order to gain useful physical information from the spectral data. For example, Stark broadening depends on both plasma N_e and temperature; one of these two parameters must be estimated or calculated using an alternative method. In this study, the plasma temperature was calculated using Doppler broadening of the LA-TDLAS spectral lines later in the LPP lifecycle and extrapolated back to shorter time delay (t_d). The plasma temperature decay was seen to be proportional to e^{-1/t_d} during the absorption measurements at late time delays. By extrapolating back to earlier delay times, the temperature could be estimated at any point throughout the LPP lifecycle. Subsequently, Doppler line broadening could be considered and accounted for by setting the Gaussian width of Voigt fits which were applied to the emission peaks. This allowed measurement of Stark broadening (using the Lorentzian width of the Voigt lineshapes) and calculation of electron density. The approach of extrapolating the plasma temperature over the entire plasma lifecycle does create uncertainties in the calculations.

As such, the results for electron density should be considered qualitative rather than quantitative.

5.4 Results and discussion

5.4.1 Plasma temperature and isotope ratio calculation using LA-TDLAS of the 670.78 nm Li D lines

Figure 5.2 displays the temporal changes in emission and absorbance. The emission profile shows the area of a Voigt fit of the 670 nm Li I emission line. The 670 nm emission line showed large self-absorption and so could not be accurately quantified, and the resulting area of fit serves only as a qualitative guide to show the temporal differences between absorption and emission. The absorbance lines show two laser diode wavelengths: on peak centre of ^{7}Li D1 and away from the absorption peak at 670.740 nm. Both the emission and absorbance lines have been normalised to their maximum values for easier comparison.

The intensity of the emission signal is at its maximum a few μs after ablation and reduces in intensity fairly linearly until it is no longer detectable above the noise after around 100 μs. Both absorption profiles reach a similar maximum absorbance within 100 μs after ablation. This indicates that the absorbance at this time is not wavelength-dependent and instead that the plasma is optically thick. After 100 μs, the off-peak (670.740 nm) absorbance drops rapidly back to the pre-ablation level, whereas the peak centre absorbance remains high until about 225 μs. The severe drop to negative one absorbance exhibited by both profiles at t_d = 0 μs is a result of scattered light from the ablation laser and emission from the LPP reaching the photodiode.

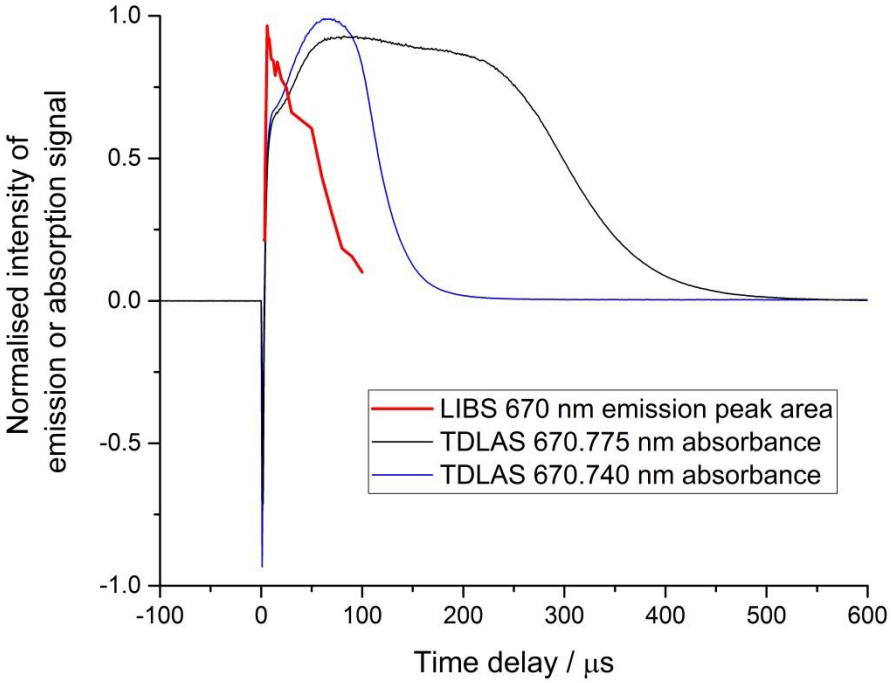

Figure 5.2. Time dependence of the emission and absorbance of the laser-produced plasma. Red line shows area of fit of the 670 nm emission line, black line gives normalised absorbance of peak centre wavelength of ^{7}Li D1 (670.775 nm) and blue line shows normalised absorbance detuned from the peak (670.740 nm). Time delay of 0 μs corresponds to the time of laser ablation pulse

The LA-TDLAS spectra could only be fitted after a time delay (t_d) of around 150 μs after the ablation pulse to allow the plasma to cool and the opacity to subside. Before this time, no absorption peaks could be identified in the spectra as the peak was not visible above the baseline. The absorption signals persisted for around 500 μs before decaying into the noise, as shown in Figure 5.3, although the maximum absorbance was very low at later time delays (e.g. 0.03 at t_d = 480 μs). The absorption spectra improve with increasing time in terms of linewidth and resolution between the peaks. However, the declining peak intensity at later time delays makes accurate spectral fitting more difficult.

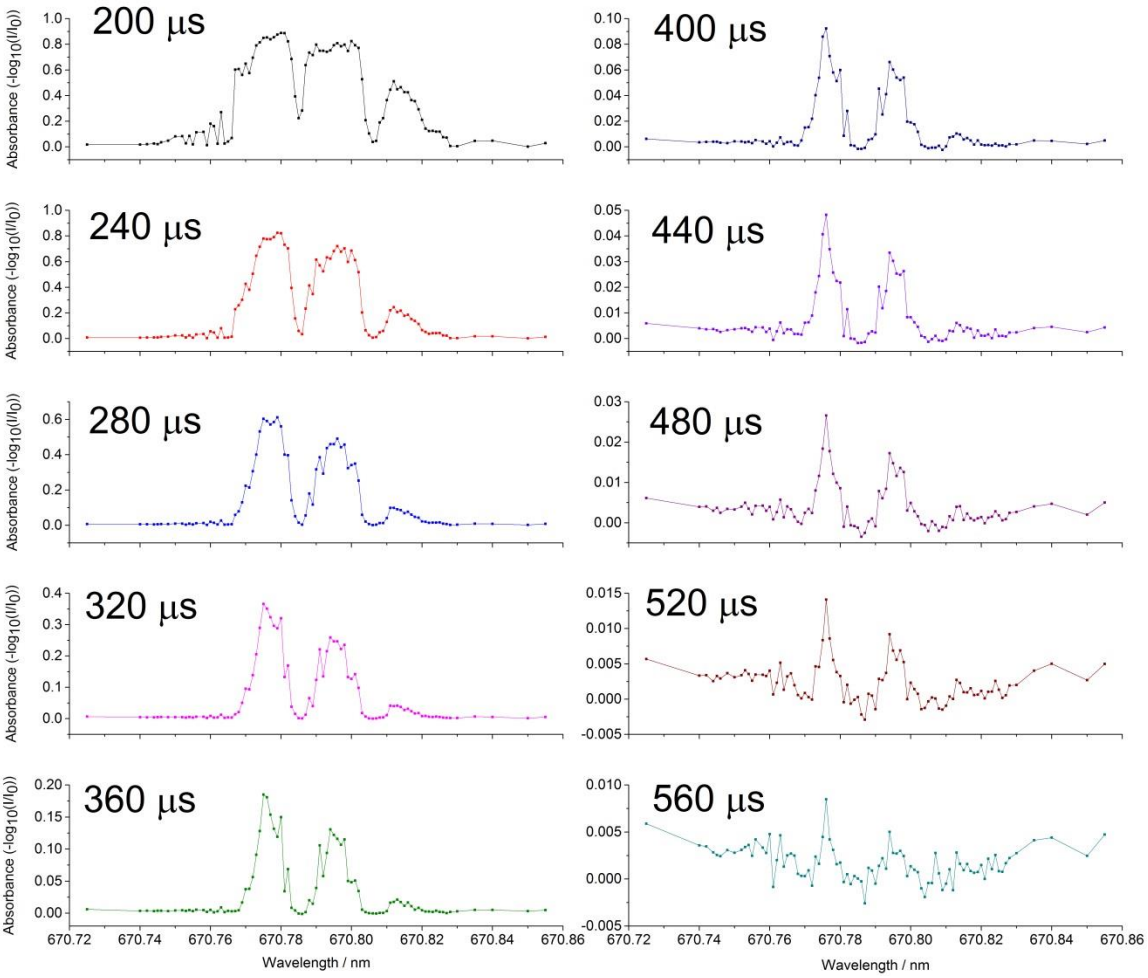

Figure 5.3. LA-TDLAS spectra of ^{6,7}Li 670.78 absorption feature at increasing measurement time delay. Pulse energy = 85 mJ/pulse.

To calculate the plasma temperature from the LA-TDLAS spectra, fits of four Voigt profiles were performed using Labview software at regular t_d intervals. However, the results indicated that there was a negligible contribution to the FWHM from the Lorentzian width. This suggests that there was no Stark broadening impacting the LPP at these long delay times. As Stark broadening is a result of an electric field, the lack of Stark broadening indicates that the plasma had fully recombined into neutral atomic species at this delay time. The LIBS spectra agree with this observation, as no emissions were detected past delay times of around 100 µs.

Because Stark broadening (and Lorentzian lineshape) could be discounted from the fitting, purely Gaussian curves were instead fitted to the spectra in order to estimate the plasma temperature using Equation (7). The oscillator strengths for each peak (given in Table 5.1)

were input to the fitting equation as constants, and the Gaussian width (w_G) and area (A) were set as shared variables. The model predicted an isotope ratio by setting a variable to represent the contribution from ^{7}Li isotope. For the ^{6}Li peaks, one minus this value was used. An example of the four Gaussian fits for t_d = 340 µs is shown in Figure 5.4. The residual of the sum of fits is shown below the spectrum. The noise as seen in the residual is high at the peak centres and low for the extremities away from the absorption feature. This shows that the noise was the result of different Li content of the plasma on a shot-to-shot basis. Spectral noise away from peak centres would indicate other sources of variation. Figure 5.5 presents the calculated temporal change in plasma temperature and the isotope ratio.

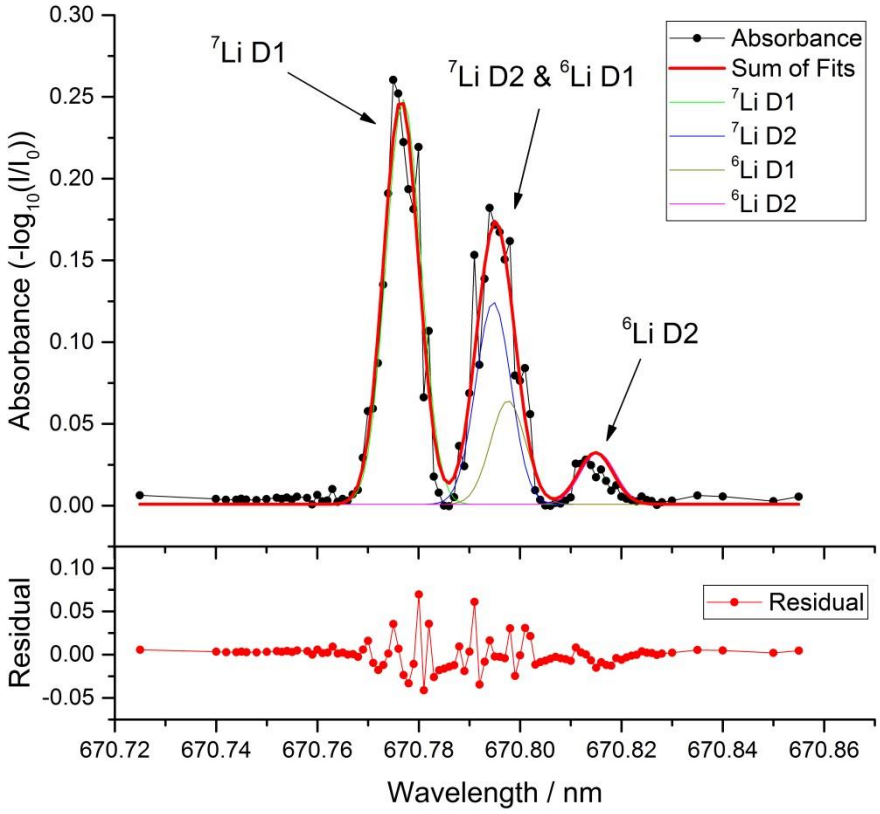

Figure 5.4. LA-TDLAS spectra at delay time of 340 µs after ablation pulse, with four fitted Gaussian peaks and residual shown below

(See Appendix Figure 8.4 for spectrum at t_d = 340 µs with error bars)

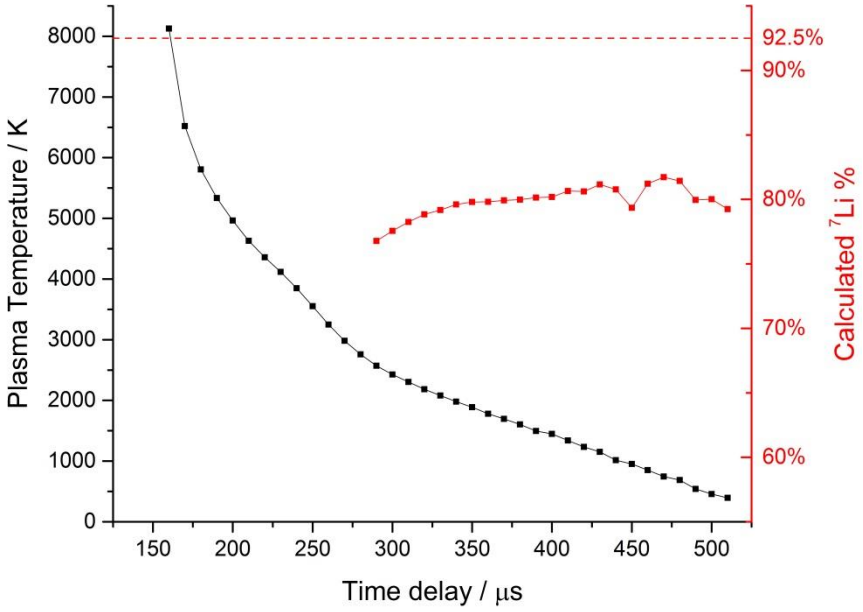

Figure 5.5. Calculated plasma temperature (black, left axis) and isotopic contribution of ^{7}Li (red, right axis) derived from fit of four Gaussian peaks on LA-TDLAS spectra. Dotted line at 92.5% shows true natural Li isotope ratio. Short time delay isotope ratio predictions were not included due to saturation of absorption spectra

The Doppler temperature calculation (Equation (7)) uses the atomic mass of the element concerned. Natural Li was used in this study, so the average atomic mass of 6.94 g mol^{-1} was used. However, the difference in mass between the two Li isotopes affects the Doppler broadening temperature calculation noticeably, as the single mass unit is comparatively large with such a small nucleus as Li. In theory it would be possible to use the isotopic mass of emitter of each peak in the TDLAS spectra to improve the accuracy of the fitting.

Phillips et al [67] discussed how the saturation of the most intense absorption peaks leads to an apparent increase in isotope ratio from the least intense peaks. Our results also show saturation may have been a source of error. The lineshapes of the absorption peaks shown in Figure 5.3 deviate from the expected Gaussian curve with a flattened top in the spectra before t_d = 280 μs. The maximum peak absorbance seen in Figure 5.3 at t_d = 200 μs is about 0.9, which corresponds to a transmission of only about 13%. At this low value, the major peaks (^{7}Li D1 and the overlapping ^{7}Li D2 and ^{6}Li D1) are saturated and give rise to an isotope prediction with inflated contribution from ^{6}Li. Only at later time delays, past 300 μs, can more accurate measurements be recorded, when the plasma is cooler and less dense and optically thin. After this time delay, Gaussian peak shapes can be observed for the

remainder of the measurements, and the calculated isotope ratio remains stable at around 80 %. The more accurate isotope ratio calculations are at later t_d values; the average relative error of prediction between 420 and 500 μs is 12.8%. Miyabe et al [68] and also Harilal et al [69] both reported a similar pattern of increased accuracy at longer time delays with their analysis of plutonium isotopes. The consistency of the calculation is promising in the cooler plasma at t_d greater than 350 μs, despite the overall signal intensity (i.e. absorbance peak maxima in Figure 5.3) being weaker at later t_d. Reducing the concentration of Li in the sample, or measuring the periphery of the plasma rather than the centre, could have reduced the impact of saturation on the absorption spectra.

The difference between the absorption characteristics of the centre and periphery of the LPP may also contribute to the uncertainty in isotope ratio measurements [67]. Studies have shown that spatial segregation can occur with light nuclei of different atomic masses (e.g. hydrogen and deuterium [70,71]) due to different expansion rates. The plasma core remains at higher temperature for longer, whereas the peripheries of the LPP are in contact with the sheath gas and lose energy more rapidly. The diameter of the plasma was not measured, but visual inspection indicated it was similar to the diameter of the collimated ECDL. It is possible that the faster migration rate of the lighter isotope could have created a higher proportion of ^{6}Li in the plasma peripheries, which enabled the ^{6}Li to cool to neutral atoms faster than the ^{7}Li. The Li D transitions at 670.78 nm are resonance lines. Therefore a higher proportion of ground state atomic ^{6}Li relative to ^{7}Li in the plasma would create an artificially high absorbance of the corresponding transitions and increase the calculated isotopic component of ^{6}Li. Additionally, the hotter centre of the plasma remains optically thick for longer than the periphery, meaning that at shorter time delays, only the peripheries of the plasma are measureable by absorption. Therefore, a faster expansion rate of the lighter isotope would mean a higher proportion of the detectable plasma was composed of ^{6}Li and also lead to uncertainty in the calculation.

The plasma temperature estimated using the LA-TDLAS Gaussian widths shown in Figure 5.5 follows an exponential decay profile. A fit of the temperature against time was therefore performed using an exponential decay function with Origin software. This yielded the relationship between plasma temperature and time delay shown below in Equation (9).

$$T = 3.57 + 23507\ \exp\left(-\frac{t_d}{133.5}\right) \quad (9)$$

5.4.2 Plasma electron density calculation using broadening of LIBS emission lines

To account for the Doppler broadening of emission lines, Equation (9) was used to estimate the plasma temperature during each LIBS measurement. This temperature was used to estimate the Gaussian linewidth caused by Doppler broadening. The LIBS spectral peaks were fitted with Voigt lineshapes, with Gaussian widths set to match the width caused by Doppler broadening. The remainder of the spectral line width (the Lorentzian width) was attributed to the Stark broadening of each transition, and was used to infer the electron density of the plasma. As stated in the introduction, it was important to understand the broadening mechanisms of the spectral lines to gain insight into the plasma condition and improve the accuracy of isotope calculations by fitting the correct lineshapes.

LIBS spectra were recorded at delay times increasing from 200 ns to 100 µs. The time gate used varied from each measurement and was increased from 100 ns to over 2 µs as the signal intensity reduced. Each spectrum therefore incorporated a short window of changing plasma conditions rather than a single absolute point in time, which reduced the accuracy of the temperature measurements slightly.

Three emission lines were not affected by self-absorption and were used for plasma N_e calculations using the Stark broadening technique: 413.26 nm, 427.31 nm and 497.17 nm. Bremsstrahlung radiation masked the emission lines before a time delay of between 3 and 5 µs, so fitting could not be achieved during that period. Similarly, at the end of the plasma lifetime, these three emissions decayed to the noise level after delays of between 40 to 50 µs, so no calculations were possible beyond this time. A line was designated as above the noise (and available for fitting) when the signal to noise ratio was greater than 2:1. Figure 5.6 shows the temporal change in electron density calculated from these three emission lines. The raw values of FWHM of each emission line are shown in the inset. The temporal change in electron density follows an exponential decay profile, although there is a large variation between the three lines – particularly at short delay times. Lower intensity of the 427.31 nm emission line made spectral fitting difficult, and resulted in an over-estimated

electron density at delays of 16 to 25 µs. The signal to noise ratio for these three emissions was quite poor – particularly for the 427.31 nm line – which increased the uncertainty. To increase the emission intensity, a longer integration time gate could be used. However, that would reduce the temporal resolution for the N_e calculations and increase the impact of non-LTE conditions on the changing LPP during each integration period. Despite this, electron densities of around 10^{16} and 10^{17} are expected for LIBS experiments under these experimental conditions, and compare well with literature values [72,73].

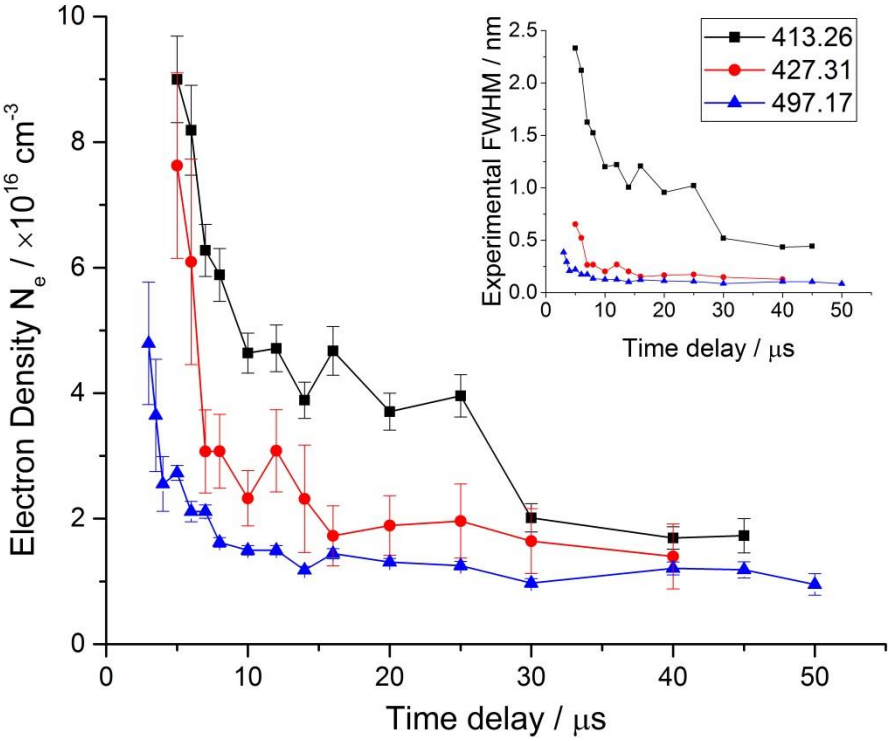

Figure 5.6. Calculated electron density of plasma using Stark width of three Li emission lines (413.26 nm; 427.31 nm; 497.17 nm). Error bars are standard error of Voigt fit of emission peaks. Inset shows experimental FWHM of emission peaks

5.4.3 Plasma temperature and isotope ratio calculations using double-pulsed laser ablation-TDLAS

Section 5.4.1 details how plasma temperature and isotope ratio can be extracted from LA-TDLAS spectra. The results showed how isotope ratio calculations were more consistent and more accurate at longer time days. Double-pulsed laser ablation has been shown in the literature to create plasma which persists for a greater time, often at lower density [74].

Lower density is expected as the plasma can expand into the rarefied gas region caused by the first laser pulse. Lower density plasma should lead to reduced spectral line broadening and sharper absorption peaks. Based on this concept, DP-LA-TDLAS was investigated as a method to improve the accuracy of the isotope ratio prediction.

Initial experiments investigated the effect of inter-pulse delay time on the temporal absorption profile. The ECDL wavelength was held stationary at the ^{7}Li D1 peak maxima (670.776 nm) as the inter-pulse delay time was increased. The absorbance at t_d = 550 µs as a function of inter-pulse delay time is shown in Figure 5.7. The absorption increases from SP-LA levels (inter-pulse delay = 0 µs) to reach a maximum at 30 µs. The absorbance then reduced back to SP-TDLAS levels – indicating that the two pulses are too far apart in time to be interacting, and instead can be thought of as two separate laser ablation events. The large increase in absorption persistence with an inter-pulse delay of 30 µs was evidence to conduct further experiments using this inter-pulse delay time.

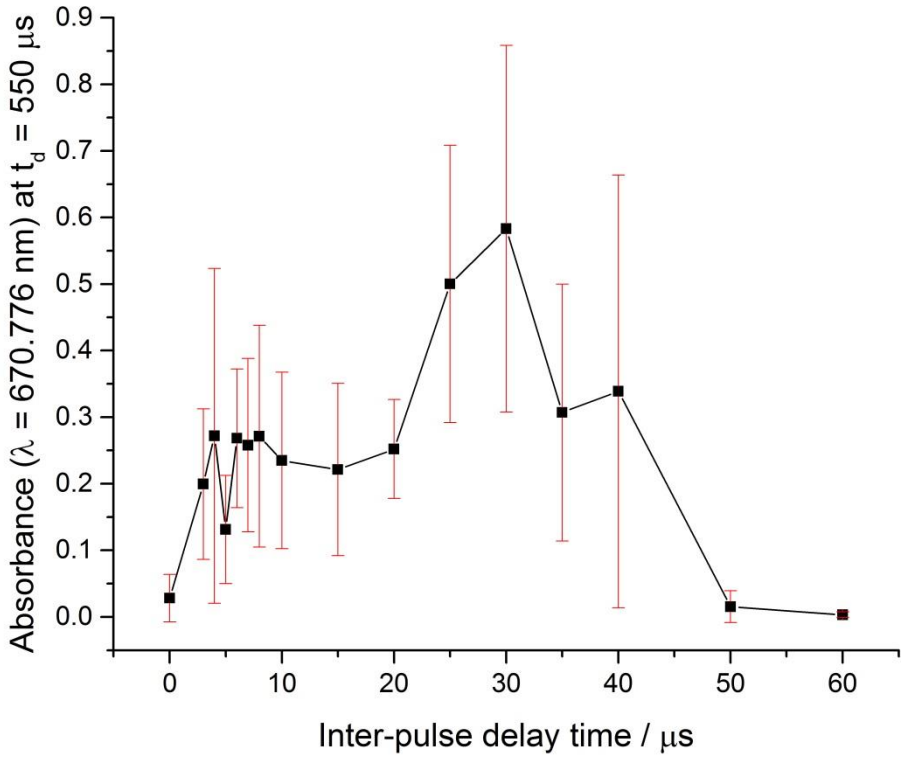

Figure 5.7. Li peak absorbance at increasing inter-pulse delay time for double-pulsed laser ablation. Note that a delay of 'zero' indicates a comparison with single-pulsed laser ablation. Error bars show ± one standard deviation

The results of DP-LA-TDLAS are displayed in Figure 5.8. A longer time delay after the ablation pulse was required before the absorption feature became visible in the DP-LA measurements compared to the SP-LA. This indicates that the plasma was optically thick for longer which agrees with prior literature on the persistence of DP-LPP. The absorption feature also remained visible for a longer time in the DP-LA-TDLAS measurements. As predicted, the FWHM of the absorption peaks are narrower because of the reduced broadening effects. However, the noise greater in the DP-LA-TDLAS spectra compared to the SP-LA.

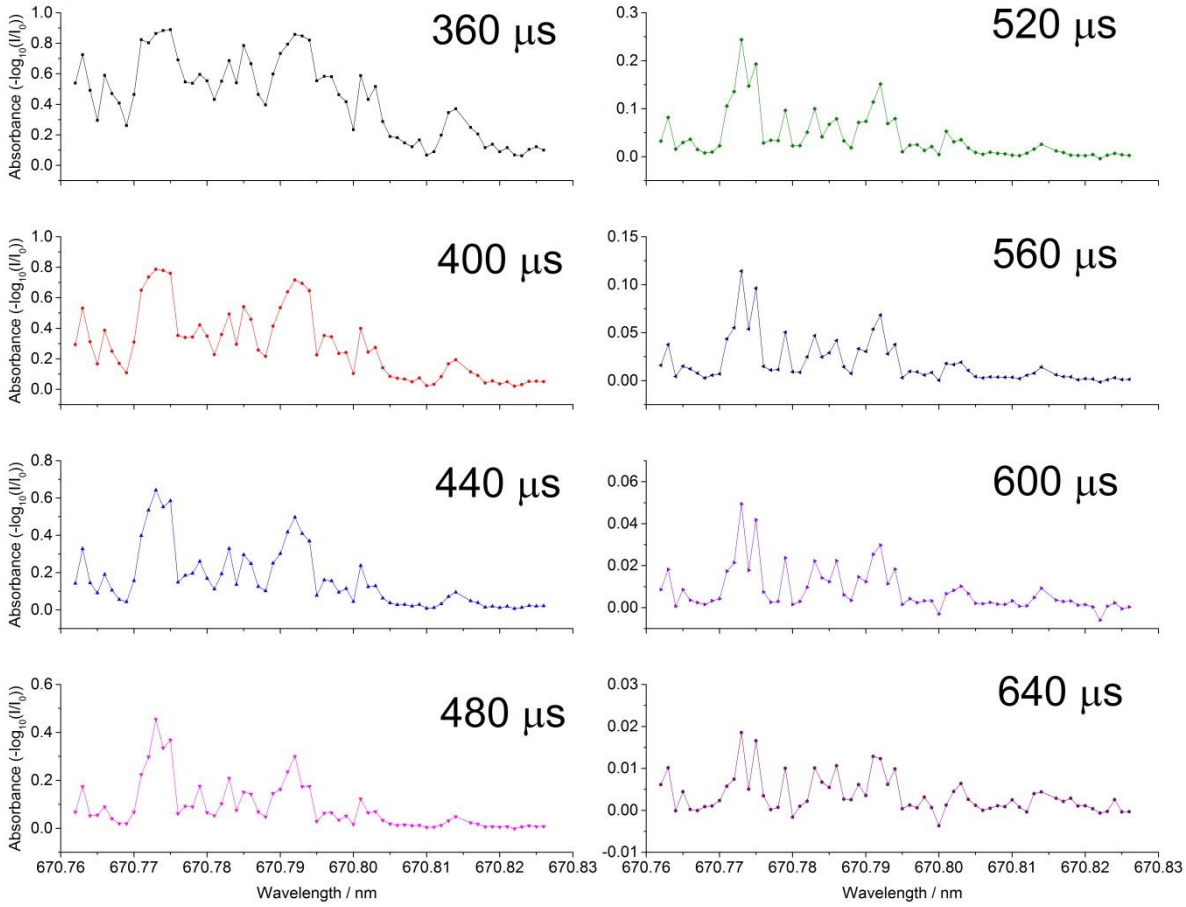

Figure 5.8. DP-LA-TDLAS spectra of Li 670.78 absorption profile with increasing time delay after ablation. Inter-pulse delay = 30 μs

(See Appendix Figure 8.5 for absorption spectrum at t_d = 440 μs with error bars showing standard deviation of absorbance)

The increased noise made spectral fitting of the absorption peaks challenging. To enable the same fitting parameters to be applied to the spectra at every time delay, the wavelength

range used for the fitting was reduced to 670.762 – 670.805 nm to only include the three highest intensity transitions. The noise was too great to identify the minor peak at higher wavelength as the high apparent baseline (caused by the noise) made fitting this region of the spectrum impossible. Additionally, peak centre and isotope ratio variables were fixed at their literature values to aid the fitting. As a result, the isotope ratio could not be determined using the DP-LA-TDLAS spectra. The increased noise in the DP-LA-TDLAS spectra was attributed to variations in the pulse energy of the laser used in these experiments on a shot-to-shot basis. The total energy of both pulses in the double pulse ablation, and also the energy distribution between those pulses, was not as consistent as the pulse energy of a single pulse.

Using this fitting procedure, the plasma temperature was calculated (shown in Figure 5.9). Compared with the SP-LA-TDLAS temperatures in Figure 5.5, the predicted temperatures are an order of magnitude lower. However, the region investigated is 150 μs later in the LPP lifecycle so a reduced temperature is expected.

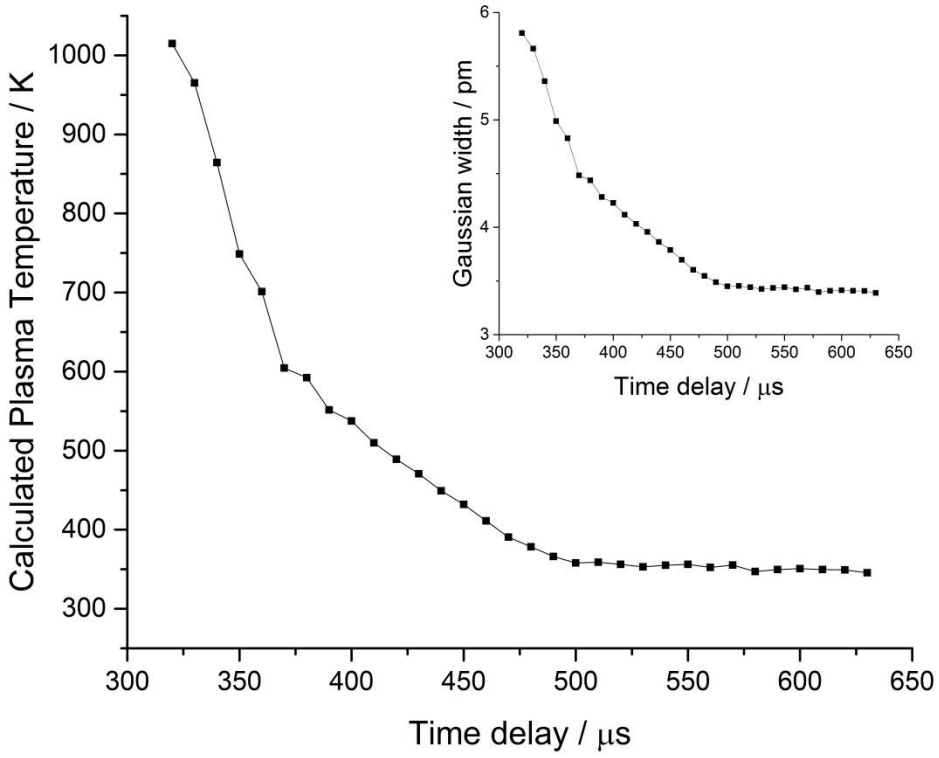

Figure 5.9. Plasma temperature calculation of DP-LA-TDLAS with FWHM of Gaussian fit inset

Fitting the exponential decay of plasma temperature from the DP-LA-TDLAS spectra (in Figure 5.9) allows the temperature to be estimated at earlier time delays in the same

manner as the SP-LA-TDLAS results were using Equation (9). The result of this exponential decay function is shown in Equation (10).

$$T = 340 + 141100\ \exp\left(-\frac{t_d}{60.28}\right) \quad (10)$$

There are significant differences between the SP- and DP-LA temperature estimates. Although the DP-LA-TDLAS results in Figure 5.9 suggest a lower final plasma temperature, the exponential temperature decay occurs at a much greater time delay. Fitting the temperature back to early in the LPP lifecycle therefore leads to a significantly higher predicted temperature. For example, the SP-LA-TDLAS temperature estimated at t_d = 1 µs was 23 × 10^3 K, whereas the DP-LA-TDLAS temperature estimated at the same time was 140 × 10^3 K. Higher temperature plasma is expected with DP-LA [74].

A potential source of error comes from the assumption of exponential decay from a maximum at t_d = 0 µs (i.e. from the moment of the second laser pulse). The complex nature of the LA process means that an exponential decay profile starting at the moment of ablation is unlikely. This is particularly true for DP-LA where interacting expanding and dissipating shockwaves from the two pulses cause different interactions between the plasma plume and sheath gas. Studies have shown that DP-LPP remains emissive for longer and the plasma conditions remain quasi-static [75]. This allows wider acquisition time gates to be used which increase the emission intensities recorded – one of the factors leading to improved analytical figures of merit. Our temperature predictions assumed a single exponential cooling rate rather than a combination of rates, which leads to increased uncertainty.

5.4.4 Plasma electron density calculation using Double-Pulsed LIBS

Figure 5.10 shows the electron density calculated during the DP-LIBS experiments. There is a much slower rate of decay from the DP-LIBS measurements than the equivalent SP-measurements (in Figure 5.6). Although the two techniques predict a similar maximum N_e, the time taken for the N_e to drop to 2 × 10^{16} cm^{-3} is between 40 and 80 µs in the DP-measurements, compared to between 8 and 40 µs for the SP-LIBS results. The DP-LIBS spectra show reduced bremsstrahlung background at shorter time delays compared to the same point in the SP-LIBS. However the intensity of the emission lines was weaker in the DP-

LIBS spectra, which made the fitting less reliable within the first 5 μs after ablation. Setting wider acquisition gates for the DP-LIBS measurements may have allowed measurements to be recorded at lower t_d, at the expense of temporal resolution. Indeed, as the LPP remains emissive for a longer time after ablation, recording fewer measurements of higher intensity spectral peaks could have increased the precision.

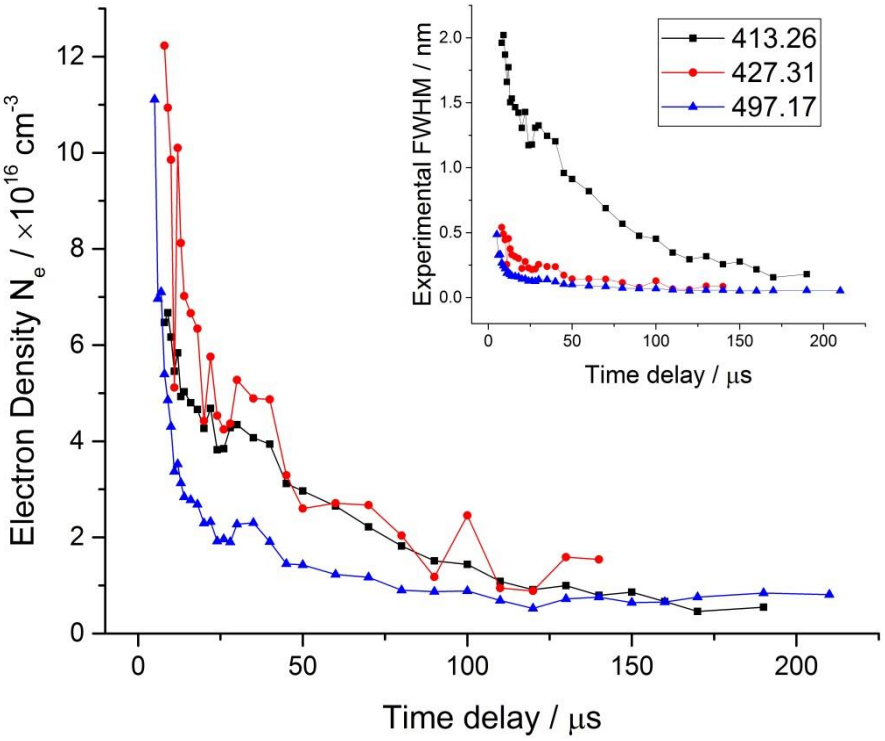

Figure 5.10. Calculated electron density of DP-LIBS plasma using Stark width of three Li emission lines. Inset shows experimental FWHM of emissions

(See Appendix Figure 8.6 for error bars showing standard error of Voigt fit)

The emissions from the DP-LIBS persisted for a longer time than for the SP-LIBS studies. Whereas the SP-LIBS emissions in Figure 5.6 decayed to the level of noise after 50 μs, the same emission in the DP-LIBS spectra were visible up to a maximum of 210 μs. Several additional interesting observations can also be noted from analysing the LIBS spectra. The reduced bremsstrahlung suggests that the plasma is less dense due to the shockwave-generated rarefied gas region caused by the first ablation pulse. In addition, boron ion (B II) lines such as 345.130 nm are observed in the early DP-LIBS spectra, whereas no species other than Li could be observed in the SP-LIBS spectra (excluding ambient gas lines from N and O). It is possible that the B lines are hidden in the bremsstrahlung radiation in the SP-

LIBS spectra. These observations of higher plasma temperature, reduced bremsstrahlung and increased intensity of ionised emission lines are similar to other comparison studies between SP- and DP-LIBS (e.g. Colao et al [23] De Giacomo et al [75] and Nagli et al [76]).

An explanation for the higher electron density of the DP-LPP shortly after ablation, combined with lower density of the plasma during recording of the TDLAS absorption spectra, is that volume of the plasma was greater. Higher temperature plasma (which is common in DP-LA and is predicted from the TDLAS fit with Equation (10) resulted in a greater degree of ionisation in the DP-LPP at short t_d. Lower density LPP resulted in less bremsstrahlung background on the emission spectra, and led to sharper absorption peaks. Greater plasma volume also increased the path length for the TDLAS measurements, which will have increased the absorbance according to the Beer-Lambert law. This is an additional reason why the absorption peaks persist for a greater duration in the DP-LA-TDLAS.

5.4.5 Discussion of DP-LA-TDLAS as viable approach to isotopic analysis

We have shown that the use of DP-LA to create the plasma for TDLAS analysis has some advantages. Reduced pressure plasma is formed using DP-LA, because the first laser pulse creates a rarefied gas region within a laser-induced shockwave. Reduced pressure plasma causes reduced linewidths of the absorption peaks in the DP-LA-TDLAS spectra. This observation could enable improved isotope ratio predictions of important elements in the nuclear fuel cycle (i.e. U and Pu) and also could allow investigation of analytes with smaller isotope shifts which is currently impossible as line broadening prevents resolution of individual isotopic peaks. Other studies have shown how the choice and pressure of the sheath gas have enhanced the absorption spectra and led to improved figures of merit (e.g. Miyabe et al 2013 [51] and 2017 [68]). However, using DP-LA creates a simulated low pressure gas environment using the rarefied gas within the laser-produced shockwave. This could allow similar spectral linewidths to be achieved without necessitating gas cylinders or vacuum pumps, which would significantly reduce the physical footprint of a technique and add portability.

The increased persistence and quasi-static nature of the DP-LPP could enable rapid wavelength ramping of an ECDL across several isotopic absorption peaks. Wavelength ramping was attempted by Liu et al [49] with their study of uranium isotopics, however the transient conditions and limited lifetime of the LPP ultimately meant a second diode laser was instead used to probe the two isotopic transitions simultaneously. Using DP-LA to lengthen the time during which the plasma is optically thin and at LTE could increase the resolution of such a wavelength ramp. Wavelength ramping could not be attempted in our study because of the limited mode-hop free tuning range of the ECDL under such a short timescale.

5.5 Conclusions

We have demonstrated an experimental setup of combined LA-TDLAS with LIBS which is capable of rapid evaluation of isotopic and elemental information from a sample, and demonstrated the feasibility of the technique with lithium samples. This combination of analytical techniques maintains the benefits of traditional LIBS (rapid, standoff, no sample preparation, non-destructive) and additionally allows isotopic measurements which are normally impossible due to the small isotope shift of electronic transitions.

A time delay of more than 200 μs after the ablation pulse was required to allow the plasma to cool before the lithium absorption peaks could be resolved. The absorption linewidth, caused by Doppler broadening, was used to calculate the plasma temperature. The temperature was extrapolated back to early delay times and used to improve the accuracy of the prediction of electron density of the laser ablation-produced plasma using the Stark broadening of three lithium emission lines in the LIBS spectra.

The accuracy of isotope ratio predictions in the lithium laser ablation-produced plasma increased at longer delay times as the plasma cooled and Doppler broadening reduced. This suggested that DP-LA might be beneficial, owing to the lower density and increased plasma lifetime. DP-LA-TDLAS was therefore investigated and was shown to improve some aspects of the absorption spectra. Absorption peaks exhibited less line broadening at late delay times under the DP-LA regime, which suggests the technique could be applied to study other elements with smaller isotope shifts which are normally unresolvable due to line broadening.

An enhancement to the LA-TDLAS technique to improve the repeatability could be achieved by using a balanced detection method for background subtraction of the absorption effects from the LPP [55]. Such experiments have been carried out in our laboratory to investigate uranium isotopics, with the challenging isotope ratio of 99.3% ^{238}U to 0.7% ^{235}U [77].

Acknowledgements

The Authors would like to thank the Atomic Weapons Establishment (AWE plc) and the EPSRC Materials for Demanding Environments Centre for Doctoral Training (M4DE CDT) for funding of the PhD research project, and AWE for the loan of the LIBS apparatus. Also, we would like to thank Andrew Murray from the University of Manchester for his help with the construction of the external cavity diode laser.

5.6 References

[1] W. Li, X. Li, X. Li, Z. Hao, Y. Lu, X. Zeng, A review of remote laser-induced breakdown spectroscopy, Appl. Spectrosc. Rev. (2018) 1–25. doi:10.1080/05704928.2018.1472102.

[2] R.C. Wiens, et al., The ChemCam instrument suite on the Mars Science Laboratory (MSL) rover: Body unit and combined system tests, Space Sci. Rev. 170 (2012) 167–227. doi:10.1007/s11214-012-9902-4.

[3] S. Palanco, C. López-Moreno, J.J. Laserna, Design, construction and assessment of a field-deployable laser-induced breakdown spectrometer for remote elemental sensing, Spectrochim. Acta - Part B At. Spectrosc. 61 (2006) 88–95. doi:10.1016/j.sab.2005.12.004.

[4] W.-B. Lee, J. Wu, Y.-I. Lee, J. Sneddon, Recent Applications of Laser-Induced Breakdown Spectrometry: A Review of Material Approaches, Appl. Spectrosc. Rev. 39 (2004) 27–97. doi:10.1081/ASR-120028868.

[5] D.W. Hahn, N. Omenetto, Laser-Induced Breakdown Spectroscopy (LIBS), Part I: Review of Basic Diagnostics and Plasma-Particle Interactions: Still-Challenging Issues Within the Analytical Plasma Community, Appl. Spectrosc. 64 (2010) 335A-366A. doi:10.1366/000370210793561691.

[6] R.E. Russo, X. Mao, J.J. Gonzalez, V. Zorba, J. Yoo, Laser ablation in analytical chemistry, Anal. Chem. 85 (2013) 6162–77. doi:10.1021/ac4005327.

[7] R. Noll, C. Fricke-Begemann, M. Brunk, S. Connemann, C. Meinhardt, M. Scharun, V. Sturm, J. Makowe, C. Gehlen, Laser-induced breakdown spectroscopy expands into industrial applications, Spectrochim. Acta - Part B At. Spectrosc. 93 (2014) 41–51. doi:10.1016/j.sab.2014.02.001.

[8] R.E. Russo, A.A. Bol'shakov, X. Mao, C.P. McKay, D.L. Perry, O. Sorkhabi, Laser Ablation Molecular Isotopic Spectrometry, Spectrochim. Acta - Part B At. Spectrosc. 66 (2011) 99–104. doi:10.1016/j.sab.2011.01.007.

[9] V.I. Babushok, F.C. DeLucia, J.L. Gottfried, C.A. Munson, A.W. Miziolek, Double pulse laser ablation and plasma: Laser induced breakdown spectroscopy signal enhancement, Spectrochim. Acta - Part B At. Spectrosc. 61 (2006) 999–1014. doi:10.1016/j.sab.2006.09.003.

[10] M. Cui, Y. Deguchi, Z. Wang, Y. Fujita, R. Liu, F.J. Shiou, S. Zhao, Enhancement and stabilization of plasma using collinear long-short double-pulse laser-induced breakdown spectroscopy, Spectrochim. Acta - Part B At. Spectrosc. 142 (2018) 14–22. doi:10.1016/j.sab.2018.02.002.

[11] P.J. Skrodzki, J.R. Becker, P.K. Diwakar, S.S. Harilal, A. Hassanein, A Comparative Study of Single-pulse and Double-pulse Laser-Induced Breakdown Spectroscopy with Uranium-containing Samples, Appl. Spectrosc. 70 (2016) 467–473. doi:10.1177/0003702815626670.

[12] J. Uebbing, J. Brust, W. Sdorra, F. Leis, K. Niemax, Reheating of a Laser-Produced Plasma by a Second Pulsed Laser, Appl. Spectrosc. 45 (1991) 1419–1423. doi:10.1366/0003702914335445.

[13] P.K. Morgan, J.R. Scott, I. Jovanovic, Hybrid interferometric/dispersive atomic spectroscopy of laser-induced uranium plasma, Spectrochim. Acta - Part B At. Spectrosc. 116 (2016) 58–62. doi:10.1016/j.sab.2015.12.006.

[14] A.J. Effenberger, J.R. Scott, Practical high-resolution detection method for laser-induced breakdown spectroscopy., Appl. Opt. 51 (2012) B165-70. doi:10.1364/AO.51.00B165.

[15] A. Hussain, X. Gao, Z. Hao, J. Lin, Combined effects of double pulses and magnetic field on emission enhancement of laser-induced breakdown spectroscopy from aluminum plasma, Optik (Stuttg). 127 (2016) 10024–10030. doi:10.1016/j.ijleo.2016.07.047.

[16] S. Eschlböck-Fuchs, P.J. Kolmhofer, M.A. Bodea, J.G. Hechenberger, N. Huber, R. Rössler, J.D. Pedarnig, Boosting persistence time of laser-induced plasma by electric arc discharge for

optical emission spectroscopy, Spectrochim. Acta - Part B At. Spectrosc. 109 (2015) 31–38. doi:10.1016/j.sab.2015.04.009.

[17] T.-L. Zhang, S. Wu, H.-S. Tang, K. Wang, Y.-X. Duan, H. Li, Progress of Chemometrics in Laser-induced Breakdown Spectroscopy Analysis, Chinese J. Anal. Chem. 43 (2015) 939–948. doi:10.1016/S1872-2040(15)60832-5.

[18] F.W.B. Aquino, E.R. Pereira-Filho, Analysis of the polymeric fractions of scrap from mobile phones using laser-induced breakdown spectroscopy: Chemometric applications for better data interpretation, Talanta. 134 (2015) 65–73. doi:10.1016/j.talanta.2014.10.051.

[19] J. Sirven, A. Pailloux, Y. M'Baye, N. Coulon, T. Alpettaz, S. Gossé, Towards the determination of the geographical origin of yellow cake samples by laser-induced breakdown spectroscopy and chemometrics, J. Anal. At. Spectrom. 24 (2009) 451–459. doi:10.1039/b821405k.

[20] J.P. Castro, E.R. Pereira-Filho, Twelve different types of data normalization for the proposition of classification, univariate and multivariate regression models for the direct analyses of alloys by laser-induced breakdown spectroscopy (LIBS), J. Anal. At. Spectrom. 31 (2016) 2005–2014. doi:10.1039/C6JA00224B.

[21] M.A. de M. Franco, D.M.B.P. Milori, P.R.V. Boas, Comparison of Algorithms for Baseline Correction of LIBS Spectra for Quantifying Total Carbon in Brazilian Soils, Sao Paulo, 2018. https://arxiv.org/pdf/1805.03695.pdf (accessed September 28, 2018).

[22] M.Z. Martin, N. Labb, N. Andre, R. Harris, M. Ebinger, S.D. Wullschleger, A.A. Vass, High resolution applications of laser-induced breakdown spectroscopy for environmental and forensic applications, Spectrochim. Acta - Part B At. Spectrosc. 62 (2007) 1426–1432. doi:10.1016/j.sab.2007.10.046.

[23] F. Colao, V. Lazic, R. Fantoni, S. Pershin, A comparison of single and double pulse laser-induced breakdown spectroscopy of aluminum samples, Spectrochim. Acta-Part B At. Spectrosc. 57 (2002) 1167–1179. doi:10.1016/S0584-8547(02)00058-7.

[24] G. Galbács, A critical review of recent progress in analytical laser-induced breakdown spectroscopy, Anal. Bioanal. Chem. 407 (2015) 7537–7562. doi:10.1007/s00216-015-8855-3.

[25] R. Hai, P. Liu, D. Wu, H. Ding, J. Wu, G.N. Luo, Collinear double-pulse laser-induced breakdown spectroscopy as an in-situ diagnostic tool for wall composition in fusion devices, Fusion Eng. Des. 89 (2014) 2435–2439. doi:10.1016/j.fusengdes.2014.04.065.

[26] R. Ahmed, M.A. Baig, A comparative study of single and double pulse laser induced breakdown spectroscopy, J. Appl. Phys. 106 (2009). doi:10.1063/1.3190516.

[27] M. Corsi, G. Cristoforetti, M. Giuffrida, M. Hidalgo, S. Legnaioli, V. Palleschi, A. Salvetti, E. Tognoni, C. Vallebona, Three-dimensional analysis of laser induced plasmas in single and double pulse configuration, Spectrochim. Acta - Part B At. Spectrosc. 59 (2004) 723–735. doi:10.1016/j.sab.2004.02.001.

[28] H. Lindner, K.H. Loper, D.W. Hahn, K. Niemax, The influence of laser-particle interaction in laser induced breakdown spectroscopy and laser ablation inductively coupled plasma spectrometry, Spectrochim. Acta - Part B At. Spectrosc. 66 (2011) 179–185. doi:10.1016/j.sab.2011.01.002.

[29] R.C. Chinni, D.A. Cremers, L.J. Radziemski, M. Bostian, C. Navarro-Northrup, Detection of uranium using laser-induced breakdown spectroscopy, Appl. Spectrosc. 63 (2009) 1238–1250. http://www.osapublishing.org/abstract.cfm?uri=as-63-11-1238.

[30] J. Klus, P. Mikysek, D. Prochazka, P. Pořízka, P. Prochazková, J. Novotný, T. Trojek, K. Novotný, M. Slobodník, J. Kaiser, Multivariate approach to the chemical mapping of uranium in sandstone-hosted uranium ores analyzed using double pulse Laser-Induced Breakdown Spectroscopy, Spectrochim. Acta - Part B At. Spectrosc. 123 (2016) 143–149. doi:10.1016/j.sab.2016.08.014.

[31] Q. Wang, J.-G. Wang, Y. Liang, X. Chen, B. Wu, Z. Ni, F. Dong, Investigation on emission spectra of reheating and pre-ablation dual-pulse laser-induced breakdown spectroscopy, 2011 Int. Conf. Opt. Instruments Technol. Optoelectron. Meas. Technol. Syst. 8201 (2011) 82012I. doi:10.1117/12.907258.

[32] R. Hai, L. Sun, D. Wu, Z. He, H. Sattar, J. Liu, W. Tong, C. Li, C. Feng, H. Ding, Enhanced laser-induced breakdown spectroscopy using the combination of circular and annular laser pulses, J. Anal. At. Spectrom. 34 (2019) 1982–1987. doi:10.1039/c9ja00230h.

[33] Y. Lu, V. Zorba, X. Mao, R. Zheng, R.E. Russo, UV fs-ns double-pulse laser induced breakdown spectroscopy for high spatial resolution chemical analysis, J. Anal. At. Spectrom. 28 (2013) 743–748. doi:10.1039/c3ja30315b.

[34] I. Choi, G.C.Y. Chan, X. Mao, D.L. Perry, R.E. Russo, Line selection and parameter optimization for trace analysis of uranium in glass matrices by laser-induced breakdown spectroscopy (LIBS), Appl. Spectrosc. 67 (2013) 1275–1284. doi:10.1366/13-07066.

[35] D.A. Cremers, A. Beddingfield, R. Smithwick, R.C. Chinni, C.R. Jones, B. Beardsley, L. Karch, Monitoring Uranium, Hydrogen, and Lithium and Their Isotopes Using a Compact Laser-Induced Breakdown Spectroscopy (LIBS) Probe and High-Resolution Spectrometer, Appl. Spectrosc. 66 (2012) 250–261. doi:10.1366/11-06314.

[36] D. Das, V. Natarajan, Absolute frequency measurement of the lithium D lines: Precise determination of isotope shifts and fine-structure intervals, Phys. Rev. A - At. Mol. Opt. Phys. 75 (2007) 1–9. doi:10.1103/PhysRevA.75.052508.

[37] G. Galbács, A Review of Applications and Experimental Improvements Related to Diode Laser Atomic Spectroscopy, Appl. Spectrosc. Rev. 41 (2006) 259–303. doi:10.1080/05704920600620378.

[38] K. Niemax, A. Zybin, C. Schnürer-Patschan, H. Groll, Semiconductor Diode Lasers in Atomic Spectrometry, Anal. Chem. News Featur. 68 (1996) 351A-356A. doi:10.1021/ac961942i.

[39] R. Hergenröder, K. Niemax, Laser atomic absorption spectroscopy applying semiconductor diode lasers, Spectrochim. Acta - Part B At. Spectrosc. 43 (1988) 1443–1449. doi:doi.org/10.1016/0584-8547(88)80183-6.

[40] K. Niemax, J. Koch, C. Schnürer-Patschan, A. Zybin, Diode laser spectrometry of environmental and industrial samples, in: Proc. SPIE 3758, Appl. Tunable Diode Other Infrared Sources Atmos. Stud. Ind. Process. Monit. II, Denver, Colorado, 1999: pp. 138–141. doi:doi:10.1117/12.366446.

[41] A. Zybin, C. Schnürer-Patschan, M.A. Bolshov, K. Niemax, Elemental analysis by diode laser spectroscopy, Trends Anal. Chem. 17 (1998) 513–520. doi:10.1016/S0165-9936(98)00063-6.

[42] H.D. Wizemann, K. Niemax, Isotope selective element analysis by diode laser atomic absorption spectrometry, Mikrochim. Acta. 129 (1998) 209–216. doi:10.1007/bf01244743.

[43] A. Zybin, V. V Liger, Y.A. Kuritsyn, Dynamic range improvement and background correction in diode laser atomic absorption spectrometry, Spectrochim. Acta - Part B At. Spectrosc. 54 (1999) 613–619. doi:10.1016/S0584-8547(98)00230-4.

[44] H.D. Wizemann, K. Niemax, Measurement of 7Li/6Li isotope ratios by resonant Doppler-free two-photon diode laser atomic absorption spectroscopy in a low-pressure graphite furnace, Spectrochim. Acta - Part B At. Spectrosc. 55 (2000) 637–650. doi:10.1016/S0584-8547(00)00198-1.

[45] J.D. Winefordner, I.B. Gornushkin, T. Correll, E. Gibb, B.W. Smith, N. Omenetto, Comparing several atomic spectrometric methods to the super stars: special emphasis on laser induced breakdown spectrometry, LIBS, a future super star, J. Anal. At. Spectrom. 19 (2004) 1061–1083. doi:10.1039/b400355c.

[46] H. Groll, G. Schaldach, H. Berndt, K. Niemax, Measurement of Cr(III)/Cr(VI) species by wavelength modulation diode laser flame atomic absorption spectrometry, Spectrochim. Acta - Part B At. Spectrosc. 50 (1995) 1293–1298. doi:10.1016/0584-8547(95)01332-9.

[47] Y. Deguchi, M. Noda, Y. Fukuda, Y. Ichinose, Y. Endo, M. Inada, Y. Abe, S. Iwasaki, Industrial applications of temperature and species concentration monitoring using laser diagnostics, Meas. Sci. Technol. 13 (2002). doi:10.1088/0957-0233/13/10/201.

[48] A. Quentmeier, M.A. Bolshov, K. Niemax, Measurement of uranium isotope ratios in solid samples using laser ablation and diode laser-atomic absorption spectrometry, Spectrochim. Acta - Part B At. Spectrosc. 56 (2001) 45–55. doi:10.1016/S0584-8547(00)00289-5.

[49] H. Liu, A. Quentmeier, K. Niemax, Diode laser absorption measurement of uranium isotope ratios in solid samples using laser ablation, Spectrochim. Acta - Part B At. Spectrosc. 57 (2002) 1611–1623.

[50] M. Miyabe, M. Oba, H. Iimura, K. Akaoka, Y. Maruyama, I. Wakaida, K. Watanabe, Ablation-initiated isotope-selective atomic absorption spectroscopy of lanthanide elements, in: T. Iguchi, K. Watanabe (Eds.), AIP Conf. Proc., American Institute of Physics, 2009: pp. 30–35. doi:10.1063/1.3115606.

[51] M. Miyabe, M. Oba, H. Iimura, K. Akaoka, Y. Maruyama, H. Ohba, M. Tampo, I. Wakaida, Absorption spectroscopy of uranium plasma for remote isotope analysis of next-generation nuclear fuel, Appl. Phys. A Mater. Sci. Process. 112 (2013) 87–92. doi:10.1007/s00339-012-7181-2.

[52] M. Miyabe, M. Oba, H. Iimura, K. Akaoka, Y. Maruyama, H. Ohba, M. Tampo, I. Wakaida, Laser ablation absorption spectroscopy for remote analysis of uranium, Hyperfine Interact. 216 (2013) 71–77. doi:10.1007/s10751-013-0845-2.

[53] M. Miyabe, M. Oba, H. Iimura, K. Akaoka, Y. Maruyama, I. Wakaida, Spectroscopy of laser-produced cerium plasma for remote isotope analysis of nuclear fuel, Appl. Phys. A Mater. Sci. Process. 101 (2010) 65–70. doi:10.1007/s00339-010-5760-7.

[54] P.J. Skrodzki, N.P. Shah, N. Taylor, K.C. Hartig, N.L. LaHaye, B.E. Brumfield, I. Jovanovic, M.C. Phillips, S.S. Harilal, Significance of ambient conditions in uranium absorption and emission features of laser ablation plasmas, Spectrochim. Acta - Part B At. Spectrosc. 125 (2016) 112–119. doi:10.1016/j.sab.2016.09.012.

[55] N.R. Taylor, M.C. Phillips, Differential laser absorption spectroscopy of uranium in an atmospheric pressure laser-induced plasma, Opt. Lett. 39 (2014) 594–597. doi:10.1364/OL.39.000594.

[56] G. Nicolaou, Determination of the origin of unknown irradiated nuclear fuel, J. Environ. Radioact. 86 (2006) 313–318. doi:10.1016/j.jenvrad.2005.09.007.

[57] X. Hou, W. Chen, Y. He, B.T. Jones, Analytical Atomic Spectrometry for Nuclear Forensics, Appl. Spectrosc. Rev. 40 (2005) 245–267. doi:10.1081/ASR-200064495.

[58] C.J. Hawthorn, K.P. Weber, R.E. Scholten, Littrow configuration tunable external cavity diode laser with fixed direction output beam, Rev. Sci. Instrum. 72 (2001) 4477–4479. doi:10.1063/1.1419217.

[59] G. Hull, LASER-INDUCED BREAKDOWN SPECTROSCOPY OF ACTINIDES – RAPID ISOTOPIC AND ELEMENTAL ANALYSIS FOR NUCLEAR FORENSICS, University of Manchester, 2020.

[60] A.N. Zaidel, V.K. Prokof'ev, S.M. Raiskii, V.A. Slavnyi, E.Y. Schreider, NIST Energy Levels and Wavelengths Bibliographic Reference #7397, in: Tables Spectr. Lines, 3rd Ed., 3rd Editio, IFI/Plenum, New York, 1970: p. 782. https://physics.nist.gov/cgi-bin/ASBib1/get_ASBib_ref.cgi?db=el&db_id=7397&comment_code=&element=Li&spectr_charge=1&ref=7397&type=.

[61] S.S. Harilal, B.E. Brumfield, N.L. Lahaye, K.C. Hartig, M.C. Phillips, Optical spectroscopy of laser-produced plasmas for standoff isotopic analysis, Appl. Phys. Rev. 5 (2018) 1–32. doi:10.1063/1.5016053.

[62] H.R. Griem, Spectral Line Broadening by Plasmas, Academic Press, New York, 1974. https://griem.obspm.fr/index.php?page=accueil.php.

[63] S. Sahal-Bréchot, M.S. Dimitrijević, N. Moreau, Virtual Laboratory Astrophysics: The STARK-B database for spectral line broadening by collisions with charged particles and its link to the European project VAMDC, J. Phys. Conf. Ser. 397 (2012). doi:10.1088/1742-6596/397/1/012019.

[64] S. Sahal-Bréchot, M.S. Dimitrijević, N. Moreau, STARK-B database, Obs. Paris, LERMA Astron. Obs. Belgrade. (2019). http://stark-b.obspm.fr (accessed November 27, 2019).

[65] N. Konjević, M. Ivković, S. Jovićević, Spectroscopic diagnostics of laser-induced plasmas, Spectrochim. Acta - Part B At. Spectrosc. 65 (2010) 593–602. doi:10.1016/j.sab.2010.03.009.

[66] W.C. Martin, W.L. Wiese, Atomic Spectroscopy - A Compendium of Basic Ideas, Notation, Data, and Formulas, Natl. Inst. Sci. Technol. (2009). https://www.nist.gov/pml/atomic-spectroscopy-compendium-basic-ideas-notation-data-and-formulas (accessed November 5, 2019).

[67] M.C. Phillips, B.E. Brumfield, N. Lahaye, S.S. Harilal, K.C. Hartig, I. Jovanovic, Two-dimensional fluorescence spectroscopy of uranium isotopes in femtosecond laser ablation plumes, Sci. Rep. 7 (2017) 1–12. doi:10.1038/s41598-017-03865-9.

[68] M. Miyabe, M. Oba, K. Jung, H. Iimura, K. Akaoka, M. Kato, H. Otobe, A. Khumaeni, I. Wakaida, Laser ablation absorption spectroscopy for isotopic analysis of plutonium: Spectroscopic properties and analytical performance, Spectrochim. Acta - Part B At. Spectrosc. 134 (2017) 42–51. doi:10.1016/j.sab.2017.05.008.

[69] S.S. Harilal, C.M. Murzyn, M.C. Phillips, J.B. Martin, Hyperfine structures and isotopic shifts of uranium transitions using tunable laser spectroscopy of laser ablation plumes, Spectrochim. Acta Part B At. Spectrosc. 169 (2020) 105828. doi:10.1016/j.sab.2020.105828.

[70] L. Mercadier, J. Hermann, C. Grisolia, A. Semerok, Plume segregation observed in hydrogen and deuterium containing plasmas produced by laser ablation of carbon fiber tiles from a fusion reactor, Spectrochim. Acta - Part B At. Spectrosc. 65 (2010) 715–720. doi:10.1016/j.sab.2010.04.011.

[71] M. Burger, P.J. Skrodzki, L.A. Finney, J. Hermann, J. Nees, I. Jovanovic, Isotopic analysis of deuterated water via single- and double-pulse laser-induced breakdown spectroscopy, Phys. Plasmas. 25 (2018). doi:10.1063/1.5042665.

[72] C. Aragón, J.A. Aguilera, Determination of the local electron number density in laser-induced plasmas by Stark-broadened profiles of spectral lines: Comparative results from H α, Fe i and Si II lines, Spectrochim. Acta - Part B At. Spectrosc. 65 (2010) 395–400. doi:10.1016/j.sab.2010.03.020.

[73] L. Pardini, S. Legnaioli, G. Lorenzetti, V. Palleschi, R. Gaudiuso, A. De Giacomo, D.M. Diaz

Pace, F. Anabitarte Garcia, G. De Holanda Cavalcanti, C. Parigger, On the determination of plasma electron number density from Stark broadened hydrogen Balmer series lines in Laser-Induced Breakdown Spectroscopy experiments, Spectrochim. Acta - Part B At. Spectrosc. 88 (2013) 98–103. doi:10.1016/j.sab.2013.05.030.

[74] D.A. Cremers, L.J. Radziemski, Handbook of Laser-Induced Breakdown Spectroscopy, Second, Wiley, 2013. doi:10.1002/9781118567371.

[75] A. De Giacomo, M. Dell'Aglio, D. Bruno, R. Gaudiuso, O. De Pascale, Experimental and theoretical comparison of single-pulse and double-pulse laser induced breakdown spectroscopy on metallic samples, Spectrochim. Acta - Part B At. Spectrosc. 63 (2008) 805–816. doi:10.1016/j.sab.2008.05.002.

[76] L. Nagli, M. Gaft, I. Gornushkin, Comparison of single and double-pulse excitation during the earliest stage of laser induced plasma, Anal. Bioanal. Chem. 400 (2011) 3207–3216. doi:10.1007/s00216-011-4806-9.

[77] G. Hull, H. Lambert, K. Haroon, P. Coffey, T. Kerry, E.D. McNaghten, C.A. Sharrad, P. Martin, Quantitative prediction of rare earth concentrations in salt matrices using laser-induced breakdown spectroscopy for application to molten salt reactors and pyroprocessing, J. Anal. At. Spectrom. (2020). doi:10.1039/D0JA00352B.

Chapter 6 - Combined laser ablation-tuneable diode laser absorption spectroscopy and laser-induced breakdown spectroscopy for rapid isotopic analysis of uranium

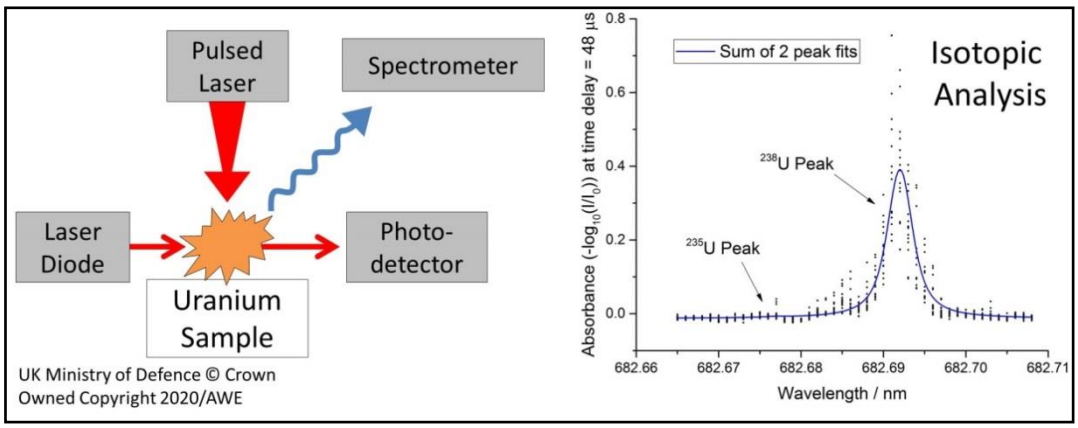

This chapter has been submitted to *Spectrochimica Acta Part B: Atomic Spectroscopy* for peer review.

Authors: Gregory Hull †[a,b], Edward D. McNaghten [c], Clint A. Sharrad [a], Philip A. Martin †[a,b]

a. Department of Chemical Engineering and Analytical Science, University of Manchester, Oxford Road, Manchester, M13 9PL

b. Photon Science Institute, University of Manchester, Oxford Road, Manchester, M13 9PL

c. AWE, Aldermaston, Reading, Berkshire, RG7 4PR

† Corresponding Authors

Author contribution: planned and constructed the balanced detection LA-TDLAS apparatus, including the external cavity diode laser; prepared the uranium samples; analysed the samples with the combined LIBS and LA-TDLAS; did the data analysis; and finally wrote the paper.

6.1 Abstract

Laser-induced breakdown spectroscopy (LIBS) can provide immediate in situ elemental characterisation of a sample from a stand-off distance with no sample preparation for bulk, minor and trace species. These attributes suggest the technique could be applied to many processes in the nuclear industry. However, at present, LIBS cannot quickly and easily be used to determine the isotopic composition of a sample, which limits its potential. We report the development of a system comprising laser ablation-tuneable diode laser absorption spectroscopy (LA-TDLAS) and LIBS which can maintain the benefits of traditional LIBS and enable isotopic analysis of certain elements, including lithium and uranium. In this feasibility study, we used this approach to analyse a uranium metal wire sample under ambient conditions of pressure and temperature. The LA-TDLAS method enabled determination of the ^{235}U:^{238}U isotopic ratio and the LIBS technique allowed electron density of the plasma to be obtained simultaneously from the same laser produced plasma. The accuracy of the isotopic analysis performed with LA-TDLAS was limited by the noise of the absorption spectra and low concentration of the minor ^{235}U isotope (0.7 %). The limit of detection was estimated to be 1.5 wt%. Using the Doppler broadening of absorption lineshapes, the plasma temperature was calculated to drop from 25 000 K to 2 000 K during the plasma lifetime. The electron density rapidly decreased from 6×10^{16} cm^{-3} immediately after laser ablation to around 3×10^{16} cm^{-3} after a few μs. The combination of LIBS and LA-TDLAS opens the possibility of rapid elemental and isotopic analysis which would be useful across the nuclear fuel cycle. Furthermore, the LA-TDLAS technique could be further developed for a portable measuring instrument for nuclear forensics applications.

Key Words:

LIBS; Tuneable diode laser absorption spectroscopy; Isotopic analysis; Nuclear forensics; Laser ablation

6.2 Introduction

Laser-Induced Breakdown Spectroscopy (LIBS) is an established elemental analysis technique which can determine the elemental composition of a sample regardless of its physical state. The analysis time is in the order of seconds and yields semi-quantitative measurements of major and trace elemental constituents at the surface, and can also measure into the bulk of a sample material. The potential for stand-off or remote LIBS has also been demonstrated using both direct line of sight [1–6] and fibre-optic cable [6–9] to direct the laser. In-line applications of LIBS in areas such as for metal casting [10–12] and waste stream monitoring [13,14] have been reported [15–18]. The emission spectra of most elements contain multiple wavelengths which enables multivariate data analysis such as Partial Least Squares regression (PLS) [19–22] and Principal Component Analysis (PCA) [23–27] to be used to increase the capability of LIBS [28,29].

The benefits which LIBS could bring to the nuclear industry have yet to be fully realised. The potential for stand-off, in situ analysis is a key advantage for nuclear and radiological samples, where machine operators can remain isolated from hazardous samples or environments [30]. Sampling in situ could deliver savings in time and cost compared to other atomic spectroscopy techniques which require sample capture, storage, transport, preparation, analysis and disposal [31]. For analysis of unknown nuclear materials, for example in nuclear forensic investigations, stand-off and in situ capabilities are extremely advantageous. The speed of LIBS measurement depends on the repetition rate of laser used, and is usually between 1 and 10 Hz for the most common apparatus of ns-length pulsed Q-switched Nd:YAG lasers. This short acquisition time enables rapid collection of numerous repeat measurements which can reduce the effect of shot-to-shot variations on the analytical capabilities. Recent advances with femtosecond laser ablation have shown a marked reduction in sample damage and improved analytical figures of merit [32,33] compared to the nanosecond LIBS regime. Compared with other atomic spectroscopy techniques such as mass spectrometry (MS), the ability of LIBS to analyse all elements within a fraction of a second, in situ, from any sample surface and without sample preparation is extraordinary. Additionally, isobaric interference can be overcome by LIBS as each element in the sample has a unique emission spectrum. The possibility of finding

spectral lines which do not overlap is a near certainty, irrespective of the number of species present in a sample.

One key hurdle to deployment of LIBS for the analysis of nuclear material is the challenge presented by isotopic-LIBS, owing to the very narrow separation of isotopic emission lines. The lightest and heaviest elements in the periodic table show the greatest isotope shift, due to mass shift dominating for the former and volume shift for the latter, while the elements in between show very small isotope shifts [34]. Even the heaviest naturally occurring element, uranium, has a maximum isotopic splitting of only 25 pm between ^{235}U and ^{238}U at the 424.437 nm emission. Resolving such narrowly separated lines necessitates high resolution spectrometers, idealised experimental conditions (such as sample preparation, sheath gas, low gas pressure etc.) and multiple measurements. All of these factors limit the usefulness of LIBS in a field-deployed scenario. Although adaptations of LIBS, such as Laser-Ablation Molecular Isotope Spectroscopy (LAMIS) [35–37], have shown potential for isotopic-speciation, more research is needed before these methods become commonplace.

A potential 'hyphenated' approach to increase the effectiveness of isotopic-LIBS could be realised by combining LIBS with other laser-based analytical techniques. Of particular interest are analyses which can interact with the same laser ablation-produced plasma (LPP) and offer complementary sample information without complications such as the need for high vacuum systems (i.e. MS). The ability to incorporate Laser Ablation (LA) with both Laser-Induced Fluorescence (LA-LIF) and Tuneable Diode Laser Absorption Spectroscopy (LA-TDLAS) was demonstrated by the Niemax group [38–40], using tuneable diode lasers as probe beams to identify isotopics of U samples. Ambient conditions such as sheath gas and gas pressure – which affect the LPP size, temperature and therefore alter the emissions – have been thoroughly investigated [41–44]. The advantages of fs over ns pulse duration in LA-TDLAS have also been studied [33,45–47]. The Miyabe group have shown numerous examples of LA-TDLAS investigations with radionuclide samples [48–50], such as how the height of probe beam above sample can influence the measurement. Bol'shakov et al [51] proposed fitting a LA-TDLAS unit to a future Mars Rover to compliment the current ChemCam instrument [3].

Improvements to the LA-TDLAS technique have been demonstrated using background subtraction methods [41–43]. Taylor and Phillips [41,42] used one 'probe' beam to interrogate the transition of interest, while a second co-propagating 'background' beam (detuned form the transition) was used to remove distorting effects caused by plasma opacity and ablated particles. Two-dimensional fluorescence spectroscopy (2DFS) has also demonstrated enhanced resolution and analytical figures of merit compared to standard TDLAS [52–54]. The ability to analyse narrowly separated uranium isotopes with 2DFS was demonstrated by Phillips et al in 2017 [53]. More recently, dual-comb spectroscopy has also shown promising results for analysing LPPs [55,56].

In this study, we have combined the isotopic speciation provided by LA-TDLAS with the emission-based LIBS technique to simultaneously determine the isotope ratio of a uranium sample and provide plasma diagnostics. We propose that a product offering in situ, stand-off quantification of elements and isotopes combined with the portability, ruggedness and low cost of laser-based spectroscopy would be well suited to deployment across the nuclear industry for environmental monitoring, inspection and for nuclear forensics. We have used the Doppler broadening of absorption peaks in LA-TDLAS spectra as a means of calculating the temporal change in plasma temperature. This technique requires knowledge of a single peak wavelength and the atomic mass of the analyte, unlike the Boltzmann plot method [57] which requires spectroscopic details of numerous atomic or ionic transitions. Using published Stark broadening parameters of uranium transitions and time-gated LIBS spectra, the electron density of the plasma was also calculated, and verified with the emission peak of an impurity element. We used the 682.691 nm uranium transition, which has an isotope split of -17 pm, to calculate the uranium isotope ratio. Although this transition has previously been analysed by LIBS [19,58–61], most absorption studies which have used this transition have done so at reduced pressure (see [39,40,54]) or with a different atomisation source such as a hollow cathode lamp [62]. To our knowledge, this is the first study on this popular uranium transition with combined emission and absorption spectroscopy conducted at atmospheric pressure. Furthermore, this is one of the first few studies [42] undertaken to study atmospheric laser ablation plasma of any uranium transition.

6.3 Materials and methods

6.3.1 Uranium samples

U metal wire (8.6 g, 1 mm diameter) of natural isotopic abundance (0.7% ^{235}U: 99.3% ^{238}U) was used in the experimental investigations. To prepare the sample, a section of the wire was manipulated into a 2-dimensional spiral shape to maximise the surface available for laser ablation, an example of which is shown in Figure 6.1. The wire spiral was then secured onto a stainless-steel disk 30 mm in diameter and 5 mm thick using a flat piece of Blu Tack™. The top surface of the wire was cleaned with grinding paper (P1200) to remove some of the black oxide layer and reveal a shiny metallic strip onto which the ablation laser was directed. This simple procedure gave an excellent homogenous surface for repeatable LA-TDLAS and LIBS measurements.

The uranium transition at 682.691 nm was chosen for investigation by absorption spectroscopy, as it is isolated from other uranium and ambient gas emission lines and persists for a long duration after the ablation process as it is a resonance transition. The isotope split of this transition is -17 pm (i.e. the emission from the minor ^{235}U isotope is 17 pm below that of the ^{238}U emission at 682.674 nm). This represents one of the largest isotope shifts in the emission spectrum of uranium. Additionally, there is good commercial availability of laser diodes at this wavelength, which reduced the cost of acquiring apparatus.

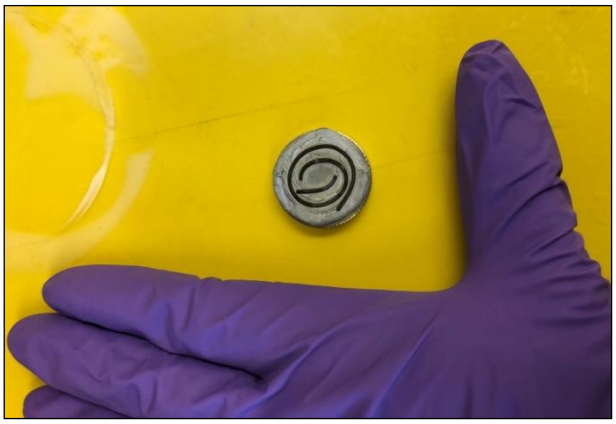

Figure 6.1. U wire sample material mounted on stainless steel disk

6.3.2 Laser ablation – tuneable diode laser absorption spectroscopy apparatus

To attain the resolution required for isotopic analysis, a laser diode (685 nm, QL68I6SA, Roithner Lasertechnik) was used in an external cavity configuration. The diode was placed into a custom-built external cavity of length around 10 mm. A similar device has been described in our previous work [64]. The multiple transverse-mode emission was forced into a single-mode of approximately 400 kHz FWHM [63]. A mode-hop free tuning range of ±0.5 nm was achievable with the External Cavity Diode Laser (ECDL) with a combination of temperature, current and grating-angle adjustments.

In order to reduce the noise of the absorption signals caused by shot-to-shot variations in the laser ablation plasma, a balanced detection method involving use of a second laser of the same type, but de-tuned from the transition of interest by 1 nm, was used. It was unnecessary to steer the emission from the second laser into an external cavity as the laser linewidth was less relevant. To spatially overlap the two beams, the diodes were orthogonally polarised and passed through a polarising beamsplitting cube (10 mm^3, Thorlabs PBS102). A second cube was used to separate the probe and background beams after the plasma for them to be individually recorded. A portion of the probe beam was analysed using an Echelle-type wavemeter (SHR model, Solar Laser Systems) with a spectral resolution of ±1 pm immediately prior to the collection photodiode. A schematic of the experimental setup is shown in Figure 6.2.

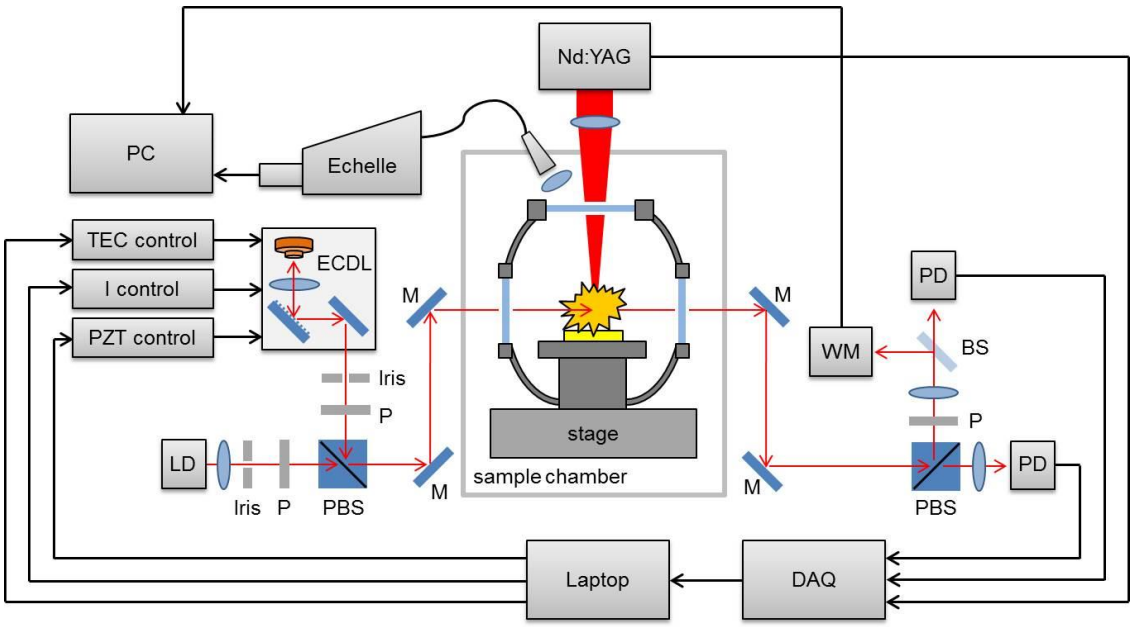

Figure 6.2. Schematic of experimental setup of hyphenated LIBS-TDLAS apparatus (ECDL: external cavity diode laser (probe beam); LD: laser diode (background beam de-tuned from atomic transition); M: mirror; P: polariser; PBS: polarising beamsplitting cube; BS: beam sampler; WM: wavemeter; PD: photodiode; DAQ: data acquisition card; TEC: thermoelectric cooler; I: current controller; PZT: piezoelectric actuator controller)

The background laser was controlled using standard laser diode current and temperature controllers (Thorlabs LDC202C and TED200C respectively) and laser mount (Thorlabs TCLDM9). The probe and background lasers were collimated over several metres before being placed into the optical setup. The diameter of each laser was set to 1 mm using two irises. The laser intensities were monitored after passing through the plasma using two identical Si photodiodes (Thorlabs DET10A2, 0.8 mm^2, 1 ns rise time) with 30 mm focussing lenses. A data acquisition (DAQ) card (National Instruments USB-6259, 1 MHz sampling rate, 16 bit) and bespoke Labview virtual instrument (National Instruments version 2016) were used to convert the photodiode voltage signals into absorbance, A, using equation (11) (where I is the voltage produced by the probe beam I_0 by the background beam). A second polariser was used before the photodiode recording the probe beam to reduce the intensity from plasma emission.

$$A = -\log_{10}\frac{I}{I_0} \qquad (11)$$

Dividing the absorbance of the probe beam by the absorbance of the background beam reduced the effects of plasma opacity, shockwaves (causing Schlieren distortions) and ablated matter (causing Rayleigh and Mie scattering) on the absorption signal [65,66]. This method significantly reduced the noise of the absorption spectra and increased the limit of detection of the LA-TDLAS technique.

6.3.3 Laser-induced breakdown spectroscopy apparatus

The LIBS apparatus comprised a Q-switched Nd:YAG laser (Spitlight 600, Innolas) operating at fundamental wavelength of 1064 nm with a 6 ns pulse duration, beam steering and light collection optics, a sample chamber and an Echelle spectrometer. The pulse energy of the laser could be controlled between 85 mJ/pulse and 600 mJ/pulse. The sample chamber (with manual xyz mobile stage) and beam focussing optics were designed and manufactured by Applied Photonics ltd (Skipton, UK). Light was collected by 2 m fibre-optic cable (200 µm core) and transferred to an Echelle spectrometer (Aryelle-Butterfly, Lasertechnik Berlin [LTB]) with ICCD camera (Andor iStar series). The resolving power of the spectrometer and camera was about 35000. The spectrometer had an acquisition rage from 250 nm to 800 nm, continuous between 250 nm and 550 nm but discontinuous above this due to the spacing of Echelle orders. All LIBS measurement variables, including camera delay time, gate width and camera-gain were controlled by Aryelle software (LTB).

6.3.4 Sampling cell

All measurements were conducted with the samples inside an air-tight stainless-steel sample cell (Scanwel ltd, Bala, UK) shown in Figure 6.3. A quartz window at the top of the cell allowed the Nd:YAG laser radiation to ablate the sample surface and for emitted light to be collected. Angled borosilicate glass windows on the sides of the cell allowed orthogonal access for the laser diodes to pass through the laser ablation plasma. Samples were prepared in an active-sample laboratory and transferred to the laser instruments inside the air-tight cell. Opening and cleaning of the cell was performed within a designated radiochemical laboratory. In this way, the optical elements, laser and personnel were shielded from the hazardous ablation-debris at all times. Although different pressures and

gases were achievable using the sample cell, experiments were conducted under air at atmospheric pressure to better simulate a field-deployed scenario.

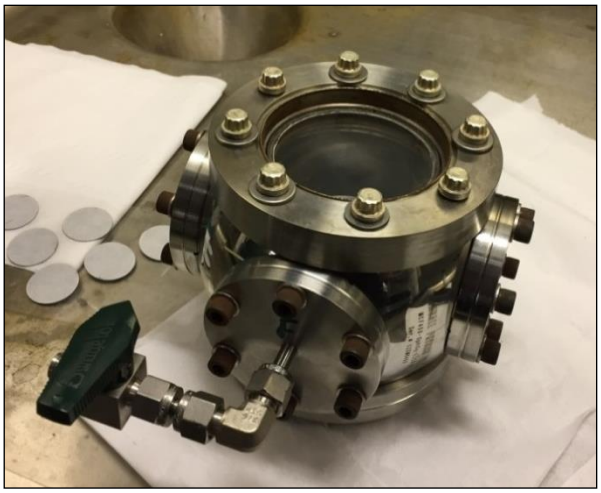

Figure 6.3 Air-tight sample cell used for analysis of hazardous samples (Scanwel Ltd.): upper face - 2mm quartz window; side faces - angled-borosilicate glass windows; front face - Swagelok valve

6.3.5 Data treatment of TDLAS and LIBS spectra

TDLAS and LIBS spectra were recorded with each ablation shot. Each measurement was recorded at a fresh spot on the sample surface with at least 0.5 mm between sampling positions to support homogeneity and avoid cratering. The TDLAS spectra were recorded at a sampling rate of 0.5 MHz, which was the highest temporal resolution possible in order to measure the probe and background beams simultaneously. 15 measurements were recorded at each probe beam (ECDL) wavelength. To reduce the variation, the spectra with the largest and smallest integrated absorption areas were removed, and the remaining 13 spectra were averaged together. The probe beam wavelength was then stepped at 1 pm intervals (the step size was limited by the resolution of the SHR wavemeter described in section 6.3.2). Origin software was used to fit Voigt profiles of the absorption spectra, with the peak centres fixed to literature values. The peaks required fixing because the minor ^{235}U (0.7%) isotope was difficult for the software to identify over the noise.

LIBS emission spectra were recorded at increasing time delays to monitor how the emission characteristics changed over time. The time gate was maintained at 200 ns. Fifteen

measurements were recorded and averaged together at each time delay. To reduce the effect of the Echelle order baseline, each Echelle order region was identified and a third order fit of the baseline was performed and subtracted from the measurement. The baseline specifically rather than any peak information was selected and accounted for by ignoring 20% of values of the highest intensity during the baseline fitting. Lorentzian lineshapes were then fitted to the peaks of interest using Labview.

For this study, three sources of line broadening were considered: Doppler, Stark and instrument broadening. The instrument broadening of the Echelle spectrometer was calculated using the spectrometer resolving power 35000. An internal Hg calibration lamp was used to visualise the emission lines, and a Gaussian profile was found to fit the emission peaks well. The instrument broadening at the 500.82 nm emission was calculated to be 14.3 pm. Doppler broadening is caused by thermal motion of atoms and also generates a Gaussian lineshape. The Gaussian full width at half maximum (w_G) caused by Doppler broadening is proportional to the square root of temperature with equation (12). Stark broadening gives rise to a Lorentzian lineshape (with width w_L) and is proportional to temperature, electron density and Stark broadening parameters which are specific to each transition. These parameters are published online for many elements (e.g. in the STARK-b database [67]) and can be used for electron density calculations using equation (13). A Voigt profile is a convolution of Gaussian and Lorentzian lineshapes.

$$w_G = \sqrt{\frac{8kT\ ln(2)}{m_A c^2}}\lambda_0 = 7.16 \times 10^{-7}\sqrt{\frac{T}{m_A}}\lambda_0 \qquad (12)$$

$$\log(w_L) = a_0 + a_1 \log(T) + a_2(\log(T)^2) \qquad (13)$$

T is temperature in Kelvin; m_A is the atomic mass; λ_0 is the peak centre wavelength; and a_0, a_1 and a_2 are Stark broadening parameters taken from the STARK-b database [67] – a_1 and a_2 are stationary whereas a_0 varies linearly with $\log_{10}(N_e)$. The contribution to broadening from ion collisions was not considered in our calculations, as this effect is estimated to be negligible compared to the electron impact broadening.

Voigt profiles were fitted to the emission lines in the LIBS spectra, with the Gaussian width set to the value of the convoluted instrument and Doppler linewidths. By accounting for the

Doppler and instrument broadening of the emission peaks, the remaining Lorentzian width can be assumed to be caused entirely by Stark broadening and can be used to calculate the electron density with Stark broadening parameters. A literature survey of uranium Stark broadening parameters revealed limited published research. However, Burger et al [68] did publish parameters for two uranium transitions (one atomic, one ionised) in 2019. Some spectroscopic details are given below in Table 6.1. Atomic parameters for one sodium emission line are also included in Table 6.1. This peak was used to validate the electron density using Stark broadening parameters from the Stark-b database [67].

Table 6.1. Emission lines in LIBS spectra used for electron density calculations (λ: wavelength; E_i and E_k: lower and upper energy levels; m_A: atomic mass)

Species	λ / nm	E_i / cm^{-1}	E_k / cm^{-1}	m_A
U I	499.01	8136	28113	238.0
U II	500.82	1772	21668	238.0
U I	682.69	0	14644	238.0
Na I	589.00	0	16973	22.99

With our measurements of the LPP electron density, there is no ambition to prove the McWhirter criterion for local thermal equilibrium (LTE) conditions. Rather, we assume that the plasma is not in LTE and caveat our results by stating they are representative only of the absorption volume in the case of TDLAS, and the averaged line-of-sight emissions from the plasma core and periphery in the case of LIBS.

6.4 Results and discussion

6.4.1 Parameter optimisation

Initial experiments were conducted to ascertain the optimum parameters for both LIBS and LA-TDLAS measurements. The effect of the pulse energy of the ablation laser was evaluated by keeping ECDL emission constant at the wavelength of the major isotope and observing the LA-TDLAS spectra with increasing ablation pulse energies. There was a significant increase in absorbance with higher pulse energies, as shown in Figure 6.4. LIBS spectra also

showed greater uranium line emission intensity at higher pulse energies and improved the signal to background ratio. No change to emission linewidth (caused by electron density and Stark broadening) was observed. As expected, the higher pulse energy ablated more material, and created a plasma with more uranium atoms and ions, which increased the absorbance and the emission signals. The increased pulse energy did, however, lead to a more noticeable cratering effect on the sample material and required a greater spacing between shots. Nonetheless, the dramatic increase in absorbance observed at higher pulse energies provided compelling evidence to use the highest possible pulse energy of 600 mJ per pulse for the remainder of the measurements.

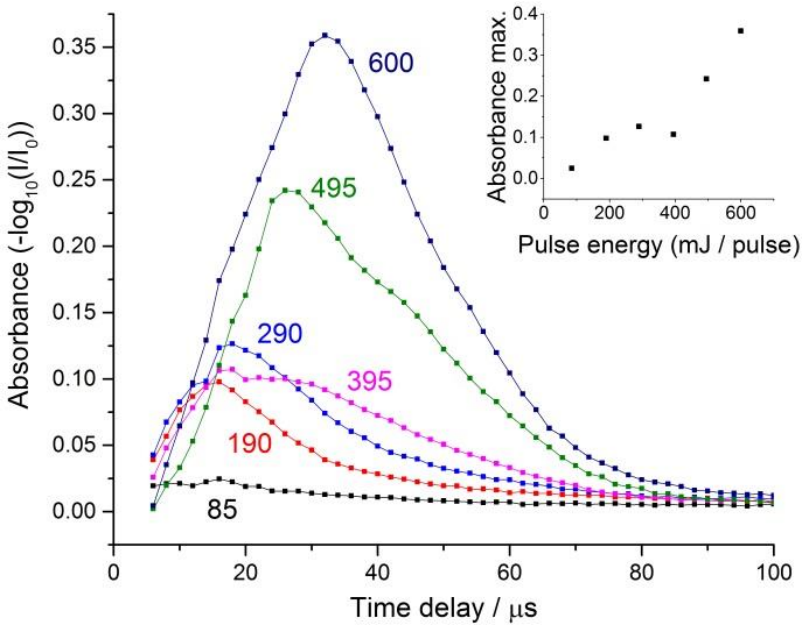

Figure 6.4. Time-resolved absorbance of ^{238}U peak recoded at various pulse energies (annotations show pulse energy in mJ). Inset shows maximum absorbance at each pulse energy

6.4.2 Tuneable diode laser absorption spectroscopy and isotope ratio predictions

The time-dependent nature of the uranium absorbance is shown in Figure 6.5 for two probe wavelengths. The black points represent the absorbance at the ^{238}U peak centre of 682.691 nm, whilst the red points give the absorbance measured 25 pm (16 GHz) below that wavelength. The peak centre absorbance shows two distinct maxima: a rapid rise in

absorbance to an initial maximum after 18 µs is followed by a second larger maximum at around 48 µs. In our previous LA-TDLAS investigations using lithium, a double absorbance maximum was not observed. However, a similar pattern was encountered by Quentmeier et al [39] with their uranium LA-TDLAS experiments, although they only observed the double peak at very low pressures (less than 4 kPa). They attributed the first peak to uranium atoms expanding with the shockwave front and the second peak to atoms which were reflected back towards the sample surface by collision with molecules of buffer gas. Harilal et al [44] also observed a double uranium peak up to pressures of 400 Torr with optical time-of-flight measurements, but they attribute the first peak to continuum and electron-excited ambient gas plasma. A more detailed discussion was provided by Harilal et al [69] who stated that, at higher gas pressures, some of the LPP plume escapes without much collision with ambient gas and creates the first peak, while the bulk of the ejected material is slowed by collisions and appears later. Their conclusions build upon previous work by Kerdja et al [70] in 1996 and Amoruso et al [71] in 2005, who both concluded that a prompt component of ejected material obeys free expansion behaviour, while the second component is more influenced by ambient gas. These peaks are dependent on different distances from the target surface depending on the ambient gas, gas pressure, analyte and pulse energy.

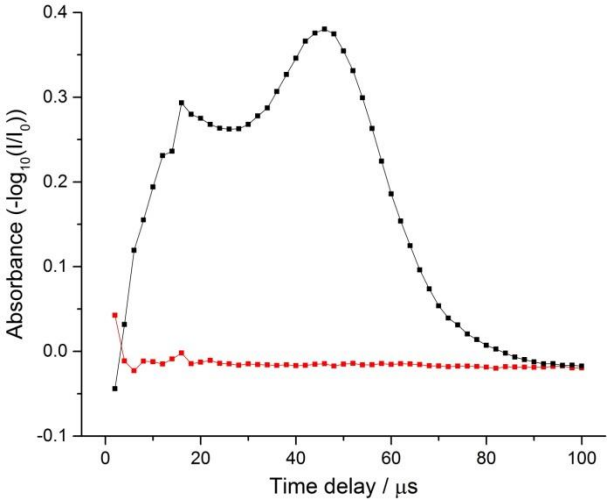

Figure 6.5. Time dependence of the uranium absorbance at a peak centre wavelength (682.691 nm – black) and off-peak (682.665 nm – red)

Hou et al [72] recently reported two plasma zones formed by femtosecond laser ablation of zirconium samples under argon at atmospheric pressure. They note that the femtosecond

laser created a weakly-ionised air channel along the laser path (due to the high power density of the fs laser pulse), which enabled a prompt plasma expansion along that axis. Although they used emission rather than absorption, their spectra showed an initial LPP plume expanding from a time delay of 500 ns which dissipated after 5 µs. A more typical spherical plasma expanded just above the sample surface and continued after the initial plume had disappeared. Although this phenomenon was achieved using the quite different fs laser ablation process, it is possible that a similar prompt plume was generated using our apparatus because of either a weakly-ionised air channel or air-breakdown above the sample surface. Indeed, our sample was positioned at the focal point of the laser where air breakdown does occur. Adjusting the axial position and height of the absorption beams and the focal point of the ablation laser to map the plasma expansion in future experiments could reveal more information about this process.

The rapid temporal changes in absorption shown in Figure 6.5 eliminate the possibility of wavelength ramping (as in scanning the ECDL wavelength to interrogate both uranium isotopes in a single ablation event). To calculate an accurate isotope ratio from the two absorption signals would require the plasma conditions to be stationary for the duration of the wavelength ramp. Figure 6.5 indicates that the plasma is constantly transient, so such a wavelength ramp would only be possible with a very short ramp time. The ECDL wavelength was controlled using piezoelectric actuators which were capable of rapid adjustment. However, control over sub-microsecond electronic outputs necessitates microcontroller electronics which were unavailable in this experiment. Additionally, the mode-hope free tuning range of our ECDL would have been insufficient to analyse both isotope transitions without temperature adjustment, which cannot take place over such a short timescale.

The limit of detection (LoD) of uranium with the LA-TDLAS method was determined from the standard deviation of the off-peak absorbance and the maximum absorbance of the peak centre line at 48 µs, using 3σ criterion shown in equation (14):

$$LoD = \frac{3\sigma_{BG}}{k} \tag{14}$$

where k is the conversion factor between absorbance and sample abundance [50]. We estimated that the concentration of the sample was 100% pure uranium at natural isotopic

composition, so contained 993 × 10^3 ppm ^{238}U. In reality this is an overestimate because of impurities such as oxidation and sodium contamination, plus some daughter nuclei from radioactive decay. Using these figures, the conversion factor k was calculated with equation (15):

$$k = \frac{0.380}{993000\ ppm} = 3.83 \times 10^{-7}\ ppm^{-1} \quad (15)$$

The standard deviation of the background was calculated at 0.00194, using a time delay region from 20 µs (after the initial jitter caused by the laser ablation had subsided) to the final time point of 100 µs. Therefore the LoD was calculated with equation (14) to be 15.2 × 10^3 ppm, or 1.52 wt%. Although the standard deviation of the baseline is good, the LoD figure is enlarged by the presumption of chemical purity in the sample, which is shown to be incorrect by the presence of impurity lines in the spectra (e.g. sodium as discussed in section 6.4.3) and the oxidised surface. Additional reactions between the LPP plume and the air atmosphere (to create uranium oxides) may further reduce the concentration of atomic uranium available for analysis by the absorption laser beams. Undertaking the analysis at different pressures or different gases could improve the LoD at the expense of measurement time and hardware footprint. Nonetheless, a LoD of 1.5 wt% of the minor ^{235}U isotope would indicate low enriched uranium which would be a useful tool for nuclear forensics, and detecting 1.5 wt% uranium ^{238}U in soil or waste water would be useful for environmental monitoring.

The off-peak centre temporal plot in Figure 6.5 demonstrates how the balanced detection method is able to remove the effects of plasma opacity and noise distortions from approximately 8 µs onward, as after this time delay the plot is stable around zero absorbance. To create absorption spectra from the temporal profiles shown in Figure 6.5, a time delay of 48 µs was chosen to maximise the peak absorbance signal. Analysing the absorbance at a time delay of 48 µs for each of the probe beam wavelengths investigated creates the absorption spectrum shown in Figure 6.6.

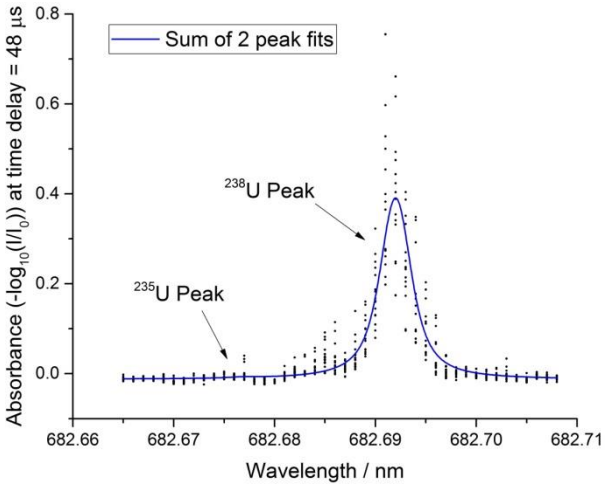

Figure 6.6. LA-TDLAS spectrum of uranium wire sample with Voigt fit of two uranium isotope peaks. Large peak at 682.692 nm is major ^{238}U isotope, ^{235}U isotope peak is at 682.677 nm

The balanced detection method reduces the standard deviation of spectral points significantly. However, despite this and the other efforts to reduce shot-to-shot variations in the plasma (such as cleaning of the sample surface with grinding paper) Figure 6.6 still displays a large range of absorption values around the ^{238}U peak centre. Interestingly, the small standard deviation at the extremities of the spectrum indicates that the spread of values around the ^{238}U peak is caused by shot-to-shot variations in the number density of absorbing species in the interrogation volume. Away from peak centre, these changes are accounted for with the second (background) laser. However, at the peak centre, the shot-to-shot variations in number density of absorbing species are evident. Although every effort was made to analyse an identical position at the top surface of the wire sample with each ablation shot, spatial alignment of the YAG laser with the middle of the wire was difficult. It is possible that minor misalignment created the LPP on a convex surface, so when the plasma plume expanded away from the surface, it ejected at a slight angle which reduced the volume being interrogated with the laser diode beams. Such a change would have affected the absorbance only around the peak centres due to the wavelength-dependent absorbance.

The spectral resolution of Figure 6.6 was limited to 1 pm wavelength steps by the resolution of the SHR wavemeter. However, this resolution made it impossible to properly identify the minor ^{235}U peak at 682.677 nm, due to the very low peak intensity and spectral noise. To fit each peak and calculate the isotope ratio, experiments were performed with higher

resolution wavelength steps across the two isotopic transitions. To generate a higher density of equally spaced analysis wavelengths around the two isotopic transitions, the piezoelectric actuator was stepped at 1 V intervals. This gave between three and four equally spaced wavelength values in place of each point in Figure 6.6, at the expense of limiting the width of the wavelength range investigated and not knowing the precise wavelength. The spectral resolution between points is assumed to be around 0.3 pm. To ensure single mode emission at each step, the temperature of the laser was continuously manually adjusted. The results of this more detailed wavelength stepped LA-TDLAS experiment are presented in Figure 6.7.

The isotope ratio ($^{235}U \div U_{total}$) predicted from the area of the two peaks is 3.21%. This is quite far removed from the natural isotopic abundance of the uranium sample (0.72%) and suggests that there are several sources of error which must be accounted for. Firstly, the spectra in Figure 6.7 show some quite high noise and, particularly with the minor ^{235}U isotope, the signal to noise ratio is poor. As discussed previously, the shot-to-shot variations were large – particularly around the peak centres. The detailed wavelength experiments in Figure 6.7 were conducted across a narrower wavelength range, so more of the data points are susceptible to changes in peak absorbance. It was not possible to perform repeat measurements for each spectrum due to the limited uranium sample size. Increasing the number of measurements could have reduced the noise and increased the precision of the isotope ratio prediction.

Phillips et al [53] reported that saturation of the fluorescence signal of the major ^{238}U isotope peak created an artificially reduced intensity, which led to incorrect isotope ratio prediction. Our group reported similar results in our previous TDLAS experiments with lithium isotopes [64]. It is possible that the major ^{238}U isotope peak suffered from saturation. The maximum absorbance reported in Figure 6.7 is only 0.4, which is below the point at which non-linear or saturation effects are usually observed. However, the balanced detection method subtracts the absorbance caused by plasma opacity, so the value of 0.4 is not representative of the total absorbance, but rather the difference between the probe and background beams. On the other hand, our previous studies showed obvious peak-flattening in the TDLAS spectra, whereas the absorbance in Figure 6.7 does not appear to suffer from this effect.

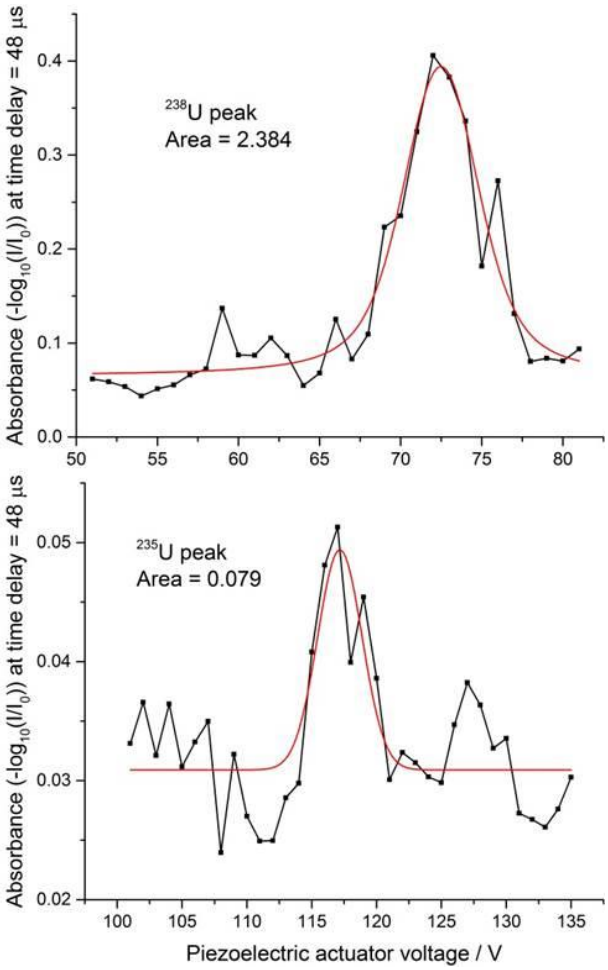

Figure 6.7. Detailed wavelength sweeps of uranium isotope peak regions, with Voigt fit in red. Upper figure - U^{238}; lower figure - U^{235}. Note the x axis scale is voltage supplied to one of the piezoelectric actuators of the ECDL rather than absolute wavelength of laser output. Note also the differing absorbance scale between the two plots. Each point is an average absorbance over 15 shots

(See Appendix Figure 8.7 for error bars showing standard deviation, and Figure 8.8 for uranium absorption spectrum with both peaks on an approximated wavelength scale)

The LA-TDLAS experiments of Miyabe et al [50] also showed less accurate isotope ratio calculations at shorter time delay because of increased Doppler and Stark broadening. The same group also thoroughly investigated the expansion dynamics of cerium isotopes under various gases and pressures [73]. They showed an increased absorption area due to Doppler splitting of absorption peaks, caused by LPP plume expansion parallel to the surface (i.e. in the direction of the TDLAS diode beams). Research into the effect of isotope mass on

expansion velocity by Burger et al [74] indicated that there was no noticeable difference between hydrogen and deuterium when they analysed ice samples. This is in agreement with the results of Dong et al [75], who analysed carbon isotopes and molecular formations with spatio-temporal emission spectra. As such, any differences in absorption characteristics between the two uranium isotopes in this study have been discounted. That being said, there has been limited research into the reaction rates of ^{235}U and ^{238}U with atmospheric oxygen [76], or on the evaporation rate of the two uranium isotopes.

6.4.3 Plasma Diagnostics

Examining the temporal changes in absorption spectra reveals information on plasma parameters such as electron density and plasma temperature. These two parameters both affect the spectral line width, so it is usual for one to be estimated or calculated from an alternative source [77]. In this study, the Doppler broadening of the absorption peaks in the TDLAS results was used to calculate the plasma temperature. By extrapolating the temperature back to early delay times, the Doppler broadening of emission lines can be accounted for, which allows the electron density to be calculated with more accuracy.

Figure 6.8 shows TDLAS spectra at increasing time delays after laser ablation. The maximum absorbance follows the double peak pattern shown in Figure 6.5 in section 6.4.2, with maxima at 16 µs and 48 µs. Interestingly, fitting these spectra with two Voigt peaks (Figure 6.9) reveals Lorentzian and Gaussian widths (w_L and w_G) which fluctuate at similar time points. The FWHM of the Voigt fits rapidly reduces to 16 µs then decays more gradually for the duration of the observable absorption signal. The double absorption peak and irregular decay of LPP temperature suggests spatial segregation of the LPP as mentioned earlier in section 6.4.2. Using a narrower diameter analysis beam for the absorption measurements could have enabled spatio-temporal mapping of the plasma, which could have offered further explanation for the double absorption peak. Once again, the spectral resolution shown in Figure 6.8 was limited to ±1 pm by the spectral resolution of the SHR wavemeter which creates the main source of uncertainty in Figure 6.9. Minor changes in absorbance at the peaks or in the wings have a large effect on the Lorentzian and Gaussian widths of fitted Voigt profiles. There appears to be a shoulder on the higher-wavelength arm of the main absorption peak in Figure 6.8. This is particularly evident at shorter time delays up to 40 µs.

It is possible that there is an overlapping uranium transition which is influencing the spectra. There are thousands of uranium transitions across the entire ultraviolet to visible wavelength range, the majority of which are un-reported, so it is not impossible that there is another transition hidden beneath the 682.691 nm emission envelope. It is also possible that the perceived shoulder is caused by uncertainty in the wavelength caused by the lack of spectral resolution of the wavemeter.

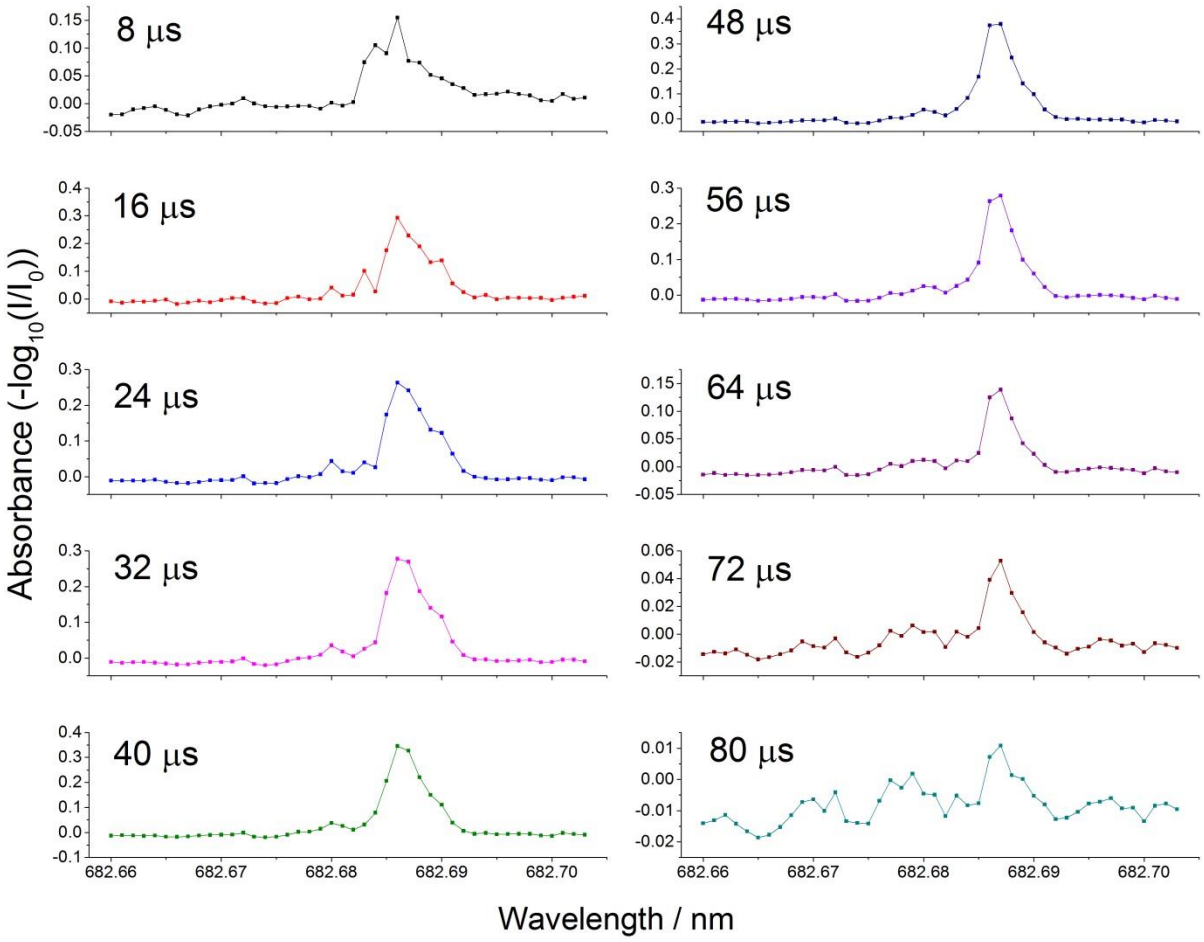

Figure 6.8. Absorption spectrum at increasing time delay after ablation pulse

(See Appendix Figure 8.9 for uranium absorption spectrum at t_d = 48 μs with error bars showing standard deviation of absorbance)

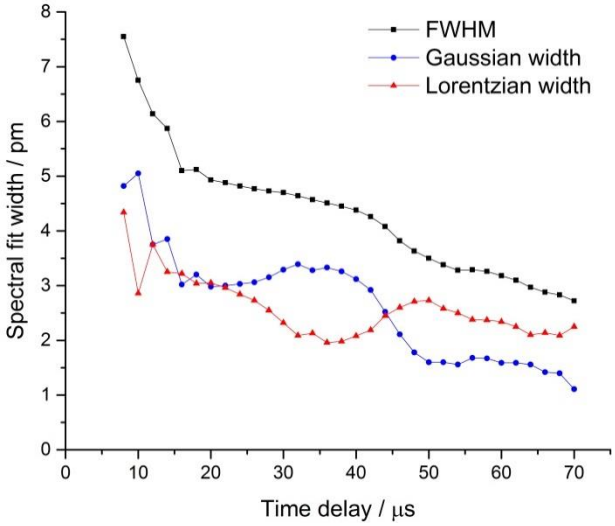

Figure 6.9. Time dependence of FWHM, Gaussian and Lorentzian widths from Voigt fits of absorption spectra (black squares: FWHM; blue circles: Gaussian width; red triangles: Lorentzian width)

Fitting the Gaussian width from Figure 6.9 with an exponential decay profile gives a relationship between time delay and temperature which is shown in equation (16). This relationship suggests that the temperature immediately after laser ablation (i.e. t_d = 1 μs) is 25000 K, which is within the estimated temperature range for LPP creation (10000 K to 40000 K). As Figure 6.8 shows, absorption peaks can be detected to a time delay of over 70 μs. At this time, the temperature is predicted to have dropped to around 2000 K.

$$T = -234.8 + 26360\ \exp\left(-\frac{t_d}{28.5}\right) \qquad (16)$$

Using the temperature estimation from equation (16), Doppler broadening can be calculated at early delay times using equation (12). This allows emission lines recorded with LIBS to be temperature-corrected as discussed in section 6.3.5.

To calculate the electron density of the plasma, the lines used by Burger et al [68] (shown in Table 6.1) were first identified in our spectra. The U I emission line at 499.01 nm was not visible at any time point so could not be utilised for electron density calculations. Presumably this was because of a combination of low number density of the excited species and a low transition strength. The U II line at 500.82 nm was visible in spectra recorded after a delay of 1.2 μs. Numerous other U I and U II lines were visible, however without Stark broadening coefficients they could not be used for electron density calculations.

Twin Lorentzian profiles were fitted to the 500.82 nm emission line and an unidentified neighbouring peak at 500.72 nm for averaged LIBS spectra at each recorded time delay. The width of the 500.82 nm line was then corrected as described in section 6.3.5. The plasma temperature was calculated for the time delay of spectral recording with equation (16). Doppler broadening for that temperature was then calculated using equation (12) and a Voigt profile was fitted to the emission peak with the Gaussian width set to a value which included contribution from the instrument and Doppler broadening. The overall contribution to the emission width from Doppler broadening was minor – not increasing above 8% for any of the temperatures predicted. This is principally because of the very heavy atomic mass of uranium (238 was used in our Doppler width calculations).

Figure 6.10 shows the electron density calculated using the procedure described. The electron density decreases within the first 5 μs before remaining fairly stable around 3×10^{16} cm^{-3} until 60 μs after the ablation pulse. There are outliers at 1.4 μs (with an electron density above 12×10^{16} cm^{-3}) and at late delay times where the electron density is calculated to drop to 1×10^{16} cm^{-3}. These uncertainties are attributed to the influence of bremsstrahlung radiation for the early time delay and to reduced signal intensity for the later measurements. The calculated electron density of around 3×10^{16} cm^{-3} is consistent with previous studies of uranium laser ablation plasmas [43,68], although experimental differences such as sample matrix, laser pulse energy, choice of sheath gas and gas pressure complicate direct comparison. The largest source of error comes from the Stark broadening parameters themselves. The literature source for the Stark broadening parameters used in this study was from Burger et al [68] who quote an estimated error margin of 45%.

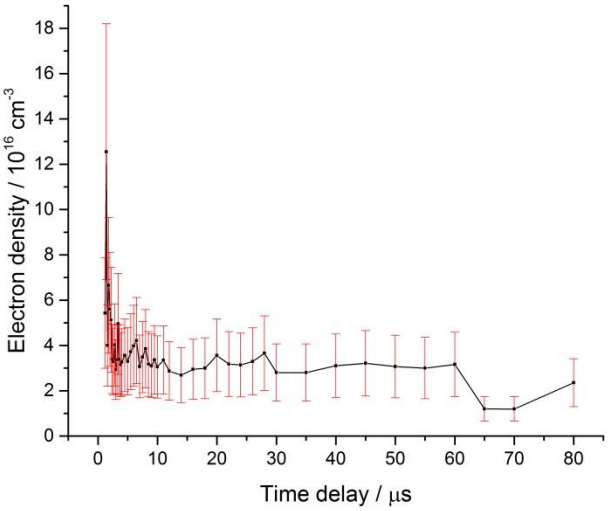

Figure 6.10. Electron density calculated from Stark width of 500.82 U II emission line against time delay after laser ablation pulse. Error bars show largest estimated source of error, the Stark broadening parameters predicted by Burger et al [68]

The electron density was also measured using the Stark broadening of a neutral sodium emission line centred at 589.00 nm ($2p^6 3p \rightarrow 2p^6 3s$; 16980 → 0 cm^{-1}) to verify the electron density calculations. This line probably resulted from surface contamination of the uranium sample, and remained intense for the full duration of the emission. Using the same methodology as for the uranium line calculations, the Doppler broadening was first subtracted from the fitted FWHM. Stark broadening parameters from the Stark-b database [67] were then used to estimate the electron density. The results indicate an electron density of between 2.25 and 1.5 × 10^{16} cm^{-3} for the first 40 μs after laser ablation, before a gradual increase up to 3 × 10^{16} cm^{-3} at a delay time of 80 μs. These values compare quite well with those measured using the U II emission in Figure 6.10, given the well reported uncertainty associated with electron density calculations [68]. However, the gradual increase after t_d = 40 μs suggested by the Na emission line is unexpected and contrasts with the U II emission. An artificially inflated line width may have been caused by self-absorption effects which are common in intense resonance lines of laser ablation plasma due to the non-local thermal equilibrium (LTE) conditions. Self-absorption tends to have more impact at later delay times as the plasma cools and the population of the lower energy level increases, so is particularly likely in this case.

To enable further study of the uranium laser ablation plasma, Stark broadening parameters for more uranium transitions could be deciphered using the combination of LA-TDLAS and LIBS demonstrated here. For Stark broadening parameters to be accurately estimated from emission spectra, both the Doppler and Stark broadening of the spectral lines should be taken into account. Using LA-TDLAS to calculate the temperature and well-studied LIBS emission lines to simultaneously calculate the electron density achieves both these objectives. Furthermore, using an emission line from a minor constituent would be possible as we have shown with sodium in this study. In this way, it is theoretically possible to calculate the Stark broadening parameters of any isolated (non-superimposed) transition observed in the LIBS spectrum. These calculations were beyond the scope of our project, but would be an interesting and useful additional study.

6.5 Conclusion

We have demonstrated a method of rapid isotopic analysis with combined laser ablation-TDLAS and LIBS. Such a technique could provide isotopic and elemental sample information, with stand-off capability, and be small and rugged enough to enable field-deployment. In this study, the absorption of uranium laser ablation plasma was investigated with LA-TDLAS using a balanced detection method of one ECDL probe beam with narrow laser linewidth and one background beam offset from the absorption features. Two absorption maxima were observed in the time-dependence of the peak absorption, temporally separated by around 30 μs. Comparing the area of absorption peaks of both uranium isotopes led to a predicted isotope ratio of around 3.2% which contrasts with the natural isotopic abundance of uranium of 0.7%. We attribute this discrepancy to a combination of high noise in the absorption spectra, the low abundance of the minor isotope and saturation of the absorption signal of the major isotope. The LoD was estimated with 3σ criterion to be 1.52 wt%. Although inflated by the incorrect assumption of 100% sample purity, this LoD would still enable identification of low enriched uranium over natural uranium, which (given the speed of measurement) would be useful in nuclear forensics and environmental monitoring. Miniaturisation of the LA-TDLAS apparatus to create a handheld device is inherently possible and would provide an additional benefit.

The plasma temperature was calculated using the Doppler broadening of absorption peaks by fitting Voigt profiles and extracting the Gaussian width. The electron density was calculated using Stark broadening of uranium and sodium emission lines. An electron density around 3×10^{16} cm^{-3} was calculated with the uranium emission, while the sodium line suggested a slightly reduced electron density between 2.25 and 1.5×10^{16} cm^{-3}, which we attributed to the impact of self-absorption.

Investigation of a double absorption peak and evidence of isotopic segregation could be achieved by spatio-temporal mapping of the ablation process using our combined LA-TDLAS and LIBS apparatus. Adjusting the height of sample relative to the focal point of the ablation laser would be a simple way to investigate the effect of a weakly-ionised air channel and air breakdown on plasma plume expansion. Additionally, studying the ablation process and plume dynamics with double-pulsed (DP-) LIBS would be an interesting further study, and the increased plasma lifetime of DP-LIBS could enable wavelength ramping to capture absorption of both isotopes during a single ablation event.

Acknowledgements

The authors would like to thank AWE and EPSRC for funding the PhD project through the Materials for Demanding Environments Centre for Doctoral Training. We would also like to acknowledge the help of Prof Andrew Murray from the University of Manchester for his help with the design and construction of the external cavity diode laser, and Dr Nicholas Stevens and AWE for providing the uranium wire samples.

6.6 References

[1] P. Fichet, P. Mauchien, C. Moulin, Determination of impurities in uranium and plutonium dioxides by laser-induced breakdown spectroscopy, Appl. Spectrosc. 53 (1999) 1111–1117. doi:10.1366/0003702991947892.

[2] P. Rohwetter, K. Stelmaszczyk, L. Woste, R. Ackermann, G. Mejean, E. Salmon, J. Kasparian, J. Yu, J.P. Wolf, Filament-induced remote surface ablation for long range laser-induced breakdown spectroscopy operation, Spectrochim. Acta - Part B At. Spectrosc. 60 (2005) 1025–1033. doi:10.1016/j.sab.2005.03.017.

[3] R.C. Wiens et al., The ChemCam instrument suite on the Mars Science Laboratory (MSL) rover: Body unit and combined system tests, Space Sci. Rev. 170 (2012) 167–227. doi:10.1007/s11214-012-9902-4.

[4] T.L. Cremers, R.C. Chinni, M. Bostian, L.J. Radziemski, C. Navarro-Northrup, C.R. Jones, L. Karch, Detection of actinide elements using LIBS, in: Proc. Inst. Nucl. Mater., 2010: p. 1. http://connection.ebscohost.com/c/articles/58108183/detection-actinide-elements-using-libs.

[5] J. Handke, F. Duschek, K. Gruenewald, C. Pargmann, Standoff detection applying laser-induced breakdown spectroscopy at the DLR laser test range, in: Proc. SPIE - Int. Soc. Opt. Eng., Orlando, Florida, 2011: p. 80180T. doi:10.1117/12.886543.

[6] W. Li, X. Li, X. Li, Z. Hao, Y. Lu, X. Zeng, A review of remote laser-induced breakdown spectroscopy, Appl. Spectrosc. Rev. (2018) 1–25. doi:10.1080/05704928.2018.1472102.

[7] S.S. Harilal, B.E. Brumfield, N.L. Lahaye, K.C. Hartig, M.C. Phillips, Optical spectroscopy of laser-produced plasmas for standoff isotopic analysis, Appl. Phys. Rev. 5 (2018) 1–32. doi:10.1063/1.5016053.

[8] R.C. Chinni, D.A. Cremers, L.J. Radziemski, M. Bostian, C. Navarro-Northrup, Detection of uranium using laser-induced breakdown spectroscopy, Appl. Spectrosc. 63 (2009) 1238–1250. http://www.osapublishing.org/abstract.cfm?uri=as-63-11-1238.

[9] X. Wan, P. Wang, Remote quantitative analysis of minerals based on multispectral line-calibrated laser-induced breakdown spectroscopy (LIBS), Appl. Spectrosc. 68 (2014) 1132–1136. doi:10.1366/13-07203.

[10] S. Palanco, S. Conesa, J.J. Laserna, Analytical control of liquid steel in an induction melting furnace using a remote laser induced plasma spectrometer, J. Anal. At. Spectrom. 19 (2004) 462–467. doi:10.1039/b400354c.

[11] G. Lorenzetti, S. Legnaioli, E. Grifoni, S. Pagnotta, V. Palleschi, Laser-based continuous monitoring and resolution of steel grades in sequence casting machines, Spectrochim. Acta - Part B At. Spectrosc. 112 (2015) 1–5. doi:10.1016/j.sab.2015.07.006.

[12] T. Hussain, M. a Gondal, Laser induced breakdown spectroscopy (LIBS) as a rapid tool for material analysis, J. Phys. Conf. Ser. 439 (2013) 13. doi:10.1088/1742-6596/439/1/012050.

[13] J.-I. Yun, R. Klenze, J.-I. Kim, Laser-induced breakdown spectroscopy for the on-line multielement analysis of highly radioactive glass melt. Part I: Characterization and evaluation of the method, Appl. Spectrosc. 56 (2002) 437–448. doi:10.1366/0003702021955097.

[14] J.-I. Yun, R. Klenze, J.-I. Kim, Laser-induced breakdown spectroscopy for the on-line multielement analysis of highly radioactive glass melt simulants. Part II: Analyses of molten glass samples, Appl. Spectrosc. 56 (2002) 852–858. doi:10.1366/000370202760171518.

[15] M. Gaft, I. Sapir-Sofer, H. Modiano, R. Stana, Laser induced breakdown spectroscopy for bulk minerals online analyses, Spectrochim. Acta - Part B At. Spectrosc. 62 (2007) 1496–1503. doi:10.1016/j.sab.2007.10.041.

[16] R. Noll, C. Fricke-Begemann, M. Brunk, S. Connemann, C. Meinhardt, M. Scharun, V. Sturm, J. Makowe, C. Gehlen, Laser-induced breakdown spectroscopy expands into industrial applications, Spectrochim. Acta - Part B At. Spectrosc. 93 (2014) 41–51. doi:10.1016/j.sab.2014.02.001.

[17] R. Noll, C. Fricke-Begemann, S. Connemann, C. Meinhardt, V. Sturm, LIBS analyses for industrial applications-an overview of developments from 2014 to 2018, J. Anal. At. Spectrom. 33 (2018) 945–956. doi:10.1039/c8ja00076j.

[18] R. Noll, H. Bette, A. Brysch, M. Kraushaar, I. Mönch, L. Peter, V. Sturm, Laser-induced breakdown spectrometry - Applications for production control and quality assurance in the steel industry, Spectrochim. Acta - Part B At. Spectrosc. 56 (2001) 637–649. doi:10.1016/S0584-8547(01)00214-2.

[19] G.C.-Y. Chan, X. Mao, I. Choi, A. Sarkar, O.P. Lam, D.K. Shuh, R.E. Russo, Multiple emission line analysis for improved isotopic determination of uranium — a computer simulation study, Spectrochim. Acta - Part B At. Spectrosc. 89 (2013) 40–49.

doi:10.1016/j.sab.2013.09.001.

[20] K. Kuhn, J.A. Meima, D. Rammlmair, C. Ohlendorf, Chemical mapping of mine waste drill cores with laser-induced breakdown spectroscopy (LIBS) and energy dispersive X-ray fluorescence (EDXRF) for mineral resource exploration, J. Geochemical Explor. 161 (2016) 72–84. doi:10.1016/j.gexplo.2015.11.005.

[21] F.R. Doucet, G. Lithgow, R. Kosierb, P. Bouchard, M. Sabsabi, Determination of isotope ratios using Laser-Induced Breakdown Spectroscopy in ambient air at atmospheric pressure for nuclear forensics, J. Anal. At. Spectrom. 26 (2011) 536–541. doi:10.1039/c0ja00199f.

[22] M.A. Sperança, D.F. Andrade, J.P. Castro, E.R. Pereira-Filho, Univariate and multivariate calibration strategies in combination with laser-induced breakdown spectroscopy (LIBS) to determine Ti on sunscreen: A different sample preparation procedure, Opt. Laser Technol. 109 (2019) 648–653. doi:10.1016/j.optlastec.2018.08.056.

[23] M.M. Tan, S. Cui, J. Yoo, S.H. Han, K.S. Ham, S.H. Nam, Y. Lee, Feasibility of laser-induced breakdown spectroscopy (LIBS) for classification of sea salts, Appl. Spectrosc. 66 (2012) 262–271. doi:10.1366/11-06379.

[24] J. Sirven, A. Pailloux, Y. M'Baye, N. Coulon, T. Alpettaz, S. Gossé, Towards the determination of the geographical origin of yellow cake samples by laser-induced breakdown spectroscopy and chemometrics, J. Anal. At. Spectrom. 24 (2009) 451–459. doi:10.1039/b821405k.

[25] M. Robel, M.J. Kristo, Discrimination of source reactor type by multivariate statistical analysis of uranium and plutonium isotopic concentrations in unknown irradiated nuclear fuel material, J. Environ. Radioact. 99 (2008) 1789–1797. doi:10.1016/j.jenvrad.2008.07.004.

[26] P. Pořízka, A. Demidov, J. Kaiser, J. Keivanian, I.B. Gornushkin, U. Panne, J. Riedel, Laser-induced breakdown spectroscopy for in situ qualitative and quantitative analysis of mineral ores, Spectrochim. Acta - Part B At. Spectrosc. 101 (2014) 155–

163. doi:10.1016/j.sab.2014.08.027.

[27] B. Bhatt, A. Dehayem-Kamadjeu, K.H. Angeyo, Rapid nuclear forensics analysis via machine-learning-enabled laser-induced breakdown spectroscopy (LIBS), AIP Conf. Proc. 060006 (2019) 1–4. doi:10.1063/1.5110124.

[28] T.-L. Zhang, S. Wu, H.-S. Tang, K. Wang, Y.-X. Duan, H. Li, Progress of Chemometrics in Laser-induced Breakdown Spectroscopy Analysis, Chinese J. Anal. Chem. 43 (2015) 939–948. doi:10.1016/S1872-2040(15)60832-5.

[29] J. El Haddad, L. Canioni, B. Bousquet, Good practices in LIBS analysis: Review and advices, Spectrochim. Acta - Part B At. Spectrosc. 101 (2014) 171–182. doi:10.1016/j.sab.2014.08.039.

[30] M.Z. Martin, S. Allman, D.J. Brice, R.C. Martin, N.O. Andre, Exploring laser-induced breakdown spectroscopy for nuclear materials analysis and in-situ applications, Spectrochim. Acta - Part B At. Spectrosc. 74–75 (2012) 177–183. doi:10.1016/j.sab.2012.06.049.

[31] E.J. Judge, J.E. Barefield, J.M. Berg, S.M. Clegg, G.J. Havrilla, V.M. Montoya, L.A. Le, L.N. Lopez, Laser-induced breakdown spectroscopy measurements of uranium and thorium powders and uranium ore, Spectrochim. Acta - Part B At. Spectrosc. 83–84 (2013) 28–36. doi:10.1016/j.sab.2013.03.002.

[32] E.L. Gurevich, R. Hergenröder, Femtosecond laser-induced breakdown spectroscopy: Physics, applications, and perspectives, Appl. Spectrosc. 61 (2007) 233–242. doi:10.1366/000370207782217824.

[33] N.L. LaHaye, M.C. Phillips, A.M. Duffin, G.C. Eiden, S.S. Harilal, The influence of ns- and fs-LA plume local conditions on the performance of a combined LIBS/LA-ICP-MS sensor, J. Anal. At. Spectrom. 31 (2016) 515–522. doi:10.1039/c5ja00317b.

[34] H.D. Wizemann, K. Niemax, Isotope selective element analysis by diode laser atomic absorption spectrometry, Mikrochim. Acta. 129 (1998) 209–216. doi:10.1007/bf01244743.

[35] R.E. Russo, A.A. Bol'shakov, X. Mao, C.P. McKay, D.L. Perry, O. Sorkhabi, Laser Ablation Molecular Isotopic Spectrometry, Spectrochim. Acta - Part B At. Spectrosc. 66 (2011) 99–104. doi:10.1016/j.sab.2011.01.007.

[36] A.A. Bol'shakov, X. Mao, J.J. Gonzlez, R.E. Russo, Laser ablation molecular isotopic spectrometry (LAMIS): current state of the art, J. Anal. At. Spectrom. 31 (2016) 119. doi:10.1039/c5ja00310e.

[37] H. Hou, G.C.Y. Chan, X. Mao, R. Zheng, V. Zorba, R.E. Russo, Femtosecond filament-laser ablation molecular isotopic spectrometry, Spectrochim. Acta - Part B At. Spectrosc. 113 (2015) 113–118. doi:10.1016/j.sab.2015.09.014.

[38] B.W. Smith, A. Quentmeier, M.A. Bolshov, K. Niemax, Measurement of uranium isotope ratios in solid samples using laser ablation and diode laser-excited atomic fluorescence spectrometry, Spectrochim. Acta - Part B At. Spectrosc. 54 (1999) 943–958. doi:10.1016/S0584-8547(99)00022-1.

[39] A. Quentmeier, M.A. Bolshov, K. Niemax, Measurement of uranium isotope ratios in solid samples using laser ablation and diode laser-atomic absorption spectrometry, Spectrochim. Acta - Part B At. Spectrosc. 56 (2001) 45–55. doi:10.1016/S0584-8547(00)00289-5.

[40] H. Liu, A. Quentmeier, K. Niemax, Diode laser absorption measurement of uranium isotope ratios in solid samples using laser ablation, Spectrochim. Acta - Part B At. Spectrosc. 57 (2002) 1611–1623.

[41] N.R. Taylor, M.C. Phillips, Measurements of Uranium Line Widths and Pressure Broadening Coefficients in Atmospheric Pressure Laser- Induced Plasmas, CLEO 2013. paper CTu2 (2013) CTu2H.2. doi:10.1364/CLEO_SI.2013.CTu2H.2.

[42] N.R. Taylor, M.C. Phillips, Differential laser absorption spectroscopy of uranium in an atmospheric pressure laser-induced plasma, Opt. Lett. 39 (2014) 594–597. doi:10.1364/OL.39.000594.

[43] P.J. Skrodzki, N.P. Shah, N. Taylor, K.C. Hartig, N.L. LaHaye, B.E. Brumfield, I. Jovanovic, M.C. Phillips, S.S. Harilal, Significance of ambient conditions in uranium

absorption and emission features of laser ablation plasmas, Spectrochim. Acta - Part B At. Spectrosc. 125 (2016) 112–119. doi:10.1016/j.sab.2016.09.012.

[44] S.S. Harilal, P.K. Diwakar, N.L. Lahaye, M.C. Phillips, Spatio-temporal evolution of uranium emission in laser-produced plasmas, Spectrochim. Acta - Part B At. Spectrosc. 111 (2015) 1–7. doi:10.1016/j.sab.2015.06.003.

[45] M.C. Phillips, S.S. Harilal, J. Yeak, Tunable Laser Absorption Spectroscopy of Uranium in Femtosecond Laser Ablation Plasmas, in: Conf. Lasers Electro-Optics, Optical Society of America, San Jose, 2016: pp. 38–39. https://www.osapublishing.org/abstract.cfm?URI=CLEO_SI-2016-STh1H.7.

[46] J.R. Freeman, S.S. Harilal, P.K. Diwakar, B. Verhoff, A. Hassanein, Comparison of optical emission from nanosecond and femtosecond laser produced plasma in atmosphere and vacuum conditions, Spectrochim. Acta - Part B At. Spectrosc. 87 (2013) 43–50. doi:10.1016/j.sab.2013.05.011.

[47] L.A. Emmert, R.C. Chinni, D.A. Cremers, C.R. Jones, W. Rudolph, Comparative study of femtosecond and nanosecond laser-induced breakdown spectroscopy of depleted uranium, Appl. Opt. 50 (2011) 313–317.

[48] M. Miyabe, M. Oba, H. Iimura, K. Akaoka, Y. Maruyama, H. Ohba, M. Tampo, I. Wakaida, Laser ablation absorption spectroscopy for remote analysis of uranium, Hyperfine Interact. 216 (2013) 71–77. doi:10.1007/s10751-013-0845-2.

[49] M. Miyabe, M. Oba, H. Iimura, K. Akaoka, Y. Maruyama, H. Ohba, M. Tampo, I. Wakaida, Absorption spectroscopy of uranium plasma for remote isotope analysis of next-generation nuclear fuel, Appl. Phys. A Mater. Sci. Process. 112 (2013) 87–92. doi:10.1007/s00339-012-7181-2.

[50] M. Miyabe, M. Oba, K. Jung, H. Iimura, K. Akaoka, M. Kato, H. Otobe, A. Khumaeni, I. Wakaida, Laser ablation absorption spectroscopy for isotopic analysis of plutonium: Spectroscopic properties and analytical performance, Spectrochim. Acta - Part B At. Spectrosc. 134 (2017) 42–51. doi:10.1016/j.sab.2017.05.008.

[51] A.A. Bol'shakov, X. Mao, C.P. McKay, R.E. Russo, Laser-ablation optical-cavity isotopic

spectrometer for Mars rovers, in: Proc. SPIE - Int. Soc. Opt. Eng. (Proceedings SPIE), 2012: pp. 83850C-83850C–7. doi:10.1117/12.919905.

[52] S.S. Harilal, N.L. LaHaye, M.C. Phillips, Two-dimensional fluorescence spectroscopy of laser-produced plasmas, Opt. Lett. 41 (2016) 3547. doi:10.1364/OL.41.003547.

[53] M.C. Phillips, B.E. Brumfield, N. Lahaye, S.S. Harilal, K.C. Hartig, I. Jovanovic, Two-dimensional fluorescence spectroscopy of uranium isotopes in femtosecond laser ablation plumes, Sci. Rep. 7 (2017) 1–12. doi:10.1038/s41598-017-03865-9.

[54] S.S. Harilal, C.M. Murzyn, M.C. Phillips, J.B. Martin, Hyperfine structures and isotopic shifts of uranium transitions using tunable laser spectroscopy of laser ablation plumes, Spectrochim. Acta - Part B At. Spectrosc. 169 (2020) 105828. doi:10.1016/j.sab.2020.105828.

[55] J. Bergevin, T.H. Wu, J. Yeak, B.E. Brumfield, S.S. Harilal, M.C. Phillips, R.J. Jones, Dual-comb spectroscopy of laser-induced plasmas, Nat. Commun. 9 (2018) 1–6. doi:10.1038/s41467-018-03703-0.

[56] Y. Zhang, C. Lecaplain, R.R.D. Weeks, J. Yeak, S.S. Harilal, M.C. Phillips, R. Jason Jones, Time-resolved dual-comb measurement of number density and temperature in a laser-induced plasma, Opt. Lett. 44 (2019) 3458. doi:10.1364/ol.44.003458.

[57] A. Safi, S.H. Tavassoli, G. Cristoforetti, S. Legnaioli, V. Palleschi, F. Rezaei, E. Tognoni, Determination of excitation temperature in laser-induced plasmas using columnar density Saha-Boltzmann plot, J. Adv. Res. 18 (2019) 1–7. doi:10.1016/j.jare.2019.01.008.

[58] G.C.-Y. Chan, I. Choi, X. Mao, V. Zorba, O.P. Lam, D.K. Shuh, R.E. Russo, Isotopic determination of uranium in soil by laser induced breakdown spectroscopy, Spectrochim. Acta - Part B At. Spectrosc. 122 (2016) 31–39. doi:10.1016/j.sab.2016.05.014.

[59] M.B. Shattan, D.J. Miller, M.T. Cook, A.C. Stowe, J.D. Auxier, C. Parigger, H.L. Hall, Detection of uranyl fluoride and sand surface contamination on metal substrates by hand-held laser-induced breakdown spectroscopy, Appl. Opt. 56 (2017) 9868.

doi:10.1364/ao.56.009868.

[60] K.R. Campbell, N.R. Wozniak, J.P. Colgan, E.J. Judge, J.E. Barefield, D.P. Kilcrease, M.P. Wilkerson, K.R. Czerwinski, S.M. Clegg, Phase discrimination of uranium oxides using laser-induced breakdown spectroscopy, Spectrochim. Acta - Part B At. Spectrosc. 134 (2017) 91–97. doi:10.1016/j.sab.2017.05.007.

[61] I. Choi, G.C.Y. Chan, X. Mao, D.L. Perry, R.E. Russo, Line selection and parameter optimization for trace analysis of uranium in glass matrices by laser-induced breakdown spectroscopy (LIBS), Appl. Spectrosc. 67 (2013) 1275–1284. doi:10.1366/13-07066.

[62] E.C. Jung, T. Kim, K. Song, C. Kim, Diode Laser-Excited Optogalvanic and Absorption Measurements of Uranium in a Hollow Cathode Discharge, Spectrosc. Lett. 36 (2003) 167–180. doi:10.1081/SL-120021823.

[63] C.J. Hawthorn, K.P. Weber, R.E. Scholten, Littrow configuration tunable external cavity diode laser with fixed direction output beam, Rev. Sci. Instrum. 72 (2001) 4477–4479. doi:10.1063/1.1419217.

[64] G. Hull, E.D. McNaghten, P. Coffey, P.A. Martin, Isotopic analysis and plasma diagnostics for lithium detection using combined laser ablation–tuneable diode laser absorption spectroscopy and laser-induced breakdown spectroscopy, Spectrochim. Acta - Part B At. Spectrosc. (2020).

[65] B.A. Bushaw, N.C. Anheier Jr., Isotope ratio analysis on micron-sized particles in complex matrices by Laser Ablation-Absorption Ratio Spectrometry, Spectrochim. Acta - Part B At. Spectrosc. 64 (2009) 1259–1265. doi:10.1016/j.sab.2009.10.002.

[66] B.A. Bushaw, N.C. Anheier, J.R. Phillips, System and method for high precision isotope ratio destructive analysis, (2013). http://www.google.com.pg/patents/US8477304.

[67] S. Sahal-Bréchot, M.S. Dimitrijević, N. Moreau, STARK-B database, Obs. Paris, LERMA Astron. Obs. Belgrade. (2019). http://stark-b.obspm.fr (accessed November 27, 2019).

[68] M. Burger, P.J. Skrodzki, I. Jovanovic, M.C. Phillips, S.S. Harilal, Laser-produced

uranium plasma characterization and Stark broadening measurements, Phys. Plasmas. 26 (2019). doi:10.1063/1.5099643.

[69] S.S. Harilal, B. O'Shay, Y. Tao, M.S. Tillack, Ambient gas effects on the dynamics of laser-produced tin plume expansion, J. Appl. Phys. 99 (2006). doi:10.1063/1.2188084.

[70] T. Kerdja, S. Abdelli, O. Ghobrini, S. Malek, Dynamics of laser-produced carbon plasma in an inert atmosphere, J. Appl. Phys. 80 (1996) 5365–5371. doi:10.1063/1.363477.

[71] S. Amoruso, R. Bruzzese, R. Velotta, N. Spinelli, M. Vitiello, X. Wang, Characterization of LaMnO 3 laser ablation in oxygen by ion probe and optical emission spectroscopy, Appl. Surf. Sci. 248 (2005) 45–49. doi:10.1016/j.apsusc.2005.03.030.

[72] H. Hou, B. Yang, X. Mao, V. Zorba, P. Ran, R.E. Russo, Characteristics of plasma plume in ultrafast laser ablation with a weakly ionized air channel, Opt. Express. 26 (2018) 13425. doi:10.1364/oe.26.013425.

[73] M. Miyabe, M. Oba, H. Iimura, K. Akaoka, Y. Maruyama, H. Ohba, M. Tampo, I. Wakaida, Doppler-shifted optical absorption characterization of plume-lateral expansion in laser ablation of a cerium target, J. Appl. Phys. 112 (2012). doi:10.1063/1.4771879.

[74] M. Burger, P.J. Skrodzki, L.A. Finney, J. Hermann, J. Nees, I. Jovanovic, Isotopic analysis of deuterated water via single- and double-pulse laser-induced breakdown spectroscopy, Phys. Plasmas. 25 (2018). doi:10.1063/1.5042665.

[75] M. Dong, X. Mao, J.J. Gonzalez, J. Lu, R.E. Russo, Carbon isotope separation and molecular formation in laser-induced plasmas by laser ablation molecular isotopic spectrometry, Anal. Chem. 85 (2013) 2899–2906. doi:10.1021/ac303524d.

[76] S.S. Harilal, E.J. Kautz, B.E. Bernacki, M.C. Phillips, P.J. Skrodzki, M. Burger, I. Jovanovic, Physical conditions for UO formation in laser-produced uranium plumes, Phys. Chem. Chem. Phys. 21 (2019) 16161–16169. doi:10.1039/c9cp02250c.

[77] S. Zhang, X. Wang, M. He, Y. Jiang, B. Zhang, W. Hang, B. Huang, Laser-induced plasma temperature, Spectrochim. Acta - Part B At. Spectrosc. 97 (2014) 13–33.

doi:10.1016/j.sab.2014.04.009.

Chapter 7 - Summary, conclusions and future work

The thesis presented results in four chapters based around two different analytical techniques: laser-induced breakdown spectroscopy (LIBS) and laser ablation-tuneable diode laser absorption spectroscopy (LA-TDLAS).

7.1 Laser-induced breakdown spectroscopy for elemental analysis of nuclear materials and environments

In this work, the overall aim was to prove that LIBS was an adequate tool for analysis of trace elements in uranium-based samples. To begin, a series of experiments using surrogate elements rather than uranium were undertaken, for easier handling and data analysis. The work in Chapter 3 was framed towards the on-line monitoring of molten salt pyroprocessing facilities, as this is one potential application of LIBS. As such, LKE salt matrices and rare earth element contaminants were used. The results show several findings which were taken forward to the analysis of uranium samples:

- Multivariate data analysis is a powerful tool that can be used to quantify trace level impurities. However, careful consideration of the data pre-processing strategy must be made. The Echelle spectrometer created an artificial intensity 'hump' in the baseline which had to be corrected using a fitting algorithm before concentration modelling. This novel approach enables more accurate comparison of emission lines, and improved the RMSECV of the modelling. Additionally, normalisation of the spectra with respect to a matrix peak (in the case of LKE, a neutral lithium peak proved suitable) improved the relationship between concentration and peak intensity, which increased the accuracy of the modelling.
- Before the experiments with different pulse energies, it was expected that increasing the pulse energy would lead to greater emission intensities and therefore improved modelling accuracy. However, the results showed that using a higher pulse energy had a detrimental impact on the emission intensity. Moreover, the sample material was used up more quickly, and so less replicate measurements could be taken.
- The sample homogeneity, particularly the texture of the surface, had a large impact on the shot-to-shot variations in emission intensity, and subsequently the accuracy of the modelling. Control of the surface was clearly important, but affecting the surface quality was non-trivial. The main method implemented to aid sample

homogeneity was to perform the LIBS measurement on a fresh sample surface position with every ablation. This was necessary to avoid sample cratering and the resulting changes in plasma plume generation and emission intensity.

With Chapter 4, the analysis moved from a previous simple salt matrix with relatively straightforward handling protocols to analysis of powdered samples of hazardous uranium-containing materials. In addition to the handling difficulties, the uranium spectrum was significantly more complex than that of the LKE, and there were 26 trace elements compared to the three present in the previous experiments. The results showed the following main conclusions:

- Two different sample sets (CRM-124 and CUP-2) were analysed in the experiments for Chapter 4. The two materials (UO_2 and uranium ore concentrate, respectively) were markedly different for many shared species. The hydrogen emission line at 656.28 nm and the ambient gas emission envelope around 821 nm were illustrated as examples. This prevented the two samples being modelled together, which highlights the need for matrix-matched reference materials.
- The accuracy and validity of the PLS modelling was improved by using pre-selected spectral regions around known emission peaks. Careful inspection of the LIBS spectrum and cross-referencing of peaks against the NIST database allowed some transitions to be identified and used for the modelling over the high density of uranium lines, rather than modelling the entire spectrum and relying on the software to select regions of interest. Using pre-selected regions, the pixels used for the PLS methodology all categorically corresponded to the emission peaks rather than to noise or uranium peaks.
- The analysis time (as in computational time) was significantly quicker with a shortened list of pixels. Although the process of peak selection requires initial investment of time, once a peak (or rather a peak region) is identified subsequent analyses can be conducted very rapidly and with increased confidence. Additionally, it would be possible to use a pre-selected or automatic list of peaks for the analysis, for example by using every peak in the NIST database belonging to a certain element. The potential risk of including some non-adequate peaks (e.g. non-isolated

peaks or peaks suffering from self-absorption) with this approach could be mitigated through computable solutions to assist in peak selection.

There are some limitations to the LIBS analysis presented in this thesis which may hinder deployment of the technique to industrial settings:

- The limit of detection (LoD) of the LIBS method is quoted down to single digit ppm levels in textbooks and published literature. However, to achieve such low LoD values numerous experimental parameters must be idealised. In the results of these experiments, significantly better LoDs were achieved using the less complex LKE matrix with fewer trace element contaminants compared to the uranium-containing samples. The limits of quantification (LoQs) of the impurity elements in the LKE experiments were calculated between 1000 and 9000 ppm. For the uranium-containing materials, the LoQ was not calculated, but the complex spectral background produced by the high density of uranium emission lines would have significantly affected the quantitative ability of the analysis. It may not be possible to achieve such low LoDs in some industrial settings, or in nuclear forensics investigations, due to the imperfections of the sample and environment.
- The need for matrix-matched samples and prior knowledge of the elements present in a sample to form a quantitative chemical profile suggests that using LIBS for the application of nuclear forensics is perhaps not ideal. After all, a sample of seized material will be of an unknown physical state and composition. However, the strength of the LIBS technique should not be judged solely by the accuracy of quantification. Rather, using LIBS from a stand-off distance to quickly achieve *qualitative* results would be of tremendous use. Qualitative answers would be adequate for initial categorisation of the material, and could inform next steps. In most industrial applications, the variety of potential materials requiring analysis may well be narrower, and so the preparation of matrix-matched samples and environments could be achievable.

Despite these limitations, the applications for LIBS across the nuclear industry are broad. The benefits of rapid, stand-off, in situ analysis present numerous opportunities for deployment. To draw back to Chapter 1, the Hot Cells at Sellafield provide an interesting

scenario for which LIBS may provide an ideal solution. Analysing unknown hazardous materials from behind a shielded window presents an opportunity to use LIBS to inform next steps and categorise the hazards, before the cell need ever be opened. Other hazardous materials such as nuclear waste or plasma-facing components from a nuclear fusion tokamak could be analysed more accurately with LIBS, as the physical nature of a sample could be controlled or at least modelled.

7.2 Laser ablation – tuneable diode laser absorption spectroscopy for isotopic analysis of nuclear materials

Research in this thesis sought to investigate laser ablation-tuneable diode laser absorption spectroscopy (LA-TDLAS). In a similar process to Chapters 3 and 4, an initial set of experiments was performed as a proof of concept study to build expertise in the experimental methodology and handling processes before moving on to uranium samples.

In Chapter 5, a proof of concept study was conducted using LA-TDLAS and LIBS to simultaneously analyse absorption and emission from lithium laser-produced plasma. Lithium was chosen for the analysis because the maximum IS (15 pm) between ^{6}Li and ^{7}Li emission lines is similar to that of the maximum uranium and plutonium ISs (25 pm and 13 pm, respectively). An external cavity diode laser (ECDL) was constructed for the experiments, to refine the wavelength of the absorption laser and to increase the spectral resolution of the resulting LA-TDLAS spectra. The following conclusions were drawn:

- The repeatability of the experiment was significantly affected by the surface of the lithium pellet sample, with minor aberrations causing major disruption to signal intensity. The low density samples suffered from cratering with prolonged sampling from the same position, and so it was necessary to move the sample to expose a fresh surface after each ablation shot. Re-creation of the pristine fresh sample surface was found to be possible by cleaning the surface with grinding paper. This saved a significant amount of time compared to fabricating fresh samples with a hydraulic pellet presser for each experiment.
- The ECDL construction was time consuming and difficult, yet completely necessary, as the spectral bandwidth of several commercial TO-can laser diodes were tested

and found to be insufficient for resolving the narrowly separated isotope shifts. The temperature of the ECDL drifted over time. When the laser was switched on, different parameters of grating angle and temperature were required to achieve a consistent wavelength. This necessitated real-time monitoring and parameter control, to ensure the correct wavelength was being achieved with single-mode emission.

- The use of double-pulsed laser ablation (DP-LA) significantly reduced the linewidth of absorption peaks in the absorption spectrum compared to single shot laser ablation. Incorporating DP-LA could enable the possibility of measuring elements with smaller IS, such as those in the centre of the periodic table. The novelty of investigating DP-LA-TDLAS presents one of the original contributions to knowledge in this thesis.
- Simultaneous acquisition of absorption and emission spectra from the laser-produced plasma enabled calculation of plasma electron density and plasma temperature, using Stark and Doppler line broadening respectively. Calculating these parameters usually requires examination of numerous spectral lines and construction of Saha-Eggert or Boltzmann plots. The method used here requires knowledge of only a single transition's Stark broadening parameters to calculate the electron density, and knowledge of the atomic mass to calculate the Doppler broadening and therefore the temperature.

Having constructed the experimental setup, created the software and gained experience with analytical methods for LA-TDLAS experiments, the switch to uranium samples prompted only minor changes in hardware to accommodate the air-tight cell needed to contain the hazardous samples. However, a combination of factors made the experiments in Chapter 6 significantly more complex than the previous studies with lithium. The main problem was the smaller isotope ratio of 0.7% ^{235}U, which meant the absorption peak was obscured by the noise. The low signal intensity necessitated adaptations to improve the spectral resolution, which resulted in the balanced detection method of a probe and background laser. The main conclusions from the uranium LA-TDLAS experiments can be summarised as follows:

- Utilising a second diode laser to remove shot-to-shot fluctuations in the plasma proved very successful in improving the quality of the absorption spectra. The

reduction in noise allowed both uranium isotopes to be measured, despite the very low abundance of ^{235}U. Indeed, the improved spectral quality enabled detailed spectral features, for example a double absorbance peak, to be observed.

- The persistence of the uranium absorption and emission signals was significantly shorter than for the lithium plasma. This could be due to a combination of differing matrix materials (low-density salt and high density metal) or the greater nuclear charge of uranium leading to faster recombination.
- Increasing the pulse energy increased the intensity of the absorption signal in an approximately linear relationship. Setting the pulse energy of the apparatus to its maximum led to the best LA-TDLAS results, so it seems logical that increasing the pulse energy further using a more powerful ablation laser could improve the results further.
- The accuracy of the isotope prediction was not good. The results indicated an isotope ratio of 3.2%, whereas the sample was of natural isotopic abundance (0.7%). Despite the improvements in noise level with the balanced detection method, a combination of the noise and possible saturation of the absorption signal of the major isotope led to sub-optimal accuracy, which is a problem for future applications of this method. However, even the ability to differentiate uranium enriched to 3% from non-enriched uranium would be extremely useful, given the advantages of the technique.

The limitations of the LA-TDLAS method with regard to nuclear forensics and other applications are below:

- Although the results of the LA-TDLAS experiments gave a stronger absorption signal at higher pulse energy, the PLS results in Chapter 3 indicated greater normalised emission intensity at lower pulse energy. The two sample matrices were significantly different (LKE salt for the PLS and uranium metal for the LA-TDLAS), so these two observations are not exactly comparable. Nonetheless, if the two methods of LIBS and LA-TDLAS were to be combined onto a single piece of apparatus for nuclear forensics, a compromise might have to be struck.
- The LoD of uranium was predicted to be worse using the LA-TDLAS method compared to the LIBS experiments with rare earth elements in Chapter 3. This

statement should be caveated with discussion of the methodology used for LoD calculation, which incorrectly estimated 100% purity of uranium metal for the LA-TDLAS results. It does however potentially challenge the LA-TDLAS method. Clearly significantly more work would need to be undertaken to estimate the LoD with different sample matrices, before this technique could be deployed.

- Finally, the overall layout of the experimental apparatus for LA-TDLAS (i.e. a laser ablation laser plus an orthogonal diode laser) does somewhat stretch the definition of 'stand-off'. The necessity for two lines of sight to a sample, moreover with one of those lines of sight uninterrupted between laser diode and a detector placed beyond the sample, complicates the arrangement compared to normal stand-off LIBS. However, a moveable probe for in situ measurements could circumvent some of this dilemma with fibre coupled lasers and by being placed close to the sample. In this way, machine operators could avoid most of the contact with the hazard.

The novelty of the research within the LA-TDLAS sections of the thesis is in the calculations of electron density and plasma temperature, and with the isotopic ratio calculations performed at atmospheric pressure, as opposed to most published literature where reduced pressure was used. Usual methods for calculating the electron density rely on numerous emission lines, whereas the Stark broadening method utilised here can be completed with knowledge of only a single emission line's Stark broadening parameters.

Although the results of the isotopic predictions are somewhat inaccurate, the sources of inaccuracy have been discussed and could potentially be mitigated in future experiments. The differentiation between natural (0.7%), low-enriched (3-5%) and weapons-grade uranium (>85%) is a very important one for nuclear security, and is achievable even with the method in its current form. It would be highly attractive to categorically achieve that differentiation from a stand-off distance in a matter of seconds with no sample preparation.

7.3 Future work

As can be concluded from the above-discussed limitations of both the LIBS and LA-TDLAS techniques, the main drawback of these methods is the precision of the results. Although the issues with precision and accuracy should not be overlooked, neither should they be overstated. The ability to rapidly interrogate a material, to ascertain its trace element

'fingerprint' irrespective of its physical state and without sample preparation, from a safe stand-off distance, would be useful in numerous fields. Enabling concurrent isotopic characterisation would present a powerful tool for the nuclear chemist to use for applications in the nuclear industry.

It seems common in the literature to overcome shortcomings in precision by controlling the sample preparation or the sheath gas and gas pressure. However, in doing so many of the benefits of LIBS are negated. The key advantage of LIBS or LA-TDLAS is not in the accuracy of the results obtained, but rather in the speed and portability of the test and its hardware. Future experimental work should focus on improving the analytical figures of merit for both the elemental and isotopic capabilities, but should not lose sight of the benefits of measuring as-received samples under air at atmospheric pressure, simulating a field-deployed nuclear forensics investigation. It is for this reason that the success of the experiments with double-pulsed laser ablation was so exciting, as no compromise on hardware footprint, sampling time or portability was needed to improve the absorption spectra. Additionally, both the LIBS and LA-TDLAS results could be improved using double pulsed laser ablation. Future experiments should extend the DP-LA-TDLAS investigations to include uranium samples, and aim to maximise the absorption signals through the best combinations of pulse lengths and inter-pulse delay.

A simple way to increase the precision of the LA-TDLAS spectrum would be to improve the ECDL wavelength stability. The temperature of the laser diode was difficult to control, but using a larger or more powerful thermoelectric cooler would enable the temperature to be maintained for longer, and so would allow better stability of the emission wavelength. The SHR wavemeter used in the uranium LA-TDLAS experiments (Chapter 6) was difficult to align and the optical fibre connections were very delicate. Investment in improved on-line wavelength monitoring apparatus (for example a Fabry-Pérot etalon device) would lead to improved reliability in future experiments. It may be possible to ramp the ECDL wavelength rapidly across one or both of the isotopic absorption peaks over a very short timescale by using microcontroller electronics. These devices have fewer channels than the larger National Instruments data acquisition cards but can read and write at much higher frequencies. By ramping the wavelength over a very short time period, the transient laser produced plasma would essentially be stationary by comparison. Other, more expensive,

hardware modifications (for example a femtosecond laser for laser ablation or a new spectrometer for the LIBS apparatus) offer feasible alternatives for improving the analytical figures of merit, but typically the cost of those devices is prohibitive.

One original aim of the PhD project, which remains somewhat un-fulfilled, was to combine both methods of LIBS and LA-TDLAS for the simultaneous elemental and isotopic analysis of uranium. The quantity of suitable sample material received was insufficient for this aim to be perfectly achieved. However, to demonstrate how both emission and absorption spectroscopy could be utilised in a hyphenated manner, the emission (LIBS) and absorption (LA-TDLAS) spectra were analysed together in the calculations of plasma temperature and electron density. In doing so, a method of calculating the electron density using Stark broadening of a single emission line was developed. As mentioned previously, calculation of both the electron density and plasma temperature from the emission spectrum is difficult, as both parameters influence the emission linewidth. Usually, one parameter is estimated, whereas in this work a complementary analytical technique was used to analyse the same plasma. Once the electron density and the temperature of the plasma have been calculated and other sources of broadening (i.e. instrument broadening) have also been accounted for, the Stark broadening parameters for other emission lines can also be calculated. This could enable the Stark broadening parameters for any suitable isolated line in the LIBS spectrum to be calculated, which would, for example, be of great interest to astrophysicists studying emissions from stellar atmospheres.

If more of the CRM-124 sample material had been available, simultaneous elemental and isotopic analysis experiments could have taken place. However, the total quantity sent by a colleague at AWE was less than 20 µg, and only about 3 or 4 µg of each particular sample (e.g. CRM-124-1). After some initial necessary LIBS measurements to ascertain the ideal experimental conditions (i.e. laser power, camera settings, sample height, powder distribution methodology etc.), there was not enough material left for an LA-TDLAS experiment. Receiving more material, and additionally experimenting on samples with varied isotopic enrichment, would have allowed more in-depth LA-TDLAS analysis with simultaneous trace element quantification using LIBS. However, there would have been serious logistical issues to overcome for both the supplier and receiver before enriched samples could have been made available, and it was deemed beyond the scope of this PhD

project. However, future experiments could be carried out using the same hardware and handling procedures as were developed for this work.

Were this work to be used as a starting point for a commercialised nuclear forensics product, a worthwhile investment would be the generation of a sample library of various nuclear materials. This should include intermediate materials produced during common processing routes in the nuclear industry, and also the 'fingerprint' of elemental impurities from ores mined at different locations around the world.

Finally, miniaturisation of the combined LIBS and LA-TDLAS apparatus is distinctly possible, to enable a handheld device capable of elemental and isotopic analysis. The additional laser (or lasers) required for LA-TDLAS could be fibre coupled to keep the electronics, laser diodes and optics secured in position and distanced from the debris produced by the laser ablation process. A balanced detection method would still be possible if polarisation-maintaining optical fibres were utilised. A high-quality off-the-shelf Littrow or Littman-Metcalf laser diode would have the benefit of not requiring constant on-line wavelength supervision, as the wavelength of commercially manufactured lasers is more consistent between uses.

Chapter 8 – Appendices

8.1 Multivariate Data Analysis Techniques and Strategies

For the multivariate analysis chapters of this Thesis, two techniques were used: Partial Least Squares regression (PLS) and Principal Component Analysis (PCA). Although the two methods are both examples of Multivariate Data Analysis (MDA), there are numerous differences between them which present opportunities and challenges. As a prelude, advantages of using multivariate over univariate analysis for spectroscopy are increased accuracy and precision. Put simply, it is more accurate to compare multiple spectral peaks across various spectra than it is to compare single peaks. Single-peak measurements carry more risk: shrinking the complexity of a whole spectrum to essentially take only one value from it exposes the analysis to issues caused by random noise or experimental error.

The main differences between PLS and PCA are covered by stating that PLS is a supervised MDA method whilst PCA is an unsupervised method. Supervised methods are more usually used for regression and classification studies, whereas unsupervised methods are favoured for interrogating sample clustering and association. Input and output data is required to produce a training set for supervised MDA methods, whereas only input data is required for unsupervised MBA. Another difference is that it is difficult to see the sequence of computer decisions (the 'trail of breadcrumbs') which lead to a produced set of variables with unsupervised techniques, whereas this process is easier with supervised methods. For LIBS analysis specifically, there have been many published examples of calibration campaigns using PLS (see references in Sections 2.4.4, 3.2 and 4.2). PCA has also been applied to LIBS (again, see references in the aforementioned Sections) for categorisation of samples.

Chapter 3 used a technique called interval PLS (iPLS) which involves breaking the spectrum into intervals of selected length to reduce the complexity of the spectra. On the first iteration, each region in turn is tested against the independent variables to test for an increase in model validity (i.e. a decrease in error of fit). The region which best increases the model validity is maintained. For the next iteration, every remaining interval is tested together with the previously selected region, and again the region which increases the validity the most is kept and taken forward to the next iterations. Once no additional interval increases the model validity, PLS is performed on all the points encompassed by the selected intervals. The interval selection process requires a decision by the user on what

interval size to use. Smaller interval sizes may only partially cover wide spectral peaks, and also modelling a greater number of narrow intervals is more computationally expensive. Also, very small intervals may start to model the spectral noise rather than peaks of interest. On the other hand, setting the intervals too wide can lead to matrix element peaks in close proximity to useful analyte peaks being included in the modelling, which can detract from the accuracy. For the PLS modelling shown in Chapter 4, iPLS was initially tested. However the regions selected by the software were identical for many of the different elements being modelled. This indicated that iPLS was not selecting relevant intervals. The process was complicated by the fact that all seven samples had increasing levels of every analyte element in the same order (i.e. sample 1 with highest concentration and sample 7 with lowest concentration), so the correlation between peak intensity and concentration was the essentially the same for each analyte element.

The PCA analysis discussed in Chapter 3 used only the peak intensity from pre-selected emission peaks on the LIBS spectra. It was a time consuming process to go through each spectrum to identify emission peaks which firstly belonged to specific analyte elements of interest and secondly did not interfere with any other spectral peaks. However this step proved necessary, as running PCA of the full spectrum did not lead to any kind clustering. There are examples in the Literature of PCA being better suited to differentiating non-chemical differences in the spectra. For example, the level of the background in the Echelle orders can indicate different physical sample conditions (e.g. surface finish, preparation method), but the same elemental concentrations of analyte and matrix.

The following data pre-processing steps were performed: normalisation of each spectrum against a matrix peak (lithium in LKE matrix Chapter 3, uranium in uranium oxide matrix Chapter 4); removal of the Echelle order ‘hump’ (shown in detail in Figure 3.5 and discussed in Section 3.3.3); repeat spectra of the same sample were then averaged.

For further information, a number of interesting textbooks are available (e.g. [1]).

8.2 External Cavity Diode Laser

The External Cavity Diode Laser (ECDL) used in Chapters 5 and 6 was constructed almost entirely from Commercial off the Shelf (COTS) components. The only exceptions to this were

two angled stainless steel pieces (used to hold the grating and reflecting mirror in the correct orientation) and one aluminium lens tube, which were manufactured by the University of Manchester workshop. One of the two angled pieces was copied from the paper by Hawthorn et al [2], and was used to hold the grating. The other piece was a slight modification to their design whereby an additional angled piece was screwed to the surface of the kinematic mount. The original design showed that part of their mount had been cut to a 45 degree angle to hold the mirror, but it was thought better to make a new piece rather than risk damaging our (quite expensive) piezo-controlled kinematic mount. Dimensions and drawings of the parts can be found in the original reference by Hawthorn et al [2] and by Arnold et al [3].Initially, COTS lens tubes from Thorlabs were used for holding the Thermoelectric Cooler (TEC), diode and lens in place. However, an aluminium part was instead constructed by the workshop to provide the correct length (18 mm) for those three components inside and to allow concentric cooling fins to be machined into the base, plus entry holes for electrical wires to power the TEC and the diode. A schematic and a photograph of the apparatus are given in Figure 8.1 and Figure 8.2, and a detailed description of the apparatus is given below.

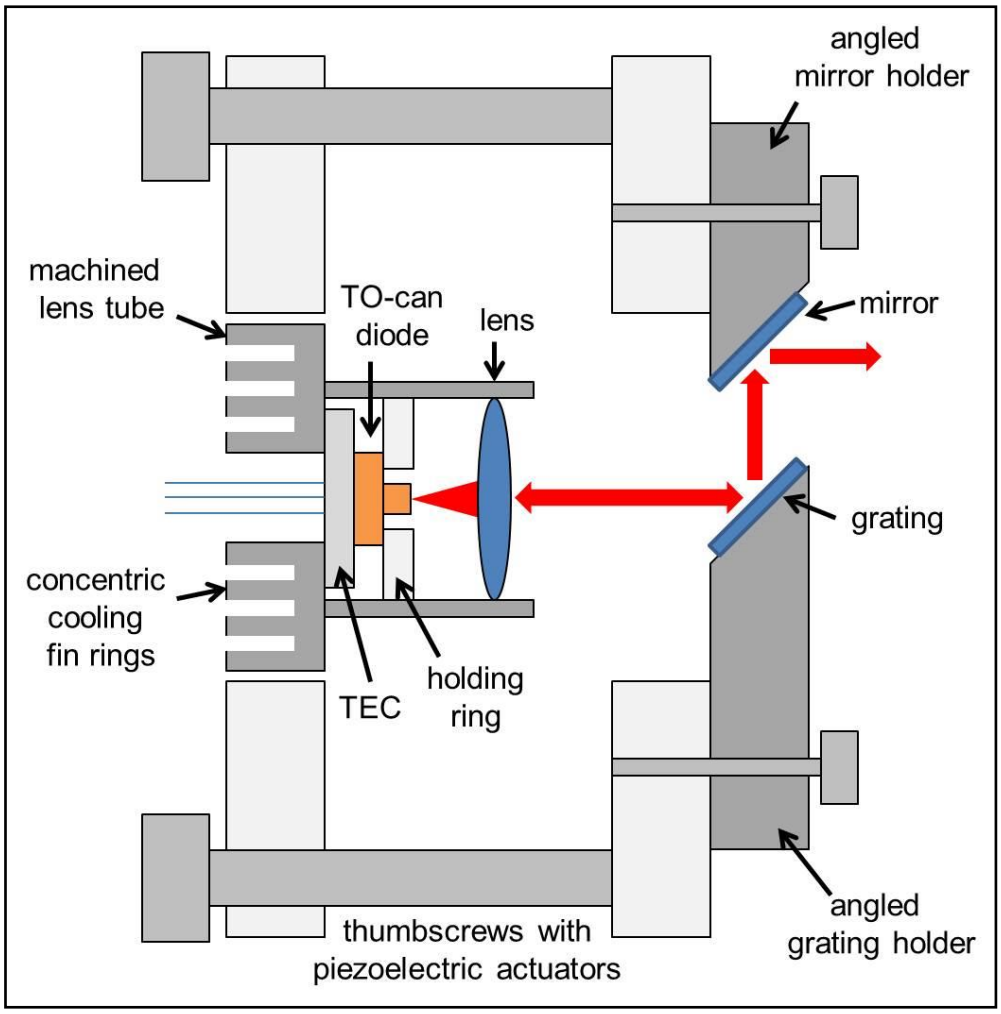

Figure 8.1. Schematic of External Cavity Diode Laser (ECDL). TEC: thermoelectric cooler

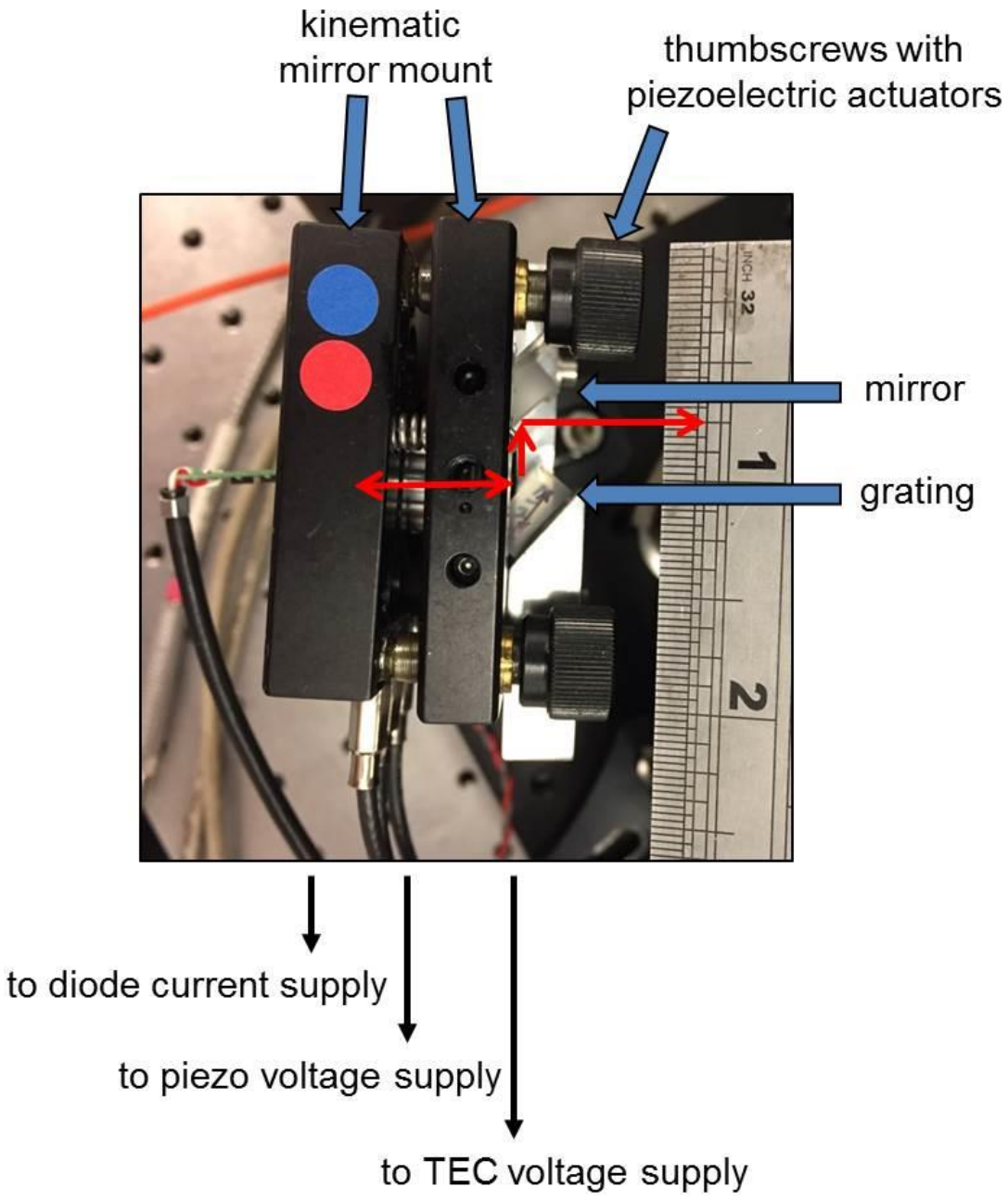

Figure 8.2. Annotated photograph of ECDL. Red arrows show direction(s) of laser

A holographic diffraction grating (Newport Scientific 33025FL01-320H, 1800 grooves/mm) was used to reflect the first order of the laser diode emission back into the laser medium, forming an external cavity. A folding mirror was fixed on the same arm as the grating and arranged in parallel – therefore as the grating arm was tuned the laser output angle remained constant. A machined aluminium lens tube with cooling fins housed the laser diode, collimating optic and a Peltier thermoelectric cooler (TEC) (1MC06-024-10H, RMT ltd., Moscow, Russia) measuring 8 mm × 8 mm × 1.8 mm. A central hole of diameter 3.4 mm

allowed the TO-can mounted laser diode to be placed in direct contact with the cold side of the TEC while the aluminium lens tube acted as a heat-sink in contact with the hot side. The laser diode and the TEC were switched on for at least one hour before each experiment to allow the temperature to stabilise. A small electrical computer fan was also positioned to blow air over the cooling fins of the lens tube to aid the cooling. This design provided excellent thermal tuning and stability for the laser once the temperature had settled. Fine-tuning the wavelength was accomplished by changing the angle of grating; this was controlled using the voltage supplied to one of the three piezoelectric actuators built into the kinematic mount by a stable high-voltage supply (Thorlabs MDT693B). The piezoelectric tuning alone enabled a mode-hop-free tuning range of up to 10 pm (6670 MHz, 0.222 cm^{-1}), and a combination of temperature, current, thumbscrew and piezoelectric tuning allowed the wavelength to be manipulated over ±0.5 nm in single mode emission. The wavelength was continuously monitored using the SHR wavemeter (accurate to ±1 pm), and the piezoelectric voltage and TEC current were adjusted to attain the necessary laser wavelength for each measurement. It was necessary to continuously manually adjust both the piezoelectric actuators and the TEC temperature to cover the full wavelength range required for analysis of the isotopic absorption peaks.

Chapters 5 and 6 state that the FWHM of the emission from the ECDL was a single mode of approximately 400 kHz. This figure is an estimation taken from the aforementioned paper by Hawthorn et al [2]. It was not possible to measure the FWHM accurately with the apparatus available. The SHR spectrometer had a resolution of only 1 pm so was not able to calculate the FWHM of the emission. Future experiments should seek to invest in a more accurate way of measuring the ECDL output, and also a more reliable way to record the wavelength in real time. The reported wavelength was very temperamental and would change by a few pm with the slightest change of angle of the fibre optic cable, or even with a change in electromagnetic field caused by moving around close to the instrument.

In order to optimise alignment of laser diode through the LPP, a sheet of burn paper angled at 45° to both the (vertical) YAG laser and (horizontal) laser diode was marked at the point of YAG laser focus. Then, without adjusting the paper, the laser diode was aligned to the centre of the scorch mark created on the burn paper. The height of the laser diode beam

above the sample surface was precisely adjusted to 1.5 mm using the periscope system, as this height maximised the absorbance from each LPP pulse.

The future work sections of Chapters 5 and 6 discuss the potential for a rapid wavelength ramp which could ramp the output wavelength across both isotopic absorption peaks during a single laser ablation event. This could increase the accuracy of the analysis, as the largest sources of error came from the inhomogeneous plasma generation. If both isotopes were analysed from a single ablation, the inhomogeneity should be completely avoided. The ramp time would have to be small enough to estimate stationary plasma conditions, which would be less than a few μs for uranium plasma but significantly longer for lithium plasma. This tuning speed should be possible with microcontroller electronics, which can read and write several channels at GHz speed (ns timescales). The Si photodiodes used in the current experimental setups have 1 ns rise times, so would be suitable for continued use. However, as stated in the previous paragraph, the ECDL required constant temperature and piezoelectric tuning to move the wavelength more than 10 pm. The setup used a TEC with a central hole to allow the TO-can diode to be in direct contact with cold side which gave very fast temperature control. However, temperature tuning on ns timescales would not be possible. That being said, rapid ramping using one of the other tuning methods – such as current tuning – would work over those short timescales. It might also be possible to increase the mode-hop-free piezoelectric tuning range with better alignment of the TO-can, lens and grating.

For further information about construction and design of the ECDL, the papers by Arnold et al [3] and Hawthorn et al [2] should be a first port of call. Their descriptions of strategies for aligning the grating and laser diode are very thorough and useful for the experimentalist. Other review articles are also available [4]. For more discussion of the theory behind external cavity lasers, tuning methods and different possible setups (i.e. prism, Littrow, Littman-Metcalf), the Master's Thesis of Martin Jackson from the University of Manchester is recommended [5].

8.3 Additional Figures

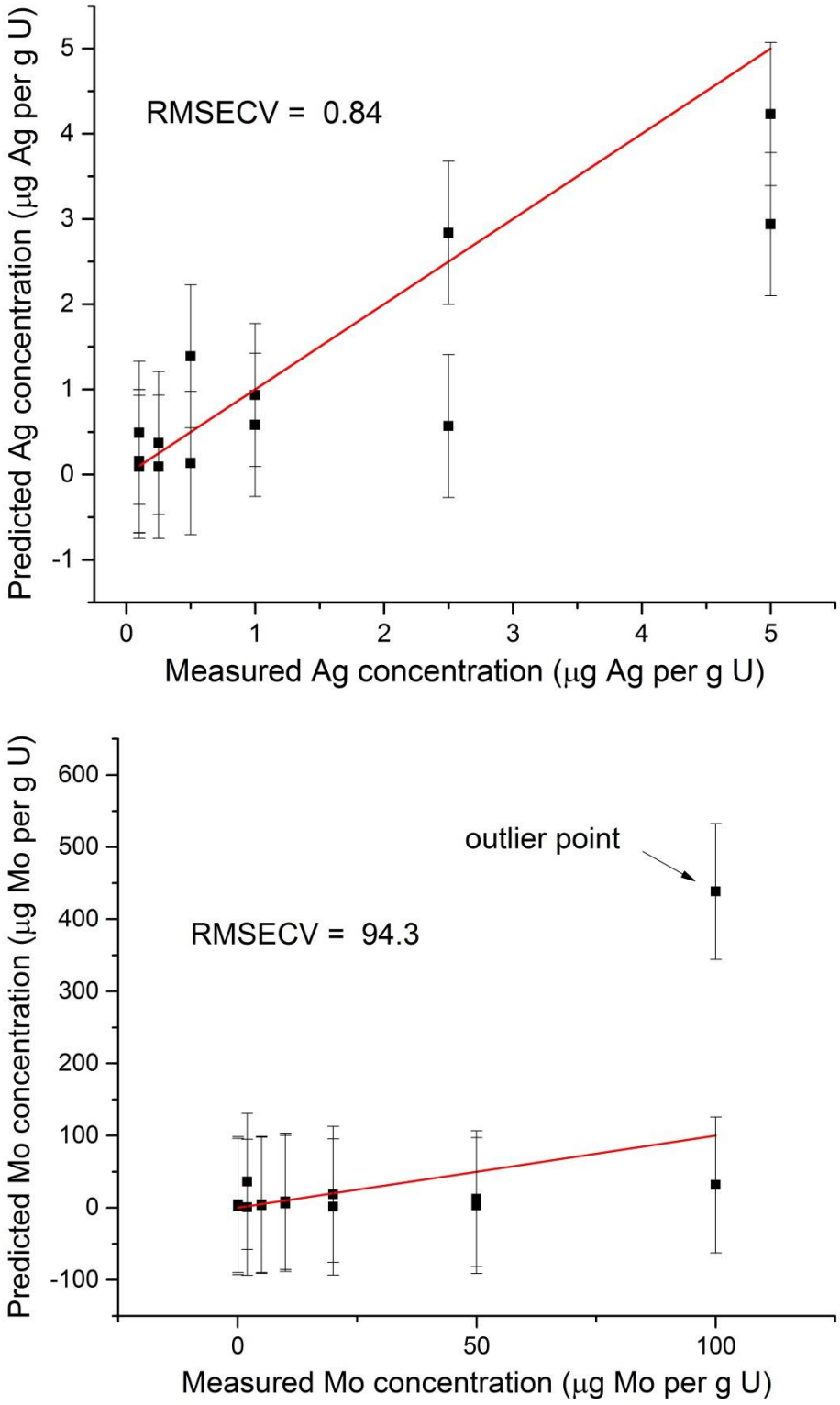

Figure 8.3. Copy of uranium PLS modelling results (same data as Figure 4.5), with error bars showing RMSECV values for each point

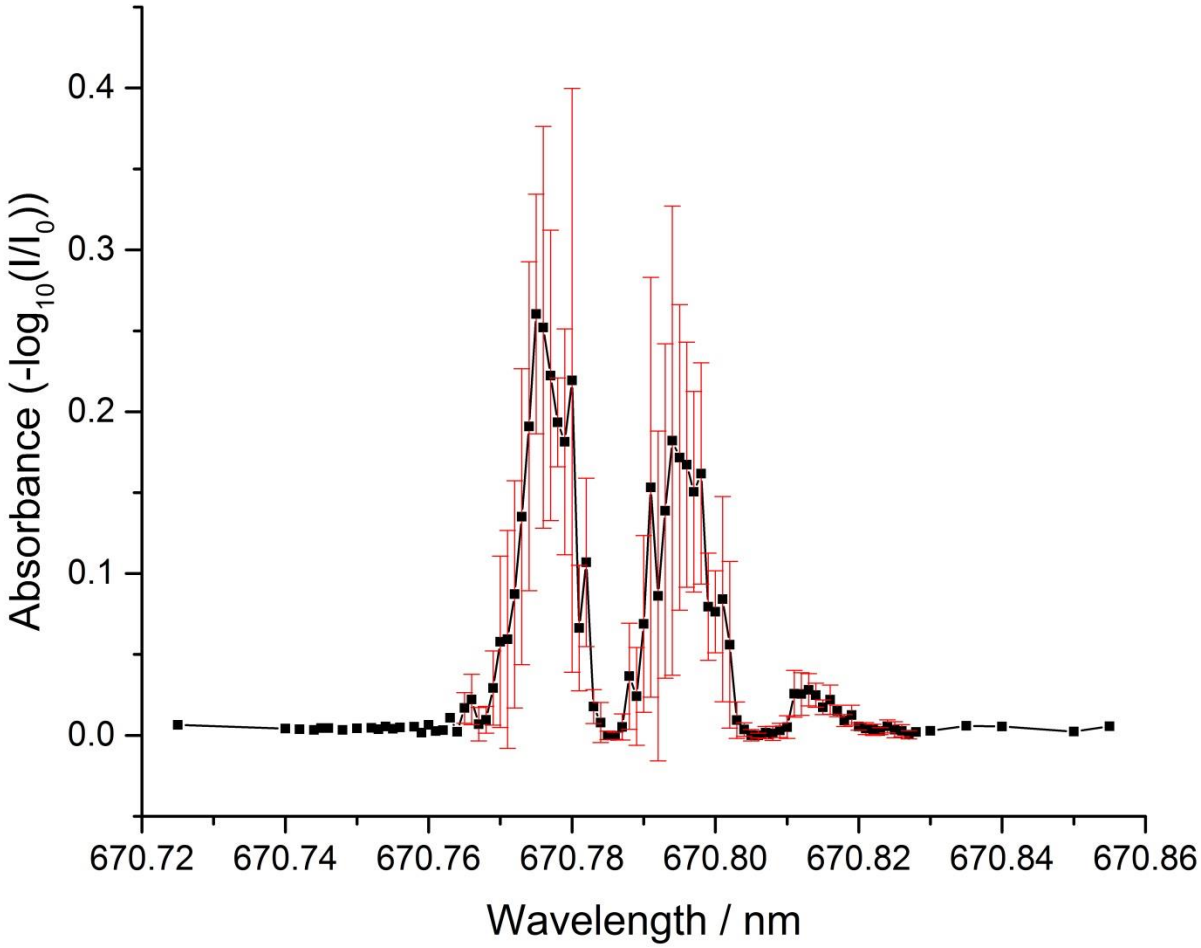

Figure 8.4. Copy of lithium absorbance spectrum at time delay of 340 µs (same data as Figure 5.3), with error bars showing ± one standard deviation of absorbance at each wavelength

Note how the standard deviation is significantly higher around each of the peak centres compared to the valley between the peaks. This is discussed in section 5.4.1.

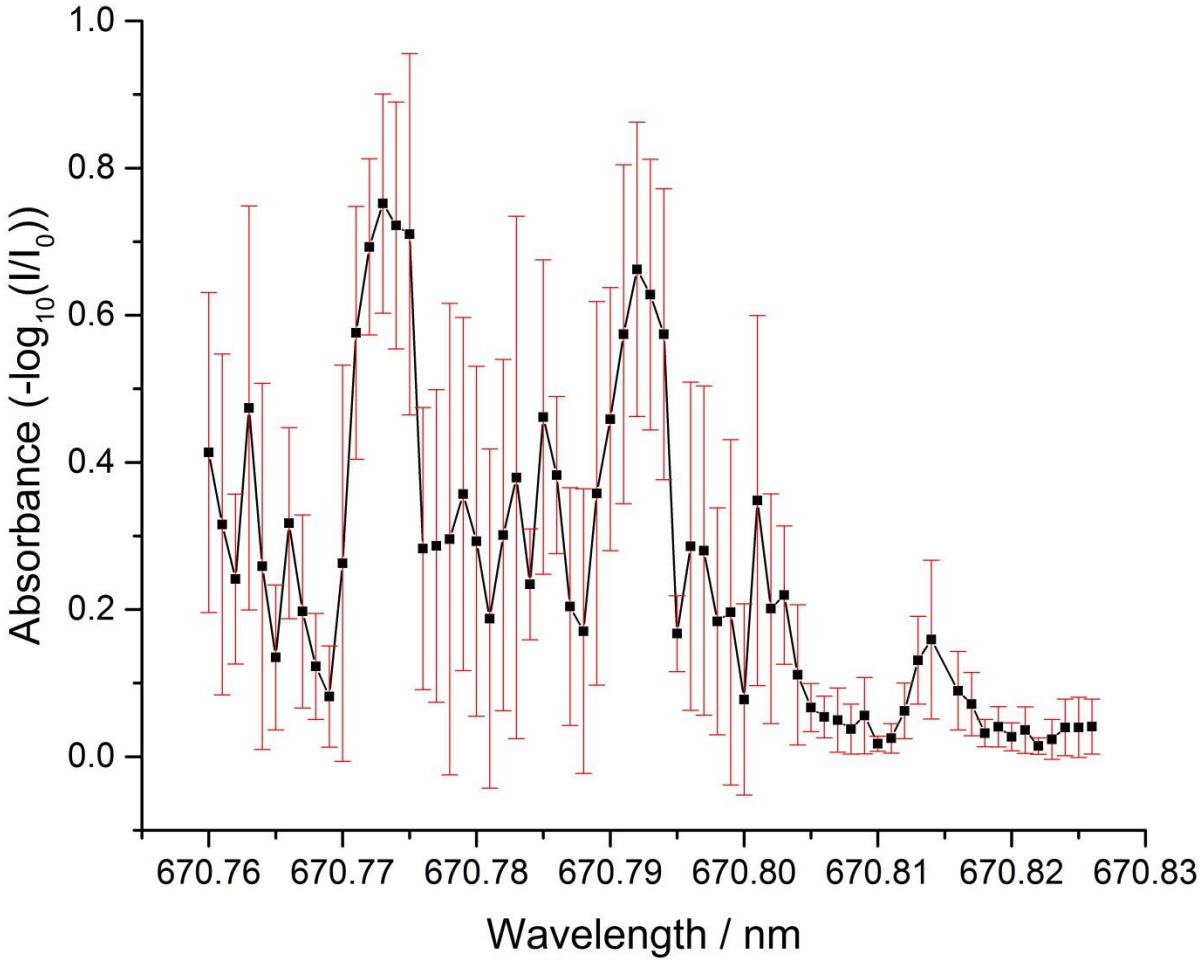

Figure 8.5. Copy of Double-Pulsed LA-TDLAS spectrum of lithium at time delay of 440 µs (same data as used in Figure 5.8), with error bars showing ± one standard deviation. Inter-pulse delay time = 30 µs

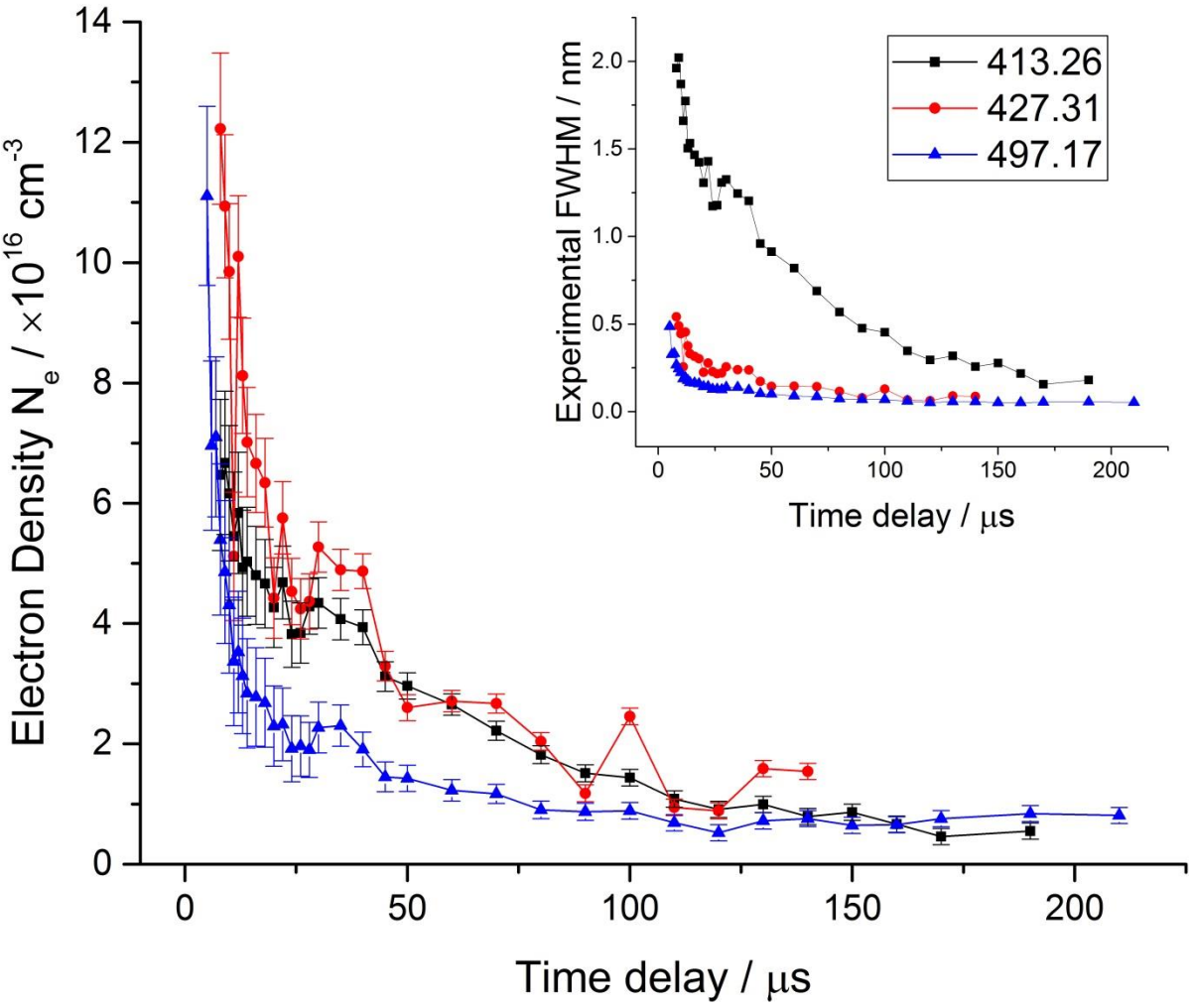

Figure 8.6. Copy of electron density calculation for DP-LA-TDLAS experiments with lithium (same data as figure 5.10). Error bars show standard error of Voigt fit

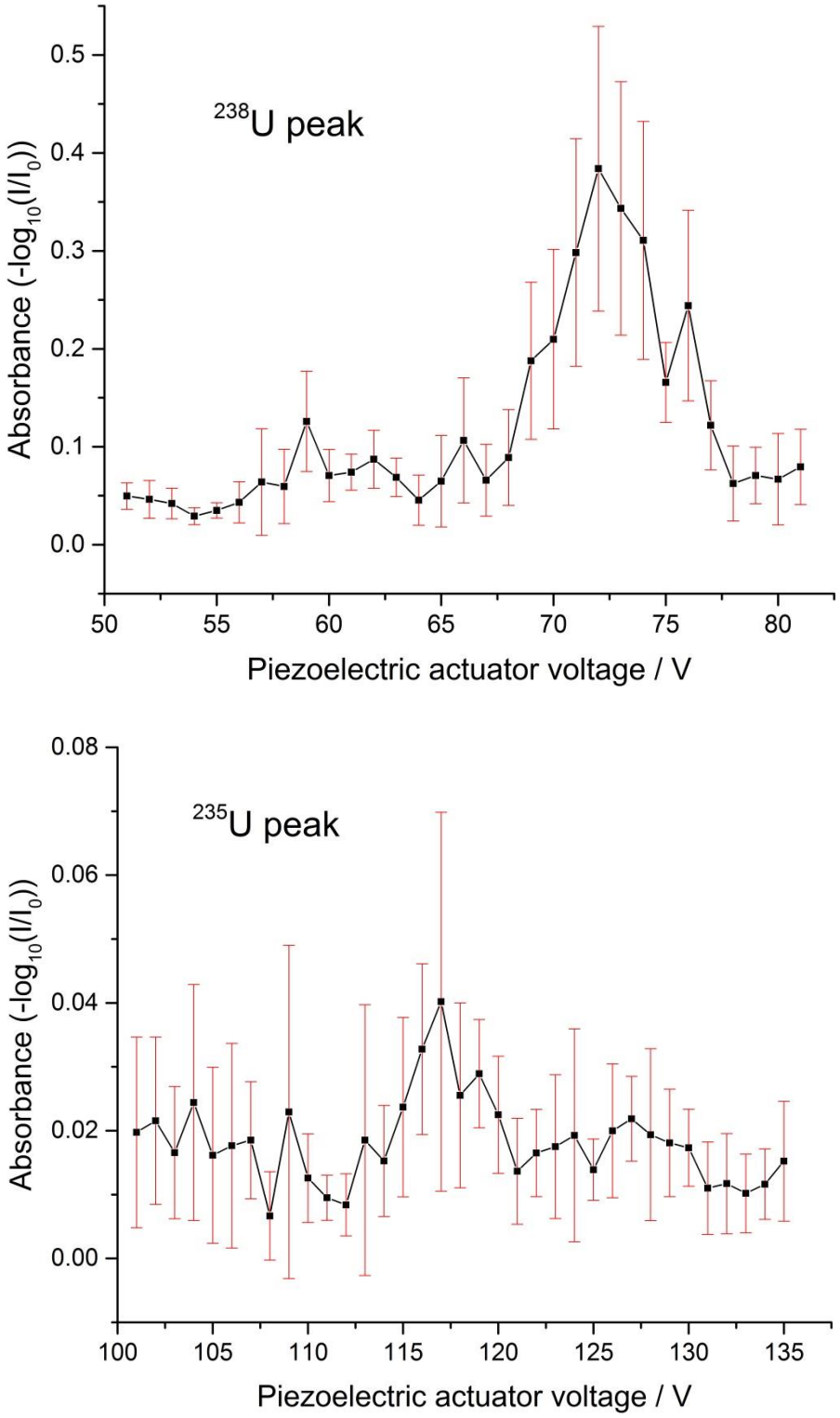

Figure 8.7. Copy of uranium absorbance spectrum at time delay of 48 μs (same data as Figure 6.7), with error bars showing one standard deviation of absorbance at each piezoelectric actuator voltage

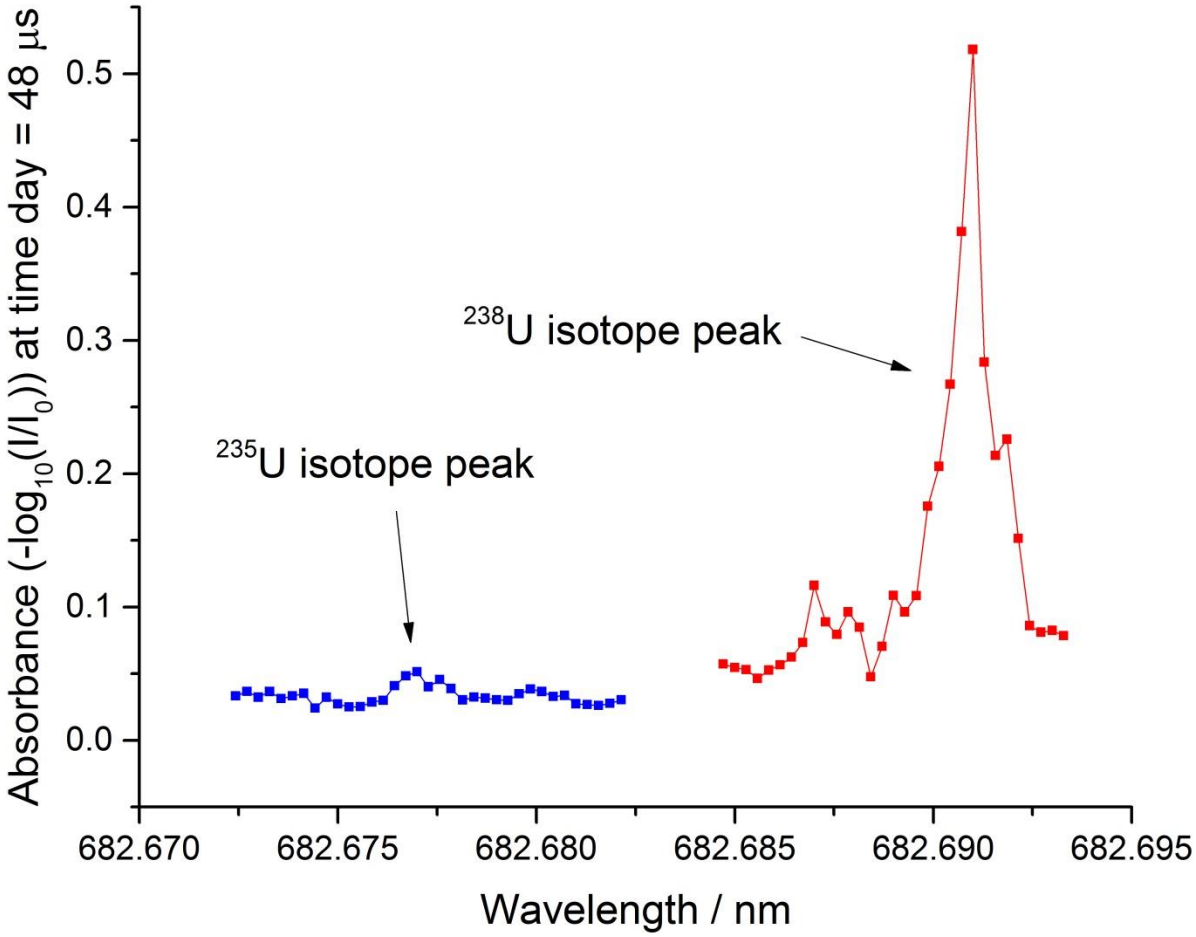

Figure 8.8. Uranium LA-TDLAS spectrum recorded using voltage stepping of the piezoelectric actuator. Same data as displayed in Figure 8.5 and Figure 6.7, but here fitted with an approximated wavelength scale to show both peaks on one spectrum

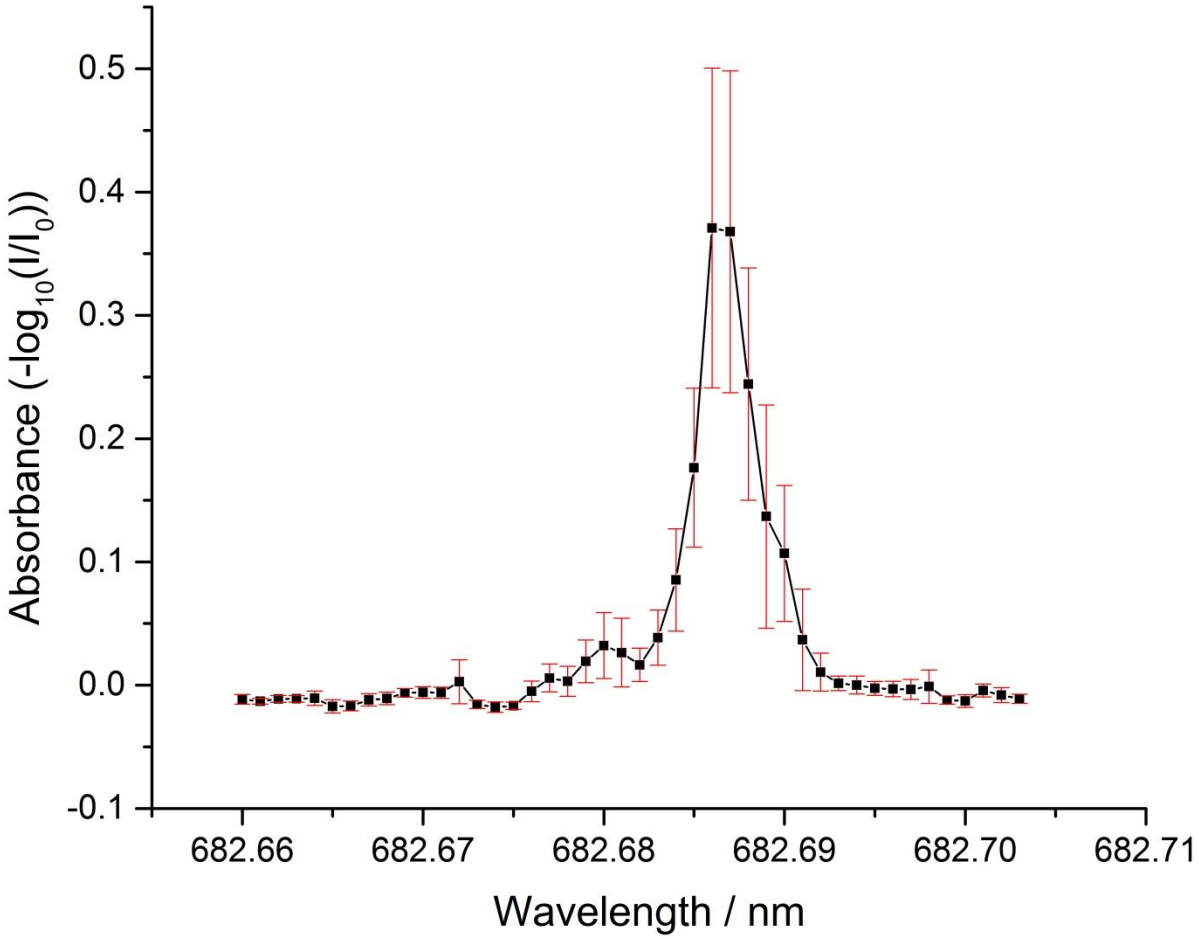

Figure 8.9. Copy of uranium LA-TDLAS spectrum measured using balanced detection setup (same data as Figure 6.8), with error bars showing ± one standard deviation

Note again (as with Figure 8.4) how the standard deviation is significantly higher around the major isotope uranium peak compared to away from peak centre, as discussed in Section 6.4.2.

References

[1] L. Eriksson, T. Byrne, E. Johansson, J. Trygg, and C. Vikström, *Multi- and Megavariate Data Analysis, Part I: Basic Principles and Applications*, 3rd ed. Umetrics Academy, 2013, 2013.

[2] C. J. Hawthorn, K. P. Weber, and R. E. Scholten, "Littrow configuration tunable external cavity diode laser with fixed direction output beam," *Rev. Sci. Instrum.*, vol. 72, no. 12, pp. 4477–4479, 2001.

[3] A. S. Arnold, J. S. Wilson, and M. G. Boshier, “A simple extended-cavity diode laser,” *Rev. Sci. Instrum.*, vol. 69, no. 3, pp. 1236–1239, Mar. 1998.

[4] B. Mroziewicz, “External cavity wavelength tunable semiconductor lasers - a review,” *Opto-Electronics Rev.*, vol. 16, no. 4, pp. 347–366, 2008.

[5] M. E. Jackson, “Design and Construction of a Temperature Controlled Littrow Mounted Extended-Cavity Diode Laser System,” University of Manchester, 2003.